

Aus dem Bereich Biophysik
Theoretische Medizin und Biowissenschaften
der Medizinischen Fakultät
der Universität des Saarlandes, Homburg/Saar

**Synthesis, endogenous detection, and mitochondrial function
of the hydroxy-substituted Coenzyme Q10 derivative HO-CoQ10**

**Dissertation zur Erlangung des Grades eines Doktors der Naturwissenschaften
der Medizinischen Fakultät**

der UNIVERSITÄT DES SAARLANDES

2019

vorgelegt von: Ewa Jasmin Slowik
geb. am: 21.03.1990 in Nürnberg

Tag der Promotion: 25.05.2020

Dekan: Prof. Dr. Michael D. Menger

Berichterstatter: Prof. Dr. Markus Hoth

Prof. Dr. Martin van der Laan

Prof. Dr. Susanne Fetzner

Contents

Summary	6
Zusammenfassung	8
1 Introduction	10
1.1 Coenzyme Q and its hydroxy analogue HO-CoQ10	10
1.2 Distribution and function of CoQ10	13
1.2.1 Intracellular distribution	13
1.2.2 Location and function in lipid bilayers.....	14
1.2.3 Physiological function	15
1.3 Mitochondrial electron transport chain	15
1.3.1 Electron transfer in respiratory chain complexes I, II, and III	16
1.3.2 Inhibitors and ROS production of respiratory chain complexes I, II, and III	17
1.3.3 Organization of respiratory chain complexes into supercomplexes	19
1.3.4 Influence of calcium on mitochondrial respiration	20
1.4 Research focus	20
2 Material and methods	22
2.1 Reagents	22
2.2 Software, general	22
2.3 Assay buffers	23
2.4 Production of HO-CoQ10	24
2.5 Structural analysis: nuclear magnetic resonance spectroscopy (NMR)	27
2.5.1 Proton NMR (^1H NMR).....	27
2.5.2 2-Dimensional NMR (2-D NMR).....	28
2.5.3 Quantitative NMR (qNMR)	28
2.6 Dissolving of CoQ10 and HO-CoQ10	28
2.7 Testing of solubility with UV/Vis spectrophotometry	29
2.8 Endogenous detection of HO-CoQ10 and CoQ10 using mass spectrometry	30
2.8.1 Mass and fragmentation analysis of pure substances: direct infusion	30
2.8.2 Testing of substance stability by ultra-high-pressure liquid chromatography coupled to mass spectrometry (UHPLC-MS).....	30
2.8.3 Detection in lipid extracts from isolated mitochondria by UHPLC-MS.....	32
2.9 Cell culture	34
2.10 Determination of metabolic turnover with the CellTiter-Blue[®] Cell Viability Assay	34

2.11	Detection of apoptosis with the protein sensor Casper-GR	35
2.12	Isolation of mitochondria	35
2.12.1	Isolation of beef heart mitochondria	36
2.12.2	Isolation of mouse heart mitochondria.....	36
2.13	Mitochondrial respiration: Clark-type electrode	38
2.13.1	Oxygraph Plus (Hansatech).....	38
2.13.2	Oxygraph 2k (Oroboros)	40
2.14	Determination of free [Ca²⁺]/[Mg²⁺] with fluorescent ratiometric dyes	42
2.15	Photometric activity assays of single respiratory chain complexes	46
2.16	Blue-native-gradient polyacrylamide gel electrophoresis of respiratory chain complexes	48
2.17	Western Blot	50
2.18	In-gel activity staining of respiratory chain complexes	50
2.19	Detection of reactive oxygen species	51
2.19.1	H ₂ O ₂ production assay using Amplex™ UltraRed	51
2.19.2	Extramitochondrial H ₂ O ₂ accumulation using Amplex™ UltraRed	52
2.19.3	Simultaneous detection of superoxide and oxygen using electron spin resonance spectroscopy	53
2.20	Low-temperature EPR of Complex I and II of the respiratory chain	54
3	Results	57
3.1	Synthesis of HO-CoQ10 in a two-phase system and identification of the main product	57
3.2	Dissolving of CoQ10 and HO-CoQ10 in aqueous media	63
3.2.1	Increased water-solubility of CoQ10 and HO-CoQ10 in a carrier complex with Cholesterol-PEG 600	65
3.3	Endogenous detection of HO-CoQ10 and CoQ10 in bovine heart mitochondria	66
3.3.1	Detection and fragmentation of CoQ10 and HO-CoQ10 by mass spectrometry	67
3.3.2	HO-CoQ10 but not CoQ10 was temperature-sensitive	69
3.3.3	HO-CoQ10 as part of mitochondrial membranes.....	70
3.4	HO-CoQ10 neither affected cell viability nor proliferation of cancer cell lines	74
3.5	Influence of HO-CoQ10 on mitochondrial respiration	76
3.5.1	Mitochondrial respiration linked to substrates of respiratory chain complex I, II, III, and IV.....	77
3.5.2	HO-CoQ10 inhibited CI-, CII-, and CIII-linked respiration	80
3.6	Ca²⁺ potentiated respiratory inhibition by HO-CoQ10	86
3.6.1	Preliminary data: Ca ²⁺ amplified HO-CoQ10-linked respiratory inhibition of mitochondria from different species	86
3.6.2	P _i reduced free Mg ²⁺ and free Ca ²⁺ concentrations in respiration buffer.....	88
3.6.3	Ca ²⁺ potentiated respiratory inhibition by HO-CoQ10.....	93

3.6.4	More hydrophilic CoQ1 did not inhibit respiration	95
3.6.5	Inhibitory Ca ²⁺ effect mediated by CoQ.....	96
3.7	HO-CoQ10 inhibited respiratory chain complexes I and II in photometric activity assays.....	97
3.7.1	CI (NADH-CoQ1 oxidoreductase) was inhibited by HO-CoQ10	97
3.7.2	CII (succinate:CoQ1 oxidoreductase) was inhibited by HO-CoQ10	101
3.7.3	CIII (decyl-ubiquinol:cytochrome c oxidoreductase) was not inhibited by HO-CoQ10	104
3.7.4	HO-CoQ10 was reduced by succinate:CoQ dehydrogenase.....	106
3.7.5	Identification of respiratory complexes and supercomplex formation.....	108
3.7.6	In-gel activity staining: HO-CoQ10 did not disturb Complex I NADH oxidase and Complex II succinate oxidase activity	109
3.8	Influence of HO-CoQ10 and CoQ10 on mitochondrial ROS production	112
3.8.1	HO-CoQ10 enhanced hydrogen peroxide production of respiring mitochondria.....	112
3.8.2	Simultaneous superoxide detection and oximetry in mitochondria using electron spin resonance spectroscopy	117
3.9	Low-temperature electron spin resonance spectroscopy (EPR) of respiratory chain complexes I and II	123
3.9.1	Reduction of Fe-S clusters from Complex I and influence of rotenone and CoQ.....	124
3.9.2	Identification of Fe-S clusters from Complex II and influence of atpenin A5.....	131
4	Discussion.....	134
	Literature	143
	Acknowledgements	157
	Publications.....	158
	Curriculum vitae	159

Summary

Quinones are redox-active molecules playing important roles in all organisms. In humans, the *para*-benzoquinone derivative Coenzyme Q10 (CoQ10) carrying a chain of 10 isoprene units and two neighbouring methoxy groups at the benzoquinone ring is found ubiquitously. It is an essential electron and proton transporter in the mitochondrial respiratory chain and fulfils various important functions like regulating redox homeostasis and membrane viscosity. In 2011, Bogeski et al. chemically modified the functional head group of CoQ10 exchanging one methoxy group by a hydroxy group. The hydroxy analogue can also be produced by CYP450 present in mitochondria and endoplasmic reticulum and is a postulated intermediate in CoQ biosynthesis that had not been detected in eukaryotes.

The aim of this thesis was to gain first insights into the biological role of the mono-demethylated Coenzyme Q10. Therefore, within this study and my precedent master thesis, the CoQ10 derivative, HO-CoQ10, was synthesized and purified in sufficient amounts for the first time. Its structure could be verified using mass spectrometry and $^1\text{H}/^{13}\text{C}$ 2-dimensional nuclear magnetic resonance spectroscopy. The synthesis was confirmed to always produce a constitutional isomer mixture of HO-CoQ10 modified at the 2- or 3-position of the quinone ring. Due to the high lipophilicity mediated by the long isoprene chain, reliable transition to the aqueous phase was crucial for experiments. An ethanolic solution of 1 mM CoQ10 and 5 mM HO-CoQ10 was stable at room temperature and could be diluted in aqueous media. Hence, most experiments were conducted with 1% ethanol resulting in a maximal concentration of 10 μM CoQ10.

To understand the physiological importance of HO-CoQ10, its endogenous occurrence was clarified using ultra-high-pressure liquid chromatography coupled to tandem mass spectrometry. In isopropanol extracts from crude bovine heart mitochondria, HO-CoQ10 was detected for the first time and estimated to have a concentration of 100 μM in mitochondrial membranes. Evaluating toxicity of exogenously applied HO-CoQ10, no effect on cancer cell lines cultivated under standard cell culture conditions was found: No interference with metabolic activity and proliferation was observed in HeLa, MelJuso and Jurkat T cells using the CellTiter-Blue[®] reduction assay and apoptosis was not induced in Jurkat T cells analysing caspase activity using Caper-GR sensor.

Detecting HO-CoQ10 in mitochondria and considering the essential role of CoQ10 in the electron transport chain, its influence on respiration was evaluated measuring oxygen consumption of isolated cardiac mitochondria from BL6N mice using a Clark-type electrode. HO-CoQ10 inhibited Complex I-, II-, and III-linked respiration. Surprisingly, also the native substance CoQ10 intervened with Complex I- and II-linked respiration, but to a lower extent than HO-CoQ10. Extramitochondrial calcium enhanced inhibition via CoQ10 and HO-CoQ10 by the same factor. Since respiration buffers contained inorganic phosphate affecting free metal concentrations, free calcium was defined using the fluorescent calcium indicator fura-2. Photometric activity assays of respiratory chain enzymes from bovine heart mitochondria showed that HO-CoQ10 but not CoQ10 inhibited both oxidoreductase activity of Complex I and II. Decyl-ubiquinol:cytochrome *c* oxidoreductase (Complex III) was unaffected. In-gel activity staining of Complex I and II did not show interference on oxidase activities indicating that HO-CoQ10 acts on Q-binding sites of the complexes. Since

CoQ10 is an important antioxidant *in vivo* but also shows prooxidant activity under distinct circumstances depending on its redox state, H₂O₂ production in the supernatant of coupled mouse heart mitochondria was examined using an HRP-based assay with Amplex[®] UltraRed. HO-CoQ10 increased Complex I- and II-linked ROS formation rate. CI-linked rates were similar for HO-CoQ10 and the ubiquinone-binding site inhibitor rotenone. Production rates induced by the Q_I-site inhibitor of Complex III, antimycin A, were considerably higher. Glycerol dehydrogenase-linked H₂O₂ production was increased by antimycin A and slightly reduced by HO-CoQ10. To assess the correlation of respiration and ROS production, oxygen consumption and superoxide production were detected simultaneously by electron spin resonance spectroscopy with the oxygen sensor trityl and the spin probe for superoxide CMH. Similar to rotenone, CM• formation rate was not influenced by HO-CoQ10. Electron distribution in Complex I-associated iron-sulphur clusters of NADH-energized bovine heart mitochondria, visualised with low-temperature electron spin resonance spectroscopy, was not altered by HO-CoQ10.

This work provides the first insight into the biological significance of the neglected hydroxy analogue of CoQ10. Focussing on mitochondrial respiration, the most studied and biologically important role of Coenzyme Q, it was found that both CoQ10 and HO-CoQ10 inhibit respiration. Enrichment of the substances was shown to decrease membrane fluidity in other studies, which might be the underlying mechanism diminishing electron transfer efficiency. Calcium potentiating the inhibition by both substances supports the observation. Due to its lower redox potential, HO-CoQ10 has been predicted to be a more potent antioxidant with a potential to substitute CoQ10 in the medication of ROS related diseases. However, it was found to inhibit activity of respiratory chain complexes and stimulated ROS production most likely via blocking Q-binding sites. Downregulation of respiration and stimulation of ROS production by HO-CoQ10, found in small portions in metabolic active heart tissue, suggests a role in regulation of energy metabolism and might act as an internal brake for growth when synthesis is upregulated.

Zusammenfassung

Synthese, endogene Detektion und mitochondriale Funktion des hydroxy-substituierten Coenzym Q10-Derivats HO-CoQ10

Chinone sind redoxaktive Moleküle, die in allen Organismen wichtige Aufgaben erfüllen. Im Menschen ist das para-Benzochinon-Derivat Coenzym Q10 (CoQ10) ubiquitär vorhanden. Am Chinonring trägt es zwei benachbarte Methoxygruppen und eine Seitekette aus zehn Isopren-Einheiten. CoQ10 ist ein essentieller Elektronen- und Protonentransporter der mitochondrialen Atmungskette und an anderen wichtigen Funktionen wie der Regulation der Redoxhomoöstase und Membranviskosität beteiligt. 2011 haben Bogeski et al. seine funktionelle Kopfgruppe chemisch modifiziert, indem sie eine der Methoxygruppen durch eine Hydroxygruppe substituiert haben. Das Hydroxy-Analogon kann auch durch CYP450-Enzyme, welche in Mitochondrien und endoplasmatischem Retikulum exprimiert sind, produziert werden und ist eine postulierte biosynthetische Vorstufe von Coenzyme Q, die jedoch in Eukaryoten bisher nicht nachgewiesen werden konnte.

In der vorliegenden Arbeit wurde erstmals die biologische Funktion von mono-demethyliertem Coenzym Q10 untersucht. Hierzu wurde das Coenzym Q10-Derivat, HO-CoQ10, im Rahmen dieser Doktorarbeit und der vorangehenden Masterarbeit synthetisiert und in ausreichender Menge aufgereinigt. Die Struktur wurde mittels $^1\text{H}/^{13}\text{C}$ 2-dimensionaler Kernspinresonanzspektroskopie verifiziert. Das Produkt besteht aus einer Mischung an Konstitutionsisomeren, welche die Hydroxygruppe an Position 2 oder 3 des Chinonrings tragen. Aufgrund der langen Isoprenkette handelt es sich um stark lipophile Substanzen, deren Übergang ins Wässrige für die folgenden Untersuchungen essentiell war. 1 mM CoQ10 und 5 mM HO-CoQ10 in ethanolischer Lösung waren bei Raumtemperatur stabil und konnten in wässrigen Medien verdünnt werden. Deshalb wurden die meisten Experimente mit 1 % Ethanol und einer maximalen CoQ10 Konzentration von 10 μM durchgeführt.

Um die physiologische Bedeutung von HO-CoQ10 zu erfassen, wurde sein endogenes Vorkommen mittels Ultra-Hochdruckflüssigkeitschromatographie-gekoppelter Massenspektrometrie aufgeklärt. In Isopropanol-Extrakten aus unaufbereitetem Rinderherzmitochondrien wurde HO-CoQ10 erstmals nachgewiesen und seine Konzentration in der Mitochondrienmembran auf 100 μM geschätzt. Die Toxizität von exogen appliziertem HO-CoQ10 auf unter Standard-Zellkulturbedingungen kultivierten Krebszelllinien wurde untersucht: Die metabolische Aktivität und Proliferation von HeLa, MelJuso und Jurkat T-Zellen, bestimmt mit Hilfe des CellTiter-Blue[®]-Reduktionsassays, war unbeeinträchtigt. Zudem konnte in Jurkat T-Zellen bei Analyse der Caspase-Aktivität mittels des Casper-GR-Sensors keine Apoptoseinduktion beobachtet werden.

Da HO-CoQ10 in Mitochondrien detektiert wurde und CoQ10 eine essentielle Rolle in der Elektronentransportkette einnimmt, wurde der Einfluss auf die Respiration untersucht. Hierfür wurde der Sauerstoffverbrauch isolierter Herzmitochondrien aus BL6N-Mäusen mit Hilfe einer Clark-Elektrode gemessen. HO-CoQ10 inhibierte Complex I-, II- und III-assozierte Atmung. Erstaunlicherweise inhibierte auch die native Substanz CoQ10 die Complex I- und II-assozierte Respiration; dies jedoch in einem geringern

Ausmaß als HO-CoQ10. Extramitochondriales Calcium steigerte die durch CoQ10 und HO-CoQ10 vermittelte Inhibition gleichermaßen. Die Puffer für Atmungsmessungen enthalten anorganisches Phosphat, welches sich auf die Konzentration an freien Metallionen auswirkt. Deswegen musste die freie Calciumkonzentration mittels des fluoreszenten Calciumindikators Fura-2 festgelegt und -gestellt werden. Photometrische Aktivitätsbestimmungen der Atmungskettenenzyme aus Rinderherzmitochondrien zeigten, dass HO-CoQ10, jedoch nicht CoQ10 Complex I- und Complex II-Oxidoreduktase-Aktivität inhibiert. Decyl-ubichinol:Cytochrom *c* oxidoreduktase (Complex III) war unbeeinträchtigt. In-Gel-Aktivitätsfärbungen stellten heraus, dass HO-CoQ10 keinen Einfluss auf die Oxidase-Aktivität von Complex I und Complex II hat. Dies deutet darauf hin, dass HO-CoQ10 auf die Q-Bindestellen wirkt. Da CoQ10 ein in-vivo wichtiges Antioxidans ist, das unter bestimmten Umständen abhängig vom Redoxzustand prooxidativ wirkt, wurde die H₂O₂-Produktion im Überstand gekoppelter Mausherzmitochondrien mit Hilfe eines HRP-basierten Assays mit Amplex® UltraRed untersucht. HO-CoQ10 erhöhte die Complex I- und Complex II-assoziierte Produktionsrate an reaktiven Sauerstoffspezies. CI-assoziierte Raten mit HO-CoQ10 waren vergleichbar mit Raten in Anwesenheit des Ubichinon-Bindestellen-Inhibitors Rotenon. Produktionsraten induziert durch den Q_i-Bindestellen-Inhibitor von Complex III, Antimycin A, waren deutlich höher. Glyceroldehydrogenase-assoziierte H₂O₂-Produktion war durch Antimycin A erhöht und durch HO-CoQ10 leicht reduziert. Um den Zusammenhang von Respiration und ROS-Produktion zu untersuchen, wurden Sauerstoffverbrauch und Superoxidproduktion simultan mittels Elektronenspinresonanzspektroskopie mit dem Sauerstoffsensor Trityl und der Superoxid-Spinsonde CMH gemessen. Vergleichbar mit Rotenon wurde die CM•-Bildungsrate auch von HO-CoQ10 nicht beeinflusst. Die Elektronenverteilung in Eisen-Schwefel-Clustern von Complex I in NADH-energetisierten Rinderherzmitochondrien wurde mittels Tieftemperatur-Elektronenspinresonanzspektroskopie visualisiert und war nicht durch HO-CoQ10 verändert.

Die vorliegende Arbeit gibt erste Hinweise auf die biologische Bedeutung des wenig beachteten Hydroxy-Analogons von CoQ10. Es konnte gezeigt werden, dass sowohl CoQ10 als auch HO-CoQ10 die mitochondriale Atmung inhibieren. Da andere Studien zeigten, dass die Anreicherung der Substanzen die Fluidität der Membran reduziert, könnte dies der zugrunde liegende Mechanismus für eine Abnahme der Elektronentransfereffizienz sein. Die Potenzierung der Inhibition durch Calcium unterstützt die Beobachtung, dass HO-CoQ10 und CoQ10 die Fähigkeit besitzen Calcium zu binden. Aufgrund des niedrigeren Redoxpotentials wurde prognostiziert, dass HO-CoQ10 ein effektiveres Antioxidans ist und das Potential besitzt, CoQ10 in der medizinischen Behandlung von ROS-korrelierten Krankheiten zu ersetzen. Allerdings zeigte sich, dass HO-CoQ10, höchstwahrscheinlich durch die Blockade von Q-Bindestellen, Atmungskettenkomplexe hemmt und ROS-Produktion stimuliert. Herunterregulation der Respiration und Stimulation von ROS-Produktion durch HO-CoQ10, das in stoffwechselaktivem Herzgewebe in kleinen Mengen gefunden wurde, weist auf Beteiligung in der Regulation von Energiestoffwechsel hin und könnte bei Hochregulation der Synthese als interne Wachstumsbremse agieren.

1 Introduction

1.1 Coenzyme Q and its hydroxy analogue HO-CoQ10

All organisms – prokaryotes as well as eukaryotes – share one important molecule to transport e^- and H^+ in many different pathways and functions: the quinone (Q in **Figure 1**). Its basic structure, the benzoquinone (BQ), takes up one electron and one proton to form a semiquinone radical (SQ^\bullet). Adding another e^- and H^+ yields its fully reduced form, the quinol (QH_2 , hydroquinone). The intermediate SQ^\bullet may form reactive oxygen species (ROS), in particular, superoxide ($O_2^{\bullet-}$) under certain conditions.^{1,2}

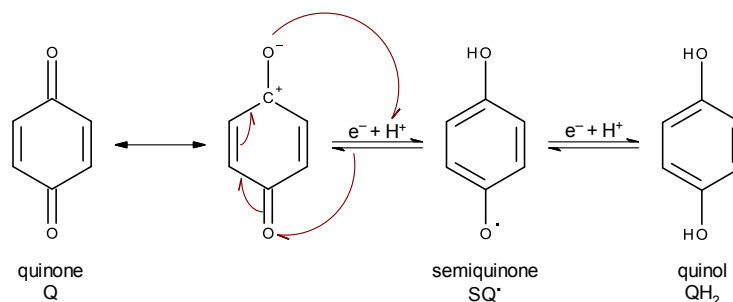


Figure 1 | Redox reaction of quinones. As an example, *para*-benzoquinone is shown. The stepwise uptake of two electrons and two protons by the quinone yields in the semiquinone radical and the fully reduced quinol, subsequently. Drawn on the basis of schemes from Ilhardt (2009), Berg (2010) and Brunmark (1989)^{1,3,4}

Among others, humans, mice, yeast, and *Escherichia coli* (*E. coli*) synthesize the quinoid Coenzyme Q (CoQ)^a which is a fully substituted *para*-benzoquinone (*p*-BQ) containing two adjacent methoxy groups, a methyl group, and an isoprene chain of species-dependent length at 2-, 3-, 5-, and 6-position of the ring, respectively. Structures of CoQs and their components are depicted in **Figure 2 a-c**. The number following CoQ reflects the number of isoprene units, e.g. the main species in mice is CoQ9, in humans CoQ10, containing 9 and 10 isoprene units. This long carbon chain, consisting of 40 successive C-atoms gives CoQ10 its hydrophobic nature. The molecules, also called ubiquinones, are found ubiquitously in all cells and subcellular compartments and are an essential part of metabolism and redox homeostasis.

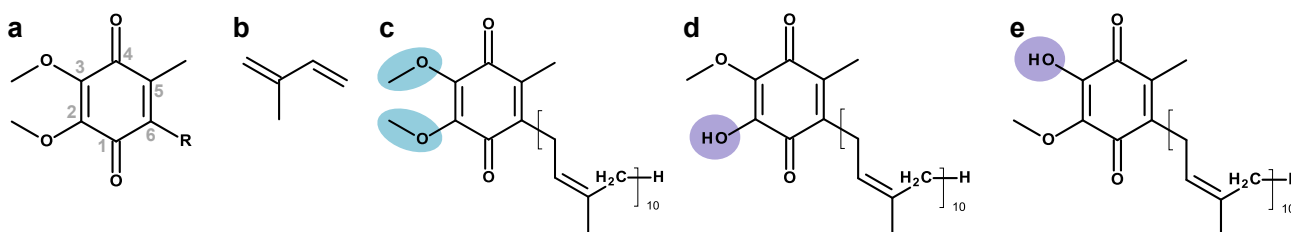


Figure 2 | Composition of Coenzyme Q and its hydroxy analogue. (a) Coenzyme Q or ubiquinone, digits indicate the position^b of the substituent on the quinone ring, R is the isoprenoid chain consisting of a species-depending number of (b) isoprene units, e.g. 10, 9, 6,

^a Coenzyme Q, CoQ, ubiquinone

^b The numbering of the position on the quinone ring follows the general IUPAC naming of Coenzyme Q but is not according to the IUPAC name of CoQ10 (see following footnotes).

and 8 in human, mice, *E. coli*, and *Saccharomyces cerevisiae* (*S. cerevisiae*), respectively. (c) Coenzyme Q10^c, (d) 2-Hydroxy Coenzyme Q10 (i.e. 2-demethyl Coenzyme Q10)^d, (e) 3-Hydroxy Coenzyme Q10 (i.e. 3-demethyl Coenzyme Q10)^e

In 2011, Bogeski et al.⁵ synthesized demethylated CoQ derivatives in which one or both methoxy groups were replaced by hydroxy groups. The products were named Hydroxy CoQ10 to emphasize the introduced functional OH-group. The structures of mono-demethylated derivatives are shown in Figure 2 d and e. Throughout this thesis, the molecule containing one hydroxy substituent at 2- or 3- position on the quinone ring will be called HO-CoQ10.

The synthesized hydroxy analogues of CoQ1 and CoQ10 showed a more negative redox potential than the native form.⁵ Hence, reduced Hydroxy CoQs have higher reducing potentials and may be better antioxidants.⁵ Indeed, reaction mixtures of hydroxy derivatives of 2,6-dimethoxy-1,4-benzoquinone have been shown to scavenge superoxide anion radicals.⁶ The reaction with superoxide was slightly faster compared to ascorbic acid and considerably faster than the reduction of superoxide by the spin probe CMH. Similarly, hydroxy derivatives of Coenzyme Q0 (Coenzyme Q not carrying an isoprene chain) had a slightly higher antioxidative potential than Vitamin E, tested by neutralization of oxidized ABTS.⁷

Surprisingly, the introduction of the hydroxy group at the quinone ring enabled BQ, Coenzyme Q0, Q1 and Q10 to bind⁶⁻⁸ and transport calcium ions.⁵ According to Bennett et al. (2002),⁹ a redox-loop mechanism was proposed where reduced quinol species bind metal ions and release them upon oxidation. The authors examined hydroxy-acetophenones^f that were proposed to complex calcium at the adjacent oxygen atoms from the keto and deprotonated alcohol group of two molecules.⁹ Hydroxy CoQs but not the native CoQs were able to bind calcium and to a lower extent magnesium.^{5,7} Transport of calcium across biomimetic membranes was shown for both Hydroxy CoQ1 and Hydroxy CoQ10 in a redox-dependent manner.

Being the most abundant ubiquinone in humans, Coenzyme Q10 and its demethylated derivative were in focus of this thesis. All before mentioned experiments with Hydroxy CoQs were performed with reaction mixtures only, so additional effects of side products cannot be excluded. In preliminary experiments in this laboratory (A. G., E. J. S.),¹⁰⁻¹² a robust synthesis and purification method for HO-CoQ10 was established. Analysing the product's fractions, non-negligible amounts of by-products have been detected. Among these were dicarboxylic acids with open ring structures. Given the distinct nature of these molecules, functional studies need to be re-examined with purified material. The main product has been proposed to be 2-HO-CoQ10 based on UHPLC-MS/MS^g and H-D exchange^h ¹H NMRⁱ data. To finally and confidently identify the product, 2-D NMR analysis of correlated ¹³C/¹H signals of the purified substance has been missing. Failing to synthesize the

IUPAC name of

^c **CoQ10:** 2-[(2E,6E,10E,14E,18E,22E,26E,30E,34E)-3,7,11,15,19,23,27,31,35,39-decamethyltetraconta-2,6,10,14,18,22,26,30,34,38-decaenyl]-5,6-dimethoxy-3-methyl-1,4-benzoquinone

^d **2-HO-CoQ10:** 2-[(2E,6E,10E,14E,18E,22E,26E,30E,34E)-3,7,11,15,19,23,27,31,35,39-decamethyltetraconta-2,6,10,14,18,22,26,30,34,38-decaenyl]-6-hydroxy-5-methoxy-3-methyl-1,4-benzoquinone

^e **3-HO-CoQ10:** 2-[(2E,6E,10E,14E,18E,22E,26E,30E,34E)-3,7,11,15,19,23,27,31,35,39-decamethyltetraconta-2,6,10,14,18,22,26,30,34,38-decaenyl]-5-hydroxy-6-methoxy-3-methyl-1,4-benzoquinone

^f IUPAC of **2,5-dihydroxyacetophenone:** 1-(2,5-dihydroxyphenyl)ethanone

^g LC-MS/MS, ultra-high-pressure liquid chromatography coupled mass spectrometry with fragment analysis

^h H-D exchange, proton-deuterium exchange

ⁱ NMR, nuclear magnetic resonance spectroscopy

compound with two hydroxy substituents in noteworthy amounts and reproducibility, suggests a minor role of *ortho*-dihydroxy quinones that might be too unstable to be of physiological relevance. Hence, this study was focussed on CoQ bearing one hydroxy group.

The methoxy substitution could be performed chemically by exposure to hydroxides^{5,10,11} and biosynthetically by catalysis with the cytochrome P450 enzyme CYP1B1.⁵ CYP1B1 is located in the ER membrane and substrate unspecific like most CYP450 enzymes. Since CYP450 enzymes catalyze *O*-dealkylations as well as aromatic hydroxylations¹³ and are colocalized together with CoQ10 in mitochondria and the endoplasmic reticulum, the conversion of CoQ10 to its demethylated form *in vivo* is very likely.

Furthermore, mono-demethyl-CoQ is the last precursor in ubiquinone biosynthesis where the quinone moiety is first hydroxylated prior to *O*-alkylation yielding a methoxy group as can be seen in **Figure 3** (first two and last two ring modifications).

In their review, Stefely and Pagliarini (2017)¹⁴ provide a comprehensive overview of Coenzyme Q biosynthesis pointing out differences in Mammalia, yeast and *E. coli*. Until today, biosynthesis is not entirely comprehended. **Figure 3** depicts the biosynthetic pathway in eukaryotes. Shortly, the precursor of the head group, hydroxybenzoic acid, is synthesized from phenylalanine or tyrosine. Isoprene subunits are provided by the mevalonate pathway and connected to polyprenyl pyrophosphate by PDSS1/PDSS2 dictating the species-dependent length of the isoprene side chain. In eukaryotes, the terminal steps, i.e. the modification of the head group after attaching the isoprenoyl residue, takes place in the mitochondrial matrix by a biosynthetic complex called the CoQ-synthome involving the enzymes COQ3-COQ9. Therefore, deficiency of any of these genes leads to accumulation of 3-polyprenyl-4-hydroxybenzoic acid (3-PP-4-HB). Though being the last precursor in Coenzyme Q synthesis in *E. coli*, HO-CoQ has never been detected in eukaryotes.^{15,16}

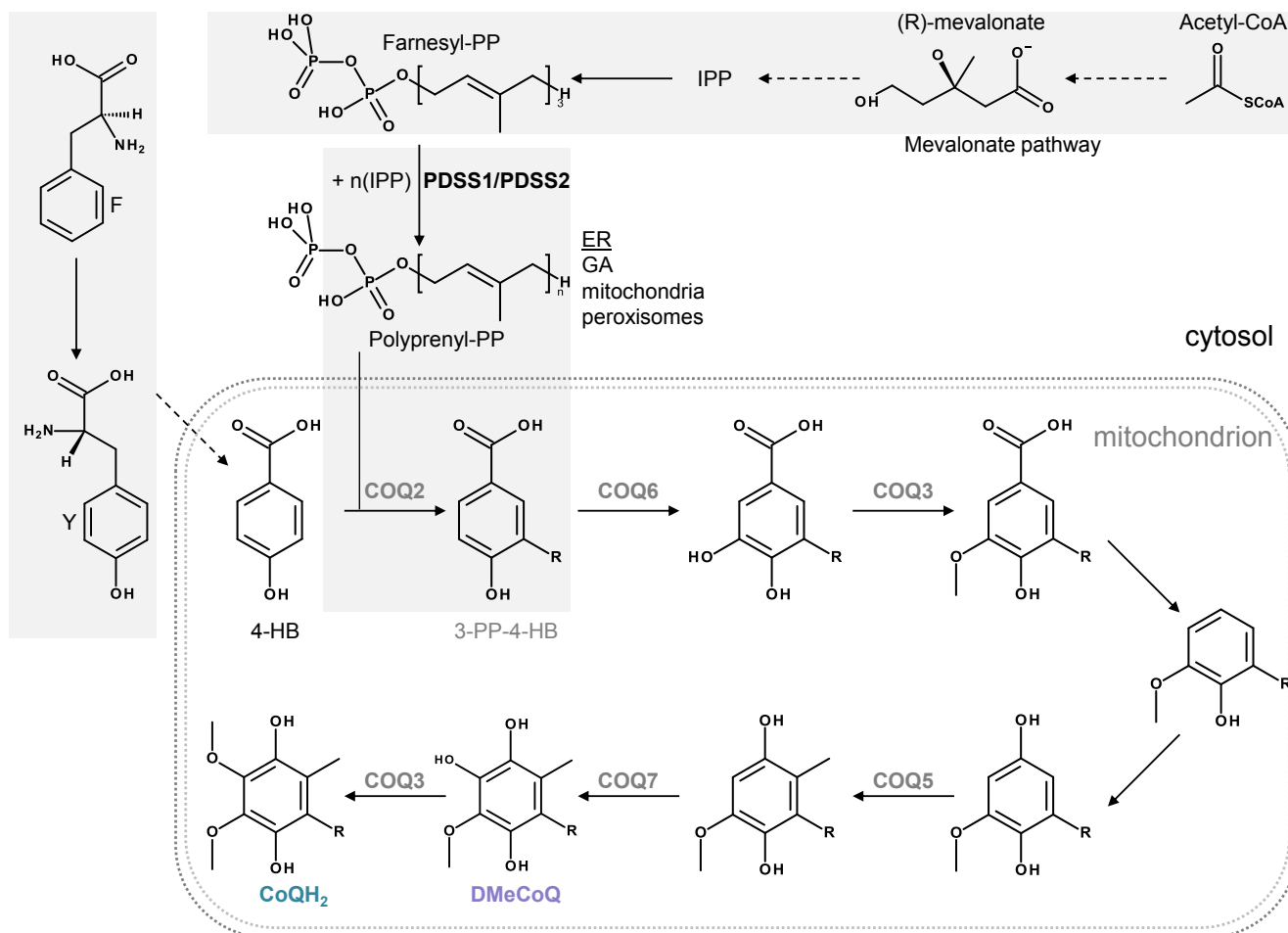


Figure 3 | Pathways of Coenzyme Q10 biosynthesis in eukaryotes. Scheme compiles information from the following reviews: Acosta (2016), Turunen (2004), Bentinger (2010).^{17–19} IPP, isopentenyl pyrophosphate; PP, pyrophosphate; F, phenylalanine; Y, tyrosine; 4-HB, 4-hydroxybenzoic acid; PDSS1/PDSS2 heterotetramer (COQ1 in *S. cerevisiae*), polypropenyl diphosphate synthase (yeast: mitochondria, mammalia: primarily ER (endoplasmic reticulum), also GA (Golgi apparatus), peroxisomes, (mitochondria)); R, isoprene side chain; COQ2, prenyltransferase (PHB-polypropenyl diphosphate transferase, rate-limiting; primarily in ER, GA, also in mitochondria and peroxisomes); 3-PP-4-HB, 3-polypropenyl-4-hydroxybenzoic acid; COQ6, Mono-oxygenase; COQ3, O-methyltransferase, COQ5, C-methyltransferase; COQ7, Hydroxylase; DMeCoQ, demethyl-CoQ, i.e. hydroxy analogue of Coenzyme Q; CoQH₂, Coenzyme Q (reduced);

1.2 Distribution and function of CoQ10

1.2.1 Intracellular distribution

Coenzyme Q is present in all cellular compartments. As shown in Table 1 Golgi vesicles, mitochondrial membranes, and lysosomes contain the highest concentrations. Taking into account the protein-to-lipid ratio of the membranes, it is obvious that CoQ concentration is especially high in inner mitochondrial membranes (IMM), closely followed by Golgi vesicles. Since 80% of lysosomal CoQ is located in their lumen²⁰ and no data on concentrations in Golgi membranes was available, it is likely to be similar for the Golgi apparatus.

Table 1 | Intracellular distribution of Coenzyme Q in rat liver.^{18,21} Cell source is unknown, except where indicated: ^brat liver cells, ^cmouse liver cells; ^dCoQ/membrane concentration was calculated by multiplication of CoQ/protein with protein/lipid ratio; ^aprotein/lipid weight ratio taken from ^{22,23} as cited in ^{24,25}

Organelle	CoQ/protein ($\mu\text{g}/\text{mg}$)	Protein/lipid ^a	CoQ/membrane ($\mu\text{g}/\text{mg}$) ^d
Mitochondria	1.4		
Outer membrane	2.2	1.2	2.6
Inner membrane	1.9	3.5	6.7
Golgi vesicles	2.6	2.5	6.5
Lysosomes	1.9		
Membrane	0.4		
Plasma membranes	0.7	1.4 ^b , 0.9 ^c	1.0 ^b , 0.6 ^c
Peroxisomes	0.3		
Endoplasmic reticulum	0.2	2.3	0.5
Rough microsomes	0.2		
Smooth microsomes	0.3		
Nuclear shell	0.2	2.1, 1.7 ^a	0.4

1.2.2 Location and function in lipid bilayers

The location of Coenzyme Q10 in the lipid bilayer has been studied thoroughly but remains controversial. Two assumptions are presented herein. Afri et al. (2004)²⁶ suggest CoQ10 to be embedded within phospholipids. Measuring NMR of CoQ10 in solvents of different polarities and incorporated into liposomes, they correlated ¹³C shifts of the ring carbons and thereby estimated the surrounding of CoQ10 in lipid membranes. As can be seen from **Figure 4 a**, the quinone head is thought to be near the polar region of the lipid bilayer although distant from the lipid-water interface. Hence, this location enables CoQ10 to increase the ordering of the acyl chains similar to cholesterol,²⁷ thereby changing membrane properties. In this model, the isoprene side chain is mainly located in the intermembrane space of the two leaflets, though a considerable part is found between lipid chains. The more polar, reduced form of ubiquinone is thought to penetrate deeper into the polar phase of the bilayer.²⁸ In contrast, in a model supported by Hauß and co-workers (2005), the complete isoprene chain is integrated in the intermembrane space.²⁹ Moreover, the quinone head is suggested to be found there, enabling quinones/hydroquinone to move freely²⁹ (compare model in **Figure 4 b**). CoQ10 was calculated to cover 10-30% of the intermembrane surface of mitochondrial membranes assuming 7 nmol CoQ per mg protein. Hence, CoQ10 could function as a physical barrier to inhibit proton leak in mitochondria as suggested by Haines (2001).³⁰ In fact, CoQ10-enriched biomimetic IMMs showed a decreased leakage of small, hydrophilic molecules.³¹ Besides, CoQ8 enrichment in the plasma membrane is a stress-response of *E. coli* exposed to hyperosmotic media providing mechanical membrane stabilization.³² Both effects have been correlated to CoQ residing in the bilayer midplane because molecules like solenasol^{31,32} and hexadecane³¹ but not the short-chained CoQs with zero to 4 isoprene units,³² that tend to penetrate the acyl chain layer of the membrane (³³ as cited in ³⁰), mimicked the effect of CoQ10³¹ and CoQ8,³² respectively.

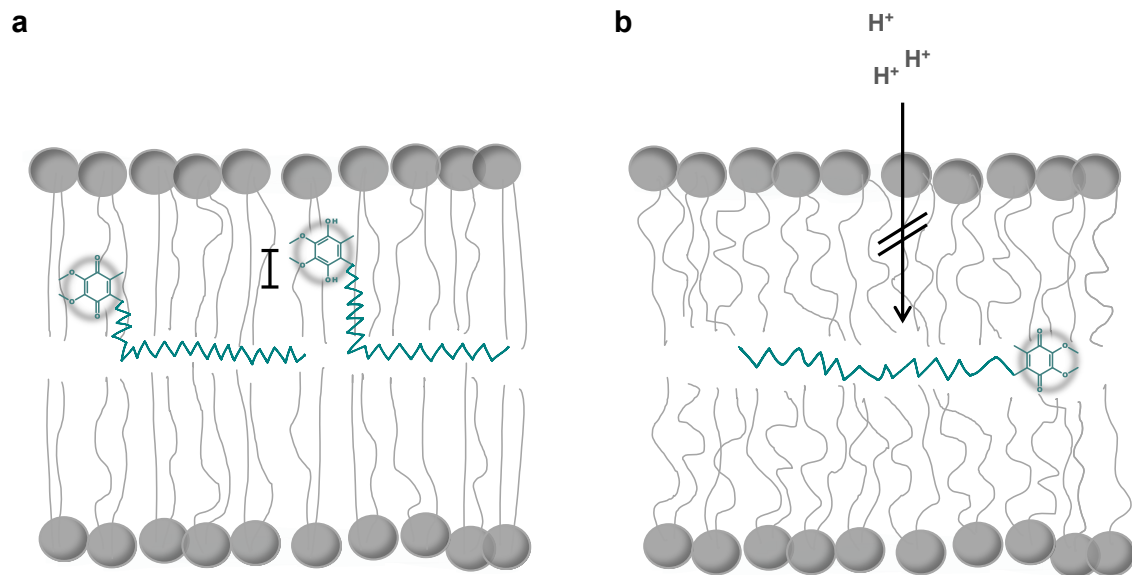


Figure 4 | Proposed location of CoQ10 in the lipid bilayer. (a) Schematic model according to Afri et al. (2004):²⁶ quinone moiety of CoQ10 is intercalating between acyl chains of phospholipids, isoprene side chain is only partly found in midplane between membrane leaflets; reduced CoQ10 (right) is thought to locate nearer to polar side than oxidized CoQ10 (left) as indicated;²⁸ (b) CoQ10 completely residing in membrane bilayer midplane according to Quinn (2012)³⁴

1.2.3 Physiological function

Coenzyme Q has been shown to exert a plethora of physiological functions. Apart from modulating biophysical properties of cellular membranes, as stated before, it represents the only known lipid-soluble antioxidant that can be de novo synthesized by animals.^{19,35} In lysosomes and the plasma membrane, it is involved in electron and proton transport via a cytosolic NADH dehydrogenase^{36–38} and a membrane-localized CoQ-dependent NADH oxidase,¹⁸ respectively. In mitochondria, CoQ is an essential cofactor of uncoupling protein (UCP)^{39,40} and inhibits the mitochondrial permeability transition pore (mPTP),⁴¹ thereby protecting cells from apoptosis induced by serum starvation, antimycin A, and C₂-ceramide.⁴²

1.3 Mitochondrial electron transport chain

Coenzyme Q is the only non-proteinogenic soluble component of the electron transfer chain transporting protons across the IMM and electrons from Complex I (CI) and Complex II (CII) to Complex III (CIII), as demonstrated in Figure 5. Apart from the classical respiratory chain complexes (RCCs), CoQ also takes up electrons from other quinone reductases such as glycerol-3-phosphate dehydrogenase (GPDH), dihydroorotate dehydrogenase and electron transfer flavoprotein oxidoreductase (ETF-QO). Electrons are further transported via cytochrome *c* to Complex IV where oxygen is the final electron acceptor. Proton translocation from the matrix into the intermembrane space via CI, CIII and CIV builds up the protonmotive force Δp consisting of ΔpH and the mitochondrial membrane potential $\Delta\psi$. ATP synthase (Complex V, CV) consumes the proton gradient to produce ATP from ADP and P_i.

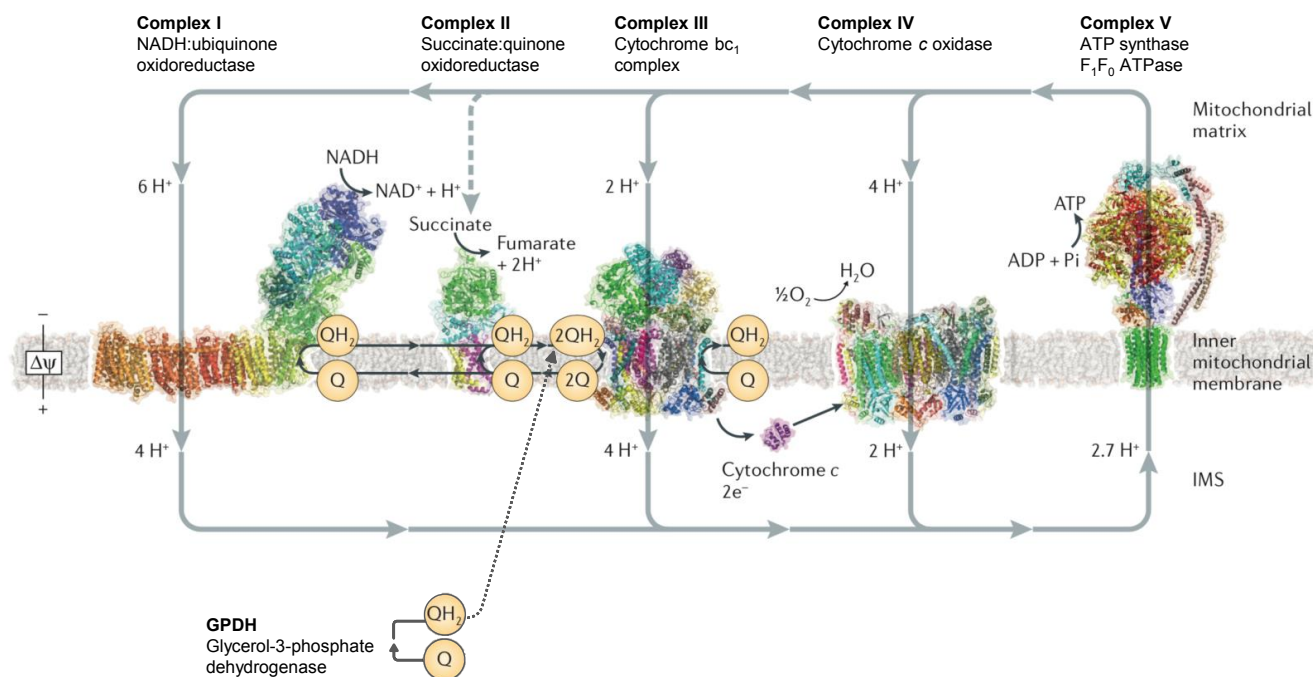


Figure 5 | Mitochondrial electron transport chain. NADH and succinate are CI and CII substrates, respectively, reducing CoQ to CoQH₂. Two CoQH₂ molecules are oxidized at CIII reducing two cytochrome *c* and one CoQ. Cytochrome *c* transfers electrons to CIV, which in turn is reducing oxygen to water. Figure was adopted from Sazanov (2015).⁴³

1.3.1 Electron transfer in respiratory chain complexes I, II, and III

Complex I (NADH:CoQ oxidoreductase) is reduced by the high-energy substrate NADH (midpoint redox potential of NADH/NAD⁺ at pH 7, $E_m = -320$ mV) originating from the citric acid cycle (CAC, Krebs cycle). The electron pathway and redox centres are illustrated in **Figure 6 a and b**.⁴³ The FMN moiety takes up two electrons from NADH oxidizing it to NAD⁺. Electrons are then singly transferred via the seven Fe-S clusters (N3 → N1b → N4 → N5 → N6a → N6b → N2) to CoQ10 accommodated in the Q-binding pocket. The reduction of N2 and the negative charges of the quinol anion or neighbouring amino acid side chains are proposed to induce conformational changes of the membrane arm allowing the transport of 4 protons into the intermembrane space. The 2Fe-2S cluster N1a is not directly involved in electron transport to CoQ, but bifurcation of FMN electrons might be necessary for N2-induced conformational changes and protection from excessive ROS production at the FMN site.

The CAC enzyme Complex II (succinate:CoQ oxidoreductase, see **Figure 6 c**) takes up 2 electrons from succinate binding to the dicarboxylate-binding site thereby reducing covalently bound FAD (succinate + FAD → fumarate + FADH₂). Since Fe-S clusters can accept only one electron at a time, electrons are transferred subsequently via the three Fe-S clusters (S-1 [2Fe-2S] → S-2 [4Fe-4S] → S-3 [3Fe-4S]) onto CoQ. The Q-binding site is located at the membrane protein interface.

The electron transport from reduced CoQ to CIII (cytochrome *bc*₁ complex) can be explained by the Q-cycle model introduced by Mitchell in 1975.⁴⁴ As shown in **Figure 6 d**,⁴³ reduced CoQ (QH₂) enters the Q_o site (Q-binding site at the outer surface of the IMM; IMS side) and transfers one electron via the 2Fe-2S cluster and cytochrome *c*₁ finally to cytochrome *c* that passes electrons on to CIV. The second electron is conducted via heme b_L and heme b_H to oxidized CoQ located at the Q_i site (Q-binding site at the inner surface of the IMM;

matrix side) reducing it to a semiquinone radical anion ($Q^{\cdot-}$). Another cycle consuming a second quinol will fully reduce the SQ^{\cdot} at the Q_i site and another cytochrome c protein. The reaction at CIII involving Q is: $2 QH_2 + Q + 2 \text{ cyt } c(\text{ox}) \rightarrow 2 Q + QH_2 + 2 H^+ + 2 \text{ cyt } c(\text{red})$. In other words per reduced ubiquinone two cytochrome c proteins are reduced and two H^+ transported across the IMM.

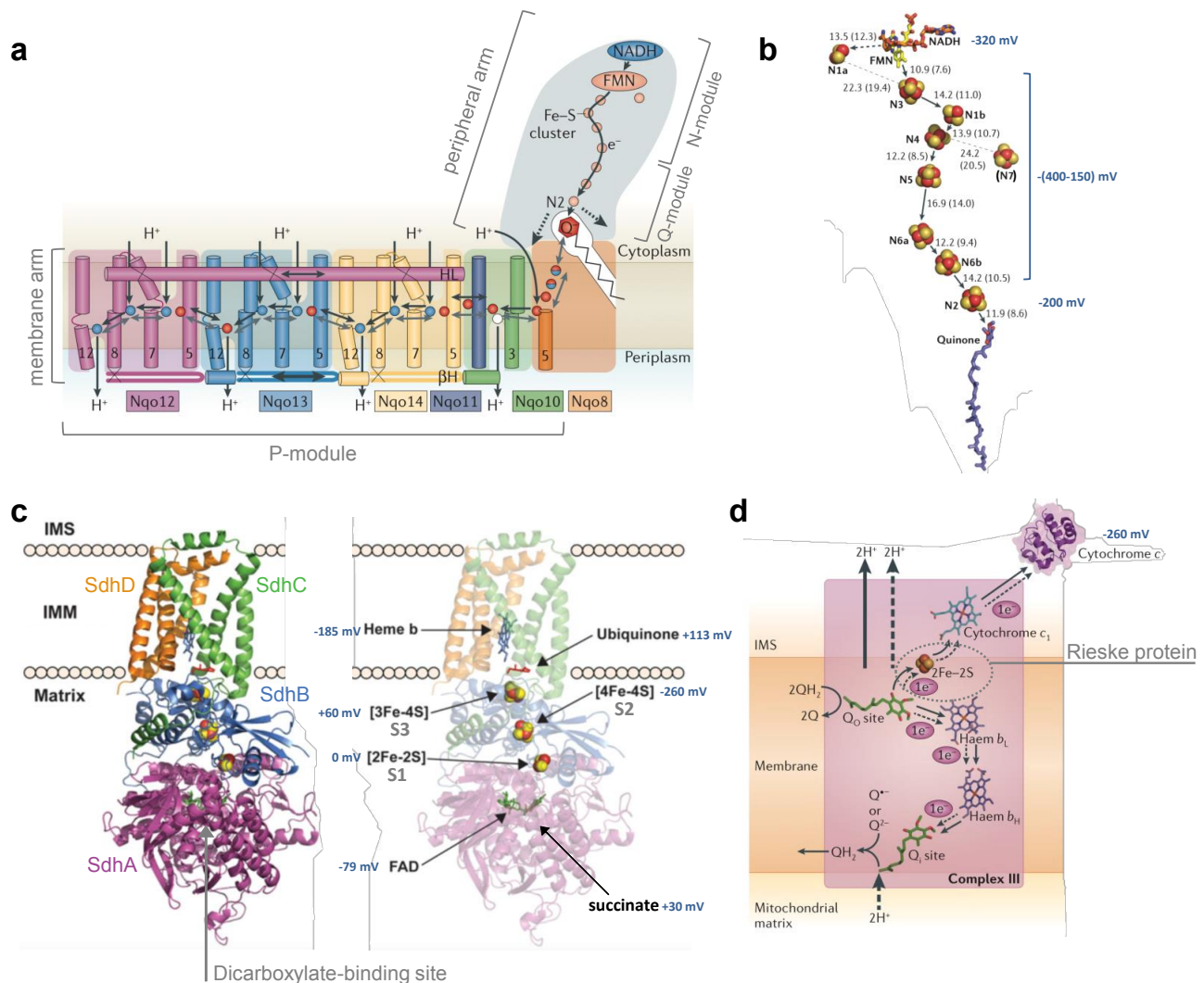


Figure 6 | Electron and proton transfer in respiratory chain complexes I (a, b),⁴³ II (c)⁴⁵ and III (d).⁴³ Figures were adopted from references as indicated, if not mentioned otherwise redox potential were excerpted from same references. (a) Coupling mechanism of CI on the basis of bacterial CI structure from *Thermus thermophilus* (core subunits labelled accordingly), e^- transfer to N2 and CoQ induces conformational changes allowing proton pumping, blue and red balls indicate key amino acids for proton transfer; (b) main electron pathway in Complex I (solid arrows); after $2 e^-$ reduction of FMN, electrons are transferred subsequently via 7 Fe-S clusters to CoQ; distances between redox centres in Å (centre-to-centre, edge-to-edge in parenthesis), N7 is only present in some bacteria e.g. *E. coli* and *T. thermophilus*, redox potential of Fe-S clusters are from *B. taurus* Complex I;⁴⁶ (c) porcine succinate dehydrogenase (CII), subunits: SdhA, FAD-binding protein; SdhB, iron-sulphur protein; SdhC and SdhD, membrane integral domain; right: electron pathway in CII from succinate to CoQ, redox potentials are from *B. taurus*;⁴⁷ (d) Q-cycle and electron transfer in Complex III, Rieske protein (ISP, iron sulphur protein) containing the Fe-S cluster accepting e^- from QH_2 at the Q_o site is indicated;

1.3.2 Inhibitors and ROS production of respiratory chain complexes I, II, and III

Mitochondrial research exploits a variety of inhibitors to dissect the electron transport chain; some of these are depicted in Figure 7 and will be described in more detail in the following chapter.

According to Fato et al. (2009)⁴⁸ Complex I inhibitors targeting the Q-binding site can be divided into two classes: Class A inhibitors like rotenone increasing ROS production and Class B inhibitors like stigmatellin, capsaicin, and reduced CoQ2, decreasing ROS production. CoQ1 but not decyl-ubiquinone potentiated ROS production induced by Class A inhibitors.^{48,49} ROS production induced by rotenone in forward electron transfer (FET) mode at CI was assigned to the backup of electrons at FMN⁵⁰ or accumulation at the final Fe-S cluster N2.⁴⁸ Superoxide and hydrogen peroxide will be produced by the reaction of oxygen with the fully reduced FMN at high NADH/NAD⁺ ratios.⁵⁰ Semiquinone radical-mediated production of superoxide was rejected because SQ• was eliminated by rotenone and piericidin A⁴⁸ and CoQ depletion did not affect ROS production rate of Complex I.⁵¹ Fato and coworkers proposed N2 to be the source of ROS.⁴⁸ Their model assumes that class A inhibitors displace CoQ from the Q-binding site allowing oxygen to pick up electrons from the iron-sulphur cluster, whereas class B inhibitors permit one-electron reduction of CoQ and therefore N2 cannot reduce oxygen.⁴⁸ In the absence of inhibitors, Complex I is a major source of ROS in reverse electron transfer (RET) mode when the CoQ pool is reduced by succinate, G3P or fatty acid oxidation and Δp is high.⁵⁰ This ROS production was shown to be rotenone-sensitive, and possible production sites are FMN and the Q-binding site.⁵⁰ Since ROS formation was pH-dependent, involvement of semiquinone or semiquinolinate is possible.⁵⁰

Complex II inhibitors are atpenin A5 (AA5), TTFA (2-Thenoyltrifluoroacetone) and mitoVES.^j In FET, when CII is reduced by succinate, the Q-binding site inhibitors induce ROS production sensitive to malonate, oxaloacetate and high succinate concentrations.⁵²⁻⁵⁴ Malonate and the CAC metabolite oxaloacetate are competitive inhibitors of the dicarboxylate-binding site. Possible ROS production sites are protein-bound FAD,^{52,53,55} terminal Fe-S cluster S3⁵⁴ and protein-bound ubisemiquinone radical. The latter was excluded due to the fact that AA5 and TTFA eliminate the SQ• signal.⁵⁴ RET-linked ROS production by Complex II was demonstrated by Quinlan et al.⁵³ Reducing the quinone pool in the presence of rotenone to inhibit RET to CI and myxothiazol to exclude CIII-linked ROS, CII produced ROS. In the absence of CIII inhibitors ROS production was considerably lower. In contrary to ROS production in FET mode where ROS production was malonate-sensitive, in RET mode ROS production could additionally be inhibited by AA5.

Antimycin A is the classical inhibitor of CIII inducing high rates of ROS. Binding to the Q reduction site (Q_i) electron transport to cytochrome b is disrupted, and bound QH₂ can only transfer one electron along the Fe-S cluster to cytochrome c. The semiquinone at the Q_o site is therefore thought to be stabilized and can react with oxygen to produce superoxide at the IMS.

The CIII inhibitors stigmatellin and myxothiazol, both binding close to the Q_o site of Complex III, reduce antimycin A-induced ROS production.^{56,57} Stigmatellin completely abolishes antimycin A-induced ROS production by inhibiting electron transfer from QH₂ to the Fe-S centre of the Rieske subunit.⁵⁶ Myxothiazol, thought to displace QH₂ from the Q_o site, on the other hand, does not fully inhibit ROS production.^{56,57} Moreover, in the absence of antimycin A, myxothiazol incubation leads to significant ROS production in presence of CI-, CII- and GDPH-linked substrates.

^j mitochondrially targeted vitamin E succinate

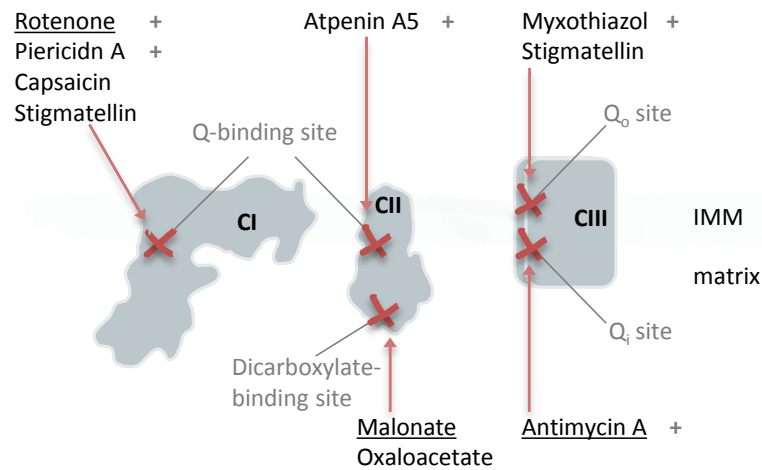


Figure 7 | Binding sites of inhibitors of the respiratory chain complexes I, II, and III. Inhibitors inducing ROS production in forward electron transfer (FET) mode are marked (+). Capsaicin, malonate, and oxaloacetate are competitive inhibitors.

1.3.3 Organization of respiratory chain complexes into supercomplexes

In 2000, Schägger et al. identified respiratory chain complexes associated to supramolecular structures, supercomplexes, when isolated mitochondria were solubilised with the mild detergent digitonin and analysed by blue-native PAGE (blue-native polyacrylamide gel electrophoresis, BN-PAGE) conserving the native structure and function of the enzymes.⁵⁸ A few years later, respirasomes, supercomplexes consisting of RCCs I₁III₁III₂IV₁ or I₁II₁III₂IV₁ together with CoQ and cytochrome *c*, were found able to respire on NADH and/or succinate.⁵⁹ The plasticity model proposed by Acín-Pérez et al. (2008) was based on the fluid model: Complexes II, III and IV are mostly found alone moving freely in the inner mitochondrial membrane, whereas most of Complex I is associated to supercomplexes (I₁III₂IV₁, I₁II₁III₂IV₁, and I₁III₂).⁵⁹ Complex III always forms dimers and is present in a supercomplex together with CIV (SC III₂IV₁).⁶⁰ CIV and CV associate to dimers (IV₂ and V₂). The existence and importance of CII within supercomplexes is disputed.^{61,62} The reason Acín-Pérez et al. only found a small portion of CII associated to respirasomes,⁵⁹ might be a more unstable interaction of CII and other RCCs. Assemblies of CII with ATP synthase isolated from human cell lines were sensitive to the Coomassie Blue stain and could only be detected in clear native conditions omitting Coomassie Blue.⁶³ This might be an important point why in many studies CII-containing supercomplexes were not detectable.⁶² Moreover, Guo et al. suggested CII to be part of human respiratory chain megacomplexes (oligomers of supercomplexes).^{64,65}

The function of supercomplexes is still under debate. Accepted advantages of supercomplex formation are the stabilization of CI by interaction with CIII⁶⁶ and CIV⁶⁷ and reduced ROS production by CI.^{68,69} Furthermore, changing supercomplex composition might be a modulator to adapt to diverse metabolic demands.⁷⁰ Supercomplexes have been proposed to increase ETC efficiency by sequestering and channelling substrates since cytochrome *c* and CoQ comigrated within supercomplexes isolated from BN-PAGE.⁵⁹ Bianchi et al. (2003)⁷¹ observed a higher NADH:cytochrome *c* oxidoreductase rate than expected from Coenzyme Q pool behaviour, which was lost after increasing theoretical distances between CI and CIII by dilution with phospholipids. Furthermore, flux control analysis of NADH oxidase showed that activity is equally influenced by CI and CIII inhibition, therefore functioning as a single enzymatic unit.^{71,72} However, Hirst and coworkers

identified major weaknesses of the performed flux control analysis⁷³ and demonstrated that CoQ is not trapped within supercomplexes but diffuses freely since NADH-reduced Q was accessible to an experimentally incorporated alternative quinol oxidase.⁷⁴ Besides, the long distance (~ 10 nm) between binding sites of CIII from CI^{65,75} and CIV,⁷⁵ respectively, speaks against quinone or cytochrome *c* channelling.⁷⁶

1.3.4 Influence of calcium on mitochondrial respiration

A rise of mitochondrial calcium levels to around 1 μM activates the citric acid cycle enzymes pyruvate dehydrogenase (PDH), glycerol-3-phosphate dehydrogenase (GPDH), NADH-isocitrate dehydrogenase (IDH) and 2-oxoglutarate dehydrogenase (ODH).⁷⁷ Calcium enables binding of PDP1 (tissue-specific PDH phosphatase isomer) to the E2 subunit of PDH, thereby activating the catalytic E1 subunit (pyruvate decarboxylase) by dephosphorylation.⁷⁷ By binding to an EF-hand Ca-binding motif of GPDH at the cytosolic surface of the IMM, calcium lowers the K_m for its substrate, glycerol-3-phosphate.⁷⁷ Similarly, calcium increases the substrate-affinities by binding to IDH and ODH.^{77,78} High ADP concentrations reduce half-maximal effective concentration for calcium in both cases.⁷⁷ Furthermore, calcium binding inactivates an inhibitory protein regulating F_1F_0 -ATPase thereby stimulating ATP synthase activity.^{79,80} Cytosolic calcium activates the mitochondrial carriers aspartate/glutamate transporter^{81,82} and ATP-Mg/ P_i carrier located in the inner mitochondrial membrane.^{82,83} On the other hand, low micromolar calcium stimulates mtNOS (mitochondrial nitric oxide synthase) that uses L-arginine for production of nitric oxide (NO).^{84,85} NO, in turn, inhibits respiration by binding to cytochrome *c* oxidase (COX, CIV).^{85,86}

1.4 Research focus

The primary goal of this thesis was to gain first insights into the biological role of HO-CoQ10, i.e. demethyl Coenzyme Q10. Since HO-CoQ10 is commercially not available, the first step was to synthesize and purify the substance in sufficiently large amounts. The structure and purity of the isolated product were analysed using electrospray ionization mass spectrometry (ESI-MS), ¹H, and ¹³C nuclear magnetic resonance spectroscopy (NMR). Even though the foundation of synthesis and purification of HO-CoQ10 had been established in preliminary experiments, it was mandatory to confirm the location of the hydroxy group applying 2-D NMR. Moreover, the integrity of the basal ubiquinone structure and stability of the synthesized compound upon storage needed to be confirmed.

Coenzyme Q is ubiquitously present in all tissues, eukaryotic cells and cellular membranes. In the view of hydroxy substitutes being precursors in CoQ10 biosynthesis and their production potentially modulated by CYP450 enzymes, the importance of these molecules is evident. In *E. coli*, demethyl-CoQ8 was detected in plasma membranes of ubiG⁻ mutants, lacking the O-methyltransferase UbiG necessary for the final step of CoQ8 synthesis.⁸⁷ Nevertheless, demethyl-CoQ has never been detected in eukaryotes.^{15,16}

In order to get an impression on the biological significance of HO-CoQ10, we first examined its presence in vivo. Lipid extracts from bovine heart mitochondria were analysed using reversed-phase ultra-high-pressure liquid chromatography coupled to tandem-mass spectrometry. This sensitive method allows a reliable identification and quantification of endogenous substances.

To evaluate the impact of HO-CoQ10 on cellular functions, CoQ10 always served as a control. Given its hydrophobic nature derived from the long isoprene chain, first solubilisation of CoQ10 and HO-CoQ10 in

aqueous media needed to be established. Then, toxicity of the substance was tested on different cancer cell lines under standard cell culture conditions determining metabolic turnover and apoptosis induction using CellTiter-Blue® and the caspase-sensitive sensor Casper-GR, respectively.

Since CoQ10 is a vital component of the electron transport chain and energy production via oxidative phosphorylation, the role of HO-CoQ10 in the mitochondrial respiration machinery was examined in detail. The significantly lowered redox potential, the ability to bind Ca^{2+} and of course modification of the functional quinone moiety might have a tremendous impact on the functionality of the molecule. To address the influence of HO-CoQ10 on oxidative phosphorylation, respiration of freshly isolated coupled mouse heart mitochondria was measured with a Clark-type electrode using saturating conditions for substrates and ADP. Established protocols to guide electrons via the respiratory chain complexes I, II, III and IV were used to investigate points of action. The influence of extramitochondrial calcium on respiration in presence of Coenzyme Q was assessed. To obtain quantitative data, free Ca^{2+} concentrations in respiration medium containing inorganic phosphate had to be precisely defined using the fluorescent ratiometric calcium indicator fura-2. In addition, oxidoreductase activity of single respiratory chain complexes was detected photometrically using specific substrate-acceptor cocktails for each individual enzyme. BN-PAGE allowed separating supercomplexes and RCCs and measuring oxidase activities without blockers against other RCCs. Since ETC activity and ROS production are closely related, H_2O_2 and superoxide production were monitored using the fluorescent-based Amplex™ UltraRed assay and the superoxide spin probe CMH detected by electrons spin resonance spectroscopy (EPR). The redox-active iron-sulphur centres of Complex I and II were studied with continuous-wave EPR at low temperatures to identify interaction sites.

2 Material and methods

2.1 Reagents

Preparation and storage protocols are indicated for sensitive substances only. Abbreviations, supplier, and catalogue number are given in parenthesis. Chemicals and equipment not mentioned were supplied by VWR, Sigma, Corning, Schott, and Fisher Scientific. Detailed material and equipment is listed within each experimental section.

- HO-CoQ10 (FW 849.32 g/mol; stored at -20 or -80 °C; 5 mM in ethanol, stored in liquid nitrogen)
- Coenzyme Q10 (**CoQ10**, FW 863.34 g/mol, OMIKRON Naturprodukte und Feinchemikalien # 101181-5 or Sigma # C9538; 1 mM in ethanol, stored in liquid nitrogen)
- Coenzyme Q1 (**CoQ1**, Sigma # C7956 or Cayman chemical # 18741; 10 mg/mL ethanolic solution, stored at -20 °C)
- Ethanol, absolute, > 99.8%, reag. Ph. Eur. absolut (**etOH**, Sigma # 32205 or VWR # 20821.321)
- **DMSO** (dimethyl sulfoxide, Sigma # D8418)
- **Sucrose** (D(+)-Saccharose; VWR # 27480.294)
- D-Mannitol (Sigma # M1902)
- KCl (potassium chloride; VWR # 26764.298)
- **NaCl** (Millipore # 1.37017.1000)
- Potassium phosphate dibasic (**K₂HPO₄**, potassium phosphate monobasic, TraceSELECT®; Sigma # 60347 (TraceSELECT®) or P5655)
- Potassium phosphate monobasic (**KH₂PO₄**, TraceSELECT®; Sigma # 229806 or # 60216)
- **HEPES** (4-(2-Hydroxyethyl)piperazine-1-ethanesulfonic acid, Sigma # H7523)
- **CaCl₂ solution, 1 M in H₂O** (Sigma # 21115)
- **MgCl₂ solution, 1 M in H₂O** (Sigma # M1028)
- **EGTA** (Ethylene glycol-bis(2-aminoethylether)-N,N,N',N'-tetraacetic acid, Sigma # E4378)
- **EDTA** (Ethylenediaminetetraacetic acid, Sigma # E6758 or ED2SS)
- KOH (potassium hydroxide; J.T. Baker # 0385; ~ 5 M at RT)
- Trizma® base (**Tris**, Tris(hydroxymethyl)aminomethane; Sigma # T1503)
- Millipore water, 18 MΩcm

2.2 Software, general

- **Origin**, versions 9.5, 2015, 2018b (OriginLab, Northampton, MA)
- Fiji,⁸⁸ *image editing*
- **Accelrys Draw** 4.1.NET; *chemical structures, calculation of exact and average molecular mass* (Accelrys. Inc.)

2.3 Assay buffers

The composition of all buffers is listed below. Concentrations are in millimolar, if not stated otherwise.

Isolation of mouse heart mitochondria⁸⁹

- Isolation solution (IS): 225 mannitol, 75 sucrose, 2 HEPES, 1 EGTA, pH 7.4 using Tris base
- Mitochondria suspension solution (MSS): 225 mannitol, 75 sucrose, 2 HEPES, pH 7.4 using Tris base

Isolation of beef heart mitochondria⁹⁰

- Heart wash solution (HWS) for isolation and suspension: 250 sucrose, 10 Tris-HCl, pH 7.8 using HCl

Respiration buffers (RB)

Phosphate concentrations are highlighted.

- RB1: 137 KCl, **2 KH₂PO₄**, 2.5 MgCl₂, 20 HEPES, 0.5 EGTA, pH 7.2 using KOH⁸⁹
- RB2: Mg²⁺ and Ca²⁺ calibration solutions
 - RB2: 137 KCl, 20 HEPES, pH 7.21 using KOH
 - Additionally containing:
 - RB2.1 : 0.1 EGTA
 - RB2.2 : 0.1 EGTA, 200 MgCl₂
 - RB2.3 : 0.1 EGTA, 2.25 mM MgCl₂
 - RB2.4 : 0.1 EGTA, 2.25 mM MgCl₂, 0.1 CaCl₂
 - RB2.5 : 10 EGTA
 - RB2.6 : 10 EGTA, 10 CaCl₂
 - Test solutions:
 - RB2.7 : **4 KH₂PO₄**, 0.5 EDTA
 - RB2.8 : **4 KH₂PO₄**, 2.5 MgCl₂, 0.1 EGTA (i.e. RB 3.1)
 - RB2.9 : **4 KH₂PO₄**, 2.5 MgCl₂, 0.5 EGTA
 - RB2.10: **4 KH₂PO₄**, 2.5 MgCl₂, 1 EGTA
 - RB2.11: **1.5 KH₂PO₄**, 2.5 MgCl₂, 0.1 EGTA
 - RB2.12: **1.5 KH₂PO₄**, 2.5 MgCl₂, 0.1 EGTA, 0.1 CaCl₂
- RB3: Ca²⁺ calibrated respiration buffer
 - RB3: **4 KH₂PO₄**, 2.5 MgCl₂, 20 HEPES, 0.1 EGTA, pH 7.21 using KOH
 - Additionally containing:
 - RB3.1 : 137 KCl
 - RB3.2 : 137 KCl, 0.1 CaCl₂
 - RB3.3 : 127 KCl, 10 NaCl
 - RB3.4: 137 KCl, 10 NaCl, 0.1 CaCl₂
 - By mixing of RB3.1 and RB3.2 or RB3.3 and RB3.4 respiration buffers with defined free Ca²⁺ concentrations were prepared according to **Figure 37 g** (p. 92) and listed below.
 - Free Ca²⁺, CaEGTA: 1.227 μM, 0.1 mM; 1 μM, 0.0959 mM; 0.5 μM, 0.0820 mM; 0.366 μM, 0.0754 mM; 0.2 μM, 0.0611 mM; 0.05 μM, 0.0255 mM;

- RB4: 600 sorbitol, 20 KH₂PO₄, 10 MgCl₂, 0.5 EDTA, pH 7.2 using KOH⁹¹

Single respiratory chain complex (RCC) activity assays and LT-EPR

- 500 mM KP_i, pH 7.4 (50 mL): 20.05 mL K₂HPO₄, 4.95 mL KH₂PO₄, 25 mL water
- Assay buffer
 - 50 mM KP_i, pH 7.4 (10x, 500 mM KP_i, 50 mL: 20.05 mL K₂PO₄, 4.95 mL KH₂PO₄, 25 mL water)
 - 10 mM Tris, pH 7.8 (pH 7.4 at 37 °C)
 - The pH of Tris-based buffers was adjusted at RT using the temperature-adjusted values for usage at 37 °C using a web-based calculator.⁹²
- Lysis buffer: hypotonic KPB, lysis buffer: 25 KP_i, 5 MgCl₂, pH 7.4

2.4 Production of HO-CoQ10

Synthesis in a two-phase system

One volume of a 4 mM CoQ10 solution in tetrahydrofuran was added to 2 volumes of 1-molar aqueous sodium hydroxide and mixed by inverting. To minimize autoxidation and thereby formation of peroxides in the organic solvent, the reaction mixture was held in an argon atmosphere. NaOH was depleted of oxygen by flushing with nitrogen for 30 min. The reaction vial was a brown glass bottle with a gas-proof lid (PTFE/silicon cap liner) and was protected from light by aluminium foil wrapping. After 24 h of incubation at RT, the reaction was stopped by removing NaOH from the organic layer.

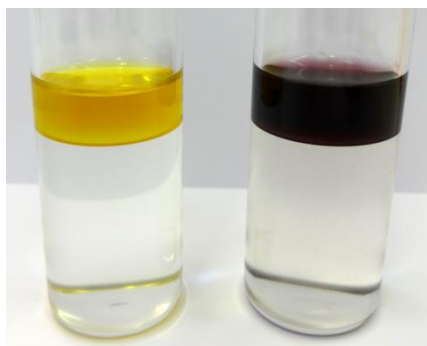


Figure 8 | Synthesis of Monohydroxy-CoQ10 from native CoQ10 and NaOH in a two-phase system. The lower aqueous phase consists of 1 M NaOH and the upper organic layer of CoQ10 in THF; reaction mixture after inverting (left) and after prolonged incubation (right); the reaction takes place in the upper organic layer.

Isolation of the product from the upper layer

The lower aqueous phase was removed with a separating funnel. To remove residual water and NaOH from the organic layer, the solution was dried over the desiccant magnesium sulphate (anhydrous MgSO₄) in a glass beaker and stirred with a glass rod.^k When added magnesium sulphate stopped clumping, the drying

^k $\text{MgSO}_4 + n \text{H}_2\text{O} \rightarrow \text{Mg}^{2+}(\text{H}_2\text{O})_n + \text{SO}_4^{2-}$

$\text{MgSO}_4 + 2 \text{NaOH} \rightarrow \text{Mg}(\text{OH})_2 + \text{Na}_2\text{SO}_4$

A better practice is to add the desiccant in small portions under constant magnetic stirring to avoid over-addition and therefore loss of product.

procedure was completed. The precipitated salts could then be removed by filtering. Product stuck to the filter and the drying agent was washed off with THF. In a bulb, the solvent was removed by rotary evaporation. Then, the product was reconstituted in a small amount of THF to aliquot it in portions of ~20 mg into autosampler vials. The solvent was evaporated at RT under a stream of nitrogen. The substance was concentrated at the bottom of the vial using a moderate N₂ flow rate. Residual THF was then removed in a desiccator under vacuum.

The reaction conditions and drying procedure of the product were partly conducted and established by Christian Holzmann under consultation with Reinhard Kappl and me.

Purification by semi-preparative high-pressure liquid chromatography

In order to isolate HO-CoQ10 the product was fractionated using semi-preparative reversed-phase high-pressure liquid chromatography (RP-HPLC). The stationary phase consisted of a C-18 modified silica gel column. The column was equilibrated and washed in between runs with the mobile phase, a 1:4-mixture (v/v) of THF and methanol + 0.1% HCOOH. The dried product was dissolved in the mobile phase with an increased THF proportion that was needed to dissolve the product (usually around 50% THF). Per run, around 30 mg product was manually loaded into the 100 µL sample loop using the leading-bubble technique with > 100 µL solution to avoid dilution of the sample with the mobile phase present in the sample loop. The pump was run at the desired flow rate of 4.4 mL/min, and simultaneously with injection the recording was started. The absorbance of the quinone ring was detected at 275 nm, and the signals were sampled every 0.48 s. To exclude collection of impurities, the starting point of product collection was chosen after the HO-CoQ10 elution peak reached the detection limit of 2.56 AU plus a delay of 6 s. The product was collected within a time interval of ~3 min and stopped when absorption dropped below 1 AU (Figure 9). The fractions of 1 day were combined right after collection and stored in a gas-tight, brown glass bottle with argon atmosphere at 4 °C. At the end of the day, the isolate was dried and stored at -20 °C. For additional separations only ~20 mg isolate was used. The first isolation run took 40 min, the next run only 30 min because the educt peak decreased remarkably. Regularly, the column was washed with 100% THF and/or with mobile phase for a prolonged time. When CoQ10 was collected, it was important to clean the needle of the fraction collector by collecting clean mobile phase after a finished run in a separate vial. After completing the purification, HO-CoQ10 was dissolved in THF and aliquoted in portions of 2-10 mg. The solvent was removed as stated before. The product was stored in glass autosampler vials with a silicone-sealed lid at -80 °C for long-term and at -20 °C for short-term storage. The yield of HO-CoQ10 was around 20%.

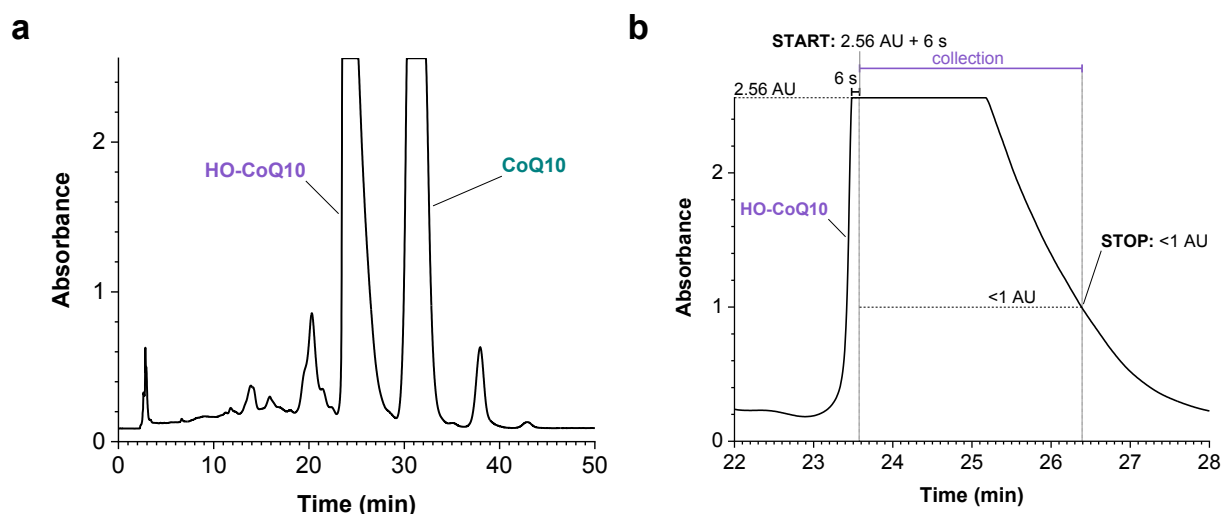


Figure 9 | Isolation of HO-CoQ10 by semi-preparative HPLC coupled to a UV/Vis detector. Absorption at 275 nm; path length, 10 mm; column was overloaded with the reaction mixture to yield a high amount of purified sample but still separated elution peaks; (a) elution profile of the reaction mixture, elution peaks of reactant CoQ10 and more hydrophilic product HO-CoQ10 are cut off due to overloading, (b) detail of collected fraction (HO-CoQ10) from (a); collection started 6 s after absorption reached maximal detection value of 2.56, collection stopped when absorption surpassed 1 AU;

Spectrophotometric analysis of the reaction course

To follow the absorption spectra of CoQ10 in the course of the reaction every hour (up to 10 h) and after 26 h a 50 to 100- μ L sample was retrieved from the upper, organic layer and centrifuged (15 min, RT) to eliminate residual NaOH. Samples were diluted in THF to result in an approximately 0.1 mM CoQ solution. The diluted CoQ10 stock solution before addition of NaOH represented time point 0. Measurements were performed with a velocity of 250 nm/min recording 1-nm steps in parafilm-sealed quartz cuvettes.

Material and equipment

- Sodium hydroxide (**NaOH**, standard volumetric solution (1M), AppliChem # A1432, 1000)
- Tetrahydrofuran (**THF**, ROTISOLV® HPLC, unstabilized, Roth # 7344.2)
- Methanol, Grad.-HPLC (**MeOH**, VWR # 20864.320 or Fisher Scientific # M/4058/17)
- Magnesium sulfate, anhydrous (**MgSO₄**; Sigma # 208094)
- **Formic acid**, p.a. (99-100%, VWR Chemicals # 20318.297)
- **Rotary evaporator** (IKA® RV 8) with integrated heating bath (IKA® HB 10) connected to a
- **Vacuum pump** (vacuubrand, PC 3001 VARIOpro with vacuum controller CVC 3000)
- **Autosampler vial** (VWR; screw cap, 9 mm, silicon, PTFE # 548-1502; vial short thread, 1.5 mL, 32x11.6 mm, clear glass # 548-0028)
- Vials, screw top with solid green Melamine cap with PTFE liner, 22 mL volume, clear glass vial: *collecting of HPLC fractions from semi-preparative HPLC* (Supelco, cat. no. 27172)
- HPLC components (Jasco) *for semi-preparative chromatography*: degasser (cat. no. DG-1580-53), low-pressure gradient unit (cat. no. LG-1580-02), intelligent HPLC pump (cat. no. PU-980), intelligent UV/Vis detector (cat. no. UV-975)

- Preparative column (material, Kromasil 100 C18; particle size, 5 μm ; length x ID, 250 x 10 mm; MZ-Analysentechnik, Part.-No.: MZ0551-250100, Ser.-No.: 24180719)
- HPLC data acquisition software (Gerhard Bracic)
- **UV/Visible Spectrophotometer** Ultrospec™ 2100 pro (GE Healthcare Life Sciences # 80211221)
- **SWIFT II Wavescan** (software for UV/Vis data collection, GE Healthcare Life Sciences)
- **Micro Cuvette** made of quartz glass SUPRASIL® (Hellma, path length 10 mm (\pm 0.1 mM))

2.5 Structural analysis: nuclear magnetic resonance spectroscopy (NMR)

All NMR experiments were recorded and analysed by (2-D NMR) or in assistance of (^1H NMR, qNMR) Dr Josef Zapp (Department of Pharmaceutical Biology, Saarland University).

Material and equipment

- 1,2,4,5-Tetrachloro-3-nitrobenzene, standard for quantitative NMR, TraceCert® (Sigma # 40384)
- Chloroform-d (CDCl_3 , \geq 99.8 atom % D, contains 0.5 wt. % silver foil as stabilizer; Sigma # 416754) or (100%, 99.96 atom % D, contains 0.5 wt. % silver wire as stabilizer, Sigma # 431915)
- Chloroform-d with internal standard tetramethylsilane (CDCl_3 , \geq 99.8 atom % D, contains 0.5 wt. % silver foil as stabilizer, 0.03% (v/v) TMS; Aldrich # 530735)
- Nuclear magnetic resonance spectrometer (Bruker), 500 MHz, probe 5 mm
DRX 500 with BBI probe
Avance I 500 with BBO or TCI probe
Avance III 500 with CPTCI probe
- **Topspin 4.0.5** (2018, Bruker BioSpin)

2.5.1 Proton NMR (^1H NMR)

Sample preparation

Dried samples were dissolved in approximately 0.6 mL deuterated chloroform (99.8% CDCl_3 , 0.2% CHCl_3 , contains 0.5 wt. % silver foil as stabilizer) and measured in capped NMR glass capillaries.

Analysis

The singlet absorption peak of the internal standard TMS (tetramethylsilane) was set to a chemical shift of 0 ppm.

Using Originlab 8.5, the absolute frequency of the spectra was calculated with formula 1.1 and then transformed into chemical shift (δ) in ppm using the detected frequency (ν) of the substance and the reference (formula 1.2). Exporting NMR spectra to JCAMP the number of intervals corresponds to the number of rows subtracted by 1; measured interval corresponds to the line of row subtracted by 1, pulse width corresponds to the first listed frequency. Sending frequency (SF01) was taken from exact measurement parameters.

Since concentrations were neglected during sample preparation, absorption intensities were normalized using the absorption integral of the last 9 vinyl protons of the side chain of each spectrum (at 5.12 and 5.06 ppm, compare Figure 15 f on p. 59). The isoprenic side chain was presumed to be intact in the molecule.

$$(1.1) \text{ absolute frequency (Hz)} = (\text{number of intervals} - \text{measured interval}) \cdot \left(\frac{\text{pulse width}}{\text{number of measured intervals}} \right) + \left(\text{sending frequency} - \frac{\text{pulse width}}{2} \right)$$

$$(1.2) \delta_{\text{substance}} (\text{ppm}) = \frac{\nu_{\text{substance}} - \nu_{\text{reference}}}{\nu_{\text{reference}}} \cdot 10^6$$

2.5.2 2-Dimensional NMR (2-D NMR)

11.8 mg HO-CoQ10 was dissolved in 0.6 mL d-chloroform. First, a ^1H NMR spectrum was recorded to confirm a usual absorption pattern. Then the sample was dried and reused for 2-dimensional NMR performing H,H-COSY, HSQC, and HBMC experiments. The analysis was performed using pulse programs from the Bruker pulse library.

2.5.3 Quantitative NMR (qNMR)

Sample preparation

The samples, around 4.5-12 mg, were accurately weighed. 500 μL d-chloroform (or 400 μL for preparation γ) and 100 μL (or 250 μL for the preparation γ) of a standard solution of 1,2,4,5-tetrachloro-3-nitrobenzene (100.3 mg in 10 mL CDCl_3) was added. The measurements were performed based on Malz (2008).⁹³ To keep the amount of substance of the sample and standard equivalent, 0.1 mL and 0.25 mL of the standard solution was added when the mass of the analyte was ~ 5 and between 4.5 and 12 mg, respectively.

Analysis

The purity of the sample was calculated in % according to Malz (2008)⁹³ using the formula below.

$$P_X = \frac{I_X}{I_{Std}} \frac{N_{Std}}{N_X} \frac{M_X}{M_{Std}} \frac{m_{Std}}{m} P_{Std}$$

P, purity in %; I, integral; N, proton count; M, molar mass; m, weighted sample; indexes X for analyte and Std for standard

The integral of the proton signal of the standard, I_{Std} , at 7.7 ppm with a proton count of $N_{Std} = 1$ was set to 100. Its purity, P_{Std} , was 99.72% according to the certificate of analysis. The molar masses are 260.89 g/mol, 863.34 g/mol, and 849.32 g/mol for the standard, CoQ10 and HO-CoQ10, respectively. The masses of the standard were either 1.003 or 2.5055 mg depending on the sample input. The integral of a proton signal of CoQ10 and HO-CoQ10 was then determined and inserted into the formula using the corresponding proton count, N_X . The chemical shift was normalized by setting the residual CHCl_3 signal to 7.26 ppm.⁹⁴

2.6 Dissolving of CoQ10 and HO-CoQ10

Ethanol solution

CoQ10 was weighed directly into a glass vial and ethanol was added to yield a concentration of 1 mM. The homogenate was heated to 40 °C in a water bath and mixed by ultrasonication from time to time until dissolution was complete. The mixture was protected from sunlight. Pre-aliquoted and dried HO-CoQ10 was treated the same way. CoQ10 and HO-CoQ10 were treated as being 100% pure as it is a lab standard for all substances and to have a general guideline. Besides, calculated volumes were added disregarding the volume

of the substance (no volumetric flask was used). Therefore, concentrations are slightly underestimated in all experiments.

Aliquots of stock solutions were stored in freezing vials with silicone-sealed lids in liquid nitrogen. Solutions were thawed at RT, vortexed thoroughly and if necessary reheated to ensure solubilisation. Handling time at RT was minimized to avoid concentration of the solution by evaporation of ethanol.

According to Park et al. (2002),⁹⁵ aqueous solutions of CoQ10 were preincubated at 37 °C for ~ 10 min whenever possible to assure solubilisation.

Water-soluble formulation with Cholesterol-PEG

Following the procedure of Borowy-Borowski,⁹⁶ CoQ10 was solubilised with Cholesterol-PEG (PCS)¹ as a carrier substance. CoQ10 and Cholesterol-PEG are used in a weight ratio of 1:3 (corresponding to a molar ratio of 1:2) and merged by two different methods: the direct melt or the solvent method.

The direct melt method requires the mixture of CoQ10 and PCS to be heated above the melting point of both substances. Since CoQ10 has a melting point around 50-52 °C⁹⁷ and PCS starts melting at RT, 60 °C was chosen to merge the molecules. The water-soluble clear melt is then diluted in aqueous solutions.

For the solvent method, solutions of CoQ10 and PCS in THF have been prepared separately. The stock solutions have been combined in a glass bulb together with water yielding a clear solution. The organic solvent was then removed by rotary evaporation, and the volume can be contracted as desired.

Material and equipment

- Chloroform (Sigma # 24216)
- Tetrahydrofuran (**THF**, ROTISOLV® HPLC, unstabilized, Roth # 7344.2)
- Dimethyl sulfoxide (**DMSO**, Sigma # D8418)
- Methanol, Grad.-HPLC (**MeOH**, VWR # 20864.320 or Fisher Scientific # M/4058/17)
- Ethanol, absolute, > 99.8%, reag. Ph. Eur. absolut (**etOH**, Sigma # 32205)
- Cholesterol-PEG 600 (**PCS**, Cholesteryl-polyethylene glycol 600 sebacate; Sigma # C1145)
- Ultrasonic bath with integrated heating (Bandelin # SONOREX SUPER RK 1028H)

2.7 Testing of solubility with UV/Vis spectrophotometry

Absorption spectra (200-900 nm) were recorded in 1-nm steps using a velocity of 250 nm/min in closed quartz cuvettes with an optical depth of 10 mm. The final volume was ~ 0.5 mL. The baseline of the solvent alone was subtracted from all traces.

Equipment

- SWIFT II Wavescan (GE Healthcare Life Sciences)
- UV/Vis spectrophotometer Ultrospec 2100 pro (GE Healthcare Life Sciences)
- Precision cells made of Quartz SUPRASIL® with PTFE stopper (volume, 400 µL; light path, 10 ± 0.1 mm, Hellma® Analytics # 115-10-40)

¹ PCS; CAS number, 69068-97-9

2.8 Endogenous detection of HO-CoQ10 and CoQ10 using mass spectrometry

The MS and LC-MS protocol was provided by Prof. Dr R. Markus Meyer. MS and LC-MS experiments were established and performed by Prof. Dr Markus R. Meyer and Dr H. J. Lilian Richter (Department of Experimental and Clinical Toxicology, Saarland University) using modified published protocols.⁹⁸⁻¹⁰⁷

2.8.1 Mass and fragmentation analysis of pure substances: direct infusion

To examine ionization and fragmentation behaviour of the analytes, direct infusion experiments were performed prior to setting experimental parameters for further analysis. 100 μM CoQ10 and HO-CoQ10 (in 90% *i*-proOH, 10% etOH) were diluted to 1 and 10 μM in eluent B and infused into the heated electrospray ionization II (HESI-II) source using a 500- μL Hamilton syringe with a constant flow of 10 $\mu\text{L}/\text{min}$.

“Mass calibration was performed prior to analysis according to the manufacturer’s recommendations using external mass calibration.”^{98,104,107} The MS conditions in negative mode were as follows: HESI, negative mode; sheath gas, nitrogen at a flow rate of 10 arbitrary units (AU); auxiliary gas switched off; vaporizer temperature switched off, spray voltage, -4.0 kV; ion transfer capillary temperature, 320 °C; and S-lens RF level, 50.0. The scan parameters were as follows: microscan, 1; resolution, 140 000; AGC target, 1e6; maximum injection time, 250 ms; MS2 isolation window, 1 m/z ; scan range, m/z 60-900; high collision dissociation (HCD) with normalized collision energy (NCE), 25-35%. Thermo Xcalibur (Software Version 2.4, Thermo Fischer Scientific) was used for data handling.

In positive mode, the following parameters were changed: HESI, positive mode; sheath gas, nitrogen at a flow rate of 12 arbitrary units (AU); spray voltage, +3.9 kV.

Material

- **Eluent B:** (acetonitrile/methanol, 1:1 (v,v); ammonium formate, 2 mM; formic acid, 0.1% (v,v); water, 1% (v,v))
- **Q-Exactive Plus system** (Thermo Fisher Scientific)
equipped with heated electrospray ionization source (HESI-II) coupled to a syringe pump
- **Xcalibur™** Software, Version 4.2, Qual Browser; *analysis of MS spectra and LC/MS chromatograms, modelling of isotope patterns* (Thermo Fisher Scientific, 2018)

2.8.2 Testing of substance stability by ultra-high-pressure liquid chromatography coupled to mass spectrometry (UHPLC-MS)

Sample preparation: substance in solid form

1 mM ethanolic stock solutions of CoQ10 and HO-CoQ10 were diluted to 100 μM in ethanol. Then, 100 μL of each solution was distributed into separate glass autosampler vials, and the solvent was evaporated under a stream of nitrogen at RT. The vials were closed with a silicone-sealed screw cap and kept in the dark. The samples were incubated for 6 d at different temperatures: -70 °C (freezer), -20 °C (freezer), 4 °C (fridge), RT (lab, drawer), and 37 °C (incubator). Then, all samples were stored at -70 °C. For measurements, the solids were reconstituted with 200 μL or 1 mL ethanol to yield 50 and 10 μM solutions, respectively.

Sample preparation: substance in solution

The following changes had been made, when the stability was tested in solution: 1 mM ethanolic solutions of CoQ10 and HO-CoQ10 were diluted 1:100 in ethanol to yield 10 μ M solutions. To every vial, 250 μ L of CoQ10 or HO-CoQ10 was added. The vials were closed tightly and incubated for 1 h at 4 $^{\circ}$ C (fridge), RT (opaque box), 37 $^{\circ}$ C (water bath) or 60 $^{\circ}$ C (thermomixer).

Detection with UHPLC-MS

Parameters for measurements shown in **Figure 21** (p. 70) are specified.

Autosampler temperature was set to 4 $^{\circ}$ C and 1 μ L sample was injected onto the column. Elution was performed using a gradient at a flowrate of 0.7 mL/min with a mobile phase consisting of water-based (eluent A) and organic solvent-based eluent (eluent B): 0-1 min 20-10% A, 1-6 min 10-0.1% A, 6-7 min hold 0.1% A, 7-7.5 min 0.1-20% A, 7.7-10.1 hold 20% A.

External mass calibration was performed prior to analysis according to the manufacturer's recommendations. The HESI-II source conditions were as follows: ionization mode, positive and negative alternating; sheath gas, 53 AU; auxiliary gas, 14 AU; sweep gas, 3 AU; spray voltage, \pm 4.0 kV; heater temperature, 438 $^{\circ}$ C; ion transfer capillary temperature, 269 $^{\circ}$ C; and S-lens RF level, 60.0.

External mass calibration was performed prior to analysis according to the manufacturer's recommendations. Mass spectrometry was performed using full scan data or product reaction monitoring using an inclusion list containing the m/z of interest (positive, m/z : 880.71770).

The settings for full scan data acquisition were as follows: resolution, 35 000; microscans, 1; automatic gain control (AGC) target, $3e6$; maximum injection time, 200 ms; and scan range, m/z 133.4-2 000. The settings for the PRM mode with an inclusion list were as follows: option "pick others", enabled; dynamic exclusion, 1 s; resolution, 17 500; microscans, 1; loop count, 5; AGC target, $2e5$; maximum injection time, 100 ms; isolation window, m/z 1.5; high collision dissociation (HCD) with normalized collision energy (NCE), 35%; spectrum data type, profile. Xcalibur Qual Browser software version 2.4 was used for data handling.

Analysis

CoQ10 was analysed in positive ionization mode as an ammonium adduct (m/z 880.7146). HO-CoQ10 was analysed in negative ionization mode in its deprotonated form (m/z 847.6618).

The content of CoQ10 and HO-CoQ10 was quantified by first determining the peak area for each signal in the respective extracted-ion chromatogram. The baseline was set for each peak, not across the whole chromatogram. Then peak areas at the lowest incubation temperature (-70 $^{\circ}$ C for long-term stability and +4 $^{\circ}$ C for short-term stability) were set to 100%.

Material and equipment

- **Autosampler vial** (VWR; screw cap, 9 mm, silicon, PTFE # 548-1502; vial short thread, 1.5 mL, 32x11.6 mm, clear glass # 548-0028)
- **Eluent A:** water; ammonium formate, 2 mM; formic acid, 0.1% (v,v); acetonitrile, 1% (v,v); pH 3
- **Eluent B:** acetonitrile/methanol, 1:1 (v,v); ammonium formate, 2 mM; formic acid, 0.1% (v,v); water, 1% (v,v)

- **Stationary phase:** Accucore PhenylHexyl column (particle size, 2.6 μm ; length x ID, 100 x 2.1 mm)
- Dionex UltiMate 3000 RS system: degasser, quaternary pump, UltiMate autosampler coupled to **Q-Exactive Plus system** (Thermo Fisher Scientific) equipped with heated electrospray ionization source (HESI-II)¹⁰⁷⁻¹⁰⁹
- **Xcalibur™** Software, Version 4.2, Qual Browser; *analysis of MS spectra and LC/MS chromatograms, modelling of isotope patterns* (Thermo Fisher Scientific, 2018)

2.8.3 Detection in lipid extracts from isolated mitochondria by UHPLC-MS

Three steps are necessary for sample preparation: 1. Protein precipitation, 2. extraction, and 3. reduction of the extract volume.

Sample preparation

Bovine heart mitochondria (isolation, see 2.12 on p. 35) were thawed on ice. In a 1.5-mL plastic tube, 10 mg (or any desired amount of) mitochondrial protein was sedimented (20.000 x g, 4 °C, 10 min) and the supernatant was disposed of.* 1 mL solvent (see listing below) was added to precipitate proteins and extract CoQ10. At this point, the internal standard (IS), 10 μL of a 100 μM CoQ4 solution in *i*-propanol, could be added. The pellet was resuspended by vortexing and loosened by hitting the vial onto the bench, if necessary. The mixture was then centrifuged (20.000 x g, 4 °C, 5 min) and 1 mL (or 0.9 mL when IS was used) of the supernatant was transferred into a glass autosampler vial (a little of the supernatant should remain on the pellet). At 50 °C (or at RT as a control) under a stream of nitrogen, the solvent was evaporated thoroughly. Samples containing water could not be dried entirely using this procedure. Thus, they were frozen at -20 °C overnight and the remaining liquid was removed in a desiccator under constant vacuum. The samples were stored at -80 °C. The precipitate was then reconstituted with 0.1 mL (or 0.09 mL when IS was used) *i*-propanol, vortexed vigorously and centrifuged (20.000 x g, 5 min) in a 1.5-mL tube to remove precipitated salts and proteins. The supernatant was then carefully transferred into an autosampler vial containing a micro-insert for small volumes.

* For the dilute-and-shoot method the following changes were applied: Only 0.09 mL *i*-propanol was added together with 0.01 mL internal standard. After centrifuging the mixture to remove precipitates, 80 μL of the supernatant was directly transferred into an autosampler vial without preceding drying procedures.

Solvent: methanol, ethanol, *n*-propanol, *i*-propanol, acetonitrile, a mixture of *i*-propanol and 10% Triton X-100 in water (1:4) or *i*-propanol and water (1:4)

Detection with UHPLC-MS

Parameters for data shown in Table 13 (p. 73)

See LC-MS conditions in section 2.8.1 (p. 30). Changes as follows:

gradient elution: 0-3 min 30-10% A, 3-8 min 10-0.1% A, 8-9 min hold 0.1% A, 9-9.5 min 0.1-30% A, 9.5-10.1 min: hold 30% A; inclusion list in positive mode: m/z 880.71770, 863.69190, 849.67550; negative: m/z 862.68760, 847.66340; scan range, m/z 233.4-3 500.

Parameters for measurements summarized in Table 12 (p. 72)

See LC-MS conditions in section 2.8.1 (p. 30). Changes as follows: inclusion list in positive mode: m/z 880.71770; negative: m/z 862.68760, 847.66340.

The HESI-II source conditions were as follows: ionization mode, positive and negative alternating; sheath gas, 52.5 AU; auxiliary gas, 13.75 AU; sweep gas, 2.75 AU; spray voltage, +3.5 and -2.5 kV, respectively; heater temperature, 437.5 °C; ion transfer capillary temperature, 268.75 °C; and S-lens RF level, 60.0 and 50, respectively.

Analysis

Protonated CoQ4, ammonium adducts of CoQ10, and HO-CoQ10 were quantified by integration of the peaks. The baseline of each peak was set for every signal separately. Peaks were smoothed using Gaussian function (7 points). Concentrations were normalized using the calibration curves of CoQ4, CoQ10 and HO-CoQ10, obtained with the same protocol as for the samples. The measurement error was calculated as the delta score in ppm: (observed mass – theoretical exact mass)/theoretical exact mass.

Material and equipment

- Coenzyme Q4 (**CoQ4**, Sigma # C2470)
- Methanol, Grad.-HPLC (**MeOH**, VWR # 20864.320 or Fisher Scientific # M/4058/17)
- Ethanol. absolute, 99.8% (Sigma # 32205)
- *n*-Propanol (1-propanol, 99.9%, HPLC grade)
- *i*-Propanol (2-propanol, HPLC grade, Fluka # 34965)
- Acetonitrile, HPLC for gradient analysis (Fisher Scientific # 10660131)
- Triton X-100 (polyethylene glycol *tert*-octylprenyl ether, eurobio # 018774, 10% in water)
- **Rotary evaporator** (IKA® RV 8) with integrated heating bath (IKA® HB 10) connected to a
- **Refrigerated high speed centrifuge** (Hermle # Z 32 HK)
- **Autosampler vial** (VWR; screw cap, 9 mm, silicon, PTFE # 548-1502; vial short thread, 1.5 mL, 32x11.6 mm, clear glass # 548-0028)
- Micro-inserts (for wide opening, 0.1 mL, 31x6 mm, clear glass, 15 mm top, VWR # 548-3006)
- **Eluent A:** water; ammonium formate, 2 mM; formic acid, 0.1% (v,v); acetonitrile, 1% (v,v); pH 3
- **Eluent B:** acetonitrile/methanol, 1:1 (v,v); ammonium formate, 2 mM; formic acid, 0.1% (v,v); water, 1% (v,v)
- **Stationary phase:** Accucore PhenylHexyl column (particle size, 2.6 µm; length x ID, 100 x 2.1 mm)
- Dionex UltiMate 3000 RS system: degasser, quaternary pump, UltiMate autosampler coupled to **Q-Exactive Plus system** (Thermo Fisher Scientific) equipped with heated electrospray ionization source (HESI-II)¹⁰⁷⁻¹⁰⁹
- **Xcalibur™** Software, Version 4.2, Qual Browser; *analysis of MS spectra and LC/MS chromatograms, modelling of isotope patterns* (Thermo Fisher Scientific, 2018)

2.9 Cell culture

Cells were cultured according to the lab's internal guidelines using the following media and splitting protocols:

- **Jurkat, Clone E6-1**
Medium: RPMI + 10% FCS + 1% P/S
Splitting: 3 x per week (1:3 – 1:6)
- **Jurkat pCasper** (Clone E6-1 stably transfected with pCasper3-GR vector, generated by Christian Backes¹¹⁰)
Medium: RPMI + 10% FCS + 1% P/S, 0.8 mg/mL G418
Splitting: 3x per week (1:4 – 1:6)
- **MelJuso**
Medium: RPMI 1640 + 10% FCS
Splitting: 2 x per week (1:10 – 1:12)
The cells are washed with PBS and incubated with trypsin for 1 min. After removing trypsin, the cells are detached by hitting the flask and medium is added.
- **HeLa**
Medium: DMEM medium, 10% FCS
Splitting: 3 x per week (1:3 or 1:5)
The cell layer is washed with PBS and incubated with TrypLE for 3 min. The cells are then resuspended in medium.

Material

- DMEM medium (life technologies, Gibco™ # 41966052)
- TrypLE™ Express Enzyme (Thermo Fisher Scientific, Gibco™ # 12604013)
- RPMI 1640 Medium + L-glutamine (life technologies, Gibco™ # 21875-034)
- Fetal bovine serum (FCS, life technologies, Gibco™ # 10270106)
- Penicillin-Streptomycin (10 000 U/mL penicillin, 10 000 µg/mL streptomycin, 100x concentrate, life technologies, Gibco™ # 15140-122)
- G418 (Calbiochem # 345810-5)
- Jurkat, Clone E6. 1 (ATCC # TIB-152™)
- MelJuso (Department of Dermatology, Venereology and Allergology, University Hospital of Saarland)
- HeLa (DSMZ)

2.10 Determination of metabolic turnover with the CellTiter-Blue® Cell Viability Assay

50 000 cells (Jurkat) were seeded in a volume of 180 µL cell culture medium approx. 1 h before addition of substances into 96-well plates. 5 000 adherent cells (MelJuso and HeLa) per well were seeded 3 h prior to treatment to guarantee adhesion of the cells. The cells were then treated with 20 µL of a stock solution of the indicated substance or vehicle to yield the desired quinone concentrations and 1% ethanol as final concentration. Stock solutions were first prepared in ethanol and then diluted 1:10 in medium for each

concentration to exclude concentration errors because of possible unstable solution in medium. The dilution was preincubated at 37 °C to ensure dissolution of CoQ.

After 2, 24, 48 and 72 h of incubation at 37 °C (5% CO₂), 20 µL of CellTiter-Blue® Reagent was added and mixed by moving the plate horizontally. Resorufin fluorescence was measured (exc. 535 nm, em. 590 nm) after 3 h of incubation (37 °C, 5% CO₂) using a plate reader. Before the measurement, the plate was shaken for 30 s (linear, 1 mm amplitude) followed by 30 s of rest to settle down the cells. The fluorescence was detected at 3 points per well (3, linear) using 5 light flashes, an integration time of 40 µs, a settle time of 10 µs, and a gain of 80.

Material and equipment

- CellTiter-Blue® Cell Viability Assay (Resorufin, Promega # 8081)
- Cell culture media, see section 2.9
- 96-Well plates, black, transparent bottom (BD Falcon™ # 353219)
- Plate reader (Tecan, Infinite M200 PRO)

2.11 Detection of apoptosis with the protein sensor Casper-GR

50 000 E6-1 pCasper cells were seeded in a volume of 180 µL in cell culture medium into a 96-well plate, approx. 1 h before adding the substances. 20 µL of stock solution of a substance or vehicle was added to yield indicated concentrations with 1% ethanol as final concentration. The samples were prepared in triplicates and incubated at 37 °C and 5% CO₂ during the measurement. After approx. 40 min, the measurement was started and green, red and FRET fluorescence was detected every 15 min for 24 h using a 10 x objective (Olympus).

The measurement was designed, conducted and analysed together with Carsten Kummerow (Department of Biophysics).

Material and equipment

- **Jurkat pCasper** (Clone E6-1 stably transfected with pCasper3-GR vector (Evrogen), generated by Christian Backes)^{110,111}
- **Medium:** RPMI + 10% FCS + 1% P/S (cf. section 2.9)
- 96-well microplate (flat bottom, black/clear bottom, Corning™ # 353219)
- BD Pathway Bioimager 855 imaging system (BD Biosciences)
- Fiji⁸⁸ *for image processing*

2.12 Isolation of mitochondria

To isolate crude mitochondria four steps are necessary: a) collection of material, b) tissue homogenization and cell disruption, c) elimination of whole cells, tissue, and nuclei by a slow centrifuging step, and d) enrichment of mitochondria by high-speed centrifugation. Material, solutions and tools were kept on ice at any time possible. Centrifugation steps were carried out at 4 °C. Protein concentration was determined by a Lowry protein assay according to the manufacturer's guidelines.¹¹² The standard assay protocol was employed at a final volume of 920 µL (plastic cuvettes), and the microplate assay protocol (transparent well plates; Tecan, Infinite M200 PRO) was used for mouse and beef heart mitochondria, respectively. Crude mitochondrial

extracts are mitochondria-enriched preparations contaminated with lysosomes, peroxisomes, and microsomes that need to be purified by differential centrifugation when contaminations are interfering with planned experiments.

2.12.1 Isolation of beef heart mitochondria

The procedure was adapted from Lenaz and Palotti (2001)⁹⁰ and carried out as follows:

- a) Beef hearts were collected as soon as possible after slaughtering (up to 2 hours thereafter) and transported in a plastic bag covered with ice. Blood was washed off using cold tap water. Connective tissue and fat were removed generously. The heart was opened and the left ventricle was divided into smaller sections to ensure thorough cooling of the tissue. 2-cm filet cubes were weighed and washed with ice-cold D-PBS several times to eliminate blood, and finally with HWS. During this procedure, the flesh was stored either in a plastic bag surrounded by crushed ice or in a crystallizing dish filled with ice-cold buffer.
- b) Together with HWS (1:1, weight/weight), the cubes were transferred into a high-performance blender. The material was homogenized for 20 s at minimal speed and twice for 12.5 s at the highest speed, as this blending protocol resulted in the highest yield of mitochondrial protein. Between the blending steps, splattered material was transferred back into the bulk with a common household silicon dough scraper. The homogenate was transferred into a glass beaker and the pH readjusted to 7.5 using 5 M Tris. Mixing was achieved best using the dough scraper.

The homogenate was transferred into 50-mL tubes and centrifuged at 1200 x g for 15 min. After transferring the supernatant into a fresh tube, it was subjected to another centrifugation step to eliminate tissue material thoroughly. Then, lipid granules were removed by filtering through a double layer of cheesecloth supported by a glass funnel.

- c) Mitochondria were pelleted at 20 000 x g (15 min) and the supernatant was discarded entirely. The pellet's surface was washed carefully by pipetting a small volume of HWS onto the tube wall and tilting the tube carefully. After carefully disposing of the buffer, lipids attached to the tube walls were wiped off with lint-free paper cloths. With a glass rod, the pellet was loosened, starting from the borders to its centre without applying pressure. Mitochondria were resuspended in HWS (around 20 x volume of pellet) using a serological pipette and centrifuged (20 000 x g, 15 min).

Finally, the pellet was suspended in ~3 x HWS (v/v) to yield a concentration of ~40 mg/mL. Mitochondria were stored long-term in liquid nitrogen and in aliquots of 0.5 or 1 mg during measuring periods at -70 °C.

2.12.2 Isolation of mouse heart mitochondria

The protocol was given by Nickel et al. (2015)^{113,114} and the isolation performed in collaboration with Prof. Dr Christoph Maack's group (now Department Translational Science, Universitätsklinikum Würzburg):

- a) Mice are sacrificed by an overdose of xylazine and ketamine (intraperitoneal injection of 0.3 mL of a 1:2-mixture, resulting in 66.7 mg/mL xylazine and 0.67% ketamine) and the beating heart is transferred into IS. Connected lung tissue, vessels, atria and residual blood (by opening both ventricles) are removed.
- b) The tissue is transferred into a 2-mL reaction tube filled with 0.5 mL IS (containing 0.16 mg/mL proteinase and 3.6 mg/mL BSA) and chopped into small pieces using scissors. With a 5-mL Potter-

Elvehjem grinder, the material is homogenized for 7 min avoiding any air bubble formation. At this stage, the homogenate should not contain any visible tissue chunks. Another 0.5 mL proteinase-BSA-mixture is added and the sample further homogenized for 7 min.

- c) The homogenate was transferred back into the same 2-mL reaction tube and centrifuged at 400 x g for 5 min. Its supernatant is transferred into a fresh tube and centrifuged again.

From the collected supernatant (fresh tube) mitochondria were pelleted at 7 700 x g for 10 min and washed twice with 1.4 mL MSS. Depending on its size, the pellet was resuspended in 100-200 μ L MSS yielding a concentration of 15-30 mg/mL mitochondrial protein. Samples were stored on ice for experiments with coupled mitochondria at the same day or at -70 °C/-196°C for long-term storage.

Material and equipment

Beef heart mitochondria:

- Beef heart (slaughterhouse Emil Färber GmbH & Co. KG, Standort Zweibrücken, Germany)
- Heart wash solution (**HWS**) *for isolation and suspension*: see section 0 on p. 23
- Glass rod
- 50-mL reaction tubes
- **Household blender** (Bosch, MUM 6412 Universal-Küchengerät, used with blender extension)
- **Refrigerated high speed centrifuge** (Hermle # Z 32 HK)
Swing out rotor 4 places with tubes for 50 mL (Hermle # 220.72 V06 and 605.004)

Mouse heart mitochondria:

Animal procedures were approved by the local animal ethics committee and conducted in accordance with institutional guidelines. If not mentioned otherwise (see figure legends) BL6N mice were used for all experiments.

- Mice, strain C57BL/6NCrl: Unlike Black6J mice, Black6N mice express the *Nnt* gene (male, BL/6N, C57BL/6NCrl, strain code 027; Charles River), 8-38 weeks depending on experiments
- Black6J mice (male, BL/J, C57BL/6J, JAX Mice Stock Number 000664; Charles River)
- **Ketamine**, 100 mg/mL (ketamine hydrochloride, Ursotamin®, Serumwerk Bernburg AG)
- **Xylazine**, 2% (xylazine hydrochloride, Rompun®, Bayer Vital GmbH)
- **DC™ Protein Assay** Kit II (Bio-Rad # 5000112)
- **Proteinase**, bacterial, Type XXIV (Sigma # P8038)
- **BSA**, fatty acid free (bovine serum albumin; Sigma A7030)
- Isolation solution (**IS**): see section 0 on p. 23
- Mitochondria suspension solution (**MSS**): see section 0 on p. 23
- Potter-Elvehjem grinder, **pestle**, 5 mL (A. Hartenstein # HT05)
- Potter-Elvehjem grinder, **grinding chamber**, 5 mL (A. Hartenstein # HZ05)
- 2-mL plastic reaction tubes

2.13 Mitochondrial respiration: Clark-type electrode

Oxygen consumption was measured using a Clark-type electrode. Two instruments were used: 1. Oxygraph Plus (Hansatech Instruments) provided by Prof. Dr Christoph Maack (now Department Translational Science, Universitätsklinikum Würzburg) and 2. Oxygraph-2k (Oroboros Instruments) provided by Prof. Martin van der Laan (Department of Medical Biochemistry & Molecular Biology, Saarland University). Used substrate cocktails to feed electrons into one of the respiratory chain complexes and inhibitors to block the respective complex are listed below.

Table 2 | Substrates and inhibitors for respiration via the different respiratory chain complexes. The solvents of the substances' stock solutions are noted in parenthesis. RB, respiration puffer; the preparation of the stock solutions is mentioned within the material section, the reduction of duroquinone on p. 47.

Complex	I	II	III	IV
Substrate	5 mM pyruvate (RB)	0.5 μ M rotenone (DMSO)	800 μ M duroquinol (ethanol)	0.5 mM TMPD (water)
	5 mM malate (water)	10 mM succinate (water)		1 mM ascorbate (water)
Inhibitor	0.5 μ M rotenone (DMSO)	5 mM malonate (water) atpenin A5 (DMSO)	10 μ M antimycin A (DMSO)	1 mM cyanide (RB)

The polarographic oxygen sensor was used in amperometric mode and consisted of a silver/silver chloride anode and gold or platinum cathode for the Oroboros and Hansatech setup, respectively. Oxygen was measured in the KCl reservoir separated from the sample chamber by a gas-permeable membrane (FEP for Oroboros, PTFE for Hansatech). The current was detected as an amperometric signal and converted into voltage.

2.13.1 Oxygraph Plus (Hansatech)

Set-up and calibration of the instrument

Parameters: stirrer, 900 rpm; polarization voltage, 0.7 V, data recording interval, 0.1 s; electrolyte solution, 1 M KCl;

Prior to starting experiments, the electrode was mounted and the chamber assembled on a daily basis. Then, a two-point oxygen calibration in distilled water was performed using an excess of $\text{Na}_2\text{S}_2\text{O}_4$ (one spatula tip) to deplete oxygen ($\text{S}_2\text{O}_4^{2-} + \text{O}_2 + \text{H}_2\text{O} \rightarrow \text{HSO}_4^- + \text{HSO}_3^-$).¹¹⁵ After one day of measuring or when noise increased, the Ag/AgCl anode was polished.

Detection of mitochondrial respiration

Respiration buffer was added to the chamber set to 37 °C. After detection of a stable baseline, mitochondria suspended in MSS were added using standard plastic pipettes. The volume of the chamber was 1 mL after

addition of mitochondria. The chamber was then closed airtight and substances were added using a Hamilton syringe.

Table 3 | Addition of substances for respiration measurements with the Hansatech Oxygraph Plus. Final volume, 1 mL; MHM, mouse heart mitochondria; PM, pyruvate and malate; r, rotenone; S, succinate; H₂-duroQ, duroquinol; asc, ascorbate; A, ADP; sample, CoQ/solvent control/inhibitor; *concentration variable

	Complex I	MHM	Temperature: 37 °C		
Stock solution		0.5 M	0.1 M		1 µM*
Volume (µL)	5-20	10	10		10
Substance	MHM	PM	ADP		<u>sample</u>
Final concentration	200 µg/mL	5 mM	1 mM		0.01 µM
Time (min:s)	1:00	3:30	5:00		6:00
	Complex II	MHM	Temperature: 37 °C		
Stock solution		0.5 mM	1 M	0.1 M	1 µM*
Volume (µL)	5-20	1	10	10	10
Substance	MHM	r	S	ADP	<u>sample</u>
Final concentration	200 µg/mL	0.5 µM	10 mM	1 mM	0.01 µM
Time (min:s)	1:00	2:30	3:30	5:00	6:00
	Complex III	MHM	Temperature: 37 °C		
Stock solution		80 mM	0.1 M		1 µM*
Volume (µL)	5-20	10	10		10
Substance	MHM	H ₂ -duroQ	ADP		<u>sample</u>
Final concentration	200 µg/mL	0.8 mM	1 mM		0.01 µM
Time (min:s)	1:00	3:30	4:00		4:45
	Complex IV	MHM	Temperature: 37 °C		
Stock solution		0.8 M	0.2 M	0.1 M	1 µM*
Volume (µL)	5-20	5	5	10	10
Substance	MHM	asc	TMPD	ADP	<u>sample</u>
Final concentration	200 µg/mL	2 mM	0.5 mM	1 mM	0.01 µM
Time (min:s)	1:00	2:30	3:30	4:00	4:45

Analysis

Oxygen consumption rate was calculated with OriginLab using linear fitting (after ADP addition), and linear or exponential-linear ($y = p_1 \cdot e^{\frac{x}{p_2}} + p_3 + p_4 x$) fitting (after sample addition, samples were tested for convergent fit of exp.-lin. Function, usually: linear, controls/CoQ10 and exp.-lin., HO-CoQ10). Selected time intervals for CI and CII were: ADP, 30 s after ADP addition until end of interval (i.e. 30 s) and sample, 30 s after sample addition until 60 s before total O₂ depletion. For CIII: ADP, 15 s after ADP addition until end of interval

(i.e. 30 s) and sample, 10 s after sample addition until 20 s before total O₂ depletion. For CIV: ADP, 15 s after ADP addition until end of interval (i.e. 30 s) and sample, 10 s after sample addition until 20 s before total O₂ depletion.

2.13.2 Oxygraph 2k (Oroboros)

Set-up and calibration of the instrument

Parameters: polarization voltage, 0.8 V; gain, 1; stirrer speed, 750 rpm; data recording interval, 2 s; electrolyte solution, 1 M KCl; O₂ solubility factor of medium F_M, 0.92 (in consultation with manufacturer).

Before starting experiments, the condition of the setup was judged and calibrated (R1, R0) on a daily basis using the desired respiration buffer according to the manufacturer's guideline:¹¹⁶

- fast, monoexponential rise of oxygen signal upon restarting magnetic stirring ("stirrer test": stirrers turned off for 30 s)
- oxygen signal of the air saturated buffer (R1) is 1-3 μA at sea level and slope of oxygen change approaching 0 with a noise of ideally $\pm 2 \text{ pmol}\cdot\text{s}^{-1}\cdot\text{mL}^{-1}$ (max. ± 4)
- oxygen consumption rate of the electrode (measured after closing the chamber); if it was higher than $4 \text{ pmol}\cdot\text{s}^{-1}\cdot\text{mL}^{-1}$, the buffer was probably contaminated and exchanged by a freshly thawed aliquot
- zero oxygen condition of the chamber (R0) was determined from the first measurement where oxygen was consumed completely (raw signal max. 5% of R1)

If a, b or d were not acceptable, POS (polarographic oxygen sensor) service¹¹⁷ including cleaning the gold cathode, the Ag/AgCl anode, and mounting the electrode with the oxygen-permeable FEP membrane was executed. Then, background correction values were determined, with minor changes to the manual,¹¹⁸ as follows: $\sim 10 \text{ mg}$ sodium dithionite ($\text{Na}_2\text{S}_2\text{O}_4$) was dissolved in $\sim 2.1 \text{ mL}$ Mir05 in a 2-mL tube to minimize air exposure. The stock solution's potency was determined by adding $2 \mu\text{L}$ of the solution to each chamber and calculating the loss of O₂ concentration per μL . Titrations were performed manually using a $50\text{-}\mu\text{L}$ Hamilton syringe. The calculated volume for each O₂ concentration was added and fine-tuned if necessary. The O₂ concentrations and recording intervals were: air-saturated (10 min), $< 100 \mu\text{M}$ (20 min), $< 50 \mu\text{M}$ (20 min), $< 23 \mu\text{M}$ (20 min), $0 \mu\text{M}$ (5 min). Excess of $\text{Na}_2\text{S}_2\text{O}_4$ ($100 \mu\text{L}$) was added to establish the zero oxygen condition. Y-intercept of the fitted function for background correction should have an average value of $-3 \text{ pmol}\cdot\text{s}^{-1}\cdot\text{mL}^{-1}$ (max. -4).

Detection of mitochondrial respiration

Before each measurement 2.25 mL respiration buffer was pipetted into the chamber, the stopper was closed and excessive buffer was removed from the receptacle leaving 2 mL in the chamber. When the buffer had equilibrated to $37 \text{ }^\circ\text{C}$ and the slope of O₂ change had been $< 10 \text{ pmol}\cdot\text{s}^{-1}\cdot\text{mL}^{-1}$, the measurement was restarted to record a new experiment. Mitochondria were thawed (yeast mitochondria, YM) and/or stored (MHM) on ice and prediluted in ice-cold respiration buffer shortly prior to starting the measurement. The final volume was $120 \mu\text{L}$ for one or $220 \mu\text{L}$ for both chambers. A 1:1 mixture of pyruvate (1 M in RB) and malate (1 M in H₂O) was prepared freshly and kept on ice. Rotenone was protected from light, thawed and kept at RT. ADP was thawed and stored on ice. Duroquinol was prepared according to procedure in section "Quinone

reduction” on p. 47. Using Hamilton syringes, mitochondria (500 μ L syringe and careful pipetting not to expose the sample to high shear forces), substrates, ADP and CoQs or inhibitors were added at defined times according to the tables below. Usually, measurements were stopped after depletion of oxygen in the chamber.

Table 4 | Addition of substances for respiration measurements with the Oroboros Instr. Oxygraph 2k. Final volume, 2 mL; MHM, mouse heart mitochondria; BHM, beef heart mitochondria; YM, yeast mitochondria; PM, pyruvate and malate; r, rotenone; S, succinate; A, ADP; sample, CoQ/solvent control/inhibitor; *concentration variable

	Complex I	MHM	Temperature: 37 °C		
Stock solution	1 mg/mL	0.5 M	0.5 M		1 μ M*
Volume (μ L)	100	20	4		20
Substance	MHM	PM	A		<u>sample</u>
Final concentration	50 μ g/mL	5 mM	1 mM		0.01 μ M*
Time (min:s)	1:00	3:30	08:00		10:30

	Complex II	MHM	Temperature: 37 °C		
Stock solution	1 mg/mL	1 mM	1 M	0.5 M	1 μ M*
Volume (μ L)	100	1	20	4	20
Substance	MHM	r	S	ADP	<u>sample</u>
Final concentration	50 μ g/mL	0.5 μ M	10 mM	1 mM	0.01 μ M*
Time (min:s)	1:00	2:30	3:30	08:00	10:30

	Complex II	YM	Temperature: 30 °C		
Stock solution	10 mg/mL	1 M	0.5 M		1 μ M*
Volume (μ L)	20	20	4		20
Substance	YM	S	ADP		<u>sample</u>
Final concentration	100 μ g/mL	10 mM	1 mM		0.01 μ M*
Time (min:s)	1:00	6:30	09:30		11:30

Analysis

The oxygen consumption rate was calculated online using the 1st derivative of the oxygen concentration in 20 s intervals calculated by DatLab. Average oxygen consumption rates for each condition were calculated as the mean within 30 or 60 s before the subsequent addition for substrate and ADP-dependent respiration or within a 3-min interval 1 min before oxygen depletion.

Material

- Na₂S₂O₄ (sodium **dithionite**, sodium hyposulfite; Sigma-Aldrich # 71699)
- **Ammonia** solution, 25% (Merck Millipore # 1.05432.1011)
- **OroboPOS-Polishing Powder** for cathode cleaning (Oroboros Instr. # 26510-01)
- **OroboPOS-Polishing Cloth** for cathode cleaning (Oroboros Instr. # 26520-01)
- Mir05 (for instruction and composition, see: ¹¹⁹)
 - **Taurine** (2-aminoethanesulfonic acid; Alfa Aesar # A12403)

- **Lactobionic acid** (4-O-β-D-Galactopyranosyl-D-gluconic acid, Acros Organics # ACRO167111000 or Aldrich # 153516)
- **Sodium pyruvate** (Sigma, # P2256)
- L-(–)-Malic acid (**malate**, Sigma, # M1000; 1 M in H₂O at pH 7 adjusted with KOH, stored at -20 °C)
- **Succinate** (sodium succinate dibasic hexahydrate; Sigma-Aldrich # S2378; 1 M in H₂O at pH 7 adjusted with HCl, stored at -20°C)
- **Duroquinone** (2,3,5,6-Tetramethyl-1,4-benzoquinone; Sigma # D223204)
- Sodium borohydride (**NaBH₄**, Sigma-Aldrich # 452882)
- N,N,N',N'-Tetramethyl-*p*-phenylenediamine dihydrochloride (**TMPD**, FW 237.17, Acros Organics # 42060050; 200 mM in H₂O, stored at -20 °C)
- Ascorbic acid (**asc**, Merck # 1004680100; 800 mM in H₂O at pH 7 adjusted with NaOH, stored at -20 °C)
- Adenosine 5'-diphosphate monopotassium salt dihydrate (**ADP**, Sigma, # A5285)
- **Rotenone** (Sigma # R8875; 1 mM in DMSO, stored at -20°C, discarded after thawing)
- **Malonic acid** (Sigma # M1296; 1 M in H₂O, add a small volume of water, titrate to pH 6.0 with 5 M KOH in 2-μL steps, fill up to 1 M, prepared daily)
- **Atpenin A5** (AA5, CAYMAN # 11898; 1 or 10 mM in DMSO, stored at -20 °C)
- **Antimycin A** from *Streptomyces* sp. (~ 532 g/mol, Sigma # A8674; 40 mM in DMSO, stored at -20 °C)
- **Oligomycin** from *Streptomyces diastochromogenes* (FW(A, 65%) 791, (B) 805.1, (C) 775.1; Sigma # 04876; 25 mM in DMSO, stored at -20 °C)
- **KCN** (potassium cyanide, FW 65.12, Sigma # 60178; 100 mM stock solution in RB was stored in aliquots at -80 °C and discarded after thawing once)
- **CCCP** (carbonyl cyanide 3-chlorophenylhydrazone; Sigma # C2759; 1 mM in DMSO, stored at -20 °C)
- **Embelin** (2,5-dihydroxy-3-undecyl-2,5-cyclohexadiene-1,4-dione; Sigma # E1406)
- RB, see p. 23
- Oxygraph Plus (Hansatech Instruments)
Oxygraph Software *for recording* (Version 1.02, Hansatech Instruments)
- Oxygraph-2k Series G (**O2k**, Oroboros Instruments Corp; O2k-Core # 10000-02 and O2k-Chambers # 23100-01)
Datlab 7 Software for data recording and evaluation of oxygen consumption rates, OCR (Oroboros Instruments Corp; Version 7.0.0.1045)

2.14 Determination of free [Ca²⁺]/[Mg²⁺] with fluorescent ratiometric dyes

When phosphates are present in solutions, free calcium and magnesium concentrations cannot be reliably calculated. Hence, free magnesium and calcium concentrations needed to be determined experimentally using the Mg²⁺ and Ca²⁺ indicators mag-fura-2 and fura-2, respectively (compare **Figure 10 a** and **b**). The ratiometric indicators shift their excitation maxima to shorter wavelengths when binding calcium but maintain their

emission maximum at 510 nm (ϵ). The excitation wavelengths at 340 and 380 nm were chosen to minimize cross-excitation of the other species.

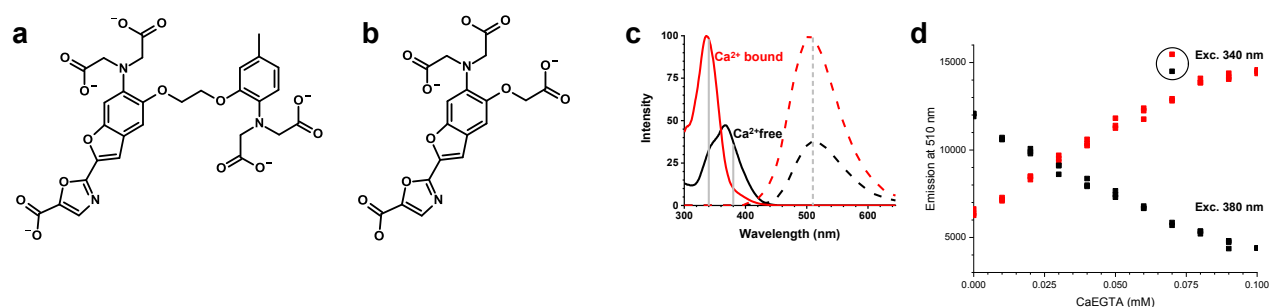


Figure 10 | Ratiometric and fluorescent Ca²⁺ and Mg²⁺ sensors. (a) Fura-2 and (b) mag-fura-2, (c) excitation (solid line) and emission (dashed lines) of fura-2 in its Ca²⁺-bound (red) and Ca²⁺-free state (black), vertical lines mark excitation (340 and 380 nm) and emission wavelengths (510 nm) used for ratiometric analysis shown in (d): change of emission of 340 and 380 nm excitation with increasing free Ca²⁺ concentrations, circled data points were technical outliers and therefore excluded from the analysis.

The procedure was based on the calibration protocol for Ca²⁺ indicators provided by Thermo Fisher Scientific.¹²⁰ Per experiment (calibration of mag-fura-2, calibration of fura-2, Ca²⁺ concentrations curve in RB) two solutions were prepared beforehand and stored at -20 or +4 °C: a high calcium or magnesium solution and a zero calcium/magnesium solution listed below (concentrations are given in mM).

Calibration of mag-fura-2 to determine free Mg²⁺ concentrations:

- Zero Mg solution (RB2.1): 137 KCl, 20 HEPES, 0.1 EGTA, pH 7.21 using KOH
- High Mg solution (RB2.2): 137 KCl, 200 MgCl₂, 20 HEPES, 0.1 EGTA, pH 7.21 using KOH

Calibration of fura-2 to determine free Ca²⁺ concentrations:

- Zero Ca solution (RB2.3): 137 KCl, 2.25 MgCl₂, 20 HEPES, 0.1 EGTA, pH 7.21 using KOH
- High Ca solution (RB2.4): 137 KCl, 2.25 MgCl₂, 20 HEPES, 0.1 EGTA, 0.1 CaCl₂, pH 7.21 using KOH

Ca²⁺ calibration curve for respiration measurements:

- Zero Ca solution (RB3.1): 137 KCl, 4 KH₂PO₄, 2.5 MgCl₂, 20 HEPES, 0.1 EGTA, pH 7.21 using KOH
- High Ca solution (RB3.2): 137 KCl, 4 KH₂PO₄, 2.5 MgCl₂, 20 HEPES, 0.1 EGTA, 0.1 CaCl₂, pH 7.21 using KOH

The pH was adjusted at RT to the second decimal place for all solutions. The pH was measured while stirring for at least 5 more minutes after the pH had stabilized. Before an experiment the solutions were thawed, vortexed thoroughly and equilibrated to RT. The pH was verified. After adding 10 μ M mag-fura-2 or fura-2, the solutions were protected from light. The addition of the fluorescent indicators did not influence the pH. The solutions were diluted serially as specified in Table 5 and Table 6 for mag-fura-2 and fura-2 calibration, respectively: First, indicated volumes of zero Mg/Ca solutions were pipetted into reaction vials (1.5, 2 or 5 mL according to total volume). Then, high Mg/Ca solution was added to the first vial and from this predilution, the indicated volume was transferred into the next dilution etc.

Table 5 | Serial dilution of Mg²⁺ solutions for mag-fura-2 calibration. Listed are from left to right: final MgCl₂ concentrations, final free Mg²⁺ concentrations calculated with maxchelator,¹²¹ the volume of zero Mg solution (RB 2.1) and predilution needed to obtain the indicated Mg concentration in the same line. High Mg (RB2.2) containing 200 mM MgCl₂ was diluted serially with zero Mg solution. Grey, free Mg²⁺ concentrations not in EGTA buffer range;

MgCl₂ (mM)	[Mg²⁺]_{free} (μM)	Zero Mg solution (μL)	Predilution (μL)	Total volume (μL)
200	200	0	1 300 (high Mg solution)	1 300
15	14.9	2 775	225	3 000
10	9.95	1 000	2 000	3 000
5	4.97	1 900	1 900	3 800
4	3.97	700	2 800	3 500
3	2.98	800	2 400	3 200
2.5	2.48	400	2 000	2 400
2	1.98	300	1 200	1 500
1	0.99	500	500	1 000
0.1	0.099	900	100	1 000
0.01	0.0099	900	100	1 000
0	0	1 000	0	1 000

Table 6 | Serial dilution of Ca²⁺ solutions for fura-2 calibration. Listed are from left to right: final CaEGTA concentrations, final free Ca²⁺ concentrations calculated with maxchelator,¹²¹ the volume of zero Ca solution (RB2.3 or RB3.1) and predilution needed to obtain the indicated Ca concentration in the same line. High Ca (RB2.4 or 3.2) containing 0.1 mM CaEGTA was diluted serially with zero Ca solution. Grey, free Ca²⁺ concentrations not in EGTA buffer range;

CaEGTA (mM)	[Ca²⁺]_{free} (μM)	Zero Ca²⁺ solution (μL)	Predilution (μL)	Total volume (μL)
0.1	3.99	0	5 500 (high Ca solution)	5 500
0.09	1.29	500	4 500	5 000
0.08	0.631	500	4 000	4 500
0.07	0.376	500	3 500	4 000
0.06	0.243	500	3 000	3 500
0.05	0.162	500	2 500	3 000
0.04	0.107	500	2 000	2 500
0.03	0.0699	500	1 500	2 000
0.02	0.0408	500	1 000	1 500
0.01	0.0181	1 000	500	1 000
0	0	1 000	0	1 000

200 μL of each solution was transferred into black 96-well plates to be measured in technical triplicates. Solutions without indicator were run in parallel as background controls. The plate was incubated at 37 °C and its lid removed to detect fluorescence. The plate reader Infinite M200 PRO (Tecan) was set to top reading mode, a gain of 150, 10 flashes, 40 μs integration time and 2 000 μm Z-position. First, the single excitation wavelengths 340 and 380 nm (± 4.5 nm) were detected at 510 nm (± 10 nm). Then excitation spectra (exc. at 250-450 nm, em. at 510 nm) were recorded.

Analysis

Excitation spectra of dilutions were compared, and dilutions were reliable when an isosbestic point was visible. Outliers due to measurement errors were excluded from further analysis (see Figure 10 d).

Background-corrected fura ratios were calculated. Since background without fluorescence indicator was similar for all solutions, high Ca/Mg solutions were chosen to be subtracted. The mean of the background ($F_{340,\text{BG}}$ and $F_{380,\text{BG}}$)^m was subtracted from every single value (F_{340} and F_{380})ⁿ: $F_{340} - F_{340,\text{BG}}$ and $F_{380} - F_{380,\text{BG}}$. Then, BG-corrected fura ratio was determined: $\text{ratio}_{\text{corr}} = (F_{340} - F_{340,\text{BG}}) / (F_{380} - F_{380,\text{BG}})$.

Fura-2 was calibrated for free Ca^{2+} concentrations in RB plotting the calculated free Ca^{2+} concentration (determined with maxchelator;¹²¹ only Ca^{2+} concentrations within the EGTA buffering range were included, cf. Table 6) against the $\text{ratio}_{\text{corr}}$ subtracted by the value without free Ca. The data were fitted using the BoxLucas1 function $y = a(1 - e^{-bx})$.

Free calcium concentrations were then recalculated inserting $\text{ratio}_{\text{corr}}$ into the determined calibration curve. Then, input CaEGTA concentrations were plotted against the recalculated free calcium concentrations.

Dissociation constants (K_d) were determined using a single excitation wavelength,¹²⁰ here 340 nm. In a double log plot, calculated free Ca^{2+} concentrations were plotted against the ratio of $(F_{340} - F_{340,\text{min}}) / (F_{340,\text{max}} - F_{340})$. The minimal fluorescence signal $F_{340,\text{min}}$ was the mean of the fluorescence signal at 340 nm of zero Ca/Mg solution with the indicator present. The maximal fluorescence signal $F_{340,\text{max}}$ was the mean of the fluorescence signal at 340 nm of high Ca/Mg solution with the indicator present. The K_d could then be calculated from the x-intercept of the linear regression line.

Material and equipment

- **Fura-2, pentapotassium salt, cell impermeant** (Fisher Scientific # F1200; stock in DMSO)
- **Mag-fura-2, tetrapotassium salt, cell impermeant** (Fisher Scientific # M1290; stock in DMSO)
- **TPEN** (N,N,N',N'-tetrakis(2-pyridylmethyl)ethylenediamine; Sigma # P4413)
- Respiration buffer (RB, see p. 23)
- Black microplate (PS, 96 well, F-bottom (chimney well); Greiner Bio-One # 655076)
- Plate reader (Tecan, Infinite M200 PRO)

^m $F_{340,\text{BG}}$: Fluorescence at exc. of 340 nm (em. 510 nm) of background control (high Ca/Mg solution without indicator)

$F_{380,\text{BG}}$: Fluorescence at exc. of 380 nm (em. 510 nm) of background control (high Ca/Mg solution without indicator)

ⁿ F_{340} : Fluorescence at exc. of 340 nm (em. 510 nm) of solutions containing indicator

F_{380} : Fluorescence at exc. of 380 nm (em. 510 nm) of solutions containing indicator

2.15 Photometric activity assays of single respiratory chain complexes

Assays were based on the protocol by Frazier et al. (2002).¹²²

Sample preparation

The activity of respiratory chain enzymes was measured using spectrophotometry. Frozen bovine heart mitochondria were subjected to three freeze-thaw cycles in liquid nitrogen either in hypotonic buffer (25 mM KPB (pH 7.4), 5 mM MgCl₂ in a concentration of 1 mg/mL; for CI and CII) or HWS (concentrated stock 30-40 mg/mL; for CIII) and stored at -70 °C.

To monitor each complex' activity without purification of the respective enzyme, only the substrate and acceptor of the RCC of interest were used. The other RCCs were inhibited. **Table 7** is summing up the substances used for each complex. Measurements were carried out in technical triplicates, at 37 °C in special UV-transparent 96-well microplates. For fluorescence-based measurements, black 96-well plates with a clear bottom were used to allow bottom reading.

Table 7 | Substances and conditions for activity measurements of respiratory chain enzymes. Absorption of underlined substances was followed at listed wavelengths.

Complex	I	II	III
Substrate	100 µM <u>NADH</u>	10 mM succinate	20 µM decyl-UQH ₂
Acceptor	50 µM CoQ1	50 <u>CoQ1</u>	10 µM <u>cytochrome c</u>
Inhibitor (other complexes)	10 µM antimycin A 1 mM KCN	2.5 µM rotenone 10 µM antimycin A 1 mM KCN	2.5 µM rotenone 1 mM KCN
Inhibitor (same complex)	0.2 µM rotenone	5 mM malonate	10 µM antimycin A
Wavelength (nm)	340	280	550

Complex I as NADH:CoQ1 oxidoreductase

NADH:CoQ1 oxidoreductase activity was followed by the loss of NADH absorption at 340 nm: NADH (reduced, absorbs at 340 nm) + H⁺ + CoQ1 (oxidized) → NAD⁺ (oxidized, no absorption at 340 nm) + H₂CoQ1 (reduced).

If not indicated otherwise, CI assay buffer contained 10 mM Tris (pH 7.4), 0.1 % (w/v) BSA, 100 µM NADH, 10 µM antimycin A and 1 mM KCN.

- CI assay buffer and a mixture of CoQ1 and CoQ of interest or ethanol were added to the wells. To account for rotenone-insensitive activity, for each sample a control containing 0.2 µM rotenone was prepared in parallel. As a vehicle control, DMSO was added to samples without rotenone. 96-well microplates were equilibrated for 10 min at 37 °C. Absorption spectra (230–900 nm, 3-nm steps) and a 5-min baseline were recorded.
- After addition of 3 µg mitochondria, Complex I activity was followed by the decrease of NADH absorption.

Complex II as succinate:CoQ1 oxidoreductase (SQR)

Succinate:CoQ1 oxidoreductase was measured at 280 nm: succinate + CoQ1 (oxidized, absorbs at 280 nm) → fumarate + H₂CoQ1 (reduced).

CII assay buffer usually contained 10 mM Tris (pH 7.4 at 37 °C), 2.5 μM rotenone, 10 mM sodium succinate, 10 μM antimycin A, 1 mM KCN. Changes are noted in figure legends.

- a) CII assay buffer was pipetted into the wells and incubated at 37 °C for 10 min. The baseline was recorded for 3 min.
- b) 3 μg mitochondria were added and the baseline was recorded for 10 min.
- c) The CoQ1 mixture (CoQ1 and CoQ of interest or ethanol) was added and CII activity was measured.

Complex III as decyl-ubiquinol:cytochrome *c* oxidoreductase

Decyl-UQH₂:cytochrome *c* oxidoreductase activity was measured by the increase of reduced cytochrome *c* at 550 nm: decyl-UQH₂ (reduced) + cytochrome *c* (oxidized) → decyl-UQ (oxidized) + cytochrome *c* (reduced, absorbs at 550 nm).

CIII assay buffer contained 50 mM KP_i (pH 7.4), 1 mM *n*-dodecyl maltoside, 0.1 % (w/v) BSA, 2.5 μM rotenone and 1 mM KCN.

- a) CIII assay buffer was added to the wells and incubated at 37 °C for 10 min; the baseline was recorded for 3 min.
- b) 3 μg mitochondria or 50 mM KP_i was added, followed by 3 min of measurement.
- c) 15 μM cytochrome *c* was added and another 3 min were recorded.
- d) Reduced decyl-UQ started the reaction that was followed by cytochrome *c* reduction.
- e) A few grains of L-ascorbic acid were put into each well to fully reduce cytochrome *c*. This value can be subtracted from each data point to analyse the turn-over of cytochrome *c* over time.

Quinone reduction

A few milligrams of sodium borohydride (NaBH₄) were weighed into a 1.5-mL reaction tube and centrifuged to focus the powdery reducing agent at the bottom of the tube. Ethanolic quinone stock solution (yellow; here: decyl-ubiquinone) and 0.5 μL of 3 M HCl were added. The solution turned transparent and was centrifuged (10 000 x g, 2 min, RT) to remove excess solid of NaBH₄. The supernatant was transferred into a new tube carefully leaving a layer of solution above the borohydride pellet not to carry any of it into the supernatant. This procedure was repeated until neither bubbles were formed upon addition of HCl nor a pellet was visible after centrifugation.

Analysis

Initial linear rates were analysed for all complexes. The dose-response curve of CII inhibition by HO-CoQ10 was fitted with the OriginLab function DoseResp ($y = A_1 + (A_2 - A_1)/(1 + 10^{(\log x^0 - x) \cdot p})$) and instrumental weighting.

Measuring parameters

Absorption was measured using a plate reader (Tecan, Infinite M200 PRO) set to 37 °C. Before starting the measurement, the plate was shaken (orbital, 6 mm amplitude) for 5 s. After a delay of 25 s, absorption was recorded every 15 s using 1 light flash. Kinetics were recorded for 2 h.

Absorption was measured at 340 (± 4.5) nm, 280 (± 2.5) nm, and 550 (± 4.5) nm for CI, CII, and CIII, respectively.

Fluorescence detection: NADH was excited at 340 (± 9) nm and emission was collected at 450 (± 20) nm using 1 light flash. The integration time was set to 20 μ s and the manual gain to 120.

Material and equipment

- β -nicotinamide adenine dinucleotide, reduced dipotassium salt (**NADH**, Sigma # N8129; aliquots of 100 mM stock in H₂O were stored at -80 °C, thawed right before use and exposed to KPBS minimal amount of time)
- **Succinate** (sodium succinate dibasic hexahydrate; Sigma-Aldrich # S2378; 1 M in H₂O at pH 7 adjusted with HCl, stored at -20°C)
- Decyl-ubiquinone (**decyl-UQ**; Sigma # D7911; 10 mM in ethanol, stored in liquid nitrogen)
- **Cytochrome c** from equine heart (MW 12,384, Sigma # C2506; 5 mM in H₂O)
- **Rotenone** (Sigma # R8875; 1 mM in DMSO, stored at -20°C, discarded after thawing)
- **Malonic acid** (Sigma # M1296; 1 M in H₂O, add small volume of water, titrate to pH 6.0 with 5 M KOH in 2- μ L steps, fill up to 1 M)
- **Antimycin A** from *Streptomyces* sp. (~ 532 g/mol, Sigma # A8674; 40 mM in DMSO, stored at -20 °C)
- **Oligomycin** from *Streptomyces diastatochromogenes* (Sigma # O4876)
- **KCN** (potassium cyanide; Sigma # 60178; 100 mM stock solution in KPBS or Tris was stored in aliquots at -80 °C and discarded after thawing once)
- Bovine serum albumin, fatty acid free (**BSA**, MW 66k, Sigma # A7030)
- UV-STAR® microplate (96 well, PS, F-bottom (chimney well); Greiner Bio-One # 655076)
- VIEWSEAL sealer, *UV-transparent foil for 96 well plates* (clear, Greiner Bio-One # 676070)
- 96-well microplate (flat bottom, black/clear bottom, Corning™ # 353219)
- Plate reader (Tecan, Infinite M200 PRO)

2.16 Blue-native-gradient polyacrylamide gel electrophoresis of respiratory chain complexes

The respiratory chain complexes were separated in their native state by blue-native gradient polyacrylamide gel electrophoresis (BN-gradient PAGE) using an established protocol provided by the working group of Prof. Dr Martin van der Laan (Department of Medical Biochemistry & Molecular Biology, Saarland University).

Gel preparation

Gradient gels are poured using a Hoefer™ gradient maker (SG30) in combination with a Gilson minipuls® peristaltic pump starting with 10% and immediately opening the 5% valve to create a continuous gradient.

After solidifying for 45 min at 4 °C, the stacking gel is layered on top. The gel is cooled until loading the samples.

Sample preparation

Mitochondria are thawed on ice and spun at maximal speed (~ 21 000 x g) for 10 min (4 °C). The supernatant is discarded and mitochondria are suspended in 50 µL solubilisation buffer with a 1 mL pipette tip avoiding bubble formation. To assure a similar degree of solubilisation up-and-down pipetting needed to be equivalent for all samples. The samples are incubated on ice for 15 min. After centrifugation (21 000 x g, 10 min, 4 °C), the supernatant is transferred to a new, pre-cooled tube. 5 µL 10x loading buffer is added and mixed carefully. Before loading 50 µL of the sample, it is centrifuged for 30 s at 21 000 x g, 4 °C.

Electrophoresis

Lanes are carefully layered with cathode buffer after loading the samples and high molecular weight marker. The gel is run for about 15 min at 100 V until samples run through most of the stacking gel. Separation is run at 600 V or at 80 V overnight. Using a water pump and magnetic stirring, the gel is continuously cooled to 4°C. To reduce background staining, the cathode buffer is replaced with fresh cathode buffer without Coomassie Blue as soon as blue dye front migrated halfway through the gel.

Material

- **3x gel buffer:** 200 mM ε-amino n-caproic acid, 150 mM Bis-Tris/HCl pH 7.0
- **Acrylamide:** 96 g acrylamide, 3 g bis-acryl, in 200 mL (49.5% T, 3% C)
- **5% acrylamide:** 3 mL 3x gel buffer, 0.91 mL acrylamide, 38 µL 10% APS, 3.8 µL TEMED, 5.014 mL H₂O
- **10% acrylamide:** 3 mL 3x gel buffer, 1.82 mL acrylamide, 1.8 mL glycerol, 30 µL 10% APS, 3 µL TEMED, 2.347 mL H₂O
- **Stacking gel (4% acrylamide):** 2.5 mL 3x gel buffer, 0.6 mL acrylamide, 30 µL 10% APS, 3 µL TEMED, 4.367 mL H₂O
- **10x anode buffer:** 500 mM Bis-Tris/HCl pH 7.0
- **10x cathode buffer:** 500 mM Tricine pH 7.0, 150 mM Bis-Tris, 0.2% Coomassie Brilliant Blue G-250
- **Loading dye (10x):** 100 mM Bis-Tris, pH 7.0, 500 mM ε-amino n-caproic acid, 5% (w/v) Coomassie Brilliant Blue G-250
- **Solubilisation buffer:** 10 g/g^o digitonin (1%) or 1.6 or 2 g/g DDM (n-dodecyl β-D-maltoside), 20 mM Tris/HCl, pH 7.4, 0.1 mM EDTA, 50 mM NaCl, 10% glycerol, 1 mM PMSF (0.1 M in isopropanol, - 20°C)
- *n*-Dodecyl β-D-maltoside (**DDM**, Sigma-Aldrich # D4641)
- Digitonin (Matrix Bioscience # 60105; 5% in H₂O, heated to dissolution (< 100°C), stored at 4°C)
- High molecular weight marker (GE Healthcare)
- Hoefer gel system (SE600 series)
- Hoefer™ gradient maker SG30
- Gilson minipuls® 3

^o g/g, mass of detergent per mass of mitochondrial protein

2.17 Western Blot

The protocol was provided by and western blot was performed with Dr Karina von der Malsburg (Department of Medical Biochemistry & Molecular Biology, Saarland University).

PVDF membranes are rinsed in methanol and kept in transfer buffer until further use. The gel is soaked in 1x SDS-PAGE running buffer for approximately 5 min right before blotting. Proteins are transferred by semi-dry blotting technique applying 220 mA for 2 h. PVDF membranes are stained with Coomassie Blue staining solution and the background is eliminated using destaining solution to tag weight marker bands. Using methanol, the membranes are destained completely prior to blocking in TBS with 5% skimmed milk powder. Antibody incubations are performed for 1 h at RT or overnight at 4 °C. Washes are performed with TBST containing 5% skimmed milk powder.

Material

- **Transfer buffer:** 20 mM Tris, 150 mM glycine, 0.02% SDS, 20% methanol
- **10x TBS:** 200 mM Tris/HCl (pH 7.5), 1.25 M NaCl
- **10x TBST:** 200 mM Tris/HCl (pH 7.5), 1.25 M NaCl, 0.1% Triton X-100
- **SDS-PAGE running buffer:** 1.87 M Tris, pH 8.8
- **Staining solution:** 50% H₂O, 40% ethanol, 10% acetic acid, 1% Coomassie Brilliant Blue G-250; + a few mL methanol
- **Destaining solution:** 50% H₂O, 40% ethanol, 10% acetic acid; + a few mL methanol
- Antibodies were dissolved in TBST + 5% skimmed milk powder, used dilutions are given in parenthesis
 - Primary polyclonal rabbit antibodies were provided by Prof. Dr Peter Rehling (Department of Cellular Biochemistry, University of Göttingen)
 - ATP5B: # 4826 (1:5000)
 - Cox4-I: # 1522 (1:500)
 - Rieske: # 1512 (1:2000)
 - NDUFB8: # 3764 (1:4000)
 - Secondary antibody: Goat Anti-Rabbit IgG Antibody, HRP conjugate (Millipore # AP187P)

2.18 In-gel activity staining of respiratory chain complexes

To ensure that Coomassie Blue staining does not mask in-gel activity staining, sample buffer contained only 10% of usual Coomassie Blue concentration.¹²³ Complex I and II activity was measured on the basis of the protocol from Jung et al. (2000).¹²⁴ After electrophoresis, gels were transferred into containers filled with 10 mM Tris (pH 7.4). The stacking gel was removed and lanes or complexes were cut out to allow different incubations. In-gel activity staining was performed in well plates appropriate for the size of the gel pieces. To ensure uniform distribution of the assay buffer, well plates were incubated on a rocking shaker. During incubation, gel pieces were transferred onto a glass plate to measure formazan staining densitometrically.

Complex I

Gels were incubated with 140 μ M NADH as a Complex I substrate and 1 mg/mL NBT as acceptor. The buffer was changed from 100 mM to 10 mM Tris/HCl (pH 7.4) to match spectrophotometric assay conditions. The formazan precipitate was quantified.

Complex II

To measure Complex II activity, 84 mM succinate was used as a substrate. 0.2 mM PMS and 2 mg/mL NBT were used to detect CII activity. The buffer was changed from 50 mM KPB to 10 mM Tris/HCl (pH 7.4) without influencing the staining. KCN was omitted since background signals were higher with KCN present. EDTA was omitted to facilitate planned measurements with added calcium.

Analysis

Bands were quantified using Image Lab™. Background was subtracted and signals were normalized to a reference signal measured together with the gel to avoid measurement errors due to changes in instrument settings.

Material

- **NADH** (β -Nicotinamide adenine dinucleotide, reduced disodium salt hydrate; Sigma-Aldrich # N8129-50MG; aliquots of 100 mM stock in H₂O were stored at -80 °C and thawed right before)
- **NBT** (Nitrotetrazolium Blue chloride; Sigma-Aldrich # N6876-250MG ; 10 mg/mL in H₂O for 1-2 weeks at 4°C, protect from light;)
- **Succinate** (sodium succinate dibasic hexahydrate; Sigma-Aldrich # S2378; 1 M in H₂O at pH 7 adjusted with HCl, stored at -20°C)
- **PMS** (Phenazine methosulfate; Sigma # P9625; 20 mM in H₂O stored at -20 °C for months, protect from light)
- **Rotenone** (Sigma # R8875; 1 mM in DMSO, stored at -20°C, discarded after thawing)
- **Malonic acid** (Sigma # M1296; 1 M in H₂O, add a small volume of water, titrate to pH 6.0 with 5 M KOH in 2- μ L steps, fill up to 1 M)
- **Tris base** (Trizma® base; Sigma # T1503)
- **Loading dye** (10x): 100 mM Bis-Tris, pH 7.0, 500 mM ϵ -amino n-caproic acid (prevents aggregation of proteins), 0.5% (w/v) Coomassie Brilliant Blue G-250
- Image Lab™ Software, Version 3.0.1 (2010, Bio-Rad Laboratories)
- Gel documentation system ChemiDoc™ XRS+ system (Bio-Rad Laboratories)

2.19 Detection of reactive oxygen species

2.19.1 H₂O₂ production assay using Amplex™ UltraRed

Extramitochondrial H₂O₂ production rate was detected using the Amplex™ UltraRed (AUR) assay. In a 96-well plate (black, clear bottom), 100 μ L substrate solution (2 x the final, desired concentration), 50 μ L assay buffer (4 x concentrated stock of AUR, HRP and SOD), and 50 μ L mitochondria (4 x concentrated stock, 40 μ g/mL) were pipetted.

Final concentrations in respiration buffer (RB1) were: 100 µg/mL mitochondria, 50 µM AUR, 0.5 U/mL HRP, 50 U/mL SOD, 10 µM CoQ, 1% solvent (ethanol or water), 0.5 µM rotenone, 5 mM malonate, 10 µM antimycin A, 1 mM KCN, 5 mM pyruvate/malate, 10 mM succinate, 1 mM ADP.

For mitochondria and the ADP-inhibitor mixture a multichannel pipette, for substrate and assay buffer a stepper pipette was used.

2.19.2 Extramitochondrial H₂O₂ accumulation using Amplex™ UltraRed

To detect extramitochondrial H₂O₂ accumulation, mitochondria were incubated at 37 °C in a 24-well cell culture plate in absence of AUR and HRP. Every 2 min samples were resuspended, 2 x 50 µL were retrieved, transferred to a 96-well plate (black, clear bottom) where 50 µL assay buffer (RB1, 100 µM AUR, 1 U/mL HRP) was preadded shortly before, and fluorescence was recorded. The starting volume was 1.4 mL respiration buffer (RB1). 0.2 mg/mL mitochondria, 5 mM P/M, 1 mM ADP, and sample (10 µM CoQ, 1% solvent, 10 µM antimycin A) were added at indicated times.

Measuring parameters

Fluorescence was measured in bottom reading mode using a plate reader (Tecan, Infinite M200 PRO) set to 37 °C. Before starting the measurement, the plate was shaken (orbital, 6 mm amplitude) for 5 s. After a delay of 5 s, fluorescence was recorded once or every 3 min for 2 h using multiple reads per well (3x3) and the following parameters: excitation, 535 (± 9) nm; emission, 590 (± 20) nm; gain, 55; number of flashes, 2; lag time, 40 µs.

Analysis

To calculate the H₂O₂ production rate, AUroX traces were differentiated (1st derivative) using 5 data points at a time and Savitzky-Golay smoothing (2nd order polynomial regression). The maximal production rate was compared between samples.

Material

- **Amplex™ UltraRed** reagent (AUR, Thermo Fisher Scientific, Invitrogen™ # A36006)
- Superoxide dismutase from bovine erythrocytes (**SOD**, Sigma # S7571; 10 kU/mL in H₂O)
- Peroxidase from horseradish, Type VI-A (**HRP**, Sigma # P6782 (type VI-A) or # P8415 (type XII))
- Hydrogen peroxide (**H₂O₂**, 30 wt. % in H₂O, Sigma # 216763)
- RB1 (see p. 23)
- **Sodium pyruvate** (Sigma, # P2256)
- L-(–)-Malic acid (**malate**, Sigma, # M1000; 1 M in H₂O at pH 7 adjusted with KOH, stored at - 20 °C)
- **Succinate** (sodium succinate dibasic hexahydrate; Sigma-Aldrich # S2378; 1 M in H₂O at pH 7 adjusted with HCl, stored at - 20°C)
- Glycerol-3-phosphate (**G3P**, Sigma # G7886; 0.9 M in H₂O, stored at - 20 °C)
- Adenosine 5'-diphosphate monopotassium salt dihydrate (**ADP**, Sigma # A5285)
- **Rotenone** (Sigma # R8875; 1 mM in DMSO, stored at - 20°C, discarded after thawing)

- **Malonic acid** (Sigma # M1296; 1 M in H₂O, add a small volume of water, titrate to pH 6.0 with 5 M KOH in 2- μ L steps, fill up to 1 M)
- **Antimycin A** from *Streptomyces* sp. (~ 532 g/mol, Sigma # A8674; 40 mM in DMSO, stored at - 20 °C)
- 96-well microplate (flat bottom, black/clear bottom, Corning™ # 353219)
- Plate reader (Tecan, Infinite M200 PRO)
- Origin 2018.b, Minitool for differentiation

2.19.3 Simultaneous detection of superoxide and oxygen using electron spin resonance spectroscopy

Freshly isolated mitochondria were incubated for 3 min at 37 °C together with the substrate in RB1. Then trityl, ADP and CMH were added rapidly. The sample was then transferred into a 50- μ L glass capillary and measured immediately.

Measuring parameters

Sample temperature, 37 °C; microwave attenuation, 10 dB; microwave power, 20 mW; modulation amplitude, 0.79G; receiver gain, 60 dB; modulation frequency, 100 kHz; conversion time, 10 s; time constant, 10 ms; centre field, 3466 G (3 G before trityl signal, 3 G after neighbouring CMH signal); sweep width, 20 G; microwave frequency, 9.5 GHz;

Analysis

Absorption intensity was quantified as the peak-to-peak height of the first derivative of the absorption spectrum (Figure 11). The CM radical (nitroxyl radical) absorption intensity was converted using 100 μ M tempol as a standard for nitroxyl radical concentration. According to recent publications^{125,126} not the commonly used peak width but the signal height of the oxygen-dependent saturation of the trityl signal was analysed.

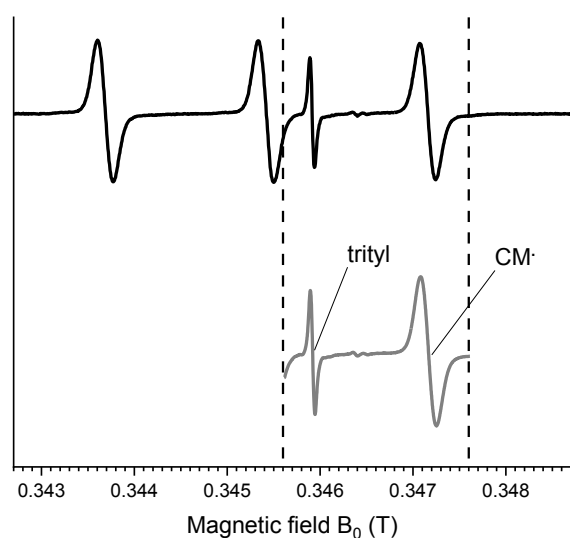


Figure 11 | Comparison of standard CMH measurement (top) to CMH/trityl detection with reduced field sweep width and shortened time interval (bottom).

Material

- 4-Hydroxy-2,2,6,6-tetramethylpiperidine 1-oxyl (**tempol**, 4-Hydroxy-TEMPO; Sigma # 56516)
- **CMH** (1-hydroxy-3-methoxycarbonyl -2,2,5,5-tetramethylpyrrolidine, Noxygen # NOX-02.1-50mg; 10 mM in oxygen-depleted water containing 25 μ M DF/5 μ M DETC, stored in aliquots at -20 °C)
- Tetrathiatriarylmethyl solution (**trityl**, OXO-63, oxygen label, 200 μ M aqueous solution, Noxygen # NOX-15.1-200 μ M)
- Diethyldithiocarbamic acid sodium salt (**DETC**, Noxygen # NOX-10.1-1g)
- Deferoxamine methanesulfonate salt (**DF**, Noxygen # NOX-09.1-100mg)
- RB1 (see p. 23)
- **Sodium pyruvate** (Sigma, # P2256)
- L-(–)-Malic acid (**malate**, Sigma, # M1000; 1 M in H₂O at pH 7 adjusted with KOH, stored at -20 °C)
- Adenosine 5'-diphosphate monopotassium salt dihydrate (**ADP**, Sigma, # A5285)
- **Rotenone** (Sigma # R8875; 1 mM in DMSO, stored at -20°C, discarded after thawing)
- **Malonic acid** (Sigma # M1296; 1 M in H₂O, add a small volume of water, titrate to pH 6.0 with 5 M KOH in 2- μ L steps, fill up to 1 M)
- **Antimycin A** from *Streptomyces* sp. (~ 532 g/mol, Sigma # A8674; 40 mM in DMSO, stored at -20 °C)
- Disposable **capillary** pipettes with ring mark, Ringcaps® (50 μ L, Noxygen # NOX-G.6-MC)
- PT-Capillary, gas permeable capillary (Noxygen # NOX-A.8.2-PT)
- **Critoseal** (Noxygen # NOX-A.3-VP)
- Electron paramagnetic resonance spectrometer (Bruker # ESP300, microwave controller # ER048R, cavity # ST9010N)
- Temperature & Gas Controller BIO-III (Noxygen # NOX-E.4-TGC)
- **LilaX** to record EPR spectra at 37 °C (in-house software, Gerhard Bracic)
- **Medeia** to read out EPR spectra (in-house software, Gerhard Bracic)

2.20 Low-temperature EPR of Complex I and II of the respiratory chain

Sample preparation

BHM in HWS were thawed on ice and subjected to three freeze-thaw cycles using liquid nitrogen. 1.5 mg BHM were suspended in 130 μ L KP_i (pH 7.4) and filled into a glass EPR tube using a long plastic tube attached to a Hamilton syringe to avoid air bubble formation. The samples were frozen stepwise in liquid nitrogen starting from bottom to top of the tube to prevent bursting of the glass tube due to volume expansion. The sample was then transferred into the cavity and measured at temperatures between 5 and 40 K. The temperature was adjusted and maintained accurately by a constant flow of liquid or gaseous helium. To add substrates or inhibitors, the samples were thawed and 10 μ L of a stock solution was added. When increasing concentrations were added to the same sample, the difference of the already contained and the desired concentration was added. Mixing was achieved by tapping the tube. The sample was concentrated at the bottom of the tube by abrupt shaking. Workflow is depicted in [Figure 12](#).

For Complex I, assay buffer additionally contained 0.1% BSA. For every measuring temperature, a baseline was recorded with buffer only.

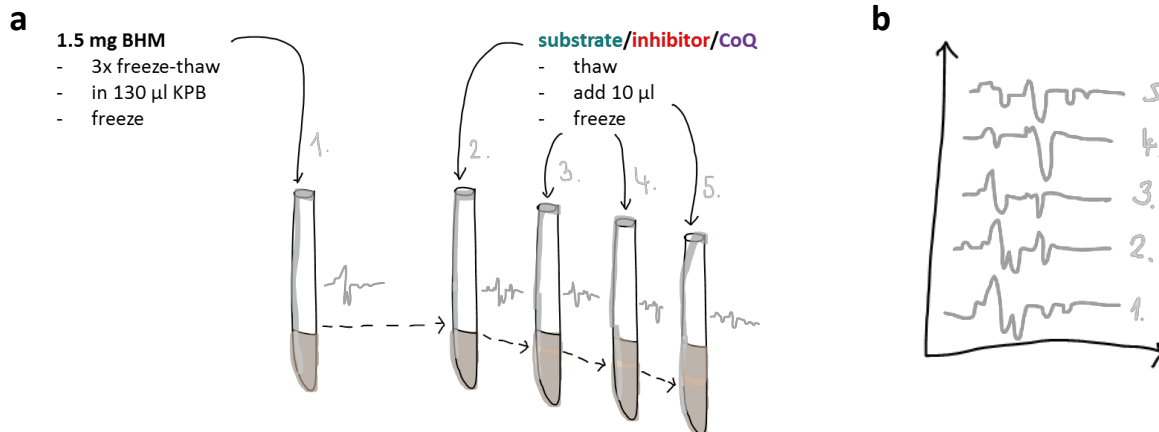


Figure 12 | Addition and measuring protocol of BHM for EPR measurements at low temperature. (a) BHM were lysed and transferred into a glass tube in a volume of 130 µL assay buffer, sample was frozen and a spectrum recorded. After recording, the sample was thawed and substances were added in a volume of 10 µL thereby increasing the sample volume by 10 µL for every addition. (b) Upon freezing the sample a spectrum was recorded and measurements originating from one sample were plotted in one diagram from bottom (first measurement) to top (last measurement).

Measuring parameters

Sample temperature, 8-9 K; microwave attenuation, 15 dB; microwave power, 6.331 mW; modulation amplitude, 3 G; modulation frequency, 100 kHz; sweep width, 800 G; conversion time, 81.92 ms; time constant, 41 ms; centre field, 3366 G; microwave frequency, 9.43 GHz;

For each measurement of a sample 12 and in case of buffer controls 24 scans were summed up.

Analysis

Baselines were corrected using Xepi on a Silicon Graphics O2 workstation and a polynomial fit to signal-free regions of the EPR spectra. Then, background correction was performed by subtracting the buffer control from the sample spectra, taking into account the number of scans.

Absorption signals were first marked as indicated in **Figure 13**. Then signals presumably appearing at the same g-factor were colour-coded. To identify the peaks, temperature dependence of the signals was analysed and recorded absorption patterns were compared with patterns of muscle samples, isolated mitochondria and single complexes found in literature.

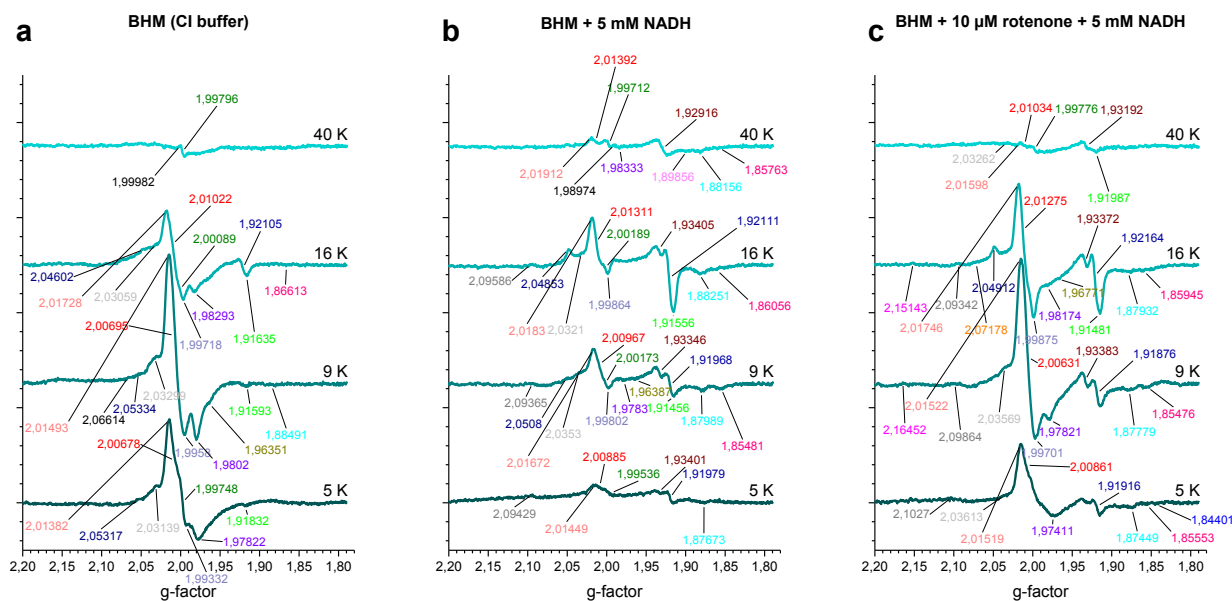


Figure 13| Objective spotting of g-factors of all EPR signals. Signals with a g-factor label above traces have a positive and negative signal portion; when g-factor label is below traces, signals have a positive or negative portion and are marked at the tip.

Material

- **BSA**, fatty acid free (bovine serum albumin; Sigma # A7030; 10% (w/v) in water)
- β -nicotinamide adenine dinucleotide, reduced dipotassium salt (**NADH**, Sigma # N8129; aliquots of 100 mM stock in H₂O were stored at -80 °C, thawed right before use and exposed to KPBS minimal amount of time)
- **Succinate** (sodium succinate dibasic hexahydrate; Sigma-Aldrich # S2378; 1 M in H₂O at pH 7 adjusted with HCl, stored at -20 °C)
- **Rotenone** (Sigma # R8875)
- **Atpenin A5** (AA5, CAYMAN # 11898; 1 or 10 mM in DMSO, stored at -20 °C)
- **Antimycin A** from *Streptomyces* sp. (~532 g/mol, Sigma # A8674; 40 mM in DMSO, stored at -20 °C)
- EPR (Elexsys 680, Bruker)
- EPR glass tube (inner diameter, 3 mm; Wilmad)
- Xepr on a Silicon Graphics O2 workstation for data recording and spectra evaluation (Bruker)
- Liquid helium continuous flow cryostat (ESR900, Oxford Instruments)
- Microwave frequency counter (5350B, HP Inc.)
- Vacuum pump
- **Medeia** for visualisation of spectra (in-house software, Gerhard Bracic)

3 Results

3.1 Synthesis of HO-CoQ10 in a two-phase system and identification of the main product

Since Coenzyme Q derivatives substituted with a hydroxy instead of a methoxy group on the quinone ring are not commercially available, the first important step of this work was to synthesize and purify these compounds in sufficient amounts. The purity was determined and the structure confirmed by mass spectrometry (MS) and nuclear magnetic resonance spectroscopy (NMR).

The synthesis of HO-CoQ10 in a two-layer system had been established in preceding experiments¹⁰⁻¹² including my master thesis and was started by adding 1 M sodium hydroxide to a solution of CoQ10 in the organic solvent tetrahydrofuran (THF) (Figure 14 a, left, detailed procedure in section 2.4, p. 24). Synthesis was easily scalable by using bigger flasks keeping the THF-to-NaOH volume ratio constant.

The alkaline demethylation of one methoxy group of CoQ10 probably follows an S_N2 mechanism (bimolecular nucleophilic substitution) as depicted in Figure 14 b and suggested for CoQ1 by Bogeski et al., though the intermediate had not been detected.⁸ The reaction involves a hydroxide anion attacking the positivated C-atom at the methoxy position of the quinone ring thereby forming a carbanion intermediate. Upon elimination of the leaving group methoxide, the quinone structure can be re-established. Due to the lipophilicity of CoQ10, a biphasic system using a strong organic solvent was advantageous. Even though THF and water are miscible, increasing the ionic strength of the aqueous phase to 1 M with NaOH results in a biphasic system. As illustrated in c, in NaOH, hydroxy anions are solvated with water molecules by formation of H-bonds. Introducing a layer of THF, apart from water molecules, some hydroxide can diffuse into the THF phase (as detected by UV/Vis spectroscopy of the organic layer, data not shown). Since THF does not offer positivated hydrogen atoms for H-bonding, solvation of HO⁻ is less effective, thus enhancing its nucleophilicity. The addition-elimination reaction takes place in the organic phase. Methoxide is cleaved off and migrating to the aqueous phase, might be protonated by water or will be stabilized by H-bonds from water. Both mechanisms may contribute to the nucleofugal activity of methoxide as leaving group.

From Figure 14 a it is evident that the reaction takes place in the upper organic phase. The course of the reaction could be followed by the colour change of this phase from yellow (Coenzyme Q10, left) to red-violet (product after 1 d incubation, right). In agreement with the colour impression, UV/Vis absorption at 430 nm decreased and a new band appeared with a bathochromic shift of 100 nm resulting in the reflection of violet light (Figure 14 d, 0 h, CoQ10 before addition of NaOH; 26 h, after incubation with NaOH for 26 h). This bathochromic shift is typical for the introduction of a hydroxy group to the benzoquinone ring.^{127,128} The absorption of the quinone ring at 280 nm declined gradually which was not solely due to appearance of reduced species but also to deprotonation of the added hydroxy group. The protonation state of the hydroxy group affected the colour: in neutral or high pH, the solution appeared violet, in low pH yellow-orange (data not shown).

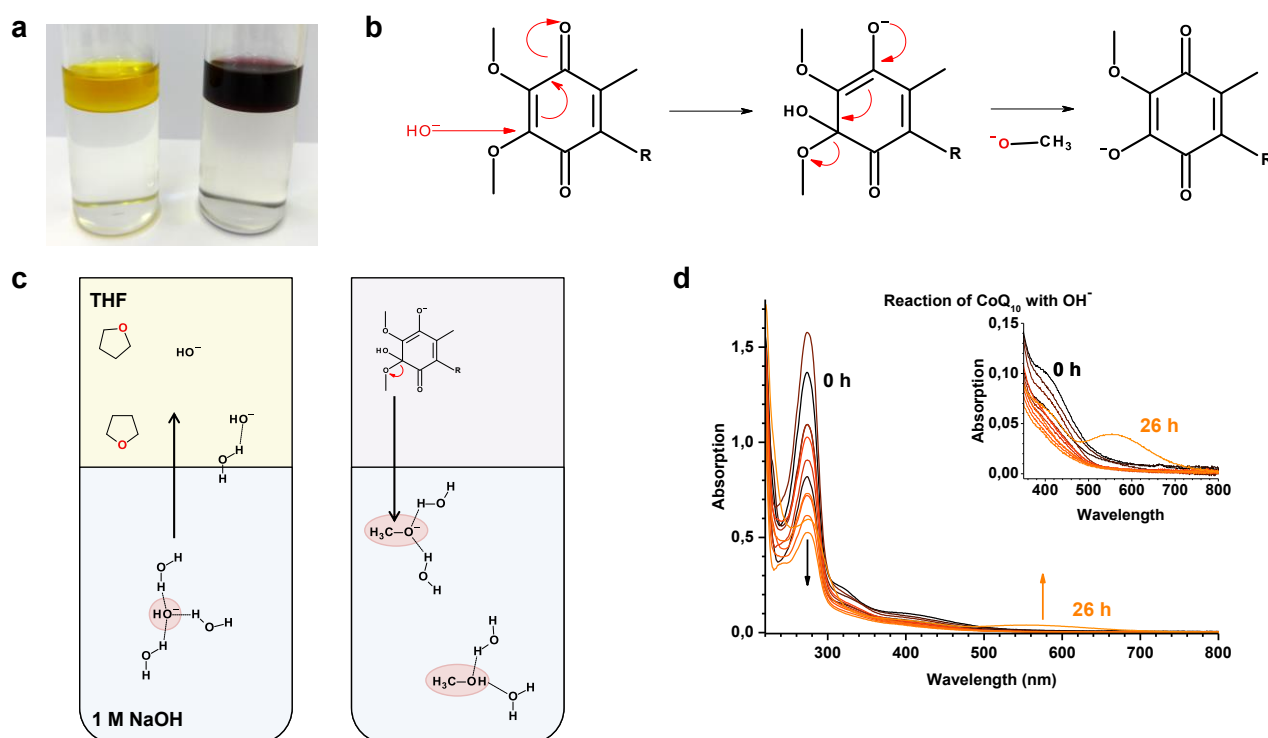


Figure 14 | Monohydroxy-CoQ₁₀ can be synthesized in a two-phase system consisting of tetrahydrofuran (THF) and 1 M NaOH. (a) 4 mM CoQ₁₀ dissolved in THF (upper phase) with 1 M NaOH (lower phase) directly after combining the reactants (left) and after 1 d incubation (right);¹¹ (b) addition-elimination mechanism of CoQ with hydroxide as *O*-nucleophile and methoxide as nucleofuge (one representative mesomeric structure of the intermediate carbanion is shown), (c) solvation/H-bonding of hydroxide (left) in aqueous (NaOH) vs. organic phase (THF) and the leaving group methoxide (right) or methanol after protonation by water; (d) UV/Vis spectra of diluted samples (0.1 mM in THF) of the upper reaction layer taken before (0 h) and during incubation with NaOH (1-26 h);¹² Experimental data are taken from my experiments preceding this thesis as indicated.

¹H-NMR, HPLC^p-MS/MS and HPLC-UV/Vis showed that after 24 h, even before the educt was consumed, the product's synthesis was saturated. Longer incubation times did not enhance the yield but led to more by-products like open ring structures with carboxylated ends (data not shown).¹¹ After stopping the reaction, the extracted and dried product mixture was purified using semi-preparative HPLC coupled to a UV/Vis detector set to maximal quinone ring absorption at 275 nm. Previous mass spectrometry analysis of the product fraction showed that the isolated product had the anticipated mass of 849 Da. From the reaction mixture the reactant, CoQ₁₀, and the product, HO-CoQ₁₀, were purified and ¹H-NMR spectra were recorded to identify the compound and to confirm the preservation of its isoprenoid chain during the reaction procedure. **Figure 15** a shows the structure of CoQ₁₀, where chemical shifts and multiplicity of proton signals are specified. From the overview of absorption spectra (**b**), it is obvious that signal patterns of CoQ₁₀ and the product are similar in shape, intensity and position, though methoxy signals at 4 ppm are decreased and shifted by 0.08 ppm (**b, c**), and two new signals at 6.5 ppm were detectable in the product (**b, d**). Besides, all signals of protons in direct vicinity to the quinone ring (**e**, methyl group at 5-position; **f**, first CH₂ of side chain) shifted in the product, whereas the proton signals derived from the isoprene side chain did not (**g**, CH groups and **h**, methyl groups of side chain). The proton count did not change for any signal except the methoxy signals (**c**). Hence, the product

^p HPLC, high pressure liquid chromatography

contains an intact isoprene side chain and is chemically modified at the methoxy position of the quinone ring. The new singlet signals at 6.05 ppm were shifted and diminished after addition of D₂O (dark blue curve in d). Thus, the H-D-exchangeable signal must be acidic and is likely to derive from a hydroxy group at the quinone ring. The two shifted methoxy signals in the product showed a peak intensity ratio of 1:2 (c) and the new signals of 2:1 (d). Furthermore, the decrease of the methoxy signals to a total proton count of 3 (c) and total proton count of the new signals of 1 (d), suggested the formation of two molecules that were modified at either the 2- or 3-position of the quinone ring.

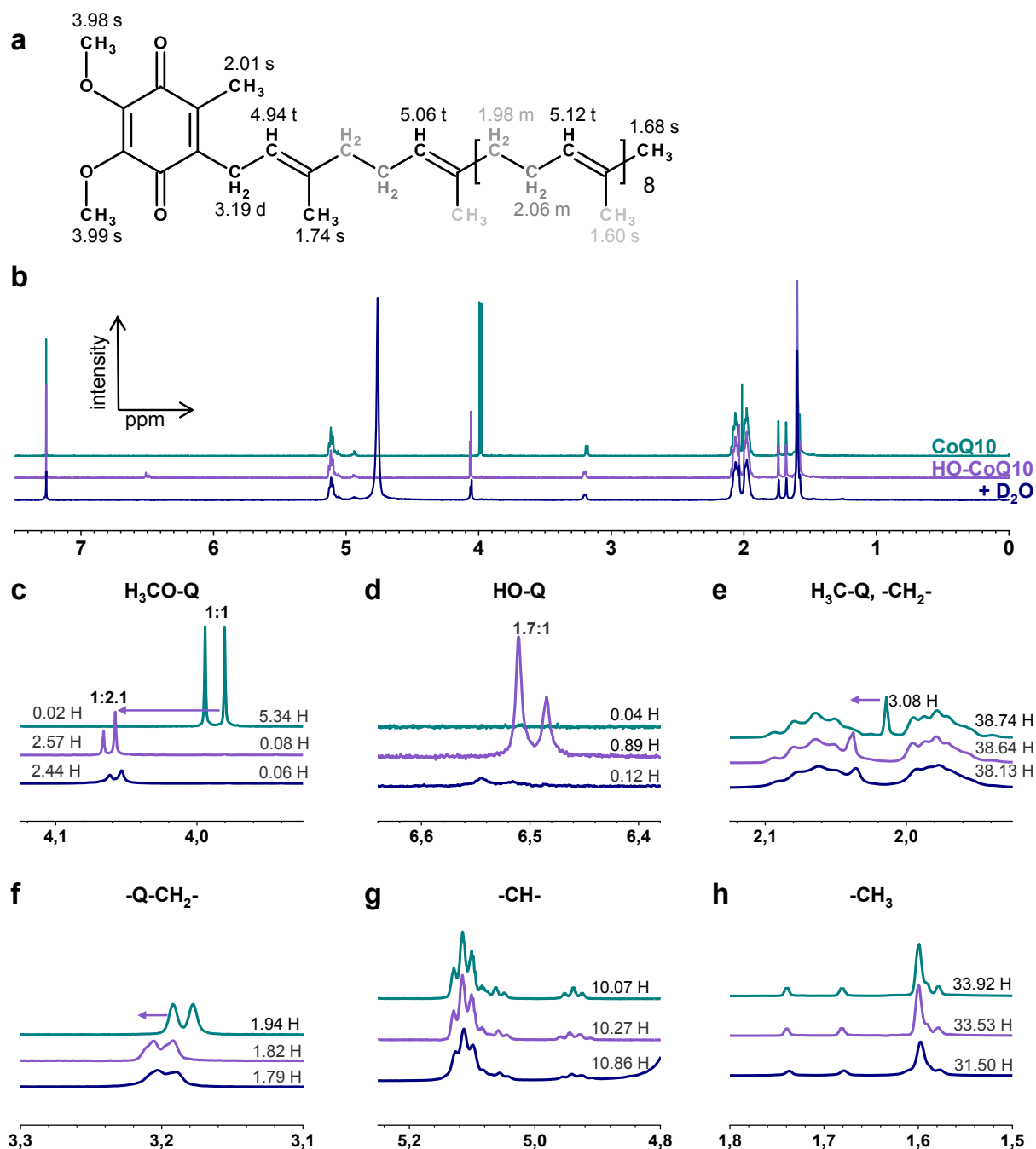


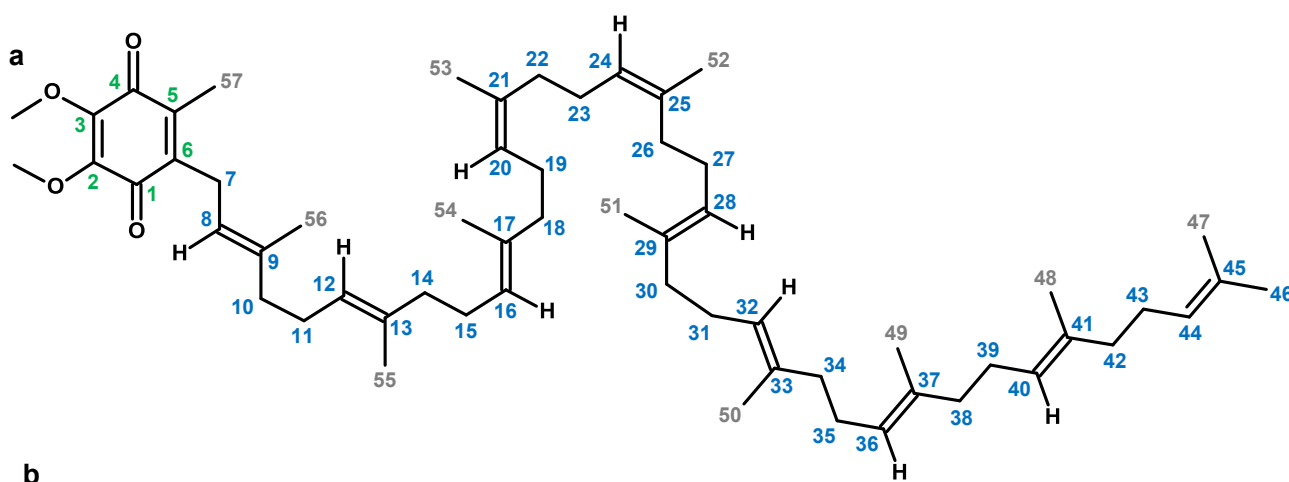
Figure 15 | Changed ¹H-NMR signals of protons in direct vicinity to the quinone moiety in the isolated product. ¹H-NMR (CDCl₃, 500 MHz, internal standard residual CHCl₃ set to 7.26 ppm); shifting of signals from the educt (CoQ10) to the product (HO-CoQ10) is highlighted with arrows (c, e, f), proton count normalized to 9 vinyl protons of the side chain (at 5.12 and 5.06 ppm) is stated. Recordings were performed during my Master thesis (2014).¹¹ (a) Structure and ¹H-NMR signal assignment of the educt Coenzyme Q10

from 2-D NMR;¹¹ multiplicity: s, singlet; d, duplet; t, triplet; m, multiplet; (b) comparison of spectra of the educt (cyan), the product (violet), and the product after addition of D₂O to test for H-D exchange (dark blue); details of ¹H signals (c) methoxy groups attached to Q shifted by 0.08 ppm, ratio of methoxy signal integrals is specified; (d) hydroxy group attached to Q, ratio of hydroxy signal integral is specified; (e) methyl group attached to Q shifted by 0.025 ppm, CH₂ groups of the side chain; (f) first CH₂ group of the side next to Q shifted by 0.015 ppm, (g) CH groups of side chain, (h) methyl groups of side chain; Q, quinone ring;

Having purified HO-CoQ10 in sufficient amounts allowed us to definitely confirm the structure of the anticipated product. The structure was determined using ¹H and ¹³C heteronuclear 2-D NMR. The proton signal at 6.05 ppm was assigned to a hydroxyl group located at 2- or 3-position of the quinone ring. The product contained two constitutional isomers. In Table 8 and Table 9, ¹³C and ¹H signals are listed and correlated signals are given in the same line.

All preparations showed two main products carrying a hydroxy group either at the position 2 or 3 on the quinone ring. The ratio of 2-HO-CoQ10 to 3-HO-CoQ10 was always 2:1 (Figure 15 c, d and Figure 16 b). Dihydroxy compounds where both methoxy groups were substituted could be detected via LC-MS in some non-purified samples, but not consistently and only minor amounts. It has been shown that high concentrations of NaOH and defined, prolonged incubation can produce didemethyl derivatives from fully substituted dimethoxyquinones.¹²⁹ Hence, reducing NaOH concentrations to yield a higher NaOH passage to the organic layer might open up the possibility to synthesize didemethylated CoQ10 derivatives.

Table 8 | 2-D NMR analysis of 2-demethyl CoQ10, i.e. 2-HO-CoQ10 (main product). (a) Structure of CoQ10 for reference and numbering of C-atoms, (b) C-atom, position of C-atom according to panel a is colour-coded: ring, green; main chain, blue; methyl groups, grey; δ , chemical shift; -, no correlation of ¹³C and ¹H-signal detected; multiplicity: br s, broad singlet; s, singlet; d, duplet; t, triplet; m, multiplet; 3H, intensity equals 3 protons; coupling constant J is given in Hertz;



C atom	δ_C	δ_H	C atom	δ_C	δ_H
2-OH	-	6.53 br s	29	134.93	-
3-OCH ₃	60.25	4.07 s (3H)	30	39.73	1.98 m
1	184.33	-	31	26.70	2.06 m
2	139.22	-	32	124.24	5.11 t (7 Hz)
3	137.10	-	33	134.93	-
4	183.95	-	34	39.73	1.98 m
5	140.65	-	35	26.70	2.06 m
6	139.33	-	36	124.24	5.11 t (7 Hz)

7	25.10	3.20 <i>d</i> (7 Hz)	37	134.90	-
8	118.54	4.94 <i>t</i> (7 Hz)	38	39.73	1.98 <i>m</i>
9	137.91	-	39	26.70	2.06 <i>m</i>
10	39.71	1.98 <i>m</i>	40	124.24	5.11 <i>t</i> (7 Hz)
11	26.45	2.06 <i>m</i>	41	134.87	-
12	123.74	5.05 <i>t</i> (7 Hz)	42	39.73	1.98 <i>m</i>
13	135.30	-	43	26.75	2.06 <i>m</i>
14	39.71	1.98 <i>m</i>	44	124.39	5.11 <i>t</i> (7 Hz)
15	26.65	2.06 <i>m</i>	45	131.24	-
16	124.10	5.11 <i>t</i> (7 Hz)	46	25.70	1.68 <i>s</i> (3H)
17	135.01	-	47	17.67	1.59 <i>s</i>
18	39.73	1.98 <i>m</i>	48	16.01	1.59 <i>s</i>
19	26.70	2.06 <i>m</i>	49	16.01	1.59 <i>s</i>
20	124.24	5.11 <i>t</i> (7 Hz)	50	16.01	1.59 <i>s</i>
21	134.93	-	51	16.01	1.59 <i>s</i>
22	39.73	1.98 <i>m</i>	52	16.01	1.59 <i>s</i>
23	26.70	2.06 <i>m</i>	53	16.01	1.59 <i>s</i>
24	124.24	5.11 <i>t</i> (7 Hz)	54	16.01	1.59 <i>s</i>
25	134.93	-	55	16.01	1.59 <i>s</i>
26	39.73	1.98 <i>m</i>	56	16.32	1.74 <i>s</i> (3H)
27	26.70	2.06 <i>m</i>	57	12.17	2.04 <i>s</i> (3H)
28	124.24	5.11 <i>t</i> (7 Hz)			

Table 9 | 2-D NMR data of 3-demethyl CoQ10, i.e. 3-HO-CoQ10 (secondary product). C-atom, position of C-atom according to **Table 8** a is colour-coded: ring, green; main chain, blue; methyl groups, grey; δ , chemical shift; -, no correlation of ^{13}C and ^1H -signal detected; multiplicity: br s, broad singlet; s, singlet; d, duplet; t, triplet; m, multiplet; 3H, intensity equals 3 protons; coupling constant J is given in Hertz;

C atom	δ_{C}	δ_{H}	C atom	δ_{C}	δ_{H}
2-OCH₃	60.25	4.06 <i>s</i> (3H)	29	134.93	-
3-OH	-	6.51 br s	30	39.73	1.98 <i>m</i>
1	183.16	-	31	26.70	2.06 <i>m</i>
2	139.13	-	32	124.24	5.11 <i>t</i> (7 Hz)
3	137.00	-	33	134.93	-
4	185.12	-	34	39.73	1.98 <i>m</i>
5	136.16	-	35	26.70	2.06 <i>m</i>
6	143.33	-	36	124.24	5.11 <i>t</i> (7 Hz)
7	25.10	3.20 <i>d</i> (7 Hz)	37	134.90	-
8	118.58	4.92 <i>t</i> (7 Hz)	38	39.73	1.98 <i>m</i>
9	137.84	-	39	26.70	2.06 <i>m</i>
10	39.71	1.98 <i>m</i>	40	124.24	5.11 <i>t</i> (7 Hz)
11	26.45	2.06 <i>m</i>	41	134.87	-
12	123.78	5.05 <i>t</i> (7 Hz)	42	39.73	1.98 <i>m</i>
13	135.26	-	43	26.75	2.06 <i>m</i>
14	39.71	1.98 <i>m</i>	44	124.39	5.11 <i>t</i> (7 Hz)
15	26.65	2.06 <i>m</i>	45	131.24	-
16	124.12	5.11 <i>t</i> (7 Hz)	46	25.70	1.68 <i>s</i> (3H)
17	135.99	-	47	17.67	1.59 <i>s</i>

18	39.73	1.98 <i>m</i>	48	16.01	1.59 s
19	26.70	2.06 <i>m</i>	49	16.01	1.59 s
20	124.24	5.11 <i>t</i> (7 Hz)	50	16.01	1.59 s
21	134.93	-	51	16.01	1.59 s
22	39.73	1.98 <i>m</i>	52	16.01	1.59 s
23	26.70	2.06 <i>m</i>	53	16.01	1.59 s
24	124.24	5.11 <i>t</i> (7 Hz)	54	16.01	1.59 s
25	134.93	-	55	16.01	1.59 s
26	39.73	1.98 <i>m</i>	56	16.32	1.74 s (3H)
27	26.70	2.06 <i>m</i>	57	11.60	2.04 s (3H)
28	124.24	5.11 <i>t</i> (7 Hz)			

For physiological experiments, it was essential to further purify the product. With each HPLC run, the purity of the preparation could be increased (Figure 16 a). The HO-CoQ10 content was determined by quantitative NMR using the hydroxy group at 6.5 ppm as a reference signal: preparation alpha (after 2 runs), 85.3%; gamma (after 3 runs), 91.4%. When the first CH₂ group of the side chain at 3.19 ppm was used as a reference, the calculated purities were 85.4% and 94.3%, respectively. Since not all hydroxy protons might have been visible due to deprotonation in the potentially acidic solvent CDCl₃, the pH-insensitive signal at 3.19 ppm should be more precise. However, contamination by the reactant CoQ10 can lead to overestimation since their signals overlap (cf. Figure 15 f). The contamination with CoQ10 was around 2% in preparation gamma, judged from the two methoxy signals at 3.9 ppm (Figure 16 c, gamma). The heights of those signals were equal which is why they can be clearly attributed to the educt. Taking into account this impurity, the total HO-CoQ10 content of preparation gamma can be calculated to be 92.3%. Considering the 2:1 ratio of the constitutional isomers, the product contained 61.5% 2-HO-CoQ10 and 30.8% 3-HO-CoQ10.

The CoQ10 content in preparation alpha was not determinable since more by-products were present (Figure 16 c, alpha, multiple peaks in methoxy region). The contamination with THF, a component of the mobile phase for chromatographic fractionation, detected at 3.74 and 1.85 ppm⁹⁴ was stable at ~ 0.5% across the preparations alpha and gamma (c, marked with *).

When the reaction was purified twice over a semi-preparative RP-HPLC (preparation alpha), at least 15.6% of the product was not the target compound as confirmed by the multitude of additional signals in the range of methoxy signal (c, alpha). When 3 purification runs were performed, the product contained only around 5.2% unknown molecules, that may be attributed to other by-products, impurities of the reactant or salt residues. If not mentioned otherwise, preparation γ was used for all experiments.

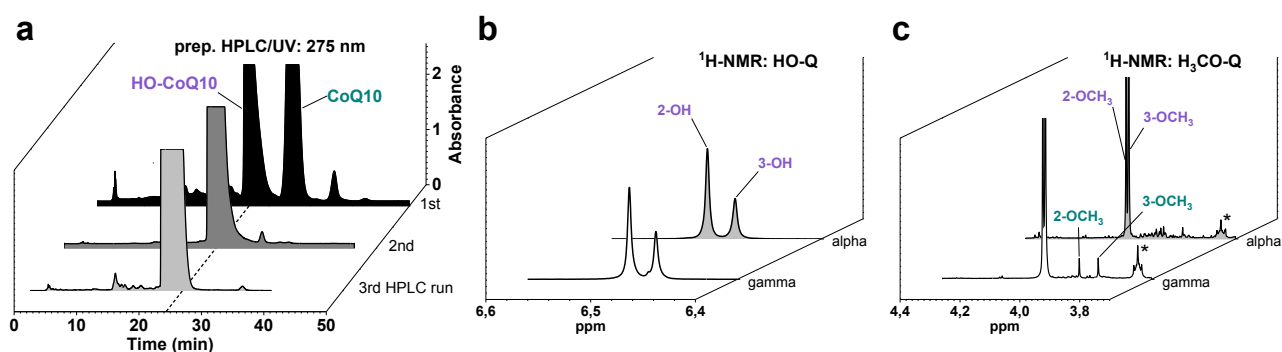


Figure 16 | 2-HO-CoQ10 was the main purified product of HO-CoQ10 synthesis. (a) Preparations were purified with semi-preparative HPLC coupled to a UV/ Vis detector (275 nm), number of run is listed; mass of injected material: 1st, 25 mg; 2nd, 14 mg; 3rd, 20 mg; from 2nd and 3rd run preparation alpha and gamma was collected, respectively; (b, c) ^1H NMR spectra (CDCl_3 , 500 MHz) of HO-CoQ10 preparations of increasing purity, completed runs of semi-preparative HPLC were: alpha, 2; gamma, 3; details of (b) hydroxy groups at 2- and 3-position on the quinone ring, integral ratios of 2-OH to 3-OH: alpha, 1.8:1; gamma, 1.7:1; (c) methoxy groups of HO-CoQ10 at 4.05 ppm (violet) and of CoQ10 at 3.9 ppm (cyan), *tetrahydrofuran impurity (3.76 ppm, multiplet), signal of methoxy signals is cut-off due to magnification to highlight small signals;

3.2 Dissolving of CoQ10 and HO-CoQ10 in aqueous media

Coenzyme Q10 is poorly water-soluble because of its highly lipophilic isoprenoid chain. Therefore, it was crucial to find a protocol to apply HO-CoQ10 and its control substance CoQ10 on biological samples. Since CoQ10 is slightly more lipophilic than HO-CoQ10, initial experiments were conducted with CoQ10 and only if successful with HO-CoQ10, additionally. There are various established methods to enhance the water-solubility of CoQ10: stock solutions in organic solvents, aqueous¹³⁰ and solid¹³¹ dispersion, and chemical modification to name a few.¹³² Since dissolving CoQ10 in an organic solvent and diluting this stock solution in buffer is the most straightforward approach, different solvents were tested and observations are summarized in Table 10.

THF and chloroform were the best solvents for CoQ10; most probably the only limiting factor for the stock solutions' concentration is their viscosity. Nevertheless, diluting these in water was not possible as the stock solution adhered to hydrophobic surfaces like pipette tips and walls of the plastic vial and did not mix with aqueous solutions.

After heating an inhomogeneous suspension of CoQ10 in DMSO, the formed solution was stable at room temperature. But as soon as it was added to water, a suspension formed. Even first dissolving CoQ10 in a strong solvent (here: THF or chloroform) and then diluting with DMSO,⁹⁵ did not improve its water solubility. The only suitable solvent was ethanol: solutions up to 1 mM CoQ10 were stable at RT after heating to ~ 40 °C and repeated mixing in an ultrasonic bath. Also, higher concentrations could be dissolved but did not stay in solution after cooling down. Still, the 1 mM stock solution could not be stored conveniently at 4 °C or -20 °C, since the substance would have precipitated. Freezing the stock in liquid nitrogen (melting point of ethanol, -114.1 °C)⁹⁷ was found to be an appropriate method for storage of aliquots: Upon thawing, mixing and warming up, the substance was redissolved easily.

Table 10 | Dissolving CoQ10 in organic solvents and performance of stock solutions after dilution in water. /, not tested; n.d., no characteristic CoQ10 UV/Vis absorption profile detectable; THF, tetrahydrofuran, CHCl₃, chloroform, DMSO, dimethyl sulfoxide; SOLN, solution; (+) hardly dissolved; SUSPN, suspension: +, inhomogenous; ++, homogenous; EMUL, emulsion; (+), not stable as emulsion; *stock solution stuck to pipette and borders of the vial, drop on surface; **stock solution stuck to pipette, vial bottom and borders; maximal possible concentration in parenthesis; the right column lists final used CoQ10 concentrations in aqueous media from stock solutions in corresponding solvents from various publications treating primary cells or cell lines with exogenous CoQ10;

Solvent	CoQ10 (μM)	RT			After heating to 40 °C		Dilution in H ₂ O	
		SOLN	SUSPN	EMUL	SOLN	Stable after cooling to RT		Final concentrations of CoQ10 in publications
THF	20-100	+			/	/	n.d.*	
CHCl ₃	1-100	+			/	/	n.d.**	50 μM ¹³³ , 58 μM ¹³⁴
DMSO	1.25		+		+	+	SUSP	20 μM ¹³⁵
THF/DMSO (1:5)	0.5		++	(+)	-	-	SUSP	
CHCl ₃ /DMSO (1:5)	0.5		++	(+)	-	-	SUSP	50 μM ⁹⁵ (stock in CH ₃ Cl/DMSO, 1% v/v DMSO)
Ethanol	1-10		+		+	+	10 μM 1% etOH	122 μM ¹³⁶ , 10 μM ¹³⁷ 10 μM from 5 mM stock ¹³⁸
Methanol	10		+?		(+)	-		200 μM ¹³⁹

Figure 17 displays the dilution of ethanolic CoQ10 and HO-CoQ10 stock solutions in water. The final concentration, here and in most of the following experiments, was 1% ethanol. Absorption spectra of 10 μM CoQ10 show the characteristic quinone absorption peak around 275 nm and absorption of visible light around 400 nm (a). Absorption intensity decreased continuously when the concentration of the CoQ10 stock solution in ethanol was increased from 1 mM to 4 mM. Even though CoQ10 could be dissolved in ethanol upon prolonged heating in concentrations up to 4 mM, dilution of these stock solutions in water containing 1% ethanol demonstrated their decreasing stability. Furthermore, concentrations higher than 1 mM CoQ10 could be dissolved in ethanol but precipitated after extended periods at RT whereas 1 mM CoQ10 remained in solution.

CoQ10 concentrations above 10 μM with a maximal solvent concentration of 1% ethanol are difficult to achieve and solvent concentrations higher than 1% ethanol should be avoided. Studies using higher CoQ10 concentrations by dilution of alcoholic solutions or strong organic solvents (Table 10, right column) are inconsistent with these observations.

Since concentrated HO-CoQ10 solutions (here: preparation alpha) were stable at RT, higher concentrations of HO-CoQ10 in 1% ethanol were achievable. The absorption spectra again show the absorption peak at 275 nm and an absorption band around 600 nm (b). The intensity of the absorption peak at 275 nm doubled when the dilution was increased from 25 to 50 μM confirming that dissolution was effective. Dilution to 100 μM HO-CoQ10 resulted in a clear solution that showed a characteristic absorption spectrum though intensity was above the linear detection limit. Working with HO-CoQ10 (especially the further purified preparation gamma)

showed that stock concentrations of 10 mM are possible but solution might be incomplete: heating time until dissolution increased and after centrifugation, the solution near the vial bottom comprised higher colour intensity. This was not the case for solutions up to 5 mM. Therefore, the maximal concentration for stock solutions in ethanol chosen was 5 mM HO-CoQ10.

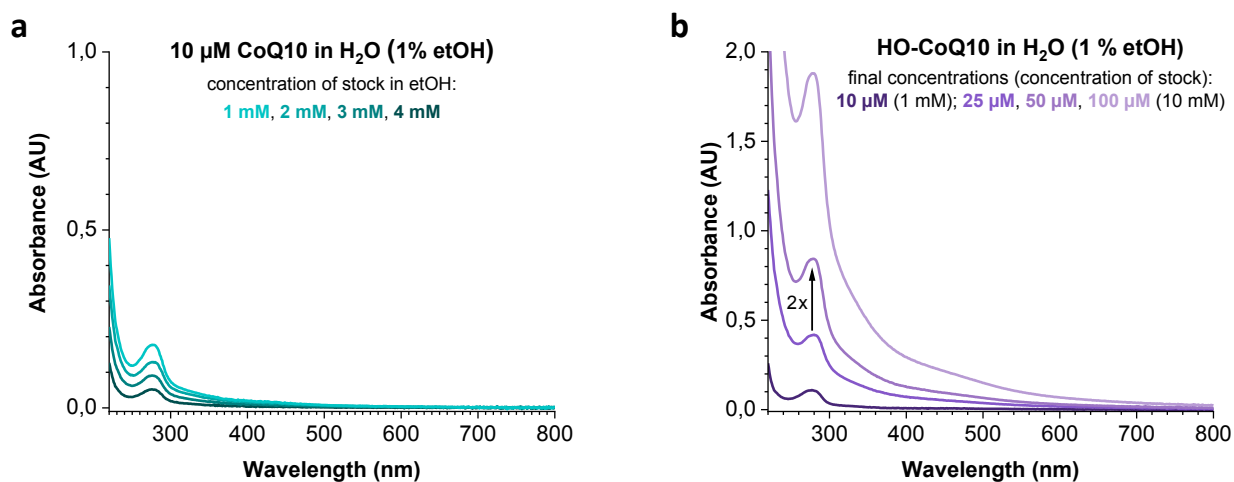


Figure 17 | Aqueous solution of CoQ10 and HO-CoQ10. UV/Vis absorption spectra of aqueous solutions of (a) CoQ10 and (b) HO-CoQ10 (preparation alpha); stock solutions were prepared in absolute ethanol and diluted in water; to obtain a final ethanol concentration of 1% from each stock solution, additional ethanol was supplied if necessary; (a) 10 µM CoQ10 diluted from stock solutions of different concentrations; (b) dilutions of HO-CoQ10 from 1 or 10 mM stock solutions, intensity of quinone absorption band at 275 nm doubled from 25 to 50 µM HO-CoQ10; shown are mean traces of duplicates in panels a and b;

3.2.1 Increased water-solubility of CoQ10 and HO-CoQ10 in a carrier complex with Cholesterol-PEG 600

Using ethanol as the solvent for stock solutions is limiting the maximal concentration in aqueous media to 10 µM and 50 µM for CoQ10 and HO-CoQ10, respectively. To increase the concentration of CoQ10 in aqueous systems, Cholesterol-PEG 600 (PCS) was tested as a carrier. Cholesterol-PEG 600 (see Figure 18 a) is a water-soluble derivative of cholesterol with a hydrophilic polyethene glycol chain forming micellar structures. According to Borowy-Borowski (2004),⁹⁶ two dissolution methods were employed: the melting method, where CoQ10 and PCS were heated above their melting points in one container, and the solvent method. For the latter, CoQ10 and PCS were first dissolved in tetrahydrofuran and then mixed with water. The organic solvent was removed to leave both substances dissolved in water.

A solution of 10 mM HO-CoQ10-PCS (1:3, wt/wt) in water is displayed in Figure 18 b showing the yellow-orange colour of HO-CoQ10 that turns violet after deprotonation of the hydroxy group by addition of NaOH (c). Stock solutions of both HO-CoQ10 and CoQ10 in water were stable at 4 °C or -20 °C after thawing. UV/Vis absorption spectra displayed in Figure 18 d and e show that concentrations higher than 100 µM in water are easily reached for both substances. Absorption at 275 nm increased by a factor of 2 when concentrations were doubled. In comparison to dilutions of stocks in ethanol (Figure 17 a), absorption intensities of diluted HO-CoQ10-PCS stocks were lower (Figure 18 e) because HO-CoQ10 has not been further purified for this preliminary experiment.

A major disadvantage of PCS formulations was an often unsuccessful dissolving process with both the melting and the solvent method. The dissolution was checked by filtering the stock solution through a 0.2-µm

membrane revealing that, repeatedly, a part of the substance was not in solution. The solvent method might have failed when CoQ10 accumulated in THF during evaporation and lost its equal distribution in the mixture. Therefore, factors like rotation speed, volume and flask surface area might be critical for the outcome. Using the melting method, it is crucial to locate CoQ10 and the PCS at the same spot in the vial to achieve proper admixing. Since CoQ10 is provided as a powder and PCS is highly viscous, transferring and weighing a preset amount of substance is challenging. This difficulty might be overcome by diluting both substances in a strong solvent like THF, and then slowly evaporating the solvent to leave the mixture at the bottom of the vial.

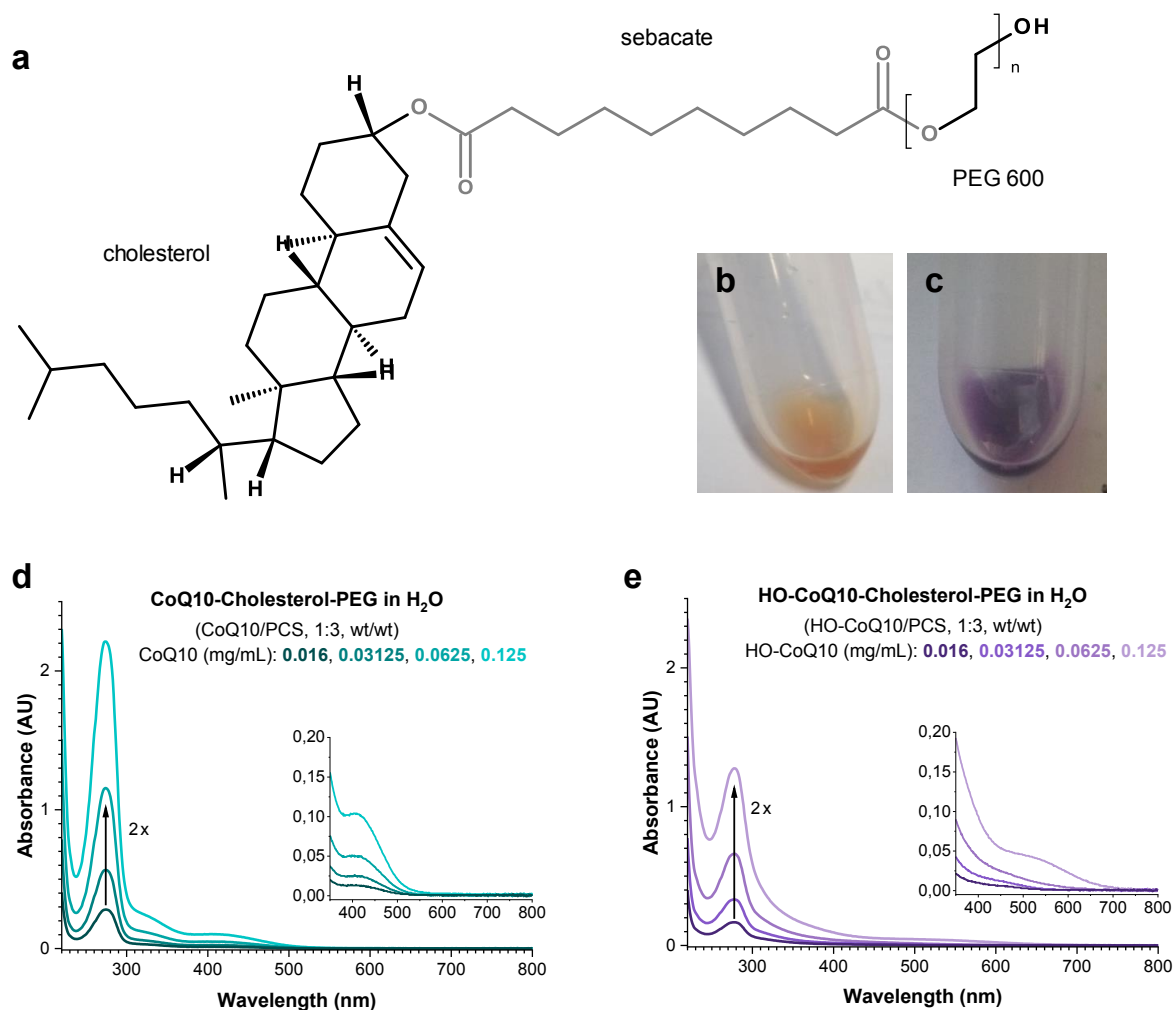


Figure 18 | Aqueous solution of CoQ10 and HO-CoQ10 using Cholesterol-PEG 600 to form nanomicelles. (a) Chemical composition of cholesterol-PEG 600: cholesterol, sebacate as a linker, and PEG 600 (polyethylene glycol with an average molecular weight of 600 u, n around 13 units); (b) stock solution of 10 mM HO-CoQ10-PCS (1:2, mol/mol; HO-CoQ10, reaction mixture) in water and (c) in 0.5 M NaOH; UV/Vis absorption spectra of dilutions of CoQ-PCS (1:3, wt/wt) stock solutions in water: (d) CoQ10-PCS, 0.016-0.125 mg/mL CoQ10 corresponds to 18.1-144.8 μ M CoQ10; (e) HO-CoQ10-PCS, 0.016-0.125 μ g/mL HO-CoQ10; PCS, Cholesterol-PEG 600; HO-CoQ10, here reaction mixture not purified via semi-preparative HPLC;

3.3 Endogenous detection of HO-CoQ10 and CoQ10 in bovine heart mitochondria

To understand the physiological importance of HO-CoQ10, its occurrence in biological material was to be clarified. The selected samples therefor were crude mitochondria of bovine heart. Cows, like humans, produce mainly CoQ with 10 subunits.¹⁴⁰ Thus, the prior purified substance HO-CoQ10 could be used as a standard to quantify its endogenous content. In contrast, in mice CoQ9 is the main endogenous species which is why

establishment of HO-CoQ9 production would have been required. Considering the greater sample size of bovine material (cow heart, ~ 6 kg; mouse heart, ~ 200 mg), working with bovine samples was beneficial. Of all organs, the heart contains the highest amount of CoQ10.¹⁴⁰ Within the cell, CoQ10 is accumulated in mitochondrial membranes.²¹ Moreover, the presence of CYP450 and the CoQ-synthome in mitochondria increases the probability of HO-CoQ10 detection.

3.3.1 Detection and fragmentation of CoQ10 and HO-CoQ10 by mass spectrometry

Ultra-high-pressure liquid chromatography coupled tandem mass spectrometry (UHPLC-MS/MS) was considered the method of choice to detect endogenous CoQ10. Hence, in a first step, the ionization behaviour of both CoQ10 and HO-CoQ10 was analysed by direct infusion mass spectrometry (DIMS) using electrospray ionization in negative and positive ionization mode. To identify the molecule, tandem-mass spectrometry (MS/MS) was applied to selected ions and molecule-specific fragmentation was analysed.

Unexpectedly, negative ionization of CoQ10 gave a molecular ion peak at a mass-to-charge ratio (m/z) of 862.6887 (Figure 19 a) and not at m/z 861.6766, the mass of deprotonated CoQ10.[¶] The found mass-to-charge ratio could be assigned to the semiquinone radical anion of CoQ10 by comparing the simulated isotope profile of its chemical composition, $C_{59}H_{90}O_4^-$, plotted in b (structure in f) to the pattern in a. The highest peak correlates to the exact mass of the ion consisting of the most abundant isotopes of all atoms. Neighbouring peaks with decreasing abundance show a difference of m/z 1 corresponding to the incorporation of one ¹³C isotope per peak with increasing m/z . The abundance of each ion in the mass spectrum correlates to the natural frequency of the isotopes. In the electron ionization mass spectrum of HO-CoQ10, a molecular ion peak was found at m/z 847.6641 corresponding to its anion (d and g). Fragmentation of the molecular ion from both CoQ10 (c, f, h) and HO-CoQ10 (e, g, h) followed the same pattern: First, loss of the methyl group(s) ($\Delta(m/z) = 15$) presumably from the methoxy group(s), followed by degradation of the isoprene chain with a base peak at m/z 219.066.

[¶] The exact mass of CoQ10 is 862.6839 g/mol.

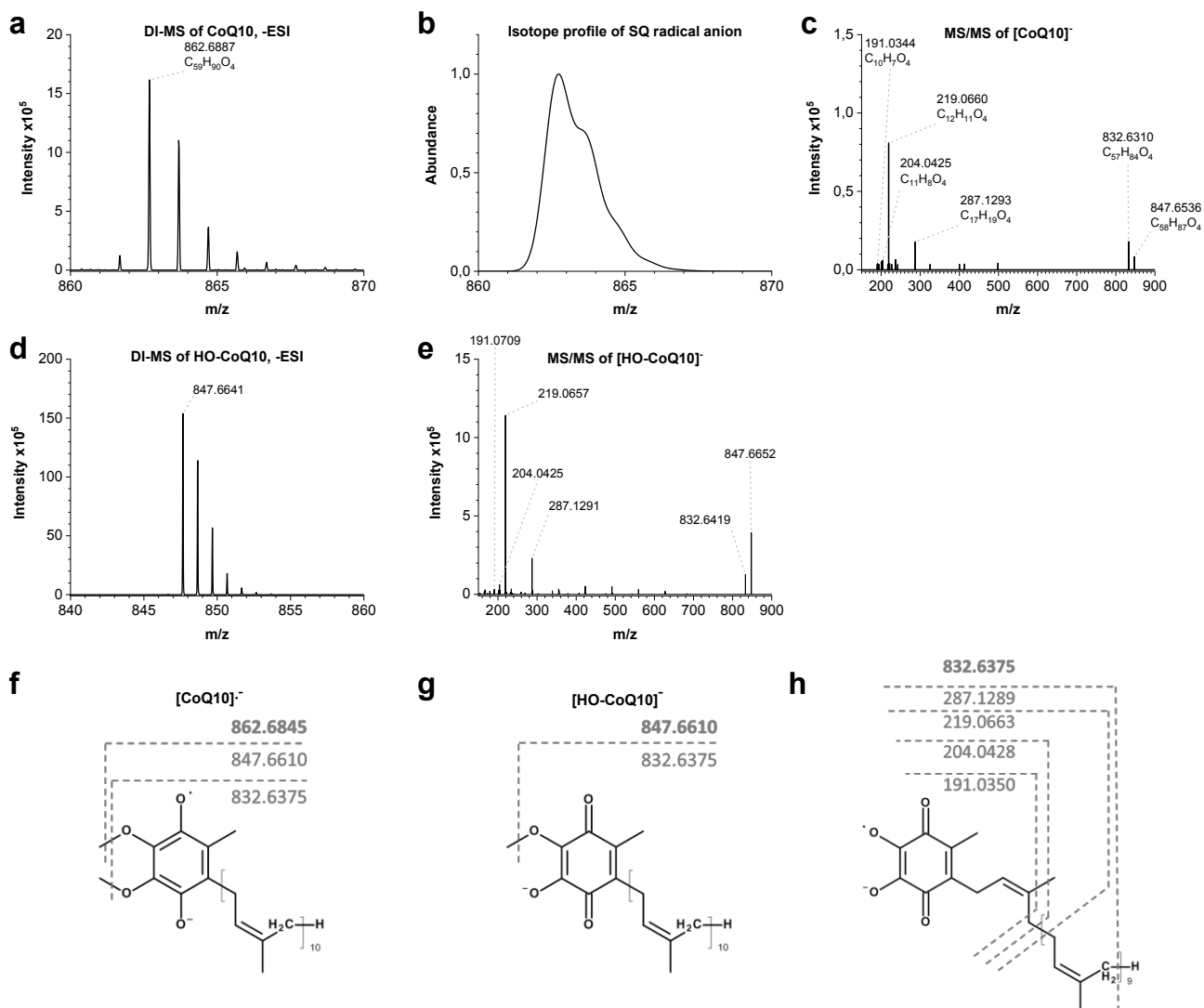


Figure 19 | CoQ10 and HO-CoQ10 detected in negative ionization mode. (a) Direct infusion mass spectrum of 1 μ M CoQ10, (b) simulated isotope distribution profile of the semiquinone radical anion ($SQ^{\cdot-}$) of CoQ10 ($C_{59}H_{90}O_4^-$) for comparison with spectrum in panel a, (c) MS/MS spectrum of $SQ^{\cdot-}$ of CoQ10 (m/z 862.40); HCD with NCE of 35%; (d) direct infusion mass spectrum of HO-CoQ10, (e) MS/MS spectrum of $[HO-CoQ10]^-$ (m/z 847.65); HCD with NCE of 25%; (f-g) Exact mass (g/mol; mass of entire depicted structure in bold), potential structures of ionized molecules and fragments (dashed lines indicate cleaved bonds, fragment mass is indicated below fragmentation line): (f) deprotonated semiquinone radical of CoQ10 with an exact mass of 862,6845 g/mol, empirical formula, $C_{59}H_{90}O_4$; fragmentation: two CH_3 groups are lost subsequently; (g) deprotonated HO-CoQ10, 847.6610 g/mol; empirical formula, $C_{58}H_{87}O_4$; fragmentation: loss of CH_3 group (h) fragmentation pattern of the didemethyl-CoQ10 fragment derived from CoQ10 or HO-CoQ10 (832.6375 g/mol, $C_{57}H_{84}O_4$): subsequent loss of 8, then 1 isoprene unit(s), 1 methyl, 1 CH group; m/z , mass-to-charge ratio; HCD, high collision dissociation; NCE, normalized collision energy;

The positive ionization spectrum of CoQ10 showed a base peak of m/z 880.7153 and molecular ion peak of m/z 863.6876 (Figure 20 a). These can be attributed to the ammonium and proton adduct of CoQ10, respectively (e). Analogous to CoQ10, positive ionization of HO-CoQ10 led to a base peak of its ammonium adduct and its less abundant protonated form (c and f). Fragmentation of CoQ10 and HO-CoQ10 resulted in a neutral loss of 666 u, equivalent to the almost complete loss of the isoprene chain leaving one methyl group behind (CoQ10: b and e, HO-CoQ10: d and f). Consequently, in contrast to negative ionization mode, in positive

ionization mode different base peaks are found for fragmented CoQ10 and HO-CoQ10 at m/z 197.08 and m/z 183.07, respectively.

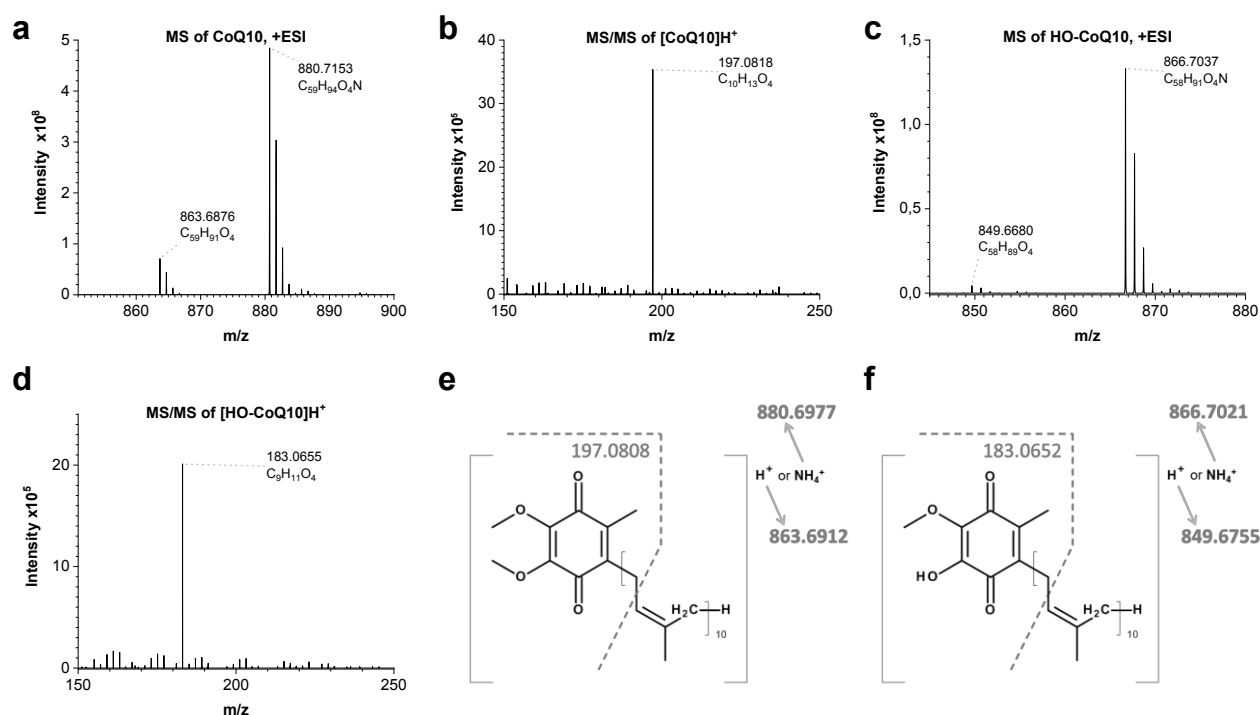


Figure 20 | CoQ10 and HO-CoQ10 detected in positive ionization mode. (a) Mass spectrum of CoQ10, (b) MS/MS spectrum of $[\text{CoQ10}]\text{H}^+$ (m/z 863.69), HCD with NCE of 35%; (c) mass spectrum of HO-CoQ10, (d) MS/MS spectrum of $[\text{HO-CoQ10}]\text{H}^+$ (m/z 849.68), HCD with NCE of 35%;

(e, f) Exact mass (g/mol; mass of entire depicted structure in bold), potential structures of ionized molecules and fragments (dashed lines indicate cleaved bonds, fragment mass is indicated below fragmentation line): (e) CoQ10 and (f) HO-CoQ10 proton and ammonium adducts; fragmentation: loss of complete side chain except for one CH_2 group; m/z , mass-to-charge ratio; HCD, high collision dissociation; NCE, normalized collision energy;

3.3.2 HO-CoQ10 but not CoQ10 was temperature-sensitive

It was important to know how heating and storing affects both CoQ10 and HO-CoQ10. Therefore, long-term stability of the solids was tested after 6 d and at different temperatures, ranging from -70 to $+37$ °C. After incubation, the substances were reconstituted in ethanol, and the content was determined via UHPLC-MS and normalized to signals from the samples stored at -70 °C. As can be deduced from Figure 21 a, CoQ10 was not sensitive to prolonged exposure up to 37 °C. In contrast, HO-CoQ10 was unstable at increased temperatures. After 6 d of incubation at RT, 30% and at 37 °C, even 92% of HO-CoQ10 was degraded. In contrast, temperatures up to 60 °C did not affect CoQ10 and HO-CoQ10 content in ethanolic solutions when incubation time was only 1 h (b).

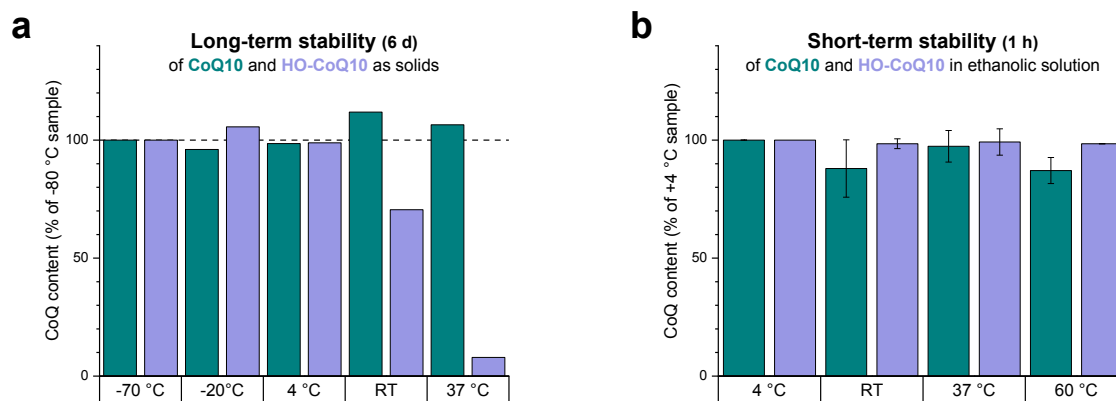


Figure 21 | Thermal stability of CoQ10 and HO-CoQ10 as a solid (a) and in an ethanolic solution (b). (a) 6 d incubation of 10 nmol CoQ10 or HO-CoQ10 (preparation alpha) in glass vials with silicon-sealed lids at different temperatures; samples were kept dark and reconstituted with 0.2 mL ethanol to yield a 50 μ M solution for quantification; (b) 1 h incubation of 250 μ L of a 10 μ M solution of CoQ10 or HO-CoQ10 (preparation alpha) in ethanol at different temperatures; (a, b) CoQs were quantified via RP-UHPLC-MS/MS analysis: CoQ10 was detected in positive ionization mode ($[\text{CoQ10}]\text{NH}_4^+$, 880.7146 m/z ; RT, 5.04 min; MS/MS, 197.0808 m/z) and HO-CoQ10 in negative ionization mode ($[\text{HO-CoQ10}]^-$, 847.6618 m/z ; RT, 4.56 min; MS/MS, 219.0658 m/z), peak areas were normalized to samples incubated at (a) -80 $^{\circ}\text{C}$ and (b) +4 $^{\circ}\text{C}$; RT, retention time; MS/MS, mass of ion emerging from fragmentation of the mentioned ion;

The experiments showed that HO-CoQ10 is sensitive to heat when the substance was exposed for long periods. Therefore, it is evident that HO-CoQ10 should be stored frozen. Although ethanolic solutions were not decomposing at 60 $^{\circ}\text{C}$ in a restricted time of 1 h, a more thorough study to evaluate stability as a solid and in solution is necessary.

3.3.3 HO-CoQ10 as part of mitochondrial membranes

The sample preparation procedure was as follows: 1. sedimentation of crude mitochondrial extract, 2. protein precipitation and lipid extraction via single phase extraction, 3. contraction of the sample volume by nitrogen gas flow at 60 $^{\circ}\text{C}$ and reconstitution in a smaller volume, 4. UHPLC-coupled tandem-mass spectrometry with electrospray ionization.

From crude heart mitochondria isolated from the left ventricle of the beef heart (Figure 22 a), lipids were extracted by single phase extraction using different solvents. The total ion current chromatogram of an exemplary lipid extract demonstrates the abundance of ionizable molecules present (b). Hence, extracted-ion chromatograms were obligatory to analyse the appearance of CoQs. As an internal standard, to compensate for variable extraction efficiency, the CoQ10 analogue CoQ4 containing 4 instead of 10 isoprene units was utilised in view of its analogy to the native substance as well as availability and price. Comparing the peak heights of CoQ ions, for both HO-CoQ10 and CoQ10 the ammonium adduct was the most abundant (c), while for CoQ4 only the protonated species was detectable in positive ionization mode. Even though deprotonated HO-CoQ10 had higher intensity than the deprotonated CoQ10 semiquinone radical, positive ionization was far more profitable. Hence, signals of ammonium adducts of CoQ10 and HO-CoQ10 and the proton adduct of CoQ4 were quantified.

For analysis of biological samples, a gradient elution protocol starting with high water content was used to eliminate components like proteins. The steepness and course of the gradient were established to separate all

three CoQs. By comparison of the retention time with standards and fragmentation of the selected ion, the analytes could be clearly assigned in the mitochondrial extract (Figure 22 d, e: ST, standards; DaS, lipid extracts). Even though for HO-CoQ10 more than one peak at $m/z \sim 866.7020$ corresponding to the ammonium adduct appeared in the EIC (d, DaS), its fragmentation resulted in one peak of $m/z 183.0653$, corresponding to the fragment ion of HO-CoQ10, eluting at the same time as the standard HO-CoQ10 identifying the peak at RT 6.8 min. Analogously, CoQ10 could be identified at RT 7.3 min.

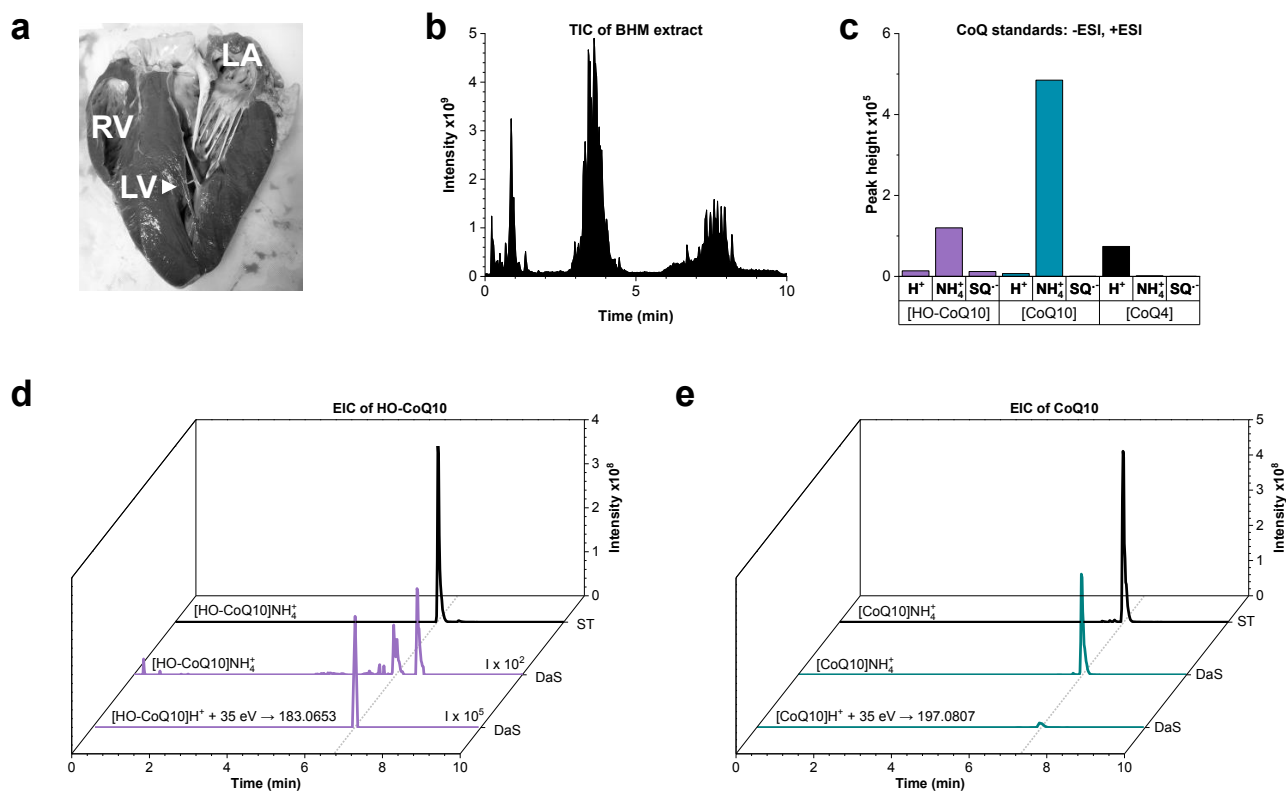


Figure 22 | HO-CoQ10 detected in bovine heart mitochondria. Crude mitochondria were isolated from the left ventricle of the (a) bovine heart: RV, right ventricle; LA, left atrium; LV, left ventricle. Samples were analysed by UHPLC-MS/MS: (b) total ion current (TIC) chromatogram of BHM extracted with the dilute-and-shoot method (DaS), (c) 10 μM CoQ standards, peak heights of detected CoQ ions in positive and negative ionization mode; positive: H^+ , H^+ adduct; NH_4^+ , NH_4^+ adduct; negative: Q^- , deprotonated quinone; SQ^- , deprotonated semiquinone radical; (d, e) extracted-ion chromatograms (EIC) of standards (ST, black line), BHM extracted with DaS (same sample as in panel b) and fragmentation of analyte: (d) HO-CoQ10 ammonium adduct, fragmentation of HO-CoQ10 proton adduct with NCE of 35% and extracted-ion at $m/z 183.0653$, fragment ion of HO-CoQ10; intensity (I) of chromatograms are magnified as stated; (e) CoQ10 ammonium adduct, fragmentation of CoQ10 proton adduct with NCE of 35% and extracted-ion at $m/z 197.0807$; NCE, normalized collision energy;

The following table provides an overview of expected (exact mass in g/mol) and observed m/z values of all analytes within this study.

Table 11 | Identified CoQ molecules with observed and theoretical exact masses. Measurement error as delta score, listed are observed masses of the CoQs in standard solutions and extracts of BHM; n.d., not detectable

Compound	Composition	Standards			Extracts	
		Exact mass (g/mol)	Observed mass (m/z)	Error (ppm)	Observed mass (m/z)	Error (ppm)

[CoQ10]H ⁺	C ₅₉ H ₉₀ O ₄ .H	863.6912	863.6887	- 2.89	863.6902	- 1.16
[CoQ10]NH ₄ ⁺	C ₅₉ H ₉₀ O ₄ .H ₄ N	880.7177	880.7149	- 3.18	880.7154	- 2.61
[CoQ10] ⁻	C ₅₉ H ₉₀ O ₄	862.6845	862.6876	3.59	862.6867	2.55
<u>CoQ10 fragments</u>						
H ⁺	C ₁₀ H ₁₂ O ₄ .H	197.0808	197.0806	- 1.01	197.0807	- 0.51
NH ₄ ⁺	C ₁₀ H ₁₂ O ₄ .H ₄ N	214.1074	n.d.			
Q ⁻	C ₁₂ H ₁₁ O ₄	219.0663	219.0656	- 3.20	219.0661	- 0.91
[HO-CoQ10]H ⁺	C ₅₈ H ₈₈ O ₄ .H ₄ N	849.6755	849.6734	- 2.47	n.d.	
[HO-CoQ10]NH ₄ ⁺	C ₅₈ H ₈₈ O ₄ .H ₄ N	866.7021	866.6996	- 2.88	866.702	- 0.12
[HO-CoQ10] ⁻	C ₅₈ H ₈₇ O ₄	847.6610	847.6640	3.54	847.6720	12.98
<u>HO-CoQ10 fragments</u>						
H ⁺	C ₉ H ₁₀ O ₄ .H	183.0652	183.0652	0	183.0653	0.55
NH ₄ ⁺	C ₉ H ₁₀ O ₄ .H ₄ N	200.0917	n.d.			
Q ⁻	C ₁₂ H ₁₁ O ₄	219.0663	219.0661	- 0.91	219.0657	- 2.74
[CoQ4]H ⁺	C ₂₉ H ₄₂ O ₄ .H	455.3156	455.3143	- 2.86	455.3150	- 1.32
[CoQ4]NH ₄ ⁺	C ₂₉ H ₄₂ O ₄ .H ₄ N	472.3421	n.d.			
[CoQ4] ⁻	C ₂₉ H ₄₂ O ₄	454.3089	454.3089	0		

Table 12 compares extraction efficiencies of different extraction solvents. Values do not reflect endogenous concentrations because concentrations were normalized to 100 µM CoQ control solutions undergoing the same procedure as the samples and not using a calibration curve. All tested solvents (methanol, ethanol, 1-propanol, 2-propanol, acetonitrile) extracted both CoQ10 and HO-CoQ10. Isopropanol was most efficient for CoQ10 extraction (11.24 nmol/mg mitochondrial protein) and acetonitrile least efficient (13% CoQ10 of *i*-prOH extract). Extracted HO-CoQ10 content, ranging between 0.02 and 0.06 nmol/mg mitochondrial protein, was more uniform using a variety of solvents. Again, propanol extracts contained more HO-CoQ10 than the ACN extract (33% HO-CoQ10 of *n*- and *i*-prOH extracts). Since 2-propanol yielded the highest extraction efficiencies for both species and is recommended to both extract CoQ10 and precipitate proteins during sample preparation,¹⁴¹⁻¹⁴³ it was chosen as the extraction solvent for further experiments.

Table 12 | Isopropanol was the most efficient extraction solvent for detection of endogenous CoQ from bovine heart mitochondria. CoQ content in nmol/mg mitochondrial protein was roughly estimated by normalizing to controls of 100 µM CoQ10 and HO-CoQ10 in 2-propanol.

Solvent	Methanol	Ethanol	<i>n</i> -Propanol	<i>i</i> -Propanol	Acetonitrile
[HO-CoQ10]NH ₄ ⁺	0.04	0.05	0.06	0.06	0.02
[CoQ10]NH ₄ ⁺	3.05	9.75	10.45	11.24	1.48

To improve extraction of CoQs, different parameters have been changed: sample input, use of surfactants, evaporation temperature, and processing of the extract. To make valid assumptions about the CoQ content per mitochondrial protein, it is important to make sure that extraction efficiency is independent of the amount of

mitochondrial input. Decreasing the amount of mitochondrial protein from 10 to 1 mg increased CoQ10 extraction efficiency per mg by a factor of 2.3 (Table 13, 1 mg and 10 mg). Also, HO-CoQ10 recovery increased but an input lower than 5 mg was very likely below the detection limit. Therefore, CoQ content per mg must be considered conditionally and has been most probably underestimated.

Since heat stability of HO-CoQ10 at least in solid form (and over prolonged periods) is questionable (cf. Figure 21 a on p. 70), drying the extracts at room temperature was compared to the standard procedure at 60 °C. Drying temperature affected CoQ extraction efficiency (Table 13, 10 mg and RT). Drying the extract without heating increased the HO-CoQ10 recovery by 55%, whereas CoQ10 recovery remained constant. Since drying at RT is time-consuming and HO-CoQ10 can be resistant to higher temperatures depending on incubation time and state (cf. Figure 21 b), the drying procedure should be revised, and additional experiments concerning the stability of HO-CoQ10 are necessary. Removing the solvent with a vacuum centrifuge with gentle heating or at RT would be a time-efficient alternative to drying the extracts under nitrogen flow.

Surfactants solubilise membrane components and have been found to increase recovery of CoQ10 in plasma samples. 10% Triton X-100 which is able to solubilise both membrane proteins and lipids¹⁴⁴ was shown to increase CoQ10 extraction efficiency by 37%.¹⁴⁵ Replacing 20% of the extraction solvent with a 10% Triton X-100 solution in water indeed increased detected HO-CoQ10 by 44% (Table 13, Trx and w). However, extraction efficiency of CoQ10 was not notably enhanced (+ 3% compared to water control). In contrast, recovery of the internal standard was one of the lowest probably due to foaming that hampered drying massively.

Another, more time efficient and robust approach is the dilute-and-shoot method, where the extract is directly measured without the intermediate step of contracting the sample volume.¹⁴⁶⁻¹⁴⁸ Despite resulting in the highest HO-CoQ10 to CoQ10 ratio (Table 13, DaS), the lowest extraction efficiencies were found using the dilute-and-shoot-method. Not only endogenous HO-CoQ10 and CoQ10 but also the internal standard CoQ4 was affected. Since the sample was not concentrated and in order to keep the volume-to-sample ratio constant, the extraction volume was 10-times lower than for the standard protocol increasing the plastic surface-to-extract ratio. Hence, the drastically reduced extraction yield might be due to quinone molecules sticking to plastic surfaces as has been observed in other studies.¹⁴⁹ To omit this disadvantage, extraction volume and material should be increased in future experiments. Also, the sample-to-solvent ratio might influence extraction efficiency since recovery of CoQ4 increased upon reduction of sample input.

Table 13 | Reducing sample-to-solvent ratio and drying temperature improved CoQ extraction. CoQ content is given in CoQ10 per mitochondrial protein (nmol/mg) and was calculated from calibration curves. Different parameters have been changed to improve extraction efficiency. 1-10 mg, input BHM (mitochondrial protein); 10 mg BHM was the standard sample input if not indicated otherwise; RT, extract was dried without heating; w, extraction solvent was a mixture of water and 2-propanol (1:4, v/v) as a control for detergent-treated sample; Trx, extraction solvent was a mixture of 10% Triton X-100 and 2-propanol (1:4, v/v); DaS, dilute-and-shoot extraction method;

Detected compound	1 mg	5 mg	10 mg	RT	w	Trx	DaS
	nmol CoQ/ mg protein						
[HO-CoQ10]NH ₄ ⁺	0.011	0.013	0.009	0.014	0.009	0.013	0.004
[CoQ10]NH ₄ ⁺	10.173	6.823	4.419	4.627	3.790	3.904	0.526
[CoQ4]H ⁺	0.063	0.060	0.053	0.044	0.044	0.013	0.052

	CoQ normalized to 10 mg (%)						
[HO-CoQ10]NH ₄ ⁺	122.2	144.4	100	155.6	100,0	144.4	44.4
[CoQ10]NH ₄ ⁺	230.2	154.4	100	104.7	85.8	88.3	11.9
[CoQ4]H ⁺	118.6	113.1	100	84.3	82.7	24.9	9.9
	Portion of HO-CoQ10 of total CoQ10 (%)						
HO-CoQ10/CoQ10 (%)	0.11	0.19	0.20	0.30	0.24	0.33	0.75

The extraction efficiency of CoQ4 was correlated with extracted concentrations of endogenous CoQ10 but not HO-CoQ10 (Table 13, CoQ normalized to 10 mg). This indicates that CoQ4 might not be an adequate internal standard for HO-CoQ10 detection. More reliable standards for both CoQ10 and HO-CoQ10 are deuterated¹⁵⁰ and propyl (or ethyl) derivatives synthesized in alkaline propanol (or ethanol)^{151,152} or CoQs with 9 isoprene units when endogenous CoQ9 is either stable or not detectable in the samples. Recovery of the analytes needs to be assessed using samples spiked with CoQ10 or HO-CoQ10 since their extraction efficiencies were not equally affected. In hindsight, it might be necessary to use one internal standard for each analyte. Nevertheless, to account for intersample variations using the same protocol, CoQ4 still is a valuable option.

The dilute-and-shoot sample left aside, all CoQ concentrations are in the expected range of 4-10 nmol CoQ10 per mg mitochondrial protein. In heart mitochondria of *Bos taurus*,¹⁵³ mouse¹⁵³⁻¹⁵⁶ and rat^{157,158} 6.5, 3.5-6 and 3-8 nmol CoQ of the main species per mg mitochondrial protein were found. The HO-CoQ10 portion of total CoQ10 content was between 0.11 and 0.75%. Taking into account the most reliable measurements (5 mg and RT), the HO-CoQ10 portion amounts to 0.3% of the total CoQ10 pool. Supposing a concentration of 0.3 mg phospholipids (PL) per mg protein in bovine heart mitochondria¹⁵⁹ and a PL density of ~ 1 mg/μL,^{160,161} CoQ10 concentration can be calculated¹⁶⁰ to be between 13 and 33 mM in the present sample. Taking into account the highest detected CoQ10 concentration and assuming a HO-CoQ10 portion of 0.3%, its concentration in mitochondria was calculated to be 100 μM.

3.4 HO-CoQ10 neither affected cell viability nor proliferation of cancer cell lines

As elaborated in the introduction, Coenzyme Q is involved in many cellular processes that influence cellular fate. Nothing, however, is known on a potential role of HO-CoQ10 present in small amounts in cell function. Moreover, there is evidence that a hydroxylated benzoquinone, embelin (2,5-dihydroxy-3-undecyl-1,4-benzoquinone), limits tumour growth.^{162,163} Hence, it was important to elucidate if and how HO-CoQ10 is influencing cell viability and proliferation. Incubation was conducted under standard cell culture conditions (respective cell culture medium; 5% CO₂).

To draw a broad picture, different cell lines were tested using the CellTiter-Blue® Assay that measures metabolic turnover by detecting the reduction of resazurin to resorufin. Measuring the turnover at different time points during several days reveals the proliferative status of the cells. There was no change in proliferation and metabolic activity when CoQ10 or HO-CoQ10 was added as ethanolic solutions to the cell culture medium of a variety of tumour cell lines (Figure 23). Tested cell lines were the melanoma cell line

MelJuso, Jurkat E6-1 T cells and the cervical cancer cell line HeLa. Noteworthy, 1% ethanol neither affected proliferation nor metabolic turnover of the cells.

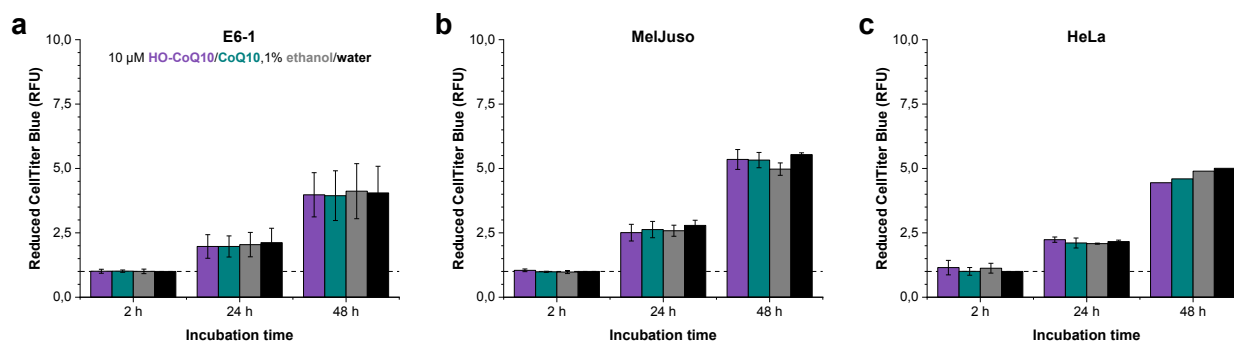


Figure 23 | HO-CoQ10 and CoQ10 did not affect cell viability and proliferation in cancer cell lines. Cells were grown under standard cell culture conditions and treated with 10 μ M HO-CoQ10, CoQ10 or solvent control (1% ethanol, water). Resazurin fluorescence, i.e. metabolic activity, was normalized to signal of control cells after 2 h (1% water; dashed line at 1 RFU, relative fluorescence unit). Tested cell lines were (a) Jurkat E6-1 T cells, (b) melanoma cell line MelJuso, and (c) cervix cancer cell line HeLa. Graphs show means \pm SEM from triplets of (a, b) 3 or (c) 2 independent experiments.

In order to identify possible effects like apoptosis induction, the stable Jurkat E6-1 T cell line expressing a fluorescent apoptosis sensor (Jurkat pCasper)¹¹⁰ was subjected to CoQs. The fluorescent FRET^r-sensor Casper-GR¹⁶⁴ (also: Casper3) detects caspase activity, one of the first steps of apoptosis induction.^{165,166} Casper-GR comprises GFP and RFP connected by a linker peptide containing a caspase target sequence. The intact protein emits green and red light upon excitation of GFP (Figure 24 a). When the linker peptide is cut by activated caspases, FRET and thereby red fluorescence is lost.

The substances were added prior to the first measurement. In a period of 24 h, every 10 min one image was taken. Figure 24 b depicts one representative image for each substance at the beginning of the incubation (40 min after sample addition) and after 24 h. Concentrations from 10 nM up to 10 μ M CoQ10 and up to 30 μ M HO-CoQ10 have been tested. HO-CoQ10, CoQ10 and 1% ethanol did not induce apoptosis over a period of 24 h since green fluorescence was not elevated in any sample but the staurosporine control. However, Jurkat T cells tend to form cell agglomerates, and a more detailed evaluation requires FACS analysis.

^r FRET, Förster resonance energy transfer

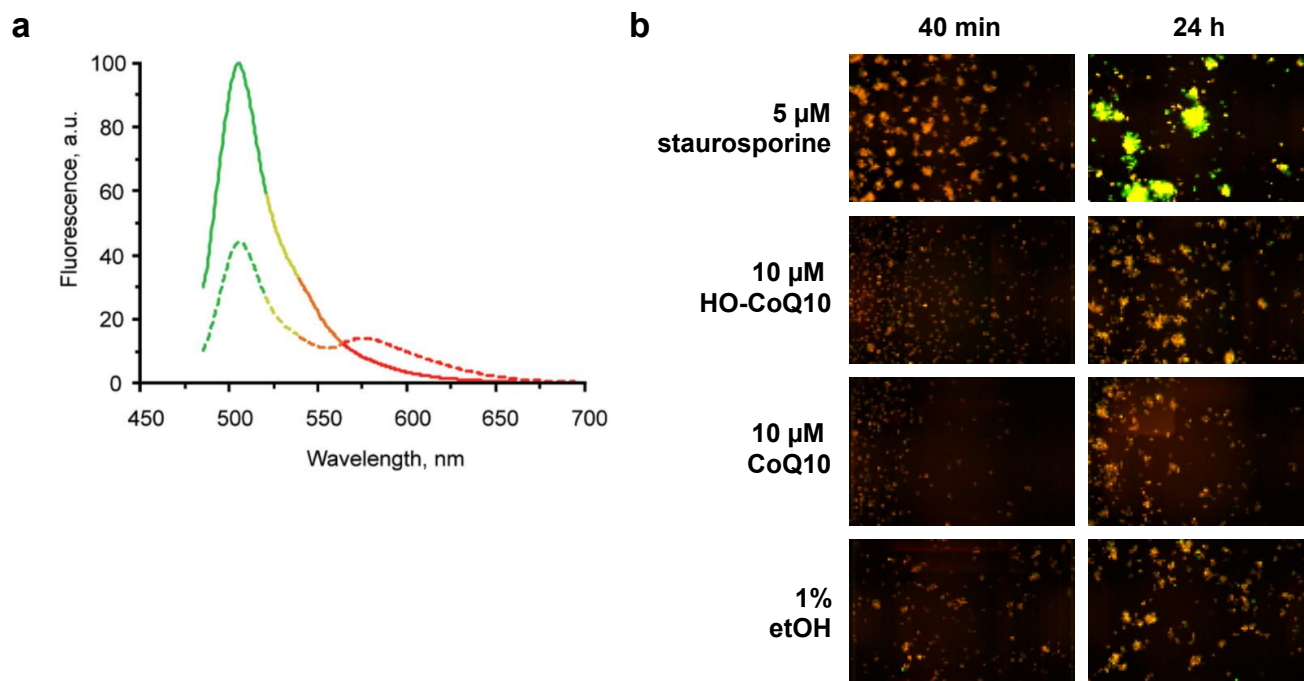


Figure 24 | HO-CoQ10 and CoQ10 did not induce apoptosis within 24 h. (a) Emission spectra of Casper-GR FRET signal (dashed line) and GFP signal after digestion by caspases (solid line), figure reproduced from Shcherbo (2009);¹⁶⁴ (b) Jurkat pCasper cells incubated under standard cell culture conditions; cells were treated with 5 μ M staurosporine to induce apoptosis as a positive control, 10 μ M HO-CoQ10 (preparation alpha), CoQ10 or vehicle (1% ethanol); green (GFP signal of pCasper) and red (FRET fluorescence of pCasper) fluorescence was merged and images after 40 min and 24 h incubation time are shown; images are representative of triplets of 1 independent experiment;

As CoQ have been applied as ethanolic solutions onto whole cells, insufficient distribution of CoQ10 within the cell might be responsible for the lack of an effect. Within this thesis, it has not been tested how much exogenously applied CoQ10 and HO-CoQ10 entered the cell. Nevertheless, Duberley et al. (2014)¹⁶⁷ detected 50-fold higher levels of CoQ10 in cells incubated with 10 μ M ethanolic CoQ10 after 5 d but did not track its intracellular distribution. Since the substances are highly lipophilic, it is likely that CoQs integrate into the plasma membrane. Because it is not yet clear where in the cell exogenous CoQ10 will be located, a positive control for known CoQ10 effects should be included. For example, the protective effect of CoQ10 can be demonstrated when cells are more susceptible to cell death by inducing apoptosis through serum starvation.⁴²

3.5 Influence of HO-CoQ10 on mitochondrial respiration

As stated before, the most studied function of Coenzyme Q is its participation in transporting electrons along and protons across the inner mitochondrial membrane. Therefore, the influence of HO-CoQ10 on respiration of viable mitochondria was investigated. As a subject, mouse heart mitochondria were chosen because isolation of these tightly coupled mitochondria was established and thoroughly studied by our cooperation partners from Prof. Dr Christoph Maack's group¹¹⁴ (now Department Translational Science, Universitätsklinikum Würzburg).

3.5.1 Mitochondrial respiration linked to substrates of respiratory chain complex I, II, III, and IV

Respiration was measured with a Clark-type electrode setup as depicted in Figure 25 a. Oxygen present in the sample chamber diffuses through the gas-permeable membrane^s into the KCl solution bridging the gold or platinum^t cathode and the silver/silver chloride anode. At the cathode, oxygen is reduced via H₂O₂ to OH⁻, in return Ag is oxidized forming silver chloride at the anode (compare reactions in b), and the generated current is detected.

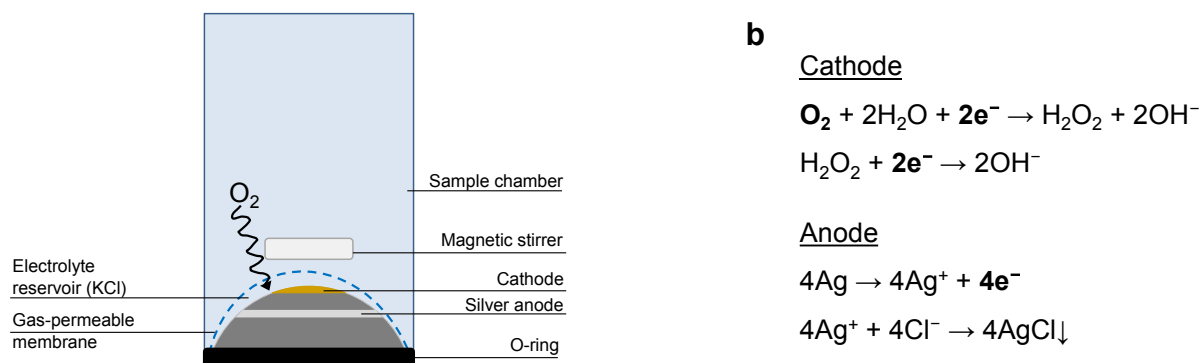


Figure 25 | Oxygen detection by the Clark-type electrode. (a) Principle setup of the used Clark-type electrodes, (b) oxygen electrode reactions: per O₂ molecule 4e⁻ are transferred.

The influence of CoQs on the respiratory chain was dissected by feeding electrons into the four respiratory chain complexes separately. The protocols were based on Nickel (2015, for Complex I)¹¹⁴ and guidelines from Mitochondrial Physiology Network by Oroboros Instruments Corp.^u

The addition protocol is illustrated in Figure 26 a: Respiration buffer was equilibrated to 37 °C in the sample chamber, and then mitochondria were added to reach the desired concentration. The addition intervals of substances were set long enough to establish a constant oxygen consumption slope. The substrate mixture, feeding electrons directly to one of the four respiratory chain complexes, was added and a saturating concentration of 1 mM ADP was supplied to fully activate oxidative phosphorylation (OXPHOS). Then, the sample substance was added to observe its influence on OXPHOS. To guarantee that the selected substrate combinations led to electron transfer via the targeted and its downstream complex(es), the inhibitors rotenone, malonate, antimycin A and KCN of complexes I, II, III, and IV, respectively, were applied (b-e).

Complex I substrates comprised a combination of 5 mM pyruvate and malate (PM, Figure 26 b) since either substrate alone only achieved less than 3% of PM-linked respiration in rat skeletal muscle mitochondria.¹⁶⁸ Pyruvate is taken up by OH⁻/pyruvate antiport or noncarrier-mediated transport at high concentrations above 5 mM.¹⁶⁹ In theory, CII-linked respiration should be possible since succinate can be formed from malate through the citric acid cycle (CAC, Krebs cycle). Nevertheless, succinate oxidation is impeded by the formation of oxaloacetate,^{170,171} the reverse reaction of fumarase producing fumarate from malate^{172,173} and the loss of 2-oxoglutarate by exchange with malate through the 2-oxoglutarate carrier.¹⁷⁴ Additionally, loss of succinate into

^s Hansatech Instr., PTFE membrane; Oroboros Instr., FEP membrane

^t Hansatech Instr., platinum cathode; Oroboros Instr., gold cathode

^u www.wiki.oroboros.at (accessed October 24, 2018)

the medium and antiport of malate/citrate reduce mitochondrial succinate concentrations.¹⁶⁹ Hence, adding PM will foremost activate Complex I respiration.¹⁶⁹

The Q-binding site inhibitor of CI, rotenone,^{175,176} as well as the inhibitors of CIII and CIV reduced PM-linked respiration drastically (Figure 26 b). Solely when malonate, a competitive inhibitor of the succinate-binding site of CII,¹⁷⁷ was added, respiration was not affected confirming that PM-linked respiration was not supported by CII. Similar behaviour was seen in studies of Lemasters et al. (1984)¹⁷⁸ where malonate reduced glutamate/malate-linked respiration by only 2.5%.

The Complex II substrate succinate is taken up via antiport of HPO_4^{2-} (Figure 26 c). The addition of rotenone was necessary to detect Complex II-linked respiration. Reports stated succinate-linked OXPHOS rate to be 50% of the rate with additional rotenone in human skeletal muscle mitochondria.¹⁷⁹ In MHM, OXPHOS rate with succinate only constituted ~ 25% of OXPHOS rate with succinate and rotenone (data not shown). Rotenone inhibits NADH-sensitive formation of the competitive CII inhibitor oxaloacetate and reverse electron flow (RET) from CII to CI with concomitant ROS formation.^{180,181} Figure 26 c shows that r/S-linked^v respiration is specific because it could only be inhibited by the downstream inhibitors antimycin A and cyanide as well as by the competitive CII inhibitor malonate.

Reduced duroquinone, tetramethyl-*p*-benzoquinol, is used as a synthetic Complex III substrate.¹⁸² Being more soluble in water and ethanol than CoQ derivatives, it can be used at high concentrations which is required to achieve a constant respiration rate (compare d using 0.8 mM duroquinol and Figure 30 c where 100 μM duroquinol was consumed after 2.5 min). As predicted, just antimycin A and cyanide inhibited duroquinol-induced respiration. Moreover, oxygen consumption with duroquinol was no artefact due to its preparation with the reductant NaBH_4 producing H_2 in presence of water which then could react with dissolved O_2 . Application of ethanol treated the same way as the duroquinol sample did not alter oxygen concentration in the chamber (data not shown; cf. quinone reduction procedure on p. 47).

TMPD, tetramethyl-*p*-phenylenediamine, was used to reduce cytochrome *c* which transfers electrons to CIV (e). The addition of ascorbate (asc) is necessary to inhibit TMPD autoxidation. Since oxidation of TMPD in presence of ascorbate in respiration buffer was negligible (asc + TMPD + ADP was ~ 1% of OXPHOS, data not shown), subtraction of the background was omitted. Inhibitors of upstream complexes did not affect CIV-linked respiration, whereas cyanide inhibited oxygen consumption.

^v r/S, rotenone/succinate

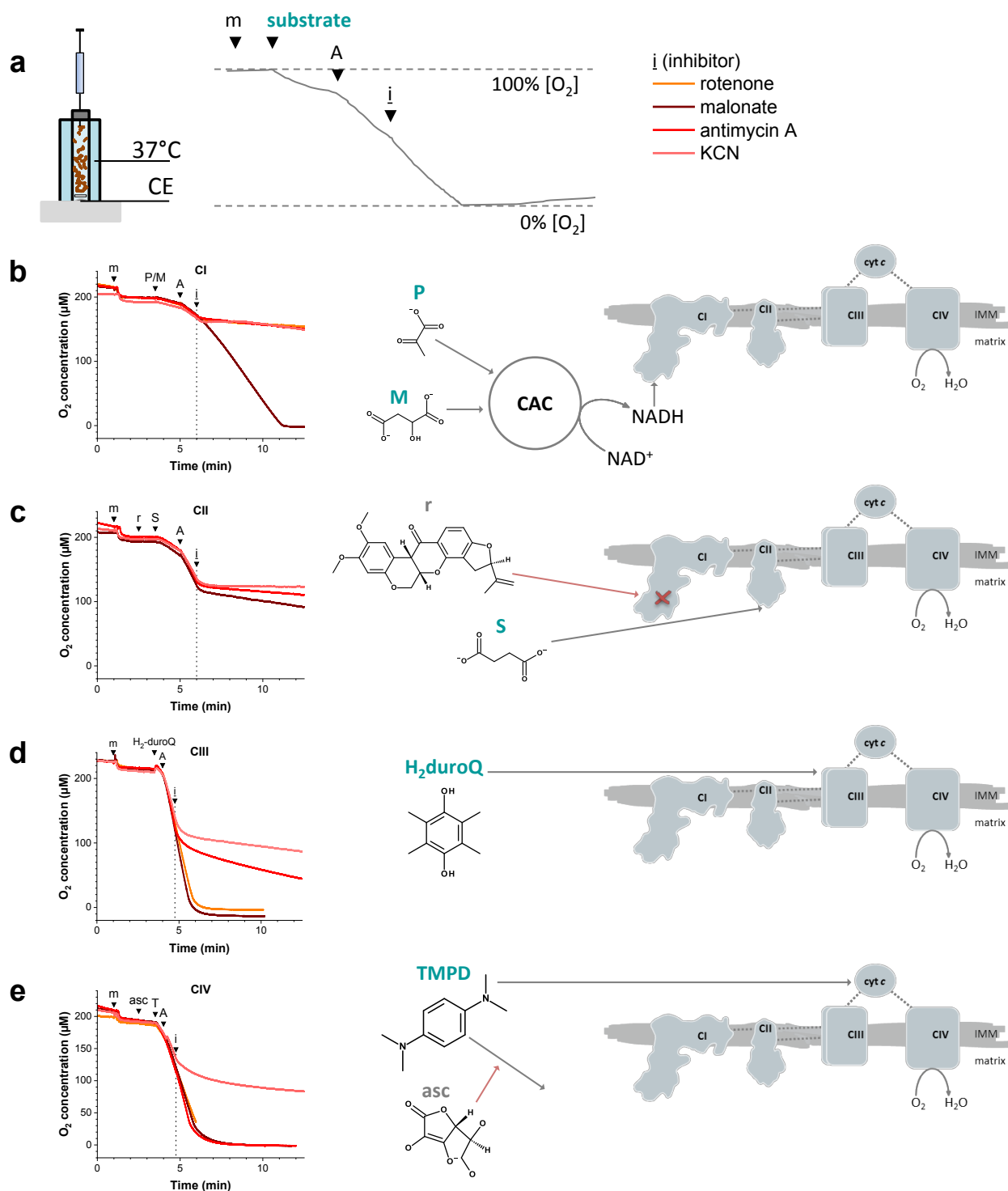


Figure 26 | Mitochondrial respiration measured by directly feeding electrons into Complex I, II, III and IV. Respiration was followed by the decrease of oxygen concentration using a Clark-type electrode. (a) Pipetting scheme was as follows: 0.2 mg/mL MHM were incubated at 37 °C in RB1, then complex-specific substrates, 1 mM ADP (A), and inhibitors for RCCs (i) were added subsequently as indicated. (b) Complex I-linked respiration using 5 mM pyruvate/malate (PM), CAC, citric acid cycle; (c) Complex II-linked respiration using 0.5 μM rotenone (r) and 10 mM succinate (S), (d) Complex III-linked respiration using 0.8 mM duroquinol (H₂-D), (e) Complex IV-linked respiration using 2 mM ascorbate (asc) and 0.5 mM TMPD (T) as substrate cocktails. Inhibitors (i) to block Complex I, II, III and IV were 0.5 μM rotenone, 5 mM malonate, 10 μM antimycin A, and 1 mM KCN, respectively. Graphs are representative of 3 independent mitochondrial preparations with similar trends. Instrument: Oxygraph Plus (Hansatech Instr.);

3.5.2 HO-CoQ10 inhibited CI-, CII-, and CIII-linked respiration

Before applying CoQs on mitochondria, their influence on the oxygen signal in air-saturated buffer was examined. Since ethanol-water solutions have a higher oxygen solubility than water alone,^{183,184} the oxygen signal rose rapidly upon application of ethanolic solutions (Figure 27). Oxygen concentration was increased by 6 and 5% after application of ethanol (a) and an ethanolic solution of HO-CoQ10 (b), respectively. Fitting the experimental data for different percentiles of ethanol from Käppeli et al. (1981),¹⁸³ addition of 1% ethanol to an aqueous solution should increase oxygen concentration by 15%. The lower increase of dissolved oxygen in the shown experiments can be explained by the slightly higher measuring temperature of 37 °C as compared to the experiments from Käppeli et al. performed at 30 °C since oxygen solubility in ethanol was shown to decrease with rising temperature.¹⁸⁴ Oxygen consumption rates were slightly increased after addition of HO-CoQ10 but also of its vehicle, ethanol, alone. This implies that respiration measurements will not be influenced by H O-CoQ10 in the chamber. Hence, CoQ can be used in experiments without altering O₂ concentration.

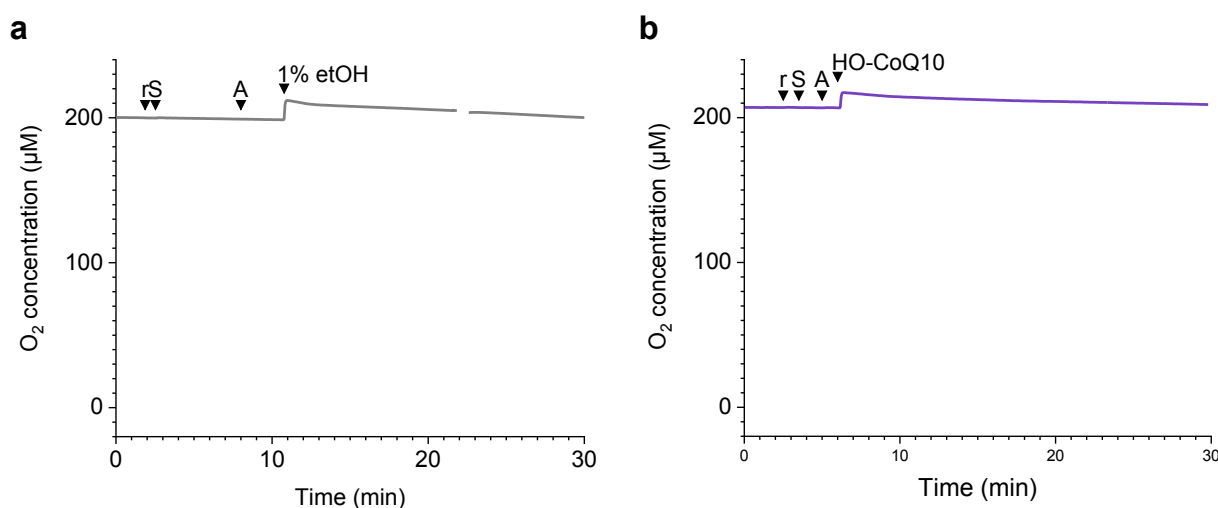


Figure 27 | HO-CoQ10 did not change O₂ concentration in respiration buffer. Oxygen levels measured with a Clark-type electrode at 37 °C, the addition protocol followed measurement of Complex II-linked respiration with subsequent addition of 0.5 µM rotenone (r), 10 mM succinate (S), 1 mM ADP (A), and (a) 1% ethanol to RB 1.2 or (b) 10 µM HO-CoQ10 to RB 3.1 without mitochondria addition. Instrument: O2k (Oroboros Instr.);

As evident from Figure 28, when 200 µg/mL mitochondria were exposed to CoQ10, ethanol or water, respiration remained unchanged. CI-linked OXPHOS rate was slightly, but not significantly, decreased by CoQ10 (a, e). Only when HO-CoQ10, in concentrations starting from 5 µM, was applied, CI- and CII-linked respiration was inhibited significantly (a, b, e, f). Remaining respiration was 39.6% and 23.0% for CI and CII (with 5 µM CoQ), respectively. On the contrary, HO-CoQ10 reduced CIII-linked respiration only after a noteworthy delay (indicated with a dashed line in c, remaining respiration 27.6% (g)). Since high concentrations (800 µM) of duroquinol were needed for Complex III-linked respiration, the inhibitory effect of HO-CoQ10 might be partially masked by oversupply of synthetic Q.

Comparing the redox potentials of duroquinone and CoQs, duroquinol is able to reduce CoQ10 but not HO-CoQ10 ($E_{p,mid}$ vs. Ag/AgNO₃ in *i*-propanol,¹⁸⁵ -0.845 V, -0.71 V and -0.925 V for duroQ/QH₂, CoQ10/H₂CoQ10 and HO-CoQ10/HO-H₂-CoQ10, respectively). Hence, added CoQ10 but not HO-CoQ10 might be present in its

quinol form during the experiments. Since reapplying duroquinol did not rescue inhibition of CIII-linked respiration by HO-CoQ10 (cf. Figure 30 c), competition by the high surplus of synthetic Q alone is doubtful. Though in this case, HO-CoQ10 was applied after consumption of 50% of only 100 μ M applied duroquinol. This opens up the possibility of HO-CoQ10 inhibiting CIII when low concentrations of CIII substrates are present.

Future work should focus on an approach to supply electrons to CIII via endogenous CoQ by its enzymatic reduction. Attempts to use glycerol-3-phosphate as a reducing equivalent for glycerol-3-phosphate dehydrogenase were unsuccessful in MHM (data not shown) due to low expression in heart tissue.^{186,187} Other Coenzyme Q reductases are e.g. DHODH (dihydroorotate dehydrogenase) and ETFQOR (electron transfer flavoprotein oxidoreductase). Nevertheless, it will be important to find a Q reductase activity not affected by HO-CoQ10.

As expected, HO-CoQ10 did not influence Complex IV-linked respiration (d, h). HO-CoQ10 affected the maximal oxidative phosphorylation rate of all respiratory chain complexes containing Q-binding sites.

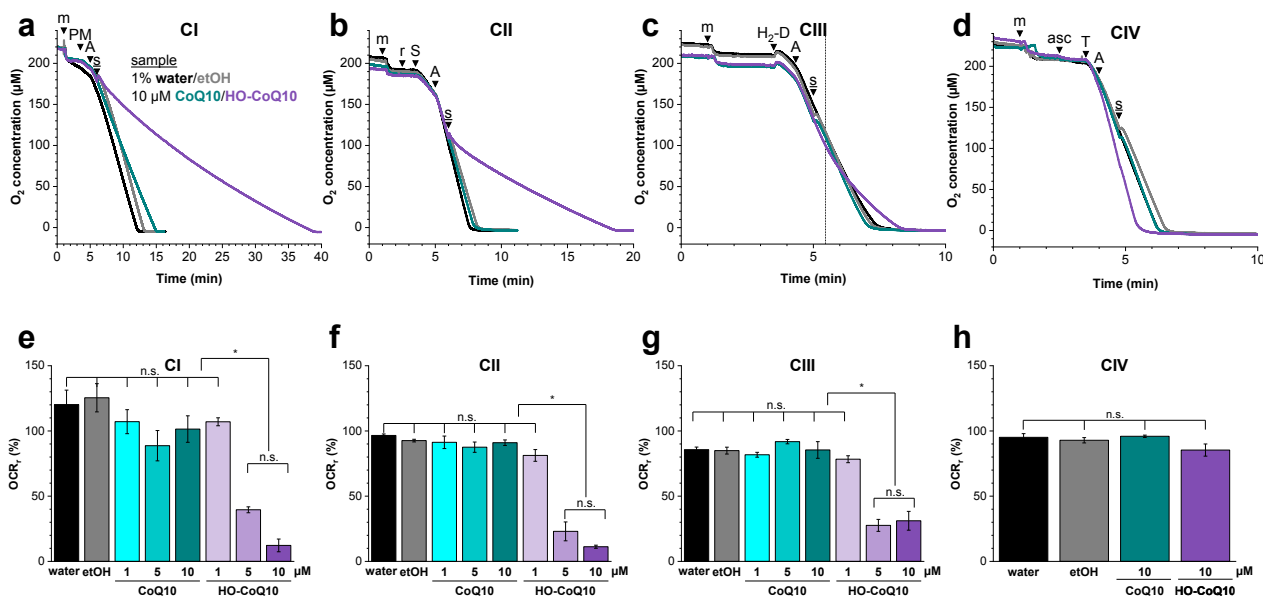


Figure 28 | HO-CoQ10 inhibited CI-, CII-, and CIII-linked respiration. Respiration was followed by the decrease of oxygen using a Clark-type electrode. 0.2 mg/mL MHM were incubated at 37 °C in RB1, then complex-specific substrates, 1 mM ADP (A), and the samples (\underline{s} ; CoQ or solvent controls) were added subsequently as indicated. (a-d) Representative measurements of the change of oxygen concentration over time, (e-h) remaining respiration after sample addition OCR_r (%) normalized to 100% ADP respiration rate (OCR_r = OCR_{after sample}/OCR_{after ADP} · 100 (%)); statistical test, one-way ANOVA: *, p ≤ 0.05; n.s. p > 0.05; (a, e) Complex I-linked respiration using 5 mM pyruvate/malate (PM), (b, f) Complex II-linked respiration using 0.5 μ M rotenone (r) and 10 mM succinate (S), (c, g) Complex III-linked respiration using 0.8 mM duroquinol (H₂-D), the dashed line in panel c marks the delay of HO-CoQ10-induced inhibition; (d, h) Complex IV-linked respiration using 2 mM ascorbate (asc) and 0.5 mM TMPD (T) as substrate cocktails. Samples (\underline{s}) were 10 μ M HO-CoQ10 (violet) or CoQ10 (cyan) and 1% ethanol (grey) or water (black). Graphs show means \pm SEM from 3 independent mitochondrial preparations. Instrument: Oxygraph Plus (Hansatech Instr.);

Figure 29 shows that respiration on succinate (a) and maximal oxidative phosphorylation (b) was strictly dependent on the mitochondrial input in the tested range of 12.5 to 200 μ g mitochondrial protein/mL ($R^2 = 0.999$). However, after addition of 0.1 μ M HO-CoQ10 respiration rate was reduced (c and d). The oxygen consumption rate normalized to mitochondrial input (O₂ flux/mass in pmol/(s · mg)) showed a typical dose-

response curve with an IC₅₀ of 64.1 $\mu\text{g}/\text{mL}$ and a ratio of 1.56 nmol HO-CoQ10 per mg mitochondrial protein (c).

Hence, to reach a roughly half-maximal inhibition of OXPHOS respiration of CII, 1.6 nmol (or 1.6 μM) HO-CoQ10 per mg (or mg/mL) mitochondrial protein is required. Accordingly, when 50 $\mu\text{g}/\text{mL}$ mitochondria were challenged with 0.1 μM HO-CoQ10 (i.e. 2 nmol HO-CoQ10/mg mt. protein), 60% of succinate-linked OXPHOS was left. In contrast, for 200 $\mu\text{g}/\text{mL}$ mitochondria 10 μM HO-CoQ10 (50 nmol HO-CoQ10/mg mt. protein) was necessary to achieve a similar inhibition. In this case, the ratio of HO-CoQ10-to-mitochondrial protein was 25 times higher compared to 50 $\mu\text{g}/\text{mL}$ mitochondria. This discrepancy demonstrates that another parameter, apart from direct RCC inhibition, must be considered because this observation cannot solely be explained by the ratio of endogenous CII content to exogenous CoQ. Since CoQ10 is highly lipophilic and either present in association to proteins, as micellar structures in aqueous environments or primarily in biological membranes, its distribution within mitochondria might play a major role. This indicates a secondary membrane-dependent effect of HO-CoQ10.

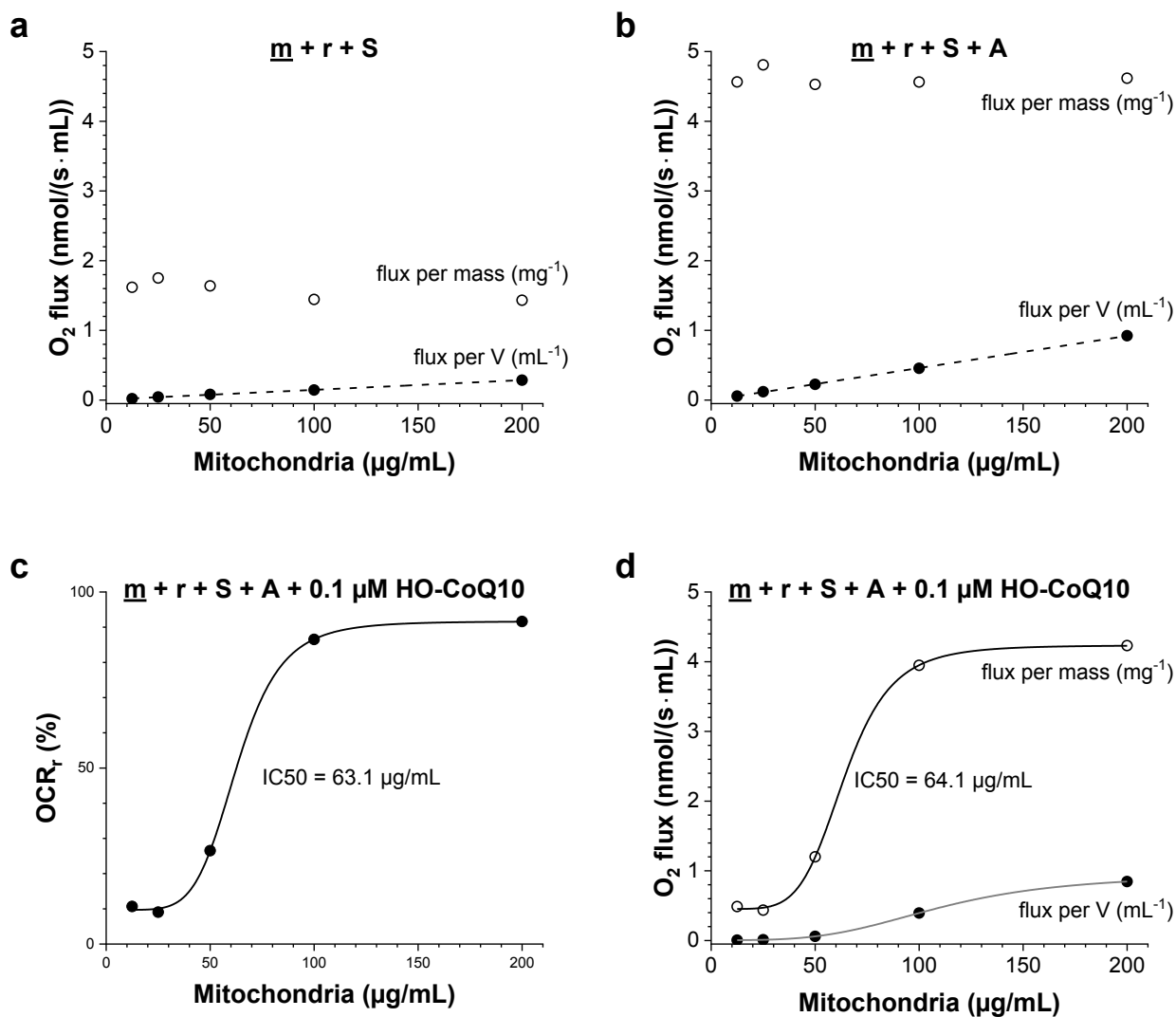


Figure 29 | HO-CoQ10-to-mitochondria ratio determines potency of inhibition of CII-linked respiration. Oxygen consumption of increasing MHM concentrations (mitochondrial protein in $\mu\text{g}/\text{mL}$) in RB3.1 was measured at 37 °C; O₂ flux (i.e. oxygen consumption rate) per volume (closed dots, pmol/(s · mL)) or normalized to mitochondrial input (open circles, pmol/(s · mg)); CII-linked respiration

on (a) substrate mixture: 0.5 μM rotenone (r), 10 mM succinate (S), (b) maximal oxidative phosphorylation with 1 mM ADP (A), and (c) after addition of 0.1 μM HO-CoQ10; (d) remaining oxygen consumption rate (OCR_r) in %, normalized to 100% ADP respiration rate;^w Linear fitting for (a) $y = 7.0612 + 1.39721x$, $R^2 = 0.99885$ and (b) $y = -0.46517 + 4.60852x$, $R^2 = 0.99987$; Logistic function $y = A_2 + (A_1 - A_2)/(1 + x/x_0)^p$ (c) per mass, $\text{IC}_{50} = 64.1 \mu\text{g}$, $R^2 = 0.99931$, $A_1 = 452.70825$, $A_2 = 4234.76717$, $x_0 = 64.10837$, $p = 5.64432$; per volume, $\text{IC}_{50} = 110.7 \mu\text{g}$, $R^2 = 1$, $A_1 = 5.75979$, $A_2 = 950.85975$, $x_0 = 110.68283$, $p = 3.51989$; and (d) $\text{IC}_{50} = 62.97751 \mu\text{g}$, $R^2 = 0.99884$, $A_1 = 9.70473$, $A_2 = 91.65275$, $x_0 = 62.97751$, $p = 5.88243$; Graphs show results from 1 independent mitochondrial preparation. Instrument: O2k (Oroboros Instr.)

On one hand, neither CoQ10 nor CoQ1 was able to rescue CI-linked respiration inhibited by HO-CoQ10 (CoQ10, see **Figure 30 a**; CoQ1, data not shown), arguing for a non-competitive inhibition mechanism. On the other hand, CoQ10 itself inhibited respiration at low mitochondrial input, so rescue of HO-CoQ10 inhibition would be unlikely (cf. **Figure 38 c** and **d** on p. 94, further discussed in **section 3.6.3**, p. 93).

Embelin,^x a structural analogue of decyl-UQ, containing two hydroxy groups in *ortho*-position to the keto groups and a side chain of 11 C-atoms, was suggested to inhibit the ETC through a light decoupling effect (structure, see insert in **Figure 30 b**).¹⁶³ Embelin inhibited Complex I-linked respiration only at high concentrations starting from 50 μM applied on 0.2 mg/mL MHM as can be seen in **b**. Even at a 100- μM concentration, the inhibition did not seem as stable as with HO-CoQ10 (cf. **Figure 28 a**, p. 81). Hence, probably distinct mechanisms are underlying the inhibitory effects of both substances. Using different mitochondrial concentrations and titration of known uncouplers should clarify this hypothesis. Addition of the uncoupler should further inhibit mitochondria when uncoupling is the underlying process. However, the remaining respiration rate was unchanged, when the influence of CCCP was tested on HO-CoQ10-dependent inhibition (data not shown). It has to be considered, that embelin was dissolved in DMSO and not like HO-CoQ10 in ethanol which might affect its localisation. Additionally, the solubility of embelin and CoQ10 are very different. So, comparisons to decyl-UQ, CoQ1 and their hydroxy analogues will be more appropriate as membrane properties and distribution will be more similar.

When mitochondria, respiring on a low concentration of decyl-ubiquinol, were treated with the CIII inhibitor antimycin A or HO-CoQ10, respiration could not be reinitiated upon readdition of decyl-ubiquinol. This indicates that CIII might only be affected at low substrate concentrations or preincubation with HO-CoQ10.

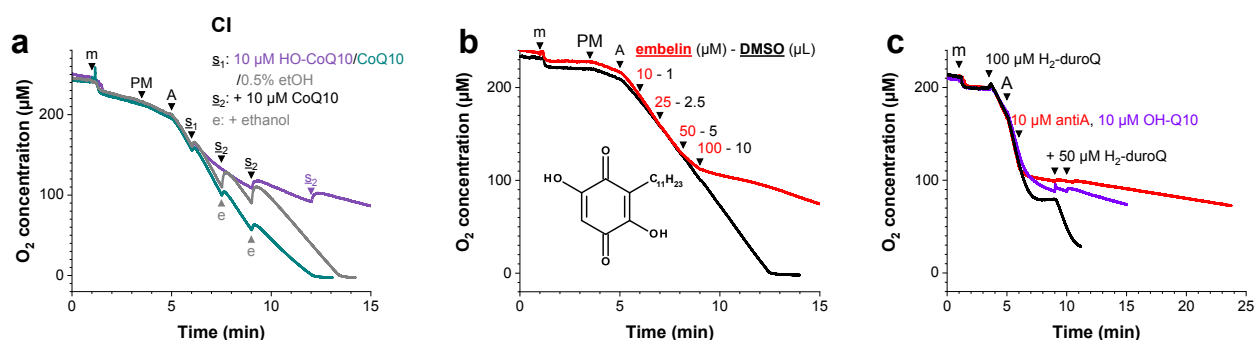


Figure 30 | CI inhibition by embelin (c) and impact of Q-readdition on CI- and CIII-linked respiration (b, c). Oxygen consumption of 200 $\mu\text{g}/\text{mL}$ MHM in RB1 was measured at 37 $^\circ\text{C}$. (a, b) CI-linked respiration with 5 mM pyruvate/malate (PM) and 1 mM ADP (A), (a)

^w $\text{OCR}_r = \text{OCR}_{\text{after sample}} / \text{OCR}_{\text{after ADP}} \cdot 100 (\%)$,

^x 2,5-dihydroxy-3-undecyl-1,4-benzoquinone

after application of CoQ or solvent, CoQ10 (or ethanol) was added in 10 μ M (10 μ L each) portions; (b) application of increasing concentrations of embelin or vehicle, final concentrations and volumes are designated; (c) CIII-linked respiration using 100 μ M duroquinol (H_2 -duroQ, stock solution 10 mM in ethanol) as a substrate and 1 mM ADP (A), respiration was inhibited with 10 μ M antimycin A (antiA) or HO-CoQ10; to check if exhaustion of the substrate was responsible for reduced respiration, 50 μ M duroquinol was applied to the control (black), antimycin A-treated (red) and HO-CoQ10-treated (violet) mitochondria. Graphs show results from 1 independent mitochondrial preparation. Instrument: Oxygraph Plus (Hansatech Instr.)

Different application methods to assess the influence of HO-CoQ10 on CI-linked respiration were tested (**Figure 31**). In all previously presented experiments, CoQs were added after stimulating full oxidative phosphorylation capacity with substrate and saturating ADP. This protocol allowed the evaluation of the respiratory control ratio (RCR) of the mitochondrial preparation in every experiment. The RCR ((OCR in presence of saturating ADP)/(OCR in presence of substrate)) provides a measure of the integrity of the outer mitochondrial membrane and therefore of the quality of mitochondrial preparations.

When CoQs were added directly after substrates, respiration was reduced by HO-CoQ10 and then was not responsive to ADP stimulation (**Figure 31 a**, violet trace). CoQ10 did not affect substrate respiration but reduced OXPHOS capacity (cyan trace), since oxygen consumption rate after ADP addition was lower than with the vehicle (ethanol, grey trace) or water (black trace). Ethanol did not influence respiration (grey trace).

In **Figure 31 b-d** mitochondria were preincubated with CoQ. In **b**, mitochondria were exposed to CoQ for 1 min before proceeding the addition protocol. To assess coupling of electron transport to ATP production, RCR was calculated as mentioned by dividing oxygen consumption rate (OCR) before and after ADP addition. Respiration was reduced by HO-CoQ10 but still reacted to PM, ADP, and oligomycin treatment. CoQ10-treated mitochondria were completely uncoupled: Although PM induced respiration at similar rates as in ethanol-treated mitochondria, respiration could neither be stimulated by ADP nor reduced by oligomycin. This behaviour is reflected in the RCR of approx. 1 and 2 after CoQ10 and HO-CoQ10 treatment compared to an RCR of 5 after incubation with ethanol. Increasing the preincubation time to 2 min, inhibition by HO-CoQ10 was stronger than for CoQ10 (**c**). However, in this experiment, CoQ10 only slightly uncoupled respiration.

In another approach (**Figure 31 d**), mitochondria were preincubated with CoQ10/HO-CoQ10 or ethanol in respiration buffer at 37 °C for 1 h before transfer to the chamber as suggested by Takahashi et al. (2013) for CoQ10.¹⁸⁸ HO-CoQ10 inhibited respiration that could not be stimulated by PM or ADP, whereas CoQ10 uncoupled respiration but did not suppress it. Only mitochondria incubated with ethanol were stimulated by PM and ADP but showed a high degree of uncoupling in this measurement. If prolonged incubation with ethanol or incubation of mitochondria at 37 °C alone led to uncoupling, needs to be examined in further experiments and control experiments without vehicle.

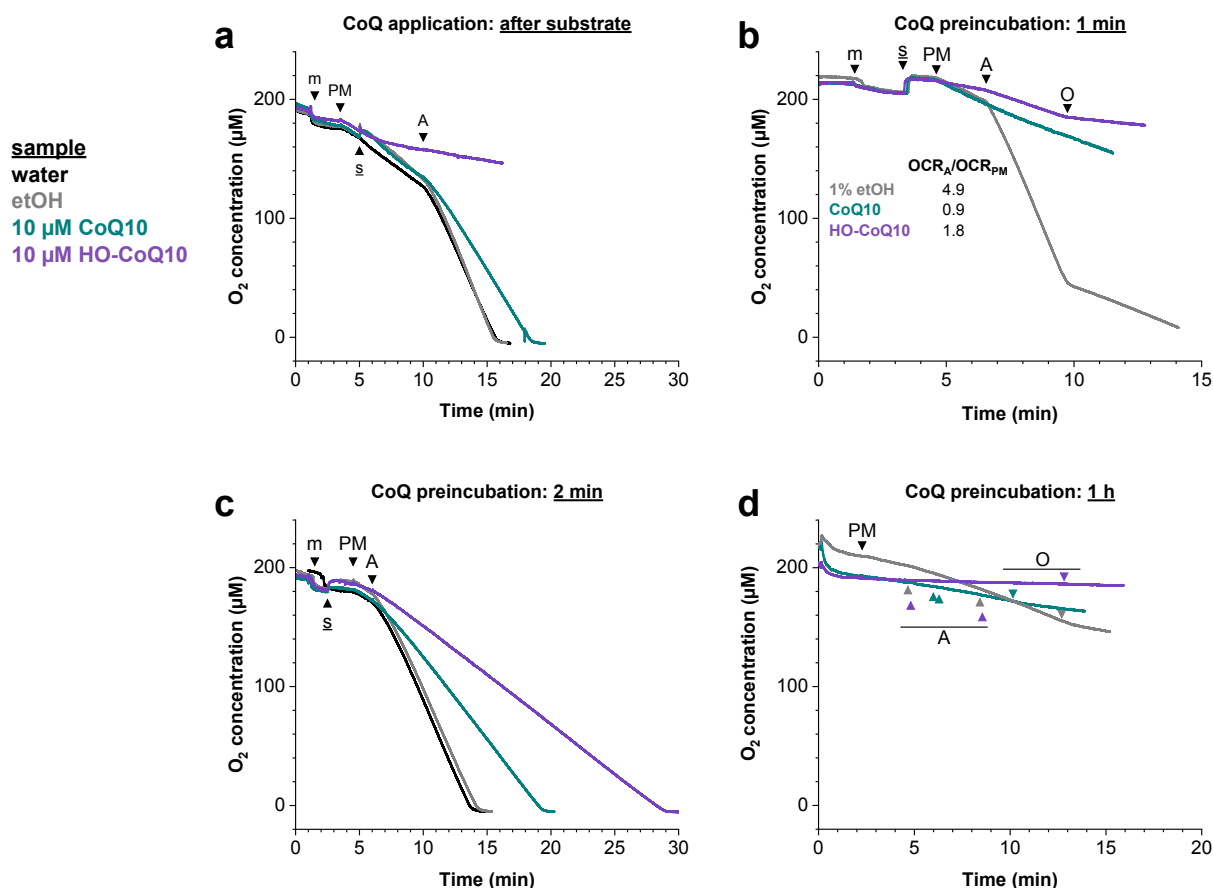


Figure 31 | Timing of CoQ application differentially influenced respiration. CI-linked respiration of 0.2 mg/mL MHM in RB1 was initiated by 5 mM pyruvate/malate (PM) and 1 mM ADP (A). The sample (s) (10 µM HO-CoQ10, CoQ10 or 1% ethanol) was added at indicated times. 1.2 µM oligomycin (O) was applied to assess coupled respiration. (a) Application of CoQ before ADP addition; preincubation of MHM with CoQ in the chamber for (b) 1 min or (c) 2 min prior to substrate addition; (d) MHM were preincubated in RB1 together with 10 µM HO-CoQ10/CoQ10 or vehicle (1% ethanol) for 1 h at 37 °C before transfer to the chamber; Graphs show results from 1 independent mitochondrial preparation (pool of (b) 3 and (d) 2 mouse hearts). Instrument: Oxygraph Plus (Hansatech Instr.), T: 37 °C;

On one hand, CoQ10 showed uncoupling effects when supplied to mitochondria before the ETC was activated (b, d). On the other hand, CoQ10 slightly reduced respiration when added after ETC substrates (Figure 31 a, and Figure 28 a).

As outlined before, CoQ10 and HO-CoQ10 are highly lipophilic and therefore experimental design is challenging. Effects might be diminished by poor and variable solubility (e.g. influenced by ambient temperature) and uptake by mitochondria. To overcome these issues, water-soluble CoQ10 formulations were used in many studies.^{188,189}

When HO-CoQ10 and CoQ10 were applied in a water-soluble formulation with Cholesterol-PEG (cf. Figure 18, p. 66), respiration was not influenced (Figure 32 a and b). It is not clear if CoQ incorporates into the inner mitochondrial membrane when it is part of a carrier complex. The complexation with PCS might only be appropriate for preincubation experiments or oral administration of high concentrations.^{96,190}

To evade these uncertainties, the small CoQ analogues Coenzyme Q1 and decyl-ubiquinone were tested on CI-linked OXPHOS (Figure 32 c). As for CoQ10 (see Figure 28, p. 81), respiration rate did not increase even though

more CoQ was available. This might be due to the fact that the endogenous CoQ10 pool is already saturated as increased respiration rates with exogenously applied CoQ10 have only been observed in CoQ-deficient mitochondria.¹⁸⁸

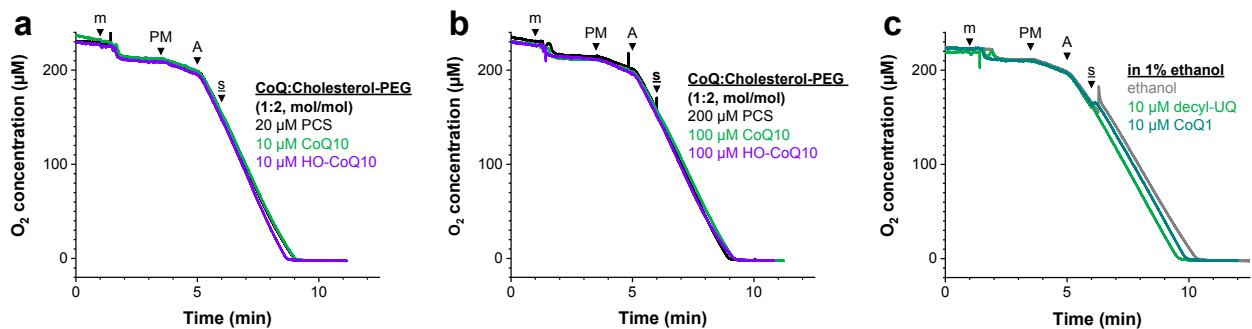


Figure 32 | Water-soluble quinones did not influence respiration. 0.2 mg/mL MHM were measured in RB1 at 37 °C. Complex I-linked respiration was induced by adding 5 mM pyruvate/malate (PM) and 1 mM ADP (A). The influence of water-soluble quinones was measured by their addition at the time marked with \underline{s} (sample): water-soluble formulation of HO-/CoQ10 with Cholesterol-PEG (1:2, mol/mol; HO-CoQ10, reaction mixture; stock in water) diluted to (a) 10 µM CoQ/20 µM PCS and (b) 100 µM CoQ/200 µM PCS final concentration; (c) 10 µM small CoQ analogues CoQ1 and decyl-UQ (stocks in 100% ethanol). Graphs show results from 1 independent mitochondrial preparation (pool of 2 mouse hearts). Instrument: Oxygraph Plus (Hansatech Instr.)

3.6 Ca²⁺ potentiated respiratory inhibition by HO-CoQ10

3.6.1 Preliminary data: Ca²⁺ amplified HO-CoQ10-linked respiratory inhibition of mitochondria from different species

All respiration experiments presented until now were conducted in Ca²⁺-free solutions. Considering the Ca²⁺ binding and transporting potential of HO-CoQ10,⁸ its inhibitory effect might have been due to depletion of mitochondria from Ca²⁺. In order to test if the inhibition could be evaded under resting cytosolic Ca²⁺ conditions, calcium chloride was added to the respiration buffer. Adding 200 nM CaCl₂ to RB1 lacking EGTA (RB1, detailed composition, see p. 23), the CI- and CII-linked oxygen consumption rate was drastically reduced in mouse heart mitochondria in comparison to Ca²⁺-free conditions (see **Figure 33 a and b**: solid line, Ca²⁺-free; dashed line, CaCl₂ added). The same was true for yeast mitochondria (c-e), where ~190 nM free Ca²⁺ (calculated considering concentrations of MgCl₂, EGTA, and the ionic strength of the buffer)^y was added and high concentrations of HO-CoQ10 were needed to inhibit respiration (c and d, 50 and 10 µM HO-CoQ10, respectively; e, 10 µM CoQ10 and vehicle control). Extraordinary high HO-CoQ10 concentrations were necessary because yeast were cultured on respiratory medium upregulating RCC expression.

^y 190 nM free Ca²⁺ is inaccurate since 20 mM P_i was not taken into account when calculating free Ca²⁺ concentrations.

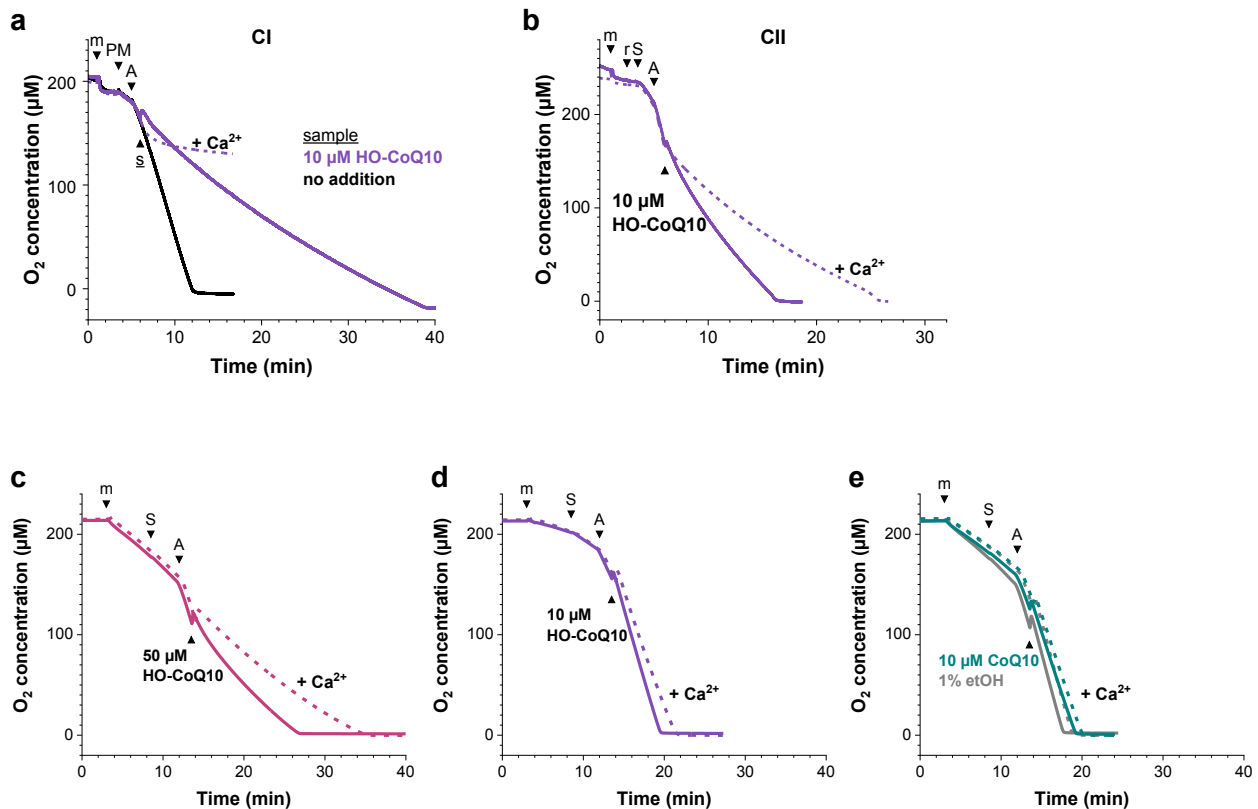


Figure 33 | Calcium potentiated the inhibitory effect of HO-CoQ10 on respiration of isolated mouse heart and yeast mitochondria. Using a Clark-type electrode, the consumption of oxygen by respiration of (a, b) 0.2 mg/mL mouse heart mitochondria in RB1 and (c-e) 0.1 mg/mL yeast mitochondria^z in RB4 was monitored at 37 °C. Mitochondria (m), substrate/s, 1 mM ADP (A) and the sample (s, HO-CoQ10, CoQ10 or 1% ethanol as final concentration) were added at the indicated times. (a) CI-linked respiration using PM (5 mM pyruvate and malate) as substrates, (b) CII-linked respiration using 0.5 µM rotenone (r) and 10 mM succinate (S) as a substrate; (c-e) CII-linked respiration using 10 mM succinate (S) as a substrate;^{aa} Graphs show results from 1 independent mitochondrial preparation. Buffer: (a, b) RB1 (with 0.5 mM EGTA) for Ca²⁺-free conditions (solid lines) or without EGTA but supplemented with 200 nM CaCl₂ (dashed lines); (c, d, e) RB4 with 0.5 mM EDTA for Ca²⁺-free conditions (solid lines) or with 0.75 µM CaCl₂ and 0.5 mM EDTA (191.2 nM free Ca²⁺, dashed lines); instrument: (a, b) Oxygraph Plus (Hansatech Instr.), (c-e) O2k (Oroboros Instr.)

To further investigate calcium dependence of the HO-CoQ10-mediated respiratory inhibition, defined free, extramitochondrial Ca²⁺ concentrations had to be set. The used respiration buffers contained high concentrations of inorganic phosphate (2-20 mM P_i). At the cytosolic pH of 7.2,¹⁹¹ potassium dihydrogen phosphate (KH₂PO₄) dissociates into dihydrogen phosphate (H₂PO₄⁻) and hydrogen phosphate (HPO₄²⁻).¹⁹² Phosphate (PO₄³⁻), that forms insoluble trimagnesium and tricalcium salts (Mg₃(PO₄)₂ and Ca₃(PO₄)₂), is not present at neutral pH.¹⁹² Single and double negatively charged phosphates form monomagnesium and dimagnesium salts (Mg(H₂PO₄)₂, slightly soluble¹⁹³ and MgHPO₄, 1.2 mM at 25 °C,^{194,195} respectively) as well as monocalcium and dicalcium salts (Ca(H₂PO₄)₂, ~ 77 mM¹⁹⁶ and CaHPO₄, 0.4 mM at 25 °C,¹⁹⁷ respectively), thus are modulating free Ca²⁺ concentrations. Since solubility of calcium and magnesium is highly variable

^z Yeast mitochondria isolated from *Saccharomyces cerevisiae* were provided by Florian Wollweber (Department of Medical Biochemistry & Molecular Biology, Saarland University)

^{aa} To measure CII-linked respiration of *S. cerevisiae* mitochondria, application of rotenone is not necessary since this yeast lacks Complex I.

depending on buffer composition and may change with formation of metal complexes, free calcium concentrations needed to be determined experimentally.

3.6.2 P_i reduced free Mg^{2+} and free Ca^{2+} concentrations in respiration buffer

The exact composition of all used respiration buffers (RB) is listed in the material and methods section on p. 23 ([RB2](#) and [RB3](#)). Even though for fluorescence-based Ca^{2+} determinations the use of concentrations higher than 1 μM fura-2 was not recommended,¹⁹⁸ 10 μM (mag-) fura-2 was used in all experiments because initial comparisons of 1 and 10 μM fura-2 showed a higher signal-to-noise ratio using 10 μM and no inner filter effects were observed (data not shown).

Strictly following the calcium calibration protocol for Ca^{2+} indicators from Thermo Fisher Scientific,¹²⁰ the calibration was performed using two solutions of RB2 (in mM: 137 KCl, 20 HEPES; pH 7.21) containing either 10 mM CaEGTA (10 mM $CaCl_2$ + 10 mM EGTA) or 10 mM EGTA and the ratiometric calcium indicator fura-2.^{bb} By mixing these solutions, free calcium concentrations between 200 nM and 40 μM were obtained.

Comparing these solutions with analogous solutions containing 4 mM P_i showed that free calcium is drastically reduced at high CaEGTA concentrations ([Figure 34](#), [blue curve](#)). This implies that not only the calculated free Ca^{2+} concentration but primarily $CaCl_2$ input is relevant for the formation and solubility of $Ca-PO_4$ salts since affinity of calcium to EGTA might be constricted by presence of P_i .

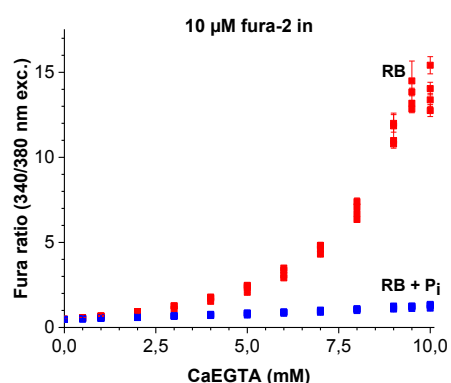


Figure 34 | High CaEGTA concentration drastically reduced free $[Ca^{2+}]$ in presence of P_i . RB2.6 (10 mM CaEGTA) was diluted stepwise with RB2.5 (Ca-free, 10 mM EGTA) to yield different free Ca^{2+} concentrations. [RB2](#) (mM): 137 KCl, 20 HEPES, pH 7.21 using KOH; [RB + \$P_i\$](#) contained 4 mM P_i additionally;

Accordingly, EGTA concentrations in calibration solutions were reduced to concentrations needed for the experiments. The EGTA concentration was set to 0.1 mM to assure the lowest impact on free Mg^{2+} . As evident from [Table 14](#), reducing calcium concentrations decreased free Mg^{2+} up to 0.9% in 0.1 mM EGTA compared to 3.6% in 0.5 mM EGTA. The lower the calcium concentration the more free EGTA is present that might complex magnesium. Additionally, P_i concentration was increased to 4 mM to assure a saturating P_i concentration needed for oxidative phosphorylation.

^{bb} Fura-2, 2-[6-[bis(carboxymethyl)amino]-5-[2-[2-[bis(carboxymethyl)amino]-5-methylphenoxy]ethoxy]-1-benzofuran-2-yl]-1,3-oxazole-5-carboxylic acid

Table 14 | Calculated free Ca^{2+} and Mg^{2+} concentrations in respiration buffer containing 0.1 mM EGTA and 0.5 mM EGTA. Free Ca^{2+} and Mg^{2+} concentrations were calculated using maxchelator.¹²¹ Grey, not reliable free $\text{Ca}^{2+}/\text{Mg}^{2+}$ concentrations because out of EGTA buffer range; buffer composition (mM): 137 KCl, 20 HEPES, 2.5 MgCl_2 , EGTA and CaEGTA (0.5 or 0.1 mM EGTA + varying CaCl_2 concentrations) as indicated, pH 7.2;

0.5 mM EGTA			0.1 mM EGTA		
CaEGTA (mM)	[Ca_{free}] (μM)	[Mg_{free}] (μM)	CaEGTA (mM)	[Ca_{free}] (μM)	[Mg_{free}] (μM)
0.5	9.09	2.25	0.1	3.99	2.25
0.45	1.43	2.25	0.09	1.29	2.25
0.4	0.651	2.23	0.08	0.631	2.25
0.35	0.381	2.22	0.07	0.376	2.24
0.3	0.245	2.21	0.06	0.243	2.24
0.25	0.163	2.21	0.05	0.162	2.24
0.2	0.108	2.20	0.04	0.107	2.24
0.15	0.0699	2.19	0.03	0.0699	2.24
0.1	0.0408	2.18	0.02	0.0408	2.24
0.05	0.0181	2.17	0.01	0.0181	2.23
0	0	2.17	0	0	2.23

Presence of metal chelators necessary for fura-2 measurements

Figure 35 reveals that the use of metal chelators like EGTA or EDTA was obligatory to detect calcium and magnesium with fura dyes. When chelators were omitted (a, d), (mag-) fura-2 already showed an excitation spectrum of its metal-bound state before any addition of Mg/Ca, hindering the capacity of fura to undergo a spectral change upon chelation. Only when EDTA was present, (mag-) fura-2 was in its unbound state (c, f, black line). With increasing Mg/Ca concentrations, the maximal absorption then shifted from 370 nm to 340 nm (c, f). Even though binding affinities of fura-2 to Ca^{2+} (K_d , 140 nM^{cc})^{120,198,199} and furaptra^{dd} to Mg^{2+} (K_d , 1.5-2 mM^{ee})²⁰⁰⁻²⁰² are high, other metals have much higher affinities, such as zinc with a 100-fold²⁰³ higher affinity to fura-2 than Ca. To avoid saturation of the indicator by traces of Zn^{2+} or other heavy metals, application of the chelator TPEN was recommended by the supplier.²⁰² Even 10-fold higher concentrations of TPEN than suggested were not able to keep fura in its non-chelated form as seen by its maximal absorption at 340 nm (h). Thus, EGTA was always present in calibration solutions, also when free $\text{Mg}^{2+}/\text{Ca}^{2+}$ exceeded the chelator's buffering capacity.

^{cc} 135 nM¹⁹⁹ in 100 mM KCl, pH 7.1-7.2, 20°C; 140 nM¹⁹⁸ in 100 mM KCl, 10 mM MOPS, pH 7.20, 0-10 mM CaEGTA, 22 °C; 145 nM¹²⁰ in 100 mM KCl, 30 mM MOPS, pH 7.2, 0-10 mM CaEGTA, 20 °C

^{dd} Furaptra, mag-fura-2

^{ee} 1.5 mM²⁰⁰ in 115 mM KCl, 20 mM NaCl, 10 HEPES, pH 7.05, 37 °C; 2 mM²⁰¹ in 90 mM KCl, 10 mM MOPS, pH 7.20±0.02, 0-200 MgCl_2 , 20 °C; 1.9 mM²⁰² in 115 mM KCl, 20 mM NaCl, 10 mM Tris, pH 7.05, 0-35 mM Mg^{2+} , 22 °C

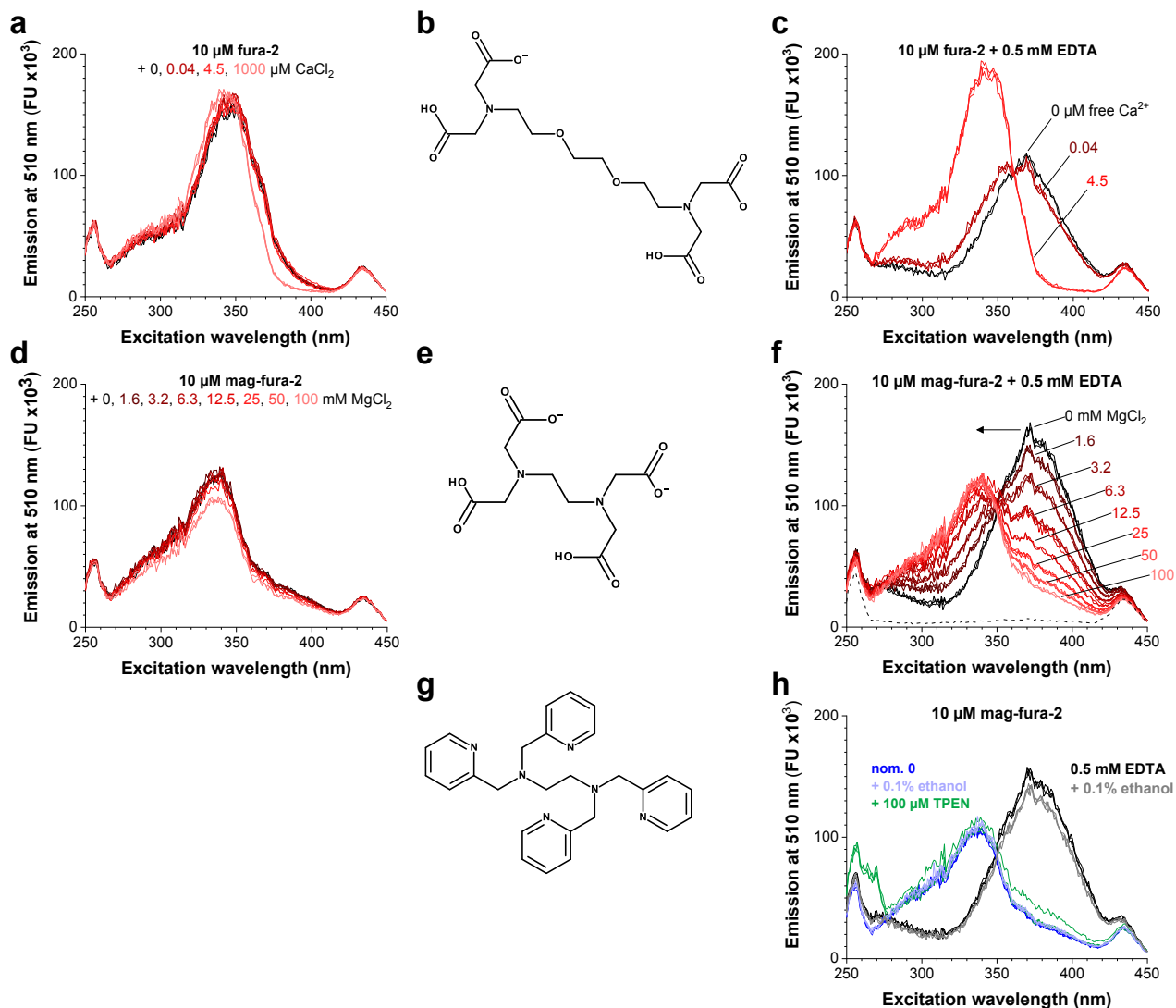


Figure 35 | Presence of metal chelators is essential to detect Ca²⁺ and Mg²⁺ using fura-2 related indicators. Fluorescence excitation spectra at 37 °C of (a, c) 10 μM fura-2 and (d, f, h) mag-fura-2 with an emission wavelength of 510 nm in RB2; solutions contained increasing concentrations of (a, c) CaCl₂ or (d, f) MgCl₂ in (a, d) absence or (c, f, h) presence of metal chelators; metal chelators are (b) EGTA for Ca²⁺, (e) EDTA for Mg²⁺, and (g) TPEN for Zn²⁺. RB2 (mM): 137 KCl, 20 HEPES, pH 7.21 using KOH

Determination of free Mg²⁺ concentration: Free Mg²⁺ concentration was reduced by P_i

First, the free Mg²⁺ concentration in respiration buffer was determined because Mg-PO₄ salts will affect the free Mg²⁺ concentration, and the fura-2 dissociation constant for calcium is Mg²⁺-sensitive (K_d of fura-2 in presence of Mg, 224 nM^{ff}).¹⁹⁹

Excitation spectra of Mg²⁺ calibration solutions in absence of P_i are shown in Figure 36 b. The clear isosbestic point at 349 nm is in agreement with literature values (e.g. 347 nm²⁰⁰) and indicates a 1:1 conversion from the mag-fura-2 ion to its chelated state upon Mg²⁺ application. The slope of the Hill plot of 1.05 (in c) agrees with a 1:1 binding of Mg²⁺ to the indicator. From the x-value at y = 0, the logarithm of the dissociation constant can

^{ff} 224 nM¹⁹⁹ in 115 mM KCl, 20 mM NaCl, 10 mM MOPS, 1 mM free Mg²⁺, pH 7.05, 37 °C

be obtained (cf. Figure 37 d). Thus, the K_d of mag-fura-2 for Mg^{2+} was determined to be 1.14 mM (mean of 5 calibrations).

The free Mg^{2+} concentration in respiration buffer containing 4 mM P_i (e) could then be calculated using the calibration line in d ($[free\ Mg^{2+}] = (ratio_{corr} - 0.27808)/0.18753$). Adding P_i resulted in chelation of 10% of the total input of 2.5 mM magnesium defined by the horizontal line in f; free Mg^{2+} further decreased at high EGTA concentrations (f).

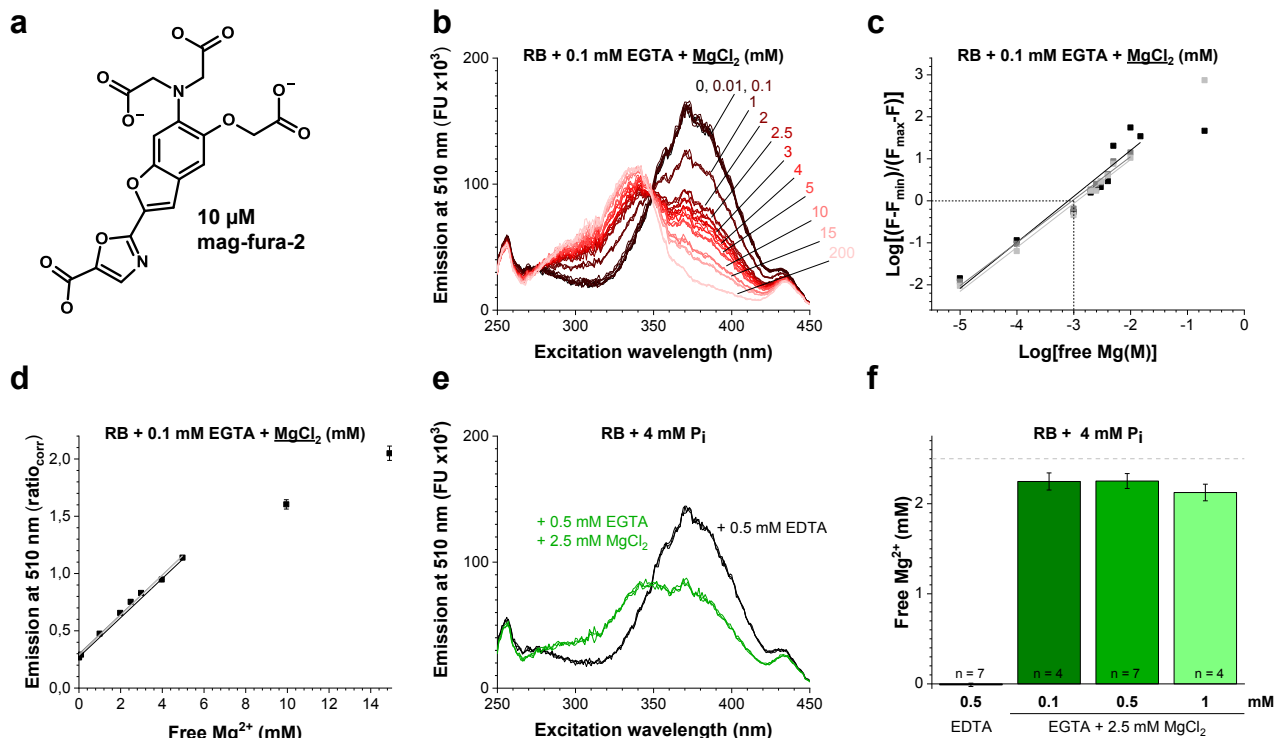


Figure 36 | Free $[Mg^{2+}]$ dropped by 10% in respiration buffer (RB) containing P_i . Free Mg^{2+} concentrations were calibrated in RB2 with 10 μM of the ratiometric Mg^{2+} indicator (a) mag-fura-2 (b-d) in RB2 with 0.1 mM EGTA and increasing $MgCl_2$ concentrations. (e, f) Free $[Mg^{2+}]$ was determined in RB2 supplemented 4 mM P_i , 2.5 mM $MgCl_2$ and EGTA/EDTA.

Measurements were performed at 37 °C. (b, e) Fluorescence excitation spectra, em. 510 nm; (c) Hill plot of fluorescence signal at 340 nm excitation, dashed lines indicate logarithm of K_d ; (d) mag-fura-2 calibration curve for free $[Mg^{2+}]$ (calculated using maxchelator)¹²¹ using the background-corrected fluorescence ratio $(F_{340}-F_{340_{BG}})/(F_{380}-F_{380_{BG}})$, i.e. Mg-free conditions were subtracted, linear fit, $y=0.27808+0.18753x$, mean \pm SEM of single excitation wavelength measurements of 3 independent serial dilutions; (f) calculated free Mg^{2+} concentrations using calibration line (d);

Buffer: RB2 (mM): 137 KCl, 20 HEPES, pH 7.21; (b-d) RB2.1/RB2.2, (e, f) without $MgCl_2$: RB2.7, with $MgCl_2$: RB2.8-RB2.10;

Determination of free Ca^{2+} concentration: Free Ca^{2+} was reduced by P_i

To determine free Ca^{2+} concentrations, 2.25 mM instead of 2.5 mM $MgCl_2$ was added to Ca^{2+} calibration solutions (RB without P_i) to mimic free Mg^{2+} concentrations in presence of P_i (Figure 36 f, 0.1 mM EGTA). Increasing CaEGTA concentrations (0.1 mM EGTA, 0-0.1 mM $CaCl_2$) were added and fura-2 fluorescence at a single excitation wavelength (Figure 37 c, 340 nm) or the ratio of 340 to 380 nm (e, g) was evaluated. The excitation spectra (b) show an isosbestic point at 361 nm.

The log-plot of fura-2 fluorescence and Ca^{2+} concentration with a slope of 1.44 implies that more than one Ca^{2+} ion is bound per fura-2 molecule (c). This discrepancy might be due to free Mg^{2+} concentrations being more variable than suggested in Table 14. Those values have been listed despite being out of the buffer range of

EGTA for Mg^{2+} . Nonetheless, the calculated K_d^{fura-2} for Ca^{2+} in RB2.3 with 106.4 nM at 37 °C (mean of 5 calibrations) was near reported values of 140 nM^{gg} at RT in high KCl solutions.^{198,199} However, the dissociation constant was expected to be higher than the reported 140 nM because temperature increase and presence of magnesium was shown to be correlated to a decrease of Ca^{2+} affinity of fura-2 analogues²⁰⁴ and fura-2¹⁹⁸, respectively.

The calibration curve of free Ca^{2+} in P_i -free respiration buffer (Figure 37 e), calculated from the mean of 3 independent measurements, was used to convert fura-2 ratios in P_i -containing buffers to free Ca^{2+} concentrations ($[Ca_{free}] = (\ln(1 - \text{ratio}_{corr}/2.89534))/2.87468$) for each CaEGTA concentration (plotted in g). In f, excitation spectra of respiration buffer containing 4 mM P_i and increasing CaEGTA concentrations again show a clear isosbestic point. However, fluorescence at 340 nm, the absorption peak of calcium-chelated fura-2, was reduced in comparison to solutions without phosphate (cf. f and b) showing that P_i limited free calcium concentrations. Plotting CaEGTA against calculated free calcium concentrations in g, desired free Ca^{2+} concentrations were chosen and prepared by dilution to the correlating CaEGTA concentration. Low free Ca^{2+} concentrations around 50 nM were not influenced by P_i concentrations up to 4 mM. Higher Ca^{2+} concentrations were drastically affected by P_i (0.08 mM CaEGTA: 1.5 mM P_i , reduction of 9%; 4 mM P_i , reduction of 29%). At potentially high free Ca^{2+} concentrations (0.09 mM CaEGTA), measuring errors were increased due to susceptible Ca^{2+} complexes and/or exceeding the indicator's measuring limit (preferable detection range $0.1-10 \cdot K_d^{205}$).

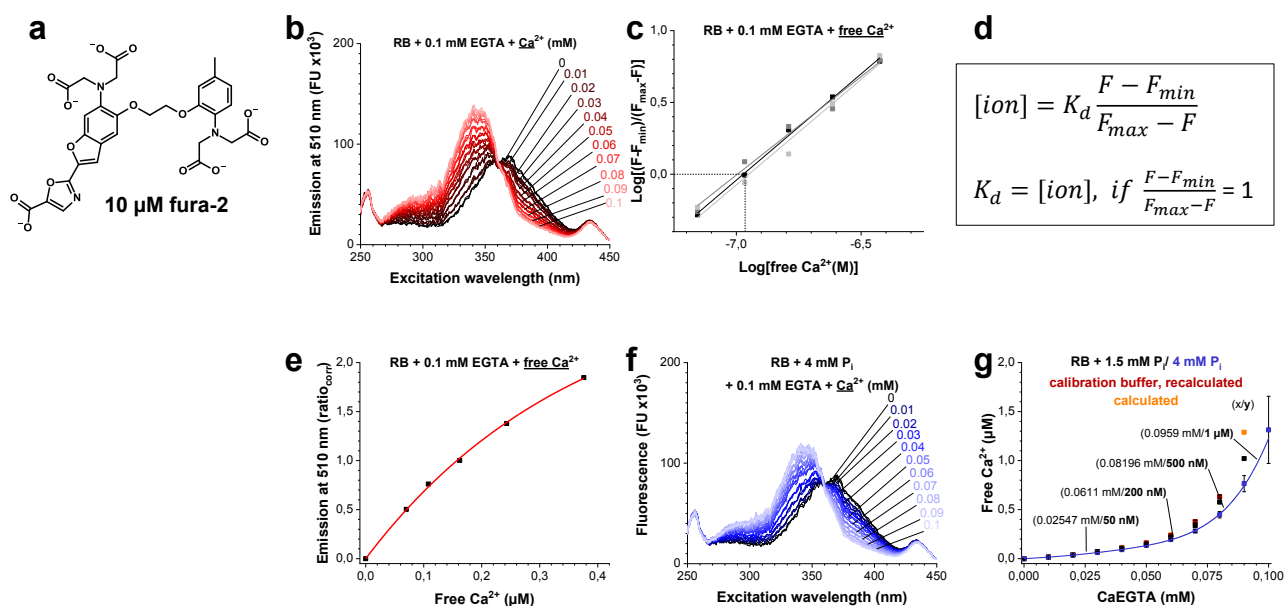


Figure 37 | P_i reduced free calcium concentrations in respiration buffer (RB). Free Ca^{2+} concentrations were calibrated in RB2 with 10 μM of the ratiometric Ca^{2+} indicator (a) fura-2 in (b, c, e) Ca^{2+} calibration solutions with 2.25 mM $MgCl_2$, 0.1 mM EGTA and increasing $CaCl_2$ concentrations. Free $[Ca^{2+}]$ was determined in (f) RB2 with 2.5 mM $MgCl_2$, 0.1 mM EGTA and increasing $CaCl_2$ concentrations supplemented with 4 mM P_i and/or (g) 1.5 mM P_i .

Measurements were performed at 37 °C. (b, f) Fluorescence excitation spectra, em. 510 nm; (c) Hill plot of fluorescence signal at 340 nm excitation, (d) determination of dissociation constant K_d , (e) fura-2 calibration curve for free $[Ca^{2+}]$ (calculated using maxchelator)¹²¹ using the background-corrected ratio $(F_{340} - F_{340_{BG}})/(F_{380} - F_{380_{BG}})$, i.e. Ca-free conditions were subtracted, fitted with BoxLucas1,

^{gg} 135 nM¹⁹⁹ in 100 mM KCl, pH 7.1-7.2 at 20 °C; 140¹⁹⁸ nM in 100 mM KCl, 10 mM MOPS, pH 7.2, 0-10 mM CaEGTA at 22 °C

$y = a(1 - e^{-bx}) = 2.89534(1 - e^{-2.87468x})$, direct weighting, mean \pm SEM of single excitation wavelength measurements of 3 independent serial dilutions; (g) calibration curve (blue): CaEGTA concentration vs. calculated free Ca^{2+} concentration in RB supplemented with 4 mM P_i (mean of 5 calibrations with instrumental weighting: $y = -3.2 \cdot 10^{-17} + 1.4x + 4.0x^2 + 1\,268.4x^3 - 3\,1930.6x^4 + 296725.5x^5$) in comparison to 1.5 mM P_i (black) or recalculated calibration buffers (red); free $[\text{Ca}^{2+}]$ was calculated using background-corrected fura-2 ratios and calibration curve from (e); calculated (orange): free $[\text{Ca}^{2+}]$ was calculated for Ca^{2+} calibration solutions using maxchelator;¹²¹ Buffer: RB2 (mM): 137 KCl, 20 HEPEs, pH 7.21; (b, c, e) RB2.3/RB2.4, (f, g) 4 mM P_i ; RB3.1/RB3.2, 1.5 mM P_i ; RB2.11/RB2.12 (4 mM P_i replaced with 1.5 mM P_i), calibration buffer: RB2.3/RB2.4;

Since free magnesium and calcium concentrations were demonstrated to be dependent on chelator and in particular on P_i concentration, respiration buffers with free Ca^{2+} were prepared according to the calibration in Figure 37. CaEGTA concentrations for used free Ca^{2+} concentrations are listed in the material and methods section on p. 23 (RB3).

3.6.3 Ca^{2+} potentiated respiratory inhibition by HO-CoQ10

Based on the calibration curve displayed in Figure 37 g (blue curve), respiration buffers with defined free Ca^{2+} concentrations could be prepared to further investigate the influence of extramitochondrial Ca^{2+} on the inhibitory effect of HO-CoQ10 on respiration.

Surprisingly, not only HO-CoQ10 but also CoQ10 showed a clear inhibitory effect on mitochondria, when tested on CI- and CII-linked respiration at low input of 50 $\mu\text{g}/\text{mL}$ mitochondrial protein. This inhibition was more effective for both HO- and CoQ10 when Ca^{2+} was present in the extramitochondrial medium.

An extramitochondrial free $[\text{Ca}^{2+}]$ of 0.2 μM did not influence CI-linked respiration (Figure 38 a; grey, dashed trace in b). Increasing the free calcium concentration to 1 μM drastically reduced substrate- and ADP-dependent respiration rates and RCR^{hh} dropped from 5.8 to 2.5. Since Complex I-linked respiration was sensitive to high Ca^{2+} concentrations (Figure 38 a), 0.2 μM extramitochondrial calcium should be preferred for CI experiments. In contrast to these experiments, calcium is known to stimulate mitochondrial energy production²⁰⁶ and was observed to increase CI-linked, ADP-stimulated respiration in pig heart²⁰⁷ and rat brain mitochondria²⁰⁸ supported by saturating glutamate and malate concentrations. However, calcium did not influence PM- and r/S-linked respiration in the latter.²⁰⁸ Denton et al. (1980) found reduced oxygen consumption of rat heart mitochondria in presence of calcium only with saturating substrate concentrations though did not further investigate this correlation.⁷⁸

Looking at individual oxygen consumption traces of CI-linked respiration, HO-CoQ10 (Figure 38 b, violet trace) but not the vehicle (1% ethanol, grey trace) hindered mitochondrial respiration, in the course of the measurement levelling off at a significantly reduced respiration rate. In the presence of 200 nM free Ca^{2+} (b, violet, dashed trace) oxygen consumption was even more impaired, substantially increasing the time for complete oxygen consumption of the chamber. 0.1 μM CoQ10 decreased respiration considerably although not to the same extent as HO-CoQ10 (c, cyan trace). Presence of calcium reduced respiration drastically. Analysing several experiments (d), HO-CoQ10 reduced remaining oxygen consumption rate more efficiently than CoQ10 and but was not more sensitive to potentiation via calcium.

^{hh} RCR, respiratory control ratio

To evaluate the Ca^{2+} effect on CoQ-dependent inhibition, the ratio dividing the remaining respiration rateⁱⁱ in presence of calcium by the one in absence of calcium was calculated^{ij} for each measurement individually and plotted in **e** and **f** for HO-CoQ10 and CoQ10, respectively. A ratio < 1 indicates that calcium is enhancing the inhibition, whereas a ratio > 1 indicates its attenuation. When 50 or 200 nM free Ca^{2+} was present, CoQ-dependent inhibition was potentiated in the majority of the cases (dots below 1 in **e**, **f**). Increasing extramitochondrial Ca^{2+} to 1 μM did not potentiate HO-CoQ10-dependent inhibition since CI-linked respiration itself was drastically lowered (**a**).

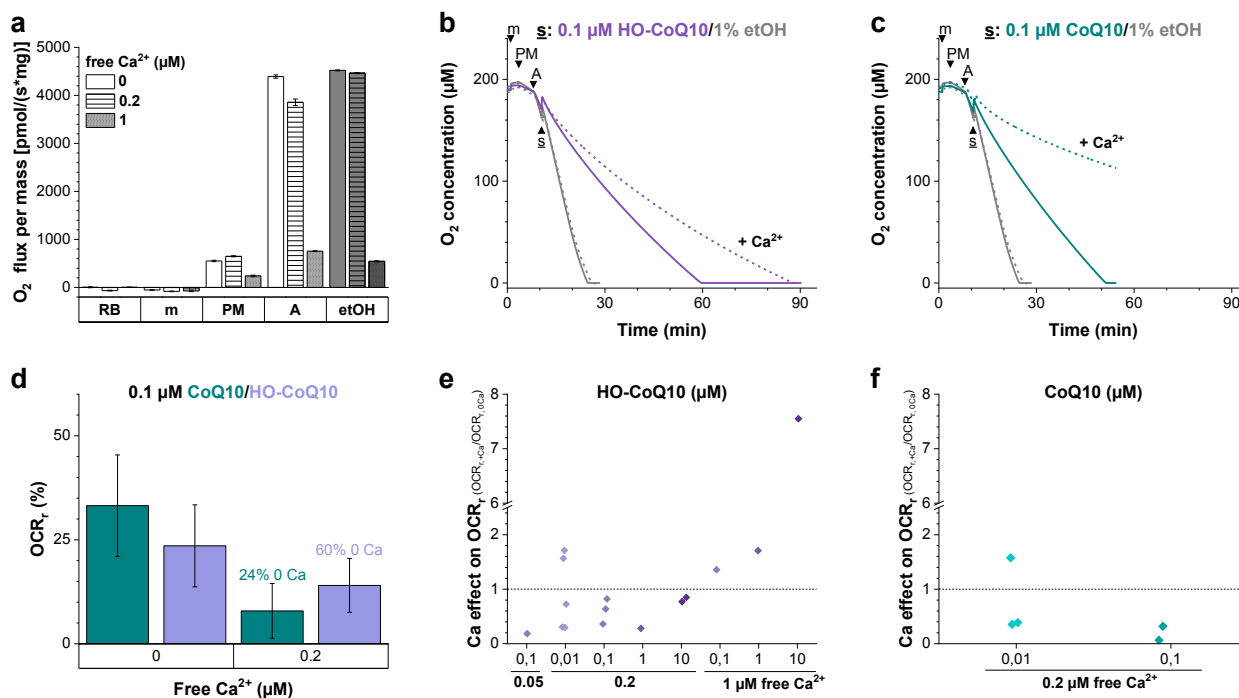


Figure 38 | Ca^{2+} potentiated inhibition of CI-linked respiration by HO-CoQ10 and CoQ10. Oxygen consumption of MHM was detected at 37 °C; CI-linked respiration of 50 $\mu\text{g}/\text{mL}$ mitochondrial protein with 5 mM pyruvate/malate (PM) as substrates. The influence of sample (**s**) on ADP-dependent respiration (1 mM ADP, A) was tested in absence (solid lines; 0 mM Ca, 0.1 mM EGTA) or presence of Ca^{2+} (dashed lines; + Ca^{2+} , 0.2 μM free Ca^{2+}) in RB3.1. (**a**) O_2 consumption rates with 1% ethanol and different free $[\text{Ca}^{2+}]$; exemplary traces show the effect of 0.1 μM (**b**) HO-CoQ10 and (**c**) CoQ10 on OXPHOS, 1% ethanol as vehicle control; (**d**) remaining oxygen consumption rate OCR_r (%), normalized to ADP respiration rate) after adding 0.1 μM CoQ; (**e**, **f**) potentiation of OXPHOS inhibition by extramitochondrial free Ca^{2+} for individual experiments expressed as Ca effect on OCR_r , the ratio of both OCR_r values, with over without free Ca^{2+} (Ca effect = $\text{OCR}_{r,+Ca}/\text{OCR}_{r,0Ca}$), when (**e**) HO-CoQ10 or (**f**) CoQ10 was present.

Buffer: RB3.1 (mM): 137 KCl, 4 KH_2PO_4 , 2.5 MgCl_2 , 20 HEPES, 0.1 EGTA, pH 7.21; 0 Ca: RB3.1, + Ca: RB3.1/RB3.2, see p. 23; analysis: mean \pm SEM of (**a**) 1, (**d**) 2, 4, 2, 3 independent mitochondrial preparations; instrument: O2k (Oroboros Instr.)

In contrast to CI-linked respiration (**Figure 38 a**), no decrease of CII-linked respiration was observed even at high Ca^{2+} concentrations up to 1.2 μM (data not shown). The exemplary trace shown in **Figure 39 a** demonstrates that 1 μM free Ca^{2+} did not influence respiration. Analogous to CI experiments, upon addition of HO-CoQ10 and CoQ10 oxygen consumption was reduced and further inhibited by extramitochondrial calcium (**b**, **c**). Looking at the overall effect (**d**), CII-linked respiration was less sensitive to CoQ-mediated inhibition than CI-linked respiration since remaining respiration rate was higher using the same concentration (cf. **Figure**

ⁱⁱ Remaining respiration rate OCR_r , respiration rate after sample application normalized to 100% ADP respiration rate, $\text{OCR}_r = \text{OCR}_{\text{after sample}}/\text{OCR}_{\text{after ADP}} \cdot 100$ (%)

^{ij} Ca^{2+} effect = $\text{OCR}_{r,+Ca}/\text{OCR}_{r,0Ca}$

38 d and Figure 39 d). Also, Ca^{2+} potentiation of CoQ-induced inhibition was less effective even though higher calcium concentrations could be applied. Independent of the HO-CoQ10 concentration, intermediate calcium between 0.366 and 1 μM was most effective always leading to a stronger inhibition (e). 200 nM and 1.2 μM free Ca^{2+} did not potentiate inhibition in most cases. Inhibition by 0.1 μM CoQ10 was potentiated by 1 μM Ca^{2+} .

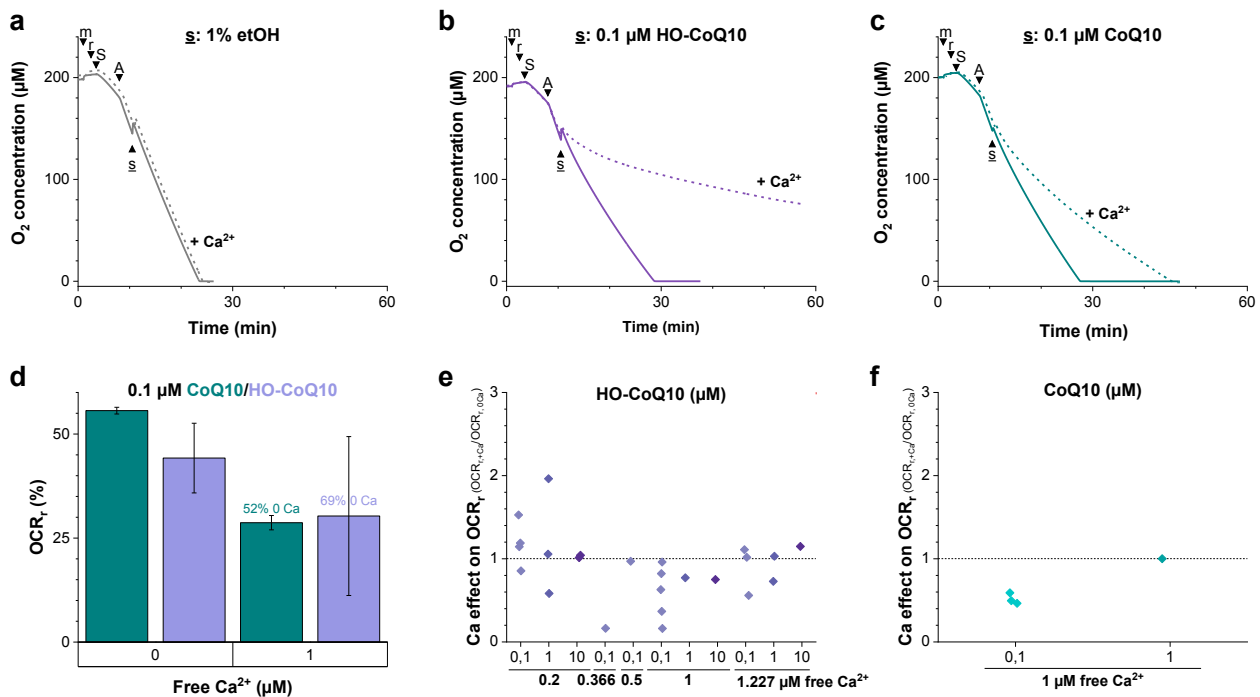


Figure 39 | Ca^{2+} potentiates inhibition of CII-linked respiration by HO-CoQ10 and CoQ10. Oxygen consumption of MHM was detected at 37 °C; CII-linked respiration of 50 $\mu\text{g}/\text{mL}$ mitochondrial protein with 0.5 μM rotenone (r) and 10 mM succinate (S) as substrate; the influence of sample (s) on ADP-dependent respiration (1 mM ADP, A) was tested in absence (solid lines; 0 mM Ca, 0.1 mM EGTA) or presence of Ca^{2+} (dashed lines; + Ca^{2+} , 1 μM free Ca^{2+}) in RB3.1; exemplary traces show the effect of (a) 1% ethanol as vehicle control, 0.1 μM (b) HO-CoQ10, and (c) CoQ10 on mitochondrial oxygen consumption; (d) remaining oxygen consumption rate OCR_r (%) after adding 0.1 μM CoQ, (e, f) potentiation of OXPHOS inhibition by extramitochondrial free Ca^{2+} expressed as Ca effect on OCR_r, the ratio of OCR_r with over without free Ca^{2+} (Ca effect = $\text{OCR}_{r,+Ca}/\text{OCR}_{r,0Ca}$), when (e) HO-CoQ10 or (f) CoQ10 was present.

Buffer: RB3.1 (mM): 137 KCl, 4 KH_2PO_4 , 2.5 MgCl_2 , 20 HEPES, 0.1 EGTA, pH 7.21; 0 Ca: RB3.1, + Ca: RB3.1/RB3.2, see p. 23 (RB3); **analysis:** (d) mean \pm SEM of 3, 10, 3, 2 independent mitochondrial preparations; **instrument:** O2k (Oroboros Instr.)

Within these experiments, the degree of inhibition was not dependent on extramitochondrial calcium concentration but on its presence. Inhibition efficiency was variable, in particular of CII, presumably due to the increased variability of Ca^{2+} concentration above 1 μM (cf. Figure 37 g). Besides, free [Ca^{2+}] can be influenced by applied substrates, CAC metabolites, and ADP not taken into account during calcium calibration experiments. Mitochondria with an RCR lower than 6 were not excluded from this analysis. RCR of mitochondria energized with CII substrates was more critical than with CI substrates. Nonetheless, the effect of CoQ and in combination with Ca^{2+} on respiration was consistent. ADP respiration rate did not always reach its maximum within the measured interval. Hence, inhibition was underestimated in those cases. Since this thesis was focussed on the effect of HO-CoQ10, to draw strong conclusions for CoQ10 further investigation is necessary.

3.6.4 More hydrophilic CoQ1 did not inhibit respiration

Since CoQ10 exhibited a similar effect on mitochondrial respiration as HO-CoQ10 and being the endogenous electron and proton transporter of the ETC, a direct effect on RCCs was considered unlikely. Addition of these

highly lipophilic substances to a mitochondrial suspension should lead to their incorporation into mitochondrial membranes as has been shown for CoQ10.²⁰⁹ Furthermore, CoQ is known to influence membrane properties as pointed out in section 1.2.2 (p. 14). One possibility to examine if CoQ10-mediated inhibition is caused by a membrane effect was the comparison to other CoQ derivatives. Through modification of the side chain, the location and therefore access of the molecule will be altered. For example, CoQ1 with only one isoprene unit as the side chain, unlike CoQ10, will take up electrons from other than the Q-binding site. Also, location in the membrane (³³ as cited in ³⁰) and transition to the membrane phase might be considerably different.

Figure 40 suggests that CoQ1 does not affect CII-linked respiration of MHM. Since CoQ1 possesses only one isoprene unit, membrane properties should be far less affected than by CoQ10. CI-linked respiration was more sensitive to CoQ10, HO-CoQ10, and calcium potentiation. Therefore, experiments need to be repeated for CI.

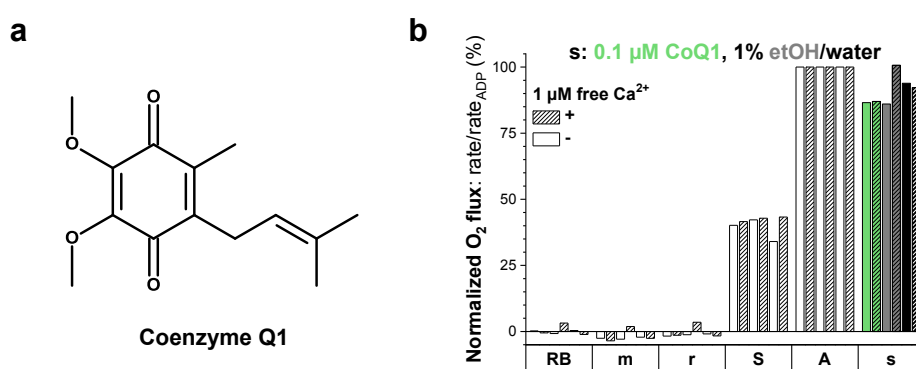


Figure 40 | CoQ1 does not inhibit CII-linked respiration. Oxygen consumption of MHM was detected at 37 °C; CII-linked respiration of 50 μg/mL mitochondrial protein with 0.5 μM rotenone (r) and 10 mM succinate (S) as substrate; the influence of Coenzyme Q1 (a) or solvent controls on ADP-dependent respiration (1 mM ADP, A) was tested in presence or absence of 1 μM free Ca²⁺ in RB3.1; (b) O₂ consumption rates normalized to 100% ADP respiration; Graph shows result from 1 independent mitochondrial preparation.

Buffer: RB3.1 (mM): 137 KCl, 4 KH₂PO₄, 2.5 MgCl₂, 20 HEPES, 0.1 EGTA, pH 7.21; **OCa:** RB3.1, +Ca: RB3.1/RB3.2, see p. 23 (RB3); **instrument:** O2k (Oroboros Instr.)

3.6.5 Inhibitory Ca²⁺ effect mediated by CoQ

The precedent experiments demonstrated strikingly that respiratory inhibition could be potentiated by calcium. To validate that this Ca²⁺ effect is associated to CoQs and is not a general feature of down-regulated respiration, commonly known CII inhibitors were examined. Two inhibitors, malonate and atpenin A5 (AA5), affecting CII at different sites were used. Furthermore, malonate, a competitive inhibitor of the dicarboxylate binding site, where electrons are accepted from succinate, is known to bind divalent metals like calcium.^{210,211} AA5 is a specific CII inhibitor mainly acting at the Q-binding site.²¹² Inhibitor concentrations were chosen to downregulate OXPHOS rate by a similar degree like CoQs (cf. Figure 39 d), i.e. 40-50%. Even though 1 μM free Ca²⁺ seemed to prolong oxygen consumption when respiration was inhibited by malonate (Figure 41 a), analysis of oxygen consumption rates normalized to ADP respiration showed that malonate-inhibited respiration was not affected by calcium (b). AA5 inhibition did not change in presence of calcium, either, as can be seen from oxygen traces (c) and OCRs (d).

Adding 1 μM free calcium did not change inhibition extent of both substances (Figure 41). Consequently, the potentiating effect of calcium on CoQ-mediated respiratory inhibition must be closely linked to CoQ molecules or their underlying mechanisms of ETC down-regulation.

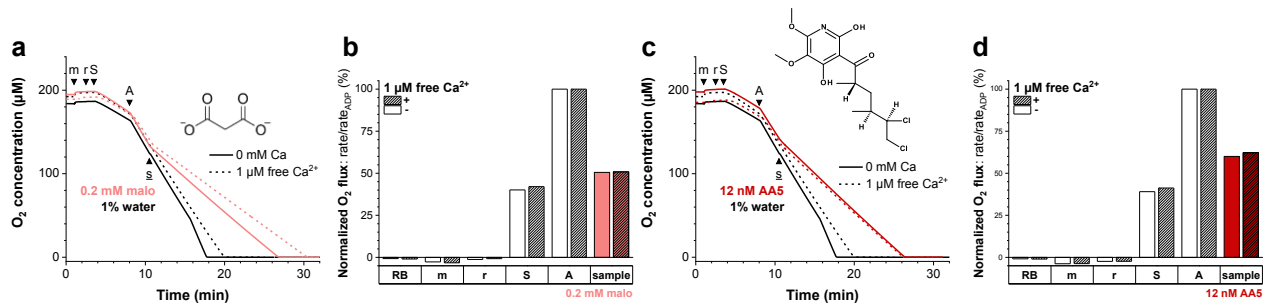


Figure 41 | Inhibition of CII-linked respiration by malonate and atpenin A5 was not Ca-dependent. Oxygen consumption of MHM was detected at 37 °C; CII-linked respiration of 50 $\mu\text{g}/\text{mL}$ mitochondrial protein with 0.5 μM rotenone (r) and 10 mM succinate (S) as substrate; the influence of a CII inhibitor (s, sample) on ADP-dependent respiration (1 mM ADP, A) was tested in absence (solid lines, -; 0.1 mM CaEGTA) and presence of Ca (dashed lines, +, 1 μM free Ca^{2+}) in RB3.1; influence of the competitive inhibitor malonate (a and b, 0.2 mM, malo) and Q-binding site inhibitor atpenin A5 (c and d, AAS, 12 nM); Graphs show results from 1 independent mitochondrial preparation.

Buffer: RB3.1 (mM): 137 KCl, 4 KH_2PO_4 , 2.5 MgCl_2 , 20 HEPES, 0.1 EGTA, pH 7.21; 0 Ca: RB3.1, + Ca: RB3.1/RB3.2, see p. 23 (RB3);
instrument: O2k (Oroboros Instr.)

3.7 HO-CoQ10 inhibited respiratory chain complexes I and II in photometric activity assays

To elucidate if HO-CoQ10 inhibits the respiratory chain at the level of single respiratory chain complexes I, II and/or III, the enzymatic activity of each complex was analysed separately. As a subject, bovine heart mitochondria were preferred over mouse heart mitochondria due to sample availability and abundance of necessary experiments to establish suitable protocols. Mitochondria were lysed by three rounds of freezing and thawing in hypotonic buffer to make the complexes accessible to their specific substrate and acceptor molecules. The assay buffer contained inhibitor cocktails to block electron transfer downstream of the acceptor molecule. When CII and CIII activities were examined, CI was additionally inhibited by rotenone to avoid reverse electron transfer from reduced CoQs. Either substrate consumption or acceptor conversion was monitored using a single absorption wavelength of the UV/Vis light spectrum. Tested CoQs were always applied together with the exogenous quinone, e.g. CoQ1 for CI, that was needed to measure RCC activity.

3.7.1 CI (NADH-CoQ1 oxidoreductase) was inhibited by HO-CoQ10

NADH:CoQ1 oxidoreductase activity assay monitoring NADH absorption

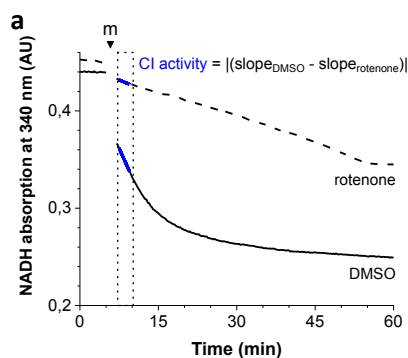
CI was measured as NADH:CoQ1 oxidoreductase activity using NADH as the substrate. Coenzyme Q1 was chosen as an artificial acceptor to pick up electrons from Complex I because its higher water-solubility facilitated handling and higher activities were achieved than with decyl-ubiquinone (data not shown). The CI-catalysed reaction was: $\text{NADH} + \text{H}^+ + \text{CoQ1} \rightarrow \text{NAD}^+ + \text{H}_2\text{CoQ1}$. The transfer of electrons from NADH to CoQ1 was followed at 340 nm where the oxidized form of NADH, NAD^+ , loses absorption intensity. Samples exposed to rotenone were run as a control to calculate CI-specific activity by subtraction of rotenone-insensitive activity resulting from electron transfer from other than the Q-binding site (Figure 42 a).

For photometric activity assays of CI, phosphate buffers are usually utilized.^{122,213–215} Phosphate buffer handling is more robust since pH is more stable with respect to temperature change ($\Delta\text{pH} < 1\%$ from 25 °C to 37 °C) and dilution of stock solutions.⁹² In **Figure 42 b**, lysis and measuring protocols were transferred from a phosphate- to a Tris-buffering system to allow measuring Ca^{2+} dependence of CI inhibition. Thereby Ca^{2+} -phosphate interactions can be excluded and defined Ca^{2+} concentrations were less prone to calculation errors. Nonetheless, Tris can also form Ca^{2+} and Mg^{2+} complexes,²¹⁶ though these are less stable than phosphate complexes. Presumably, there are no buffers available without any metal-binding capacity. Even the Good's buffer HEPES, long thought not to bind any Ca^{2+} and Mg^{2+} ,^{217,218} has been proven to bind both metals in a similar range to Tris.²¹⁹ Tris buffer at pH 7.4 and 37 °C was used. As a control, Tris buffer at pH 8 was run in parallel as this buffer composition has been suggested by Barrientos et al. (2009).¹⁸²

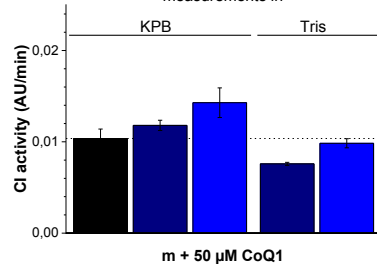
When measurements were conducted in Tris buffer, activities were reduced (**Figure 42 b**). CI activity increased with pH of the Tris-based buffer as the pH optimum for CI in human muscle mitochondria was reported to be 7.8,²²⁰ near the physiological pH of the mitochondrial matrix being between 7.8 and 8.0 depending on the examined sample.^{221,222} Lysing mitochondria in Tris buffer instead of hypotonic KPB increased CI activity since 10 mM Tris was more hypotonic. Yet, Tris at pH 7.4 was chosen for following experiments.

Then, the influence of the ethanol portion in the assay buffer was determined as shown in **Figure 42 c**. Up to 2.5% ethanol did not adversely affect CI activity. Nevertheless, 5% ethanol was chosen for further experiments to allow the highest CoQ10 concentration possible (50 μM) without overly impairing CI activity.

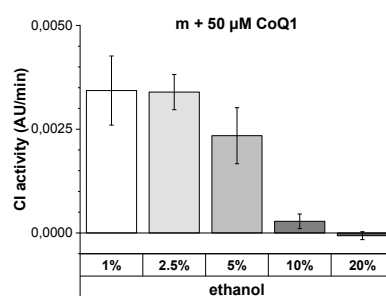
Increasing amounts of mitochondria were tested and two concentrations and two CI acceptor concentrations were used: 50 and 20 μM CoQ1 (**Figure 42 d**). Enzymatic turnover was higher with 50 μM CoQ1 but was less responsive to increasing mitochondrial input in the tested range. Besides, measurements with 50 μM CoQ1 were more stable with respect to the variability of initial slopes, but 20 μM allowed higher (OH-)CoQ10/CoQ1 ratios.



b Lysis in hypotonic KPB, Tris at pH 7.4 or Tris pH 8.0 measurements in



c



d

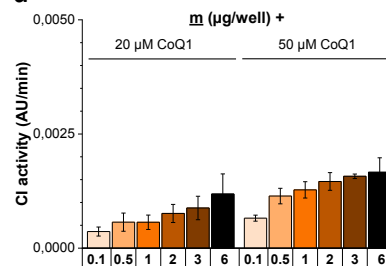


Figure 42 | Replacing KP_i with Tris buffer and increasing ethanol portion decreased CI activity. 15 $\mu\text{g}/\text{mL}$ (3 $\mu\text{g}/\text{well}$) BHM were added to assay buffer containing 100 μM NADH as substrate and 50 μM CoQ1 as acceptor; inhibition of CIII and CIV with 10 μM antimycin A and 1 mM KCN, respectively; NADH oxidation was measured at 340 nm in absence and presence of rotenone; (a) assay buffer in presence of rotenone or its vehicle DMSO was incubated at 37 °C and enzyme activity was started by adding mitochondria (m), CI activity was calculated from the initial linear phase subtracting rotenone-insensitive activity; (b) lysis and assay buffer based on KP_i were replaced by Tris buffers, lysis of BHM in hypotonic KPB or Tris-based assay buffers, measurements in assay buffer supplemented with 0.1% BSA (w/v) on basis of 50 mM KP_i (pH 7.4) or 10 mM Tris (pH 7.4/pH 8), 5.5% ethanol; (c) assay buffer containing 1-20% ethanol; (d) different mitochondrial input (μg) per well (0.2 mL) with 20 or 50 μM CoQ1, 5% ethanol; Sample: BHM subjected to 3 freeze-thaw cycles in (a) hypotonic KPB or (a-d) 10 mM Tris; buffer: (a) assay buffer: 10 mM Tris (pH 7.4 or pH 8 at 37°C) or 50 mM KP_i (pH 7.4), 10 μM antiA, 1 mM KCN, 0.02% DMSO, +/- 0.2 μM rotenone; hypotonic KPB: 25 mM KP_i , 5 mM MgCl_2 , pH 7.2; (b, c) 10 mM Tris (pH 7.4); analysis: see panel a, initial linear activity, mean \pm SEM from triplets of 3 independent mitochondrial preparations;

Using the conditions defined above, CI activity was followed when exposed to 50 μM CoQ1 and semi- or equimolar concentrations of the CoQs Coenzyme Q1, Coenzyme Q10 and HO-CoQ10 (Figure 43 a). Increasing the concentration of CoQ1 above 50 μM enhanced CI activity dose-dependently up to 1.3-fold indicating that acceptor concentration was not fully saturated. Half-equimolar Coenzyme Q10 slightly increased CI activity, whereas equimolar CoQ10 did not alter CI activity. HO-CoQ10 decreased NADH oxidation rate by 33% at equimolar concentrations. Rotenone-insensitive activities did not significantly change by CoQ addition (data not shown) indicating that HO-CoQ10 is acting on the Q-binding site.

During establishing the assay protocol, it was noticed that HO-CoQ10 did not always inhibit Complex I. Especially when rotenone-insensitive activity was high, experiments were more likely lacking an HO-CoQ10 effect. This observation is conclusive as HO-CoQ10 is expected to interact at the Q-binding site of CI and rotenone-insensitive NADH oxidation is independent of this site.

To examine if calcium potentiation of CoQ-mediated inhibition is working on enzyme level, CI activity was measured with 50 μM CoQ1 and semi-equimolar CoQ in Tris buffer enriched with different calcium concentrations (Figure 43 b-g). Nominal free calcium conditions were equivalent to those in experiments shown in Figure 43 a. No calcium-dependent effect was obvious. Looking at the control with 50 μM CoQ1 (b, grey bars), addition of ~ 0.2 and 10 μM free Ca^{2+} to the assay buffer slightly increased CI activity above nominal free calcium conditions, but completely excluding calcium from the buffer with EGTA also resulted in somewhat increased CI activity. Also, when additional CoQ1 (green bars) or CoQ10 (cyan bars) was supplied no calcium-dependent change in CI activity was visible. The effect of calcium on HO-CoQ10-dependent inhibition could not be evaluated: In conditions with nominal zero Ca^{2+} CI activity was inhibited as can be deduced from individual traces following NADH absorption during the assay (e, violet lines). However, when the buffer was supplemented with EGTA (d) and calcium (f, g), absorption at 340 nm increased upon application of mitochondria when HO-CoQ10 was supplied in absence (solid lines) as well as in presence of rotenone (dashed lines). Figure 43 c shows that the observed increase of NADH absorption cannot be due to insufficient dissolution of HO-CoQ10 in the assay buffer. When mitochondria were omitted, absorption did not increase during prolonged incubation in KP_i -based buffer. Then again, especially in assay buffers containing 10 μM Ca^{2+} , the absorption increase was most prominent implying a calcium-dependent effect. Absorption spectra of NADH were not sensitive to changing calcium concentrations (tested in Tris buffers listed in caption of Figure

43, data not shown). Hence, NADH interaction with Ca^{2+} can be excluded. To rule out a measuring artefact, experiments need to be repeated with different BHM preparations.

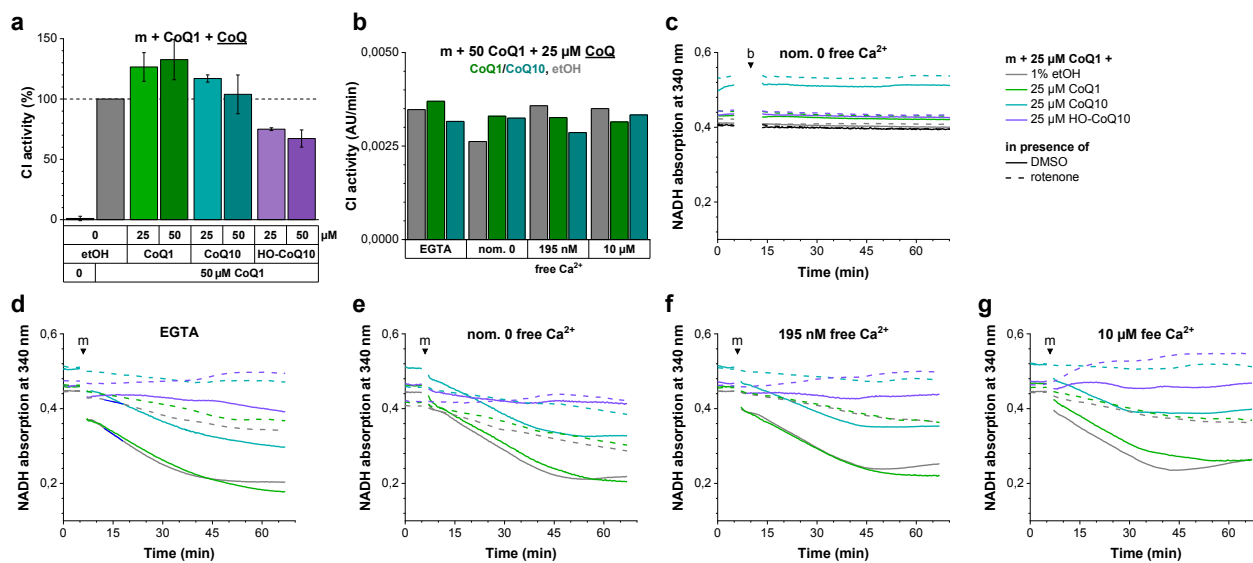


Figure 43 | HO-CoQ10 inhibited Complex I activity. 15 $\mu\text{g}/\text{mL}$ (3 $\mu\text{g}/\text{well}$) BHM were added to assay buffer containing 100 μM NADH as substrate and 50 μM CoQ1 + 25/50 μM CoQ/vehicle as acceptor cocktail. (a) Initial CI activity normalized to 50 μM CoQ1 + ethanol; (b) influence of calcium on CI activity; (c) absorption at 340 nm of control measurement adding buffer (b) instead of mitochondria (m) in presence of 100 μM NADH and 50 μM CoQ1 + 25 μM CoQ/vehicle in 50 mM KPB, pH 7.4, 0.1% BSA; (d-g) NADH absorption at 340 nm of samples analysed in panel b with different calcium concentrations, addition of mitochondria (m) is indicated, measurements in absence (solid lines) and presence of rotenone (dashed lines) are shown: (d) 1 mM EGTA, (e) nominal free Calcium, (f) 195 nM free Ca^{2+} , (g) 10 μM free Ca^{2+}

Sample: BHM subjected to 3 freeze-thaw cycles in 10 mM Tris; **buffer:** 10 mM Tris (pH 7.4 at 37 $^{\circ}\text{C}$), 10 μM antiA, 1 mM KCN, 0.02% DMSO, +/- 0.2 μM rotenone, 5.5% ethanol; (b-g) free $[\text{Ca}^{2+}]$ was calculated with maxchelator¹²¹ and adjusted as follows: EGTA, 1 mM EGTA; nom 0 Ca, assay buffer without additives; 195 nM Ca, 1 mM EGTA + 883.1 μM CaCal₂, 10 μM Ca, 1007.4 μM CaCl₂; **analysis:** see Figure 42 a, initial linear activity, mean \pm SEM from triplets of (a) 3 or (b) 1 independent mitochondrial preparation; (b) analysis of mean, not single traces;

NADH:CoQ1 oxidoreductase activity assay monitoring NADH fluorescence

Measuring CI activity following the loss of NADH absorption at 340 nm resulted in rising absorptions when samples were treated with high HO-CoQ10 concentrations (Figure 43 g). This increase might be a result of a measurement artefact caused by the changed absorption pattern of reduced CoQs. UV/Vis absorption spectra of rising NADH concentrations in Figure 44 a demonstrate that NADH not only absorbs at 340 nm but also at 280 nm, the wavelength characterising the oxidation state of quinones. In reverse, CoQs have a strong absorption band at 280 nm but also absorb at 340 nm (b-d). Plotting the absorption at 280 nm of CoQ against their concentration, extinction coefficients are similar for CoQ1, CoQ10 and HO-CoQ10 and are considerably higher than for NADH (e). As can be already seen from the UV/Vis spectrum of CoQ1 (b), absorption at 340 nm of CoQ1 is low in comparison to NADH (f). However, CoQ10 and HO-CoQ10 both absorb at 340 nm in a similar range as NADH. Moreover, this absorption may change upon reduction of CoQ.

To exclude the influence of different concentrations of CoQ and their redox state on the measurements, NADH fluorescence instead of absorption was recorded. Fluorescence of reduced CoQ10 ($\text{H}_2\text{CoQ10}$, exc. 290 nm/em. 370 nm²²³) did not interfere with NADH detection (data not shown). Different to absorption-based

measurements in the fluorescence-based CI activity assay (g), calcium increased CI activity. CI activity was clearly inhibited by 10 μM HO-CoQ10. With regard to respiration with CoQ1 alone, CI inhibition by HO-CoQ10 was more effective in presence of calcium. Since these fluorescence-based experiments were preliminary and measurement parameters were different than in absorption-based assays, more experiments are necessary to draw conclusions. Moreover, detection parameters must be optimized to increase signal-to-noise ratio. It is preferable to choose a HO-CoQ10 concentration near its IC₅₀ to allow the observation of both attenuation and potentiation of its inhibitory effect.

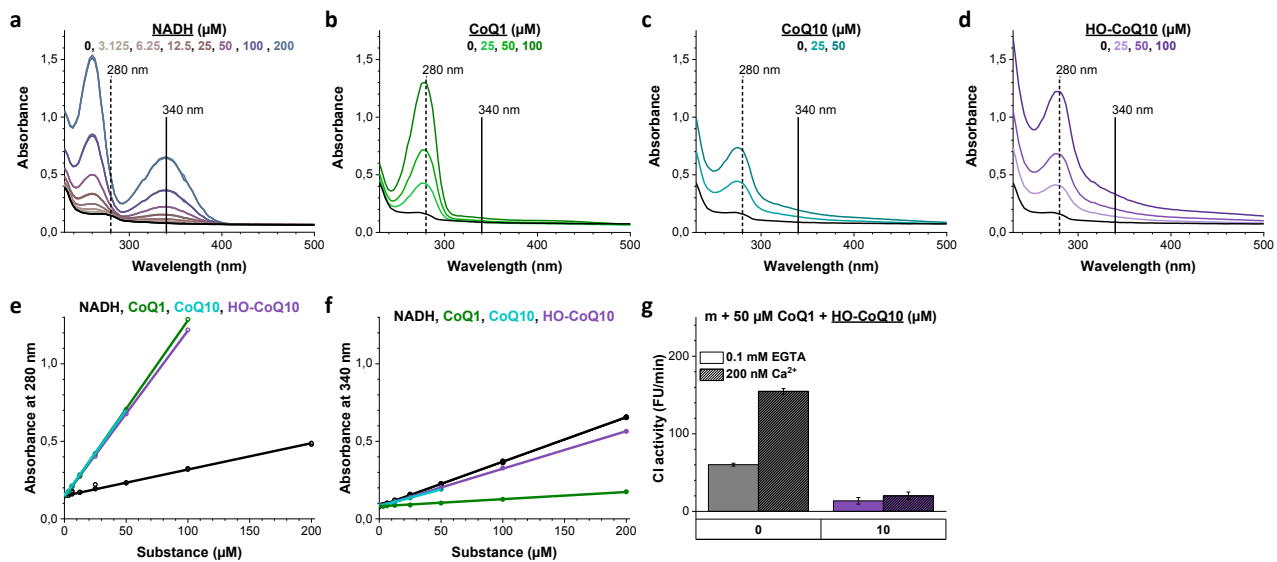


Figure 44 | NADH:CoQ1 oxidoreductase activity fluorescence assay. UV/Vis spectra of increasing (a) NADH, (b) CoQ1, (c) CoQ10 and (d) HO-CoQ10 concentrations; dependence of absorption at (e) 280 nm (characteristic CoQ absorption) and (f) 340 nm (characteristic NADH absorption), absorption values taken from measurements shown in panels a-d; (g) initial linear CI activity (NADH fluorescence detected at exc. 340 nm/em. 450 nm): 5 $\mu\text{g/mL}$ (1 $\mu\text{g/well}$) BHM were added to assay buffer containing 100 μM NADH as substrate and 50 μM CoQ1 + 25/50 μM CoQ/vehicle as acceptor cocktail;

Sample: BHM subjected to 3 freeze-thaw cycles in 10 mM Tris; buffer: 10 mM Tris (pH 7.4 at 37 °C), 10 μM antiA, 1 mM KCN, 0.02% DMSO, +/- 0.2 μM rotenone, 5% ethanol; 200 nM free [Ca²⁺], 0.1 mM EGTA + 75.8 μM CaCl₂; analysis: see **Figure 42 a**, initial linear activity, mean \pm SEM from triplets of 1 independent mitochondrial preparation;

3.7.2 CII (succinate:CoQ1 oxidoreductase) was inhibited by HO-CoQ10

CII activity was quantified by succinate:CoQ1 oxidoreductase activity following the decrease of quinone absorption at 280 nm. Succinate, applied as a substrate, feeds electrons into CII, which in return will reduce CoQ1 to its quinol form exhibiting a lowered absorbance at 280 nm.

In contrast to CI, CII activity decreased upon changing lysis and assay buffer from phosphate to Tris (**Figure 45 a**). Nevertheless, the Tris-based assay buffer was preferred in following experiments because Ca²⁺ addition will be less problematic. The drastic reduction of CII activity by malonate (**a**) proved CII specificity of the assay. CII was less sensitive to ethanol than CI but still decreased at concentrations $\geq 10\%$ (**b**). CII activity with 20 and 50 μM CoQ1 was linear up to concentrations of 10 $\mu\text{g/mL}$ (2 $\mu\text{g/well}$) mitochondrial protein, then decreased again (**c**).

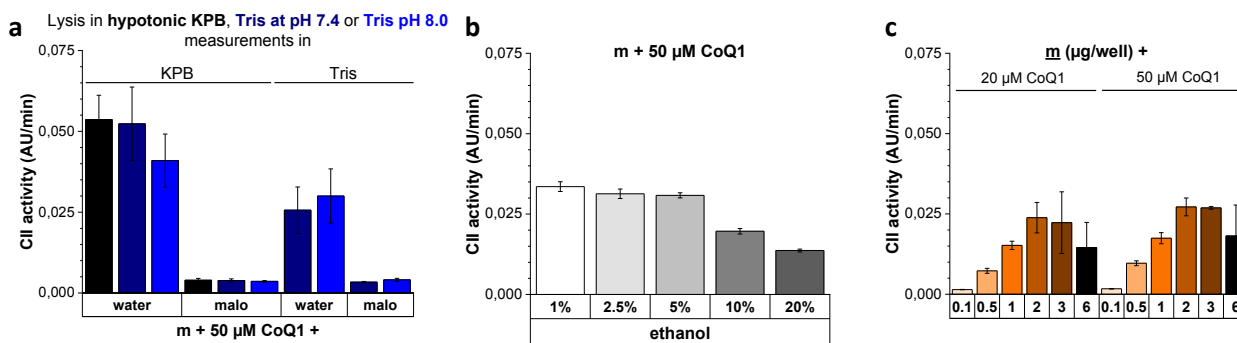


Figure 45 | Replacing KP_i with Tris buffer and increasing ethanol portion decreased CII activity. After preincubation of 15 µg/mL (3 µg/well) BHM with succinate as substrate, 50 µM CoQ1 was added to initiate CoQ turnover by Complex II. CI, CIII and CIV were inhibited. Initial linear CII activity was calculated from decrease at 280 nm (characteristic absorption of CoQ). (a) Lysis of BHM in hypotonic KPb or Tris-based assay buffers, measurements in assay buffer on basis of 50 mM KP_i (pH 7.4) or 10 mM Tris (pH 7.4/pH 8), 12.5% ethanol; (b) assay buffer containing 1-20% ethanol; (c) different mitochondrial input (µg) per well (0.2 mL) with 20 or 50 µM CoQ1, 5% ethanol;

Sample: BHM subjected to 3 freeze-thaw cycles in (a) hypotonic KPb or (a-c) 10 mM Tris; buffer: (a) 50 mM KP_i (pH 7.4) or 10 mM Tris (pH 8 or 7.4 at 37 °C), (b, c) 10 mM Tris pH 7.4 at 37 °C, 10 mM succinate, 2.5 µM rotenone, 10 µM antiA, 1 mM KCN; analysis: initial linear activity, mean ± SEM from triplets of (a) 1 or (b, c) 3 independent mitochondrial preparations;

The influence of additional CoQ was examined with 20 and 50 µM CoQ1 and different concentrations of CoQ10, HO-CoQ10 and CoQ1 as a control (Figure 46). Unlike CI, CII activity was not enhanced by additional CoQ1 confirming that CoQ1 was supplied in saturation. As can be seen from individual traces of CoQ absorption at 280 nm in a and plotting CII activity in e, initial rates did not rise with increasing CoQ1 concentration. CII activity was slightly lower when CoQ10 was present though this behaviour was not concentration-dependent in a range of 1-30 µM CoQ10 (b, e). Lower concentrations need to be tested to elucidate if CII activity can be regulated by CoQ10 supply. The slight increase in absorption after addition of mitochondria that could be observed at the beginning of all measurements (a-c) was not CII-related since it was also found when mitochondria were omitted (data not shown). Therefore, this initial increase was always excluded when determining CII activity. HO-CoQ10 clearly inhibited CII activity up to a concentration of 30 µM (c, d). The IC50 of HO-CoQ10 was 110.8 and 236.5 nM using 20 and 50 µM CoQ1, respectively (f, e). The ratios of HO-CoQ10 to CoQ1 yielding a half-maximal inhibition were similar (20 µM CoQ1, 1:0.006; 50 µM CoQ1:0.005), whereas HO-CoQ10-to-BHM ratios were differing by a factor of 2.13. Thus, in this case, HO-CoQ10 inhibition was independent of CII concentrations and dependent on CoQ1 input indicating a competition between HO-CoQ10 and CoQ1. Surprisingly, samples with 100 µM HO-CoQ10 (c, d) showed a decrease of 280-nm absorption that even superposed any artificial increase at the beginning of the measurement, hinting that HO-CoQ10 might be an alternative acceptor for CII, even though lower concentrations of HO-CoQ10 inhibited CoQ1-dependent CII activity. Potential Complex II succinate:HO-CoQ10 oxidoreductase activity is analysed in section 3.7.4 (p. 106).

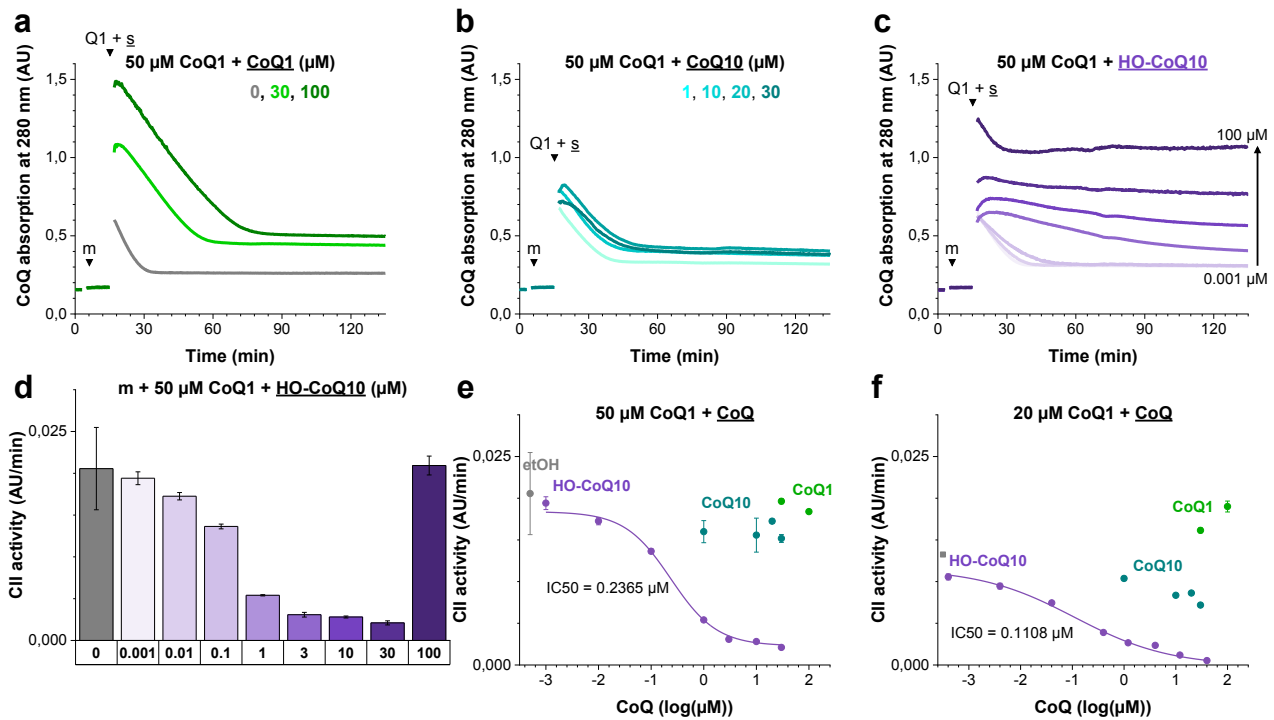


Figure 46 | HO-CoQ10 inhibited succinate:CoQ1 oxidoreductase activity. After preincubation of 5 $\mu\text{g}/\text{mL}$ (1 $\mu\text{g}/\text{well}$) BHM with succinate, 50 μM CoQ1 + increasing concentrations of HO-CoQ10, CoQ10 and CoQ1 were added to initiate CoQ turnover by Complex II. (a-c) CII activity followed at 280 nm (characteristic CoQ absorption) with 50 μM CoQ1 as an acceptor and additional (a) CoQ1 or vehicle, (b) CoQ10 or (c) HO-CoQ10; (d) influence of HO-CoQ10 on initial CII activity; concentration dependence of CII activity on additional CoQ with (e) 50 μM or (f) 20 μM CoQ1;

Sample: BHM subjected to 3 freeze-thaw cycles in 10 mM Tris; buffer: 10 mM Tris (pH 7.4 at 37 $^{\circ}\text{C}$), 2.5 μM rotenone, 10 μM antiA, 1 mM KCN, 5% ethanol; analysis: initial linear activity, mean \pm SEM from triplets of 1 independent mitochondrial preparation;

Ca-dependence of CII activity was tested with 50 μM CoQ1 and semi-equimolar CoQ in **Figure 47**. CII activity slightly increased with calcium concentration (a). Unexpectedly, CoQ10 decreased CII activity by $\sim 50\%$ as seen in **Figure 47 b**, which was unaffected by calcium. Since CoQ10 did not affect CII activity in the experiment shown in **Figure 46** (b and e) performed with another BHM preparation and lower mitochondrial input, for now, there is no strong evidence on CoQ10 impacting CII activity. However, its influence needs to be further investigated. 25 μM HO-CoQ10 decreased CII activity by over 90% at calcium concentrations up to 195 nM. With 10 μM free Ca^{2+} , inhibition was considerably attenuated (b, f). To assure that Ca effects are not covered up by a harsh inhibition, half-maximal inhibitory concentrations of HO-CoQ10 should be chosen for future experiments. Ca-dependent measurements should be repeated using 5 $\mu\text{g}/\text{mL}$ (1 $\mu\text{g}/\text{well}$) mitochondria since CII activity was already saturated with 10 $\mu\text{g}/\text{mL}$ (2 $\mu\text{g}/\text{well}$, **Figure 45 c**).

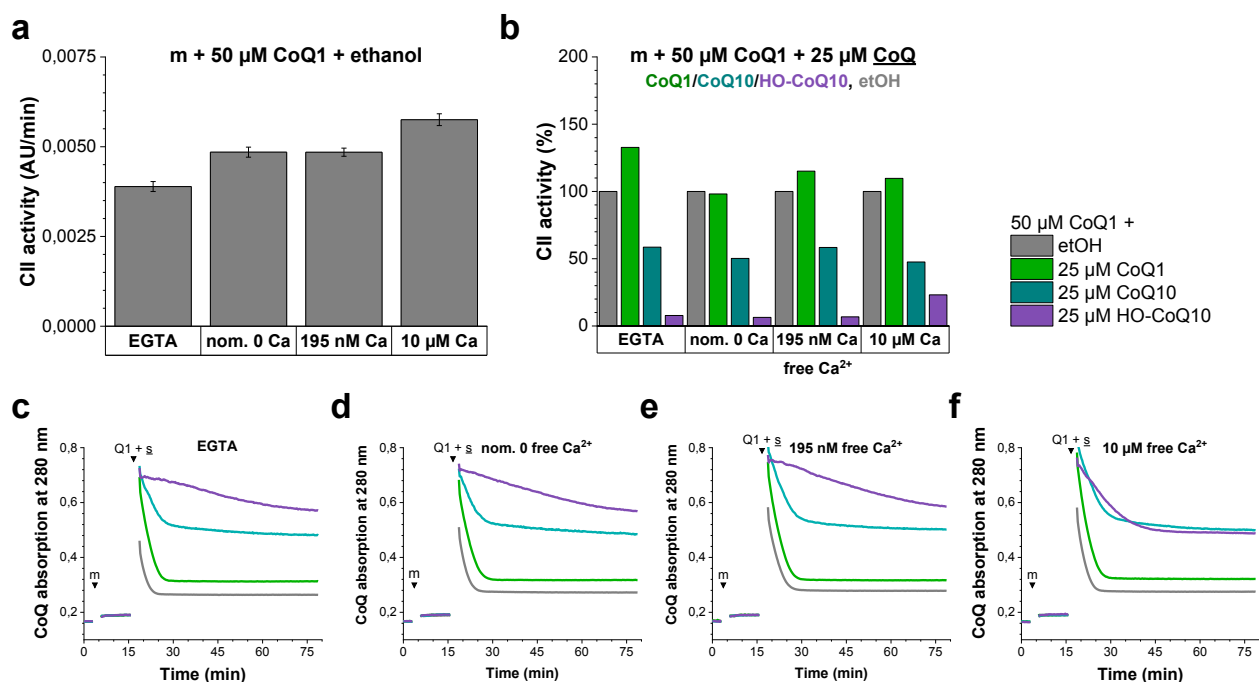


Figure 47 | Influence of calcium on CII activity. After preincubation of 15 $\mu\text{g}/\text{mL}$ (3 $\mu\text{g}/\text{well}$) BHM with succinate, 50 μM CoQ1 + 25 μM CoQ were added to initiate CoQ turnover by Complex II. CoQ1-sample mixtures were CoQ1 together with ethanol (grey), CoQ1 (green), CoQ10 (cyan) or HO-CoQ10 (violet). (a, b) Initial CII activity from measurements in Tris containing different calcium concentrations shown in panels c-f: (a) 50 μM CoQ1 + ethanol, (b) 50 μM CoQ1 + 25 μM CoQ, normalized to 50 μM CoQ1 + ethanol for every calcium concentration; (c-f) mean traces of CoQ absorption at 280 nm of experiments performed in different calcium concentrations, addition of mitochondria (m) and CoQ1-sample mixture (Q1 + s) is indicated: (c) EGTA, (d) nominal zero Ca^{2+} , (e) 195 nM free Ca^{2+} , (f) 10 μM free Ca^{2+} ;

Sample: BHM subjected to 3 freeze-thaw cycles in 10 mM Tris; buffer: 10 mM Tris (pH 7.4 at 37 $^{\circ}\text{C}$), 10 mM succinate, 2.5 μM rotenone, 10 μM antiA, 1 mM KCN, 5.5% ethanol; free $[\text{Ca}^{2+}]$ was calculated with maxchelator¹²¹ and adjusted as follows: EGTA, 1 mM EGTA; 195 nM free Ca, 1 mM EGTA + 883.1 μM CaCl_2 , 10 μM Ca, 1007.4 μM CaCl_2 ; analysis: initial linear activity, mean \pm SEM from triplets of 1 independent mitochondrial preparation;

3.7.3 CIII (decyl-ubiquinol:cytochrome *c* oxidoreductase) was not inhibited by HO-CoQ10

CIII activity was measured as decyl-ubiquinol:cytochrome *c* oxidoreductase activity. Here, decyl-UQH₂ acted as the substrate and cytochrome *c* as the acceptor for CIII electrons. CIII activity was analysed by subtracting the initial linear rate of cytochrome *c* reduction after addition of decyl-ubiquinol in absence from the rate in presence of mitochondria (Figure 48 a). To assess the influence of CoQ on CIII activity, reduced decyl-UQ was applied together with oxidized CoQ. Comparing redox potentials from the used species, only CoQ1 can be reduced by decyl-UQH₂ (Figure 48 b). Therefore, the sample with CoQ1 probably contained only reduced CoQ1 and oxidized decyl-UQ. The other mixtures contained reduced decyl-UQ and oxidized forms of HO-CoQ10 or CoQ10.

When oxidized decyl-UQ (DUQ) was added as a control for CoQ addition, CIII activity was reduced in comparison to ubiquinol with ethanol alone (Figure 48 c). This might be explained by radical formation through the disproportionation reaction of reduced and oxidized species. Radicals will be oxidized quickly in an aqueous medium, thereby reducing substrate availability. CIII activity seemed to be even more reduced when CoQ1 was added as a sample (c). Looking at the cytochrome *c* reduction rate with additional CoQ1, it was

already very high without mitochondria (d, CoQ1 + cyt c was 79% of CoQ1 + cyt c + m) indicating that H_2CoQ1 is an inappropriate substrate, possibly directly reducing cytochrome *c*. Therefore, specific CIII activity could not be measured in presence of CoQ1.

CoQ10 and HO-CoQ10 both considerably enhanced CIII activity (c). Since inhibition of CIII-linked respiration could only be observed at low substrate concentrations (cf. Figure 30 c on p. 83 and delay in Figure 28 c on p. 81), preincubation with HO-CoQ10 might still affect CIII activity. HO-CoQ10 did not negatively affect CIII activity but enhanced it slightly suggesting that HO-CoQ10 might be an endogenous CIII substrate. Like in respiration measurements an ubiquinol analogue was used as a CIII substrate. Thus, it is not clear if CIII activity controlled by endogenous CoQ10 will react the same way.

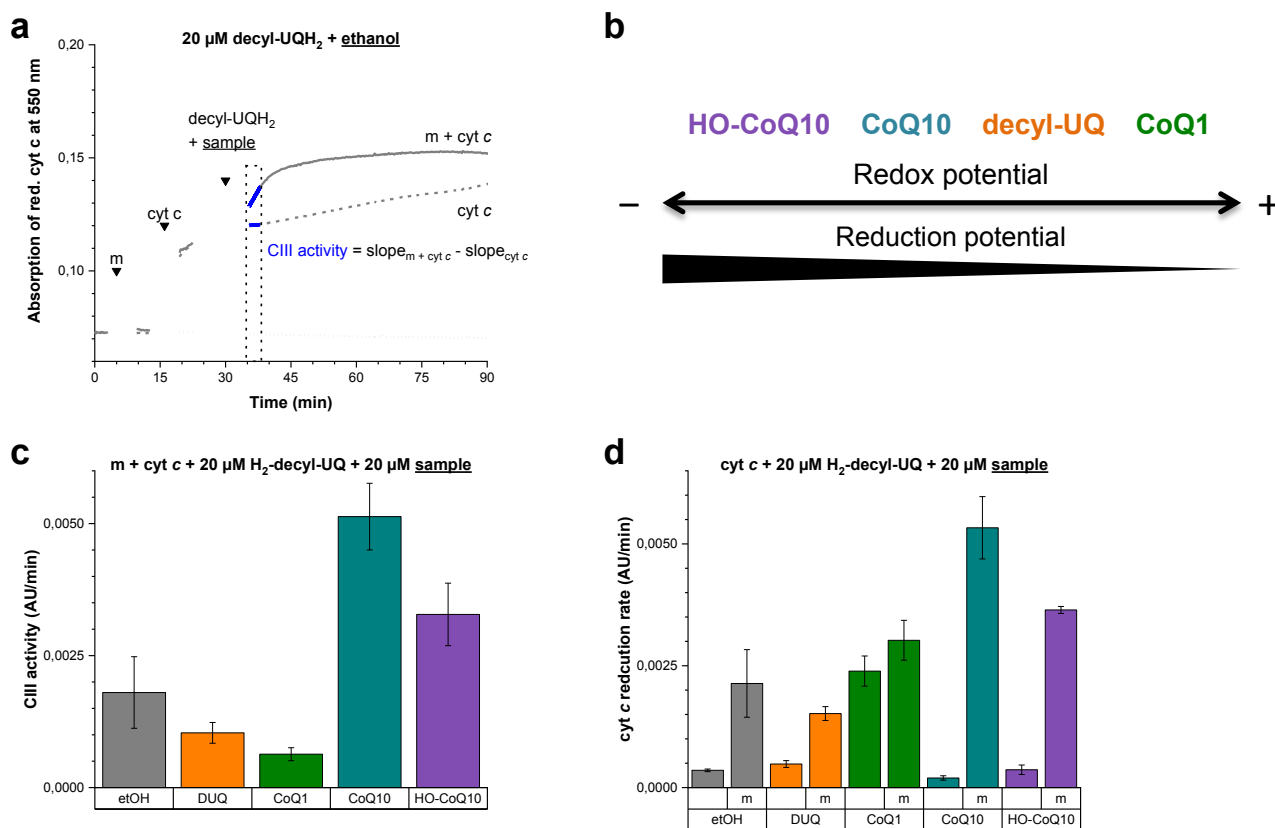


Figure 48 | HO-CoQ10 did not inhibit decyl-ubiquinol:cytochrome *c* oxidoreductase activity. After preincubation of 75 $\mu\text{g}/\text{mL}$ (15 $\mu\text{g}/\text{well}$) BHM, 10 μM cytochrome *c* was added as an acceptor for CIII. The addition of 20 μM decyl-UQH₂ + sample (20 μM CoQ or ethanol) initiated CIII turnover. Cytochrome *c* reduction was monitored at 550 nm. (a) Exemplary trace and analysis of CIII activity assay: addition of mitochondria (m), cytochrome *c* (cyt *c*) and decyl-ubiquinol-sample mixture as indicated; subsequent addition of: m + cyt *c* + CoQ (solid line), cyt *c* + CoQ (dashed line) or CoQ (dotted line); CIII activity was calculated analysing the initial rate of cytochrome *c* reduction after addition of 20 μM decyl-ubiquinol in presence of mitochondria (m + cyt *c* + CoQ) and subtracting the rate in absence of mitochondria (cyt *c* + CoQ); (b) redox and reduction potential of the used ubiquinones (on basis of voltammetric data, $E_{p,\text{mid}}$ determined in *i*-proH)^{185,224}; (c) CIII activity with decyl-ubiquinol-sample mixtures: 20 μM decyl-ubiquinol + ethanol or 20 μM decyl-ubiquinone (DUQ)/CoQ1/ CoQ10/HO-CoQ10; (d) initial rate of cytochrome *c* reduction after addition of decyl-UQH₂ with and without adding mitochondria (m), same measurements as in panel c;

Sample: BHM subjected to 3 freeze-thaw cycles in hypotonic KPB; buffer: 50 mM KP_i, 0.1% BSA, 1 mM DDM, 2.5 μM rotenone, 1 mM KCN, 2.2% ethanol; analysis: initial linear activity see panel a, mean \pm SEM from triplets of 3 independent mitochondrial preparations;

3.7.4 HO-CoQ10 was reduced by succinate:CoQ dehydrogenase

To test if HO-CoQ10 can act as an alternative acceptor for the respiratory chain complexes I and II, CoQ1 was substituted with CoQ10 and HO-CoQ10 in activity assays.

CoQ reductase activity of Complex I

NADH:CoQ oxidoreductase activity was measured with 50 μM NADH and half- or equimolar CoQ concentrations. To allow high concentrations of CoQ10, final ethanol concentration was raised to 10% despite the risk of low rotenone-insensitive activities (cf. Figure 42 c in Tris on p. 99).

Mean absorption traces at 340 nm are shown for equimolar NADH and CoQ concentrations in Figure 49 to evaluate the decrease of NADH due to CI-specific (solid lines, + DMSO) and CI-unspecific activity (dashed lines, + rotenone) after addition of mitochondria to a solution containing substrate and acceptor sample.

In absence of acceptors (Figure 49 a, ethanol), NADH concentration was constant. CI activity with 25 μM CoQ1 was not detectable (data not shown), but 50 μM CoQ1 induced NADH turnover that was higher in absence of rotenone and therefore CI specific (Figure 49 a). Neither CoQ10 nor HO-CoQ10 initiated NADH oxidation (b, c). Since CoQ10, of course, is the natural acceptor of Complex I, no conclusions can be drawn for the hydroxy derivative and the experimental setup needs to be reassessed.

There are three effects possibly masking a reduction of CoQs in these experiments: 1. As mentioned above, high ethanol concentrations reduce CI activity drastically. Hence, measurements should be repeated with lower ethanol concentrations around 5%. 2. Decreased aqueous solubility negatively affected CI activity comparing decyl-ubiquinone to CoQ1 in preliminary experiments. Since CoQ10 is even more hydrophobic than decyl-ubiquinone, it might be an inadequate substrate for in-vitro CI activity assays. For this reason, testing the demethylated derivative of CoQ1 (HO-CoQ1) as a water-soluble model for HO-CoQ10 will be more conclusive.

3. Comparison of starting values of the ethanol control with CoQ samples (Figure 49) shows that CoQs influence absorption at 340 nm (see also Figure 44 f on p. 101). Ideally, CoQ reduction at 280 nm should be followed instead of NADH oxidation. Since NADH is absorbing at 280 nm (cf. Figure 44 a and e) and its oxidation would influence absorption at this wavelength, a regeneration system for NADH (lactate + lactate dehydrogenase) needs to be included.²²⁵ Additionally, reduced and oxidized CoQ species can be quantified by HPLC.²²⁵

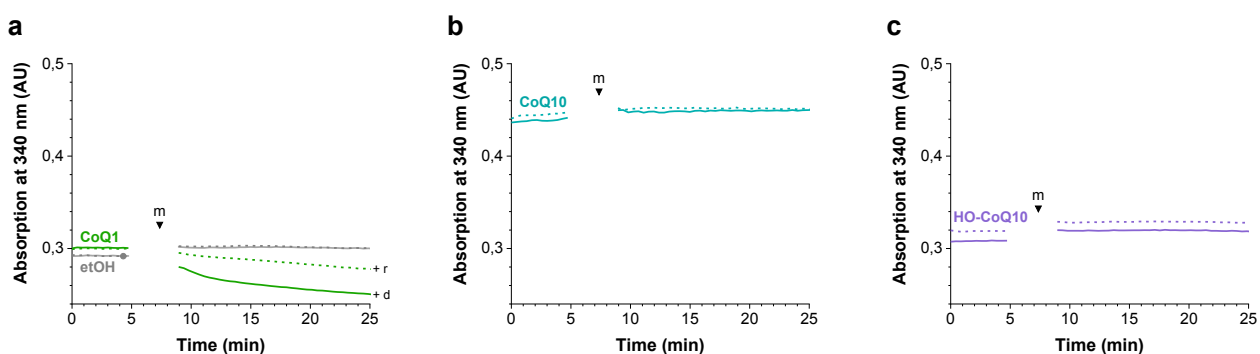


Figure 49 | Complex I activity was not detectable with CoQ10 or HO-CoQ10. 15 $\mu\text{g}/\text{mL}$ (3 $\mu\text{g}/\text{mL}$) BHM (m, see arrow) were added to assay buffer containing 50 μM NADH and 50 μM of different, tested acceptors, and NADH-characteristic absorption at 340 nm was

detected. Experiments were run in presence of rotenone (dashed lines, + r) or its vehicle DMSO (solid lines, + d) to identify CI-specific activity. Tested acceptors were (a) CoQ1 or 10% ethanol as vehicle control, (b) CoQ10, and (c) HO-CoQ10.

Sample: BHM subjected to 3 freeze-thaw cycles in hypotonic KPB; buffer: 50 mM KPi (pH 7.4), 50 μ M NADH, 1 mM KCN, 10 μ M antiA, 10% ethanol; analysis: mean of single traces from triplets of 1 independent mitochondrial preparation;

CoQ reductase activity of Complex II

Succinate:CoQ oxidoreductase activity was measured with 10 mM succinate and increasing concentrations of CoQ up to 100 μ M (Figure 50). For all tested CoQs, quinone-specific absorption at 280 nm was stable during the measurement (d-f) and decreased only upon addition of mitochondria (g-j), a measure of CII activity. CoQ10 was reducible by succinate dehydrogenase and reduction rate, at a concentration of 100 μ M, was higher than with CoQ1 (Figure 50 a, b). HO-CoQ10 was reduced only at high concentrations of 75 and 100 μ M. At concentrations lower than 50 μ M CoQ10 or 75 μ M HO-CoQ10, initial rates were affected by a primary small increase of absorption at 280 nm (b, c). This increase could also be observed at high CoQ concentrations, when mitochondria were omitted (e, f) and in precedent measurements of CII activity (cf. Figure 46 a-c on p. 103). The total decrease in absorption was significantly lower for HO-CoQ10 than for CoQ10 and CoQ1 comparing the difference in absorption values after addition of CoQ and at the endpoint of the measurement in g-j. It will be important to compare extinction factors for all three molecules in their reduced and oxidized form. For this purpose, absorption spectra of the reduced species need to be recorded. Since quinols are unstable in aqueous solution and on-site reduction by NaBH₄ is unsuitable for spectrophotometric measurements, voltammetry coupled to UV/Vis spectroscopy will be the method of choice.

CoQ10 can be used as an acceptor for CII assays and might be a better acceptor than CoQ1 at high concentrations. HO-CoQ10 seems to be an alternative acceptor to the well-established CoQ10 but shows drastically reduced kinetics. Blocking CII with malonate and atpenin A5 and therefore the reduction of CoQ10 and HO-CoQ10, will be an important control to verify CII-specificity. Like mentioned for CI, acceptor studies should be repeated with water-soluble hydroxy derivatives since solubility effects may affect kinetics.

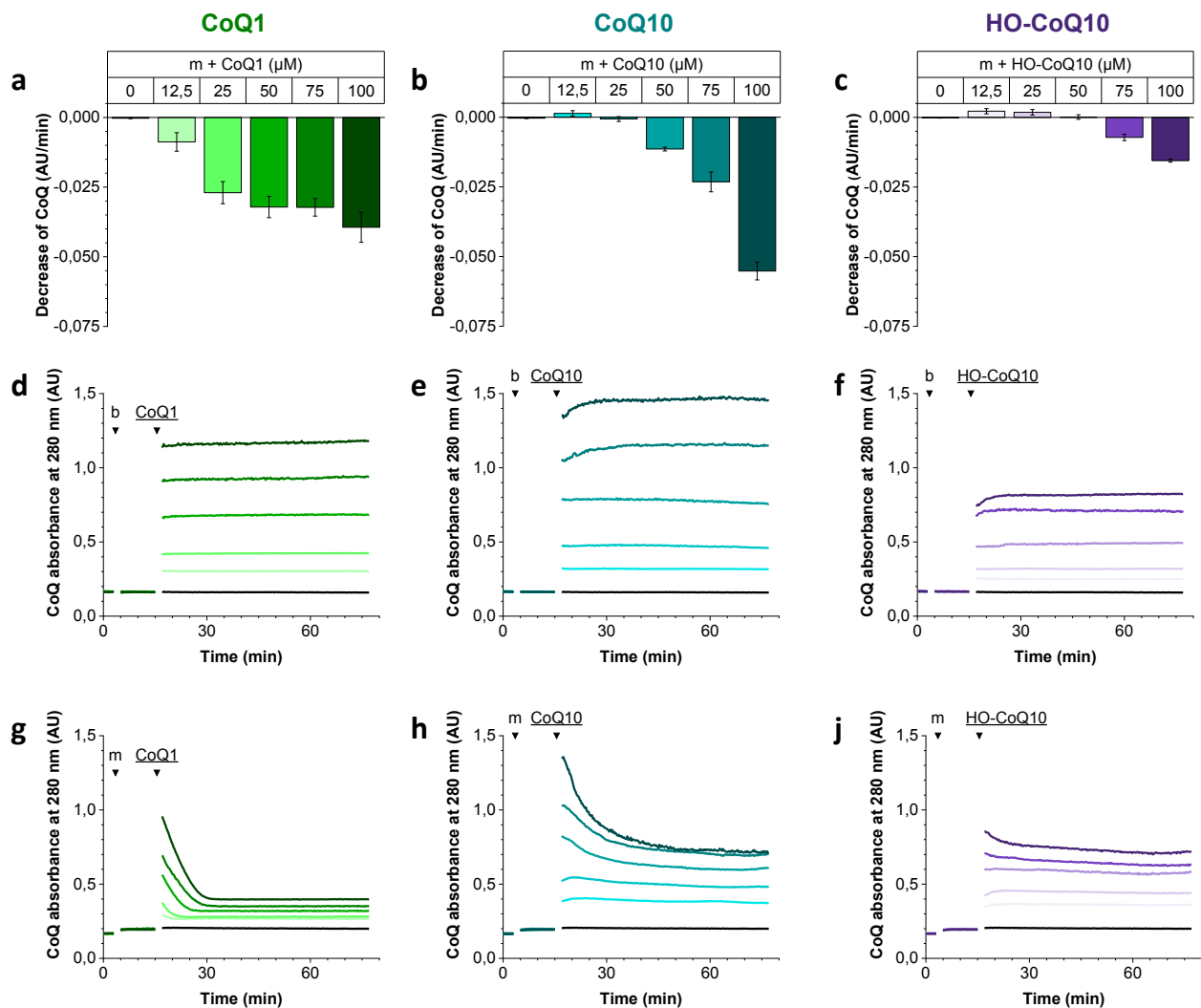


Figure 50 | HO-CoQ10 as alternative electron acceptor from CII. After preincubation of 15 $\mu\text{g}/\text{mL}$ (3 $\mu\text{g}/\text{well}$) BHM (m) with succinate, different, tested acceptors (CoQ1, CoQ10, HO-CoQ10) were added to initiate CoQ reduction by Complex II. (a-c) Initial linear succinate:CoQ oxidoreductase activity; reduction of CoQ was followed as loss of absorption at 280 nm: (d-f) control experiments adding buffer (b) instead of mitochondria (m) (g-h);

Sample: BHM subjected to 3 freeze-thaw cycles in hypotonic KPb; buffer: 50 mM KP_i (pH 7.4), 10 mM succinate, 1 mM KCN, 10 μM antimycin A, 2.5 μM rotenone, 10% ethanol; analysis: mean \pm SEM from triplets of 1 independent mitochondrial preparation;

3.7.5 Identification of respiratory complexes and supercomplex formation

Respiratory chain complexes are associated into supercomplexes within the inner mitochondrial membrane. To visualize supercomplexes (~ 2 MDa) and single complexes (down to 200 Da) in bovine heart mitochondria, gradient polyacrylamide gels were used with a stacking gel of 4% and a separating gel spanning from 5-10% acrylamide (Figure 51 a). To maintain supercomplexes and functional enzymes blue-native conditions were chosen. To solubilise the mitochondria, digitonin or dodecyl maltoside (DDM) was used. In Western blots, complexes I, III, IV, and V were detected to identify the bands in Coomassie Blue-stained gels (compare b and c with d). Human antibodies were used against subunits of the RCCs.

Complex I was detected at a molecular mass greater than 669 kDa (anti-NDUFB8 in b), in agreement with its molecular mass of around 1 MDa.²²⁶ Digitonin-solubilised BHM showed less monomeric CI than DDM-solubilised BHM, therefore more high-molecular bands indicating intact supercomplexes were present. Since

bovine Complex I consists of 45 subunits,²²⁷ bands with smaller molecular mass might be correlated to different stages of its assembly.²²⁸

Dimeric Complex III (500 kDa)²²⁶ was identified detecting the Rieske subunit at a molar mass between 440 and 669 kDa (anti-Rieske in **b**). Complex IV was found around 200 kDa as well as at higher masses (**c**, anti-Cox4-I) correlating with association to other respiratory chain complexes, e.g. III₁IV₁.²²⁶ The holo-F₁F₀ complex of ATP synthase (Complex V) was detected in its monomeric (around 700 kDa) and dimeric state; its F₁ subcomplex migrated around 440 kDa (anti-ATP5B in **c**).^{226,229-231}

Supercomplexes were identified for digitonin-solubilised mitochondria according to Schagger et al. (2001).²³⁰ Three supercomplexes were distinguishable in Coomassie Blue-stained gel consisting of one CI, a CIII dimer (I₁III₂) and one or two CIV (I₁III₂IV₁ and I₁III₂IV₂) with I₁III₂IV₁ as the most abundant supercomplex. Solubilisation with the stronger detergent DDM did not allow a clear distinction of still intact supercomplexes. Since in western blots CI, CIII (**b**), and CIV (**c**) were detectable and one band was at a similar height as the digitonin-solubilised supercomplex I₁III₂IV₁ (~1.7 MDa), stable supercomplexes solubilised with DDM probably were I₁III₂IV₁ and I₁IV₁ (~1.2 MDa) which were observed from Schagger et al. at lower DDM concentrations.²³⁰

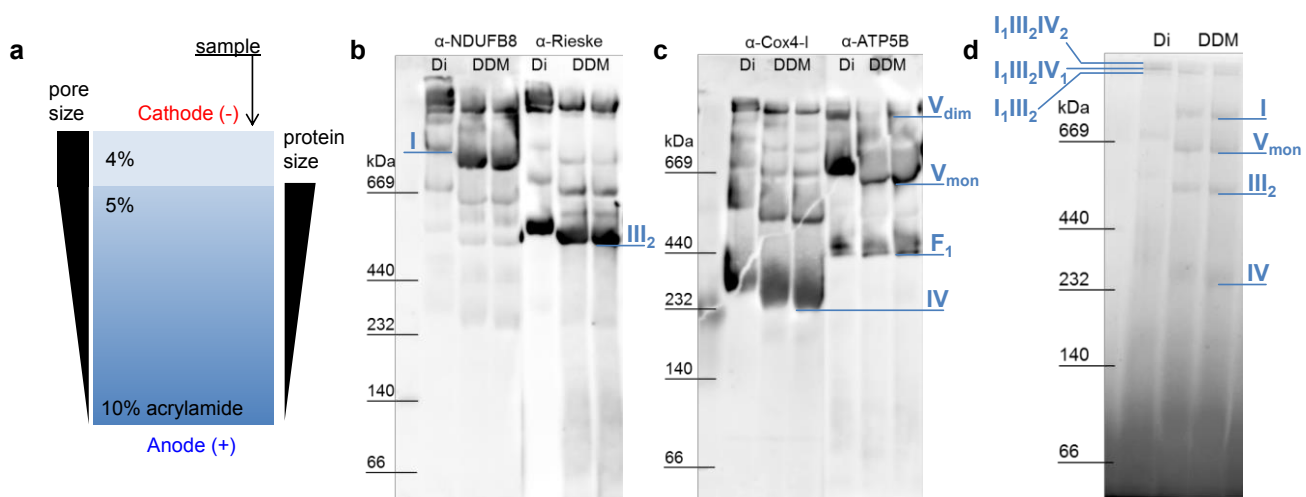


Figure 51 | Blue-native PAGE of respiratory chain complexes from bovine heart mitochondria. (a) Gradient blue-native polyacrylamide gel electrophoresis (BN-PAGE), (b and c) western blot of digitonin- (Di; Di/protein ratio 10 (g/g)) or dodecyl maltoside- (DDM; DDM/protein ratio 1.6 and 2 (g/g), from left to right) solubilised BHM with human antibodies against (b) CI (NDUFB8), CIII (Rieske), (c) CIV (Cox4-I), and CV (ATP5B) subunits; (d) Coomassie Blue staining of gel used for western blot; I-V, respiratory chain complexes I to V; V_{dim} and V_{mon}, monomeric and dimeric states of CV (ATP synthase); F₁, F₁ subcomplex of CV;

3.7.6 In-gel activity staining: HO-CoQ10 did not disturb Complex I NADH oxidase and Complex II succinate oxidase activity

Photometric activity assays of Complex I and II showed an inhibitory effect of HO-CoQ10, though, especially for CI, results were inconsistent. Furthermore, the need for artificial quinones as substrates complicated the evaluation of a direct influence of CoQs on the enzymes. In-gel activity staining has the advantage of first separating respiratory chain complexes and then measuring the activity of single complexes without interference with inhibitors or other enzymes. Enzyme activity is directly quantified through optic density of

the precipitate of a probing substance on the gel. Besides, protein content can be quantified by Coomassie Blue staining.

HO-CoQ10 did not affect Complex I NADH oxidase activity

Complex I activity was measured using NBT^{kk} as an acceptor that will form an insoluble precipitate after reduction by CI to formazan (Figure 52 a). To measure CI separately and not within supercomplexes, DDM concentration was raised to 2 g/g, the highest possible DDM concentration without expansion of the dye front into protein bands (data not shown). Although Coomassie Blue staining showed a distinct band of Complex I accumulated at its monomeric mass (b, left), in-gel activity staining could not differentiate between monomeric CI and supercomplex-bound CI (b, right). Therefore, to keep supercomplexes intact, 10 g/g digitonin was used. Like this, monomeric Complex I was still distinguishable from SC-bound CI after in-gel activity staining (lane ±d in c). Although in-gel activity staining showed another band at low molecular weight (~ 100 kDa; marked with * in b), the separation on the gel allowed a clear distinction of CI activity from CI-unspecific activities.

Even though Jung et al. (2000)¹²⁴ measured a rotenone-sensitive in-gel activity using NBT as an acceptor for CI, NBT turnover was not sensitive to rotenone in all performed experiments (Figure 52 b, c e, f). Neither prolonged preincubation of the gels with rotenone (data not shown) nor its addition during solubilisation of mitochondria (c, e) reduced in-gel activity staining. To exclude that an attenuated NBT turnover was masked by accumulation of the dye due to long incubation times, formazan precipitation was quantified at different times during the reaction. Still, CI in-gel activity was not reduced by rotenone (e, f). Actually, the used assay is well-known to detect NADH oxidase but not NADH:CoQ oxidoreductase activity and therefore cannot be sensitive to rotenone.^{232,233} Like rotenone, HO-CoQ10 did not inhibit NADH oxidase activity. Neither preincubation of mitochondria with 10 μM HO-CoQ10 during solubilisation (c, d) nor performing in-gel activity staining in presence of HO-CoQ10 (f) reduced NBT turnover. Ngu et al. (2012) observed that a mutation near the Q-binding site of Complex I reduced NADH:CoQ1 oxidoreductase but not CI content or in-gel activity, and therefore suggested a catalytic defect regarding electron passage from the final Fe-S cluster N2 to CoQ.²³⁴ Hence, it is likely that the inhibitory site of HO-CoQ10 is the Q-binding site of CII. In addition, stability of supercomplexes was not influenced by HO-CoQ10, CoQ10 or CoQ1 supplied during solubilisation of mitochondria since presence of CI and migration height of supercomplexes, probably formed by I₁III₂IV₂, I₁III₂IV₁, and I₁III₂, was similar to the vehicle control (c). Admittedly, solubility of CoQs might have been compromised due to the low temperature necessary for mitochondria solubilisation. To examine SC integrity in more detail electrophoresis run time and/or acrylamide gradient should be adjusted. Furthermore, mitochondria collected from respiration measurements in which CoQs are supplied at 37 °C and demonstrably exert an effect on mitochondrial ETC should be used for further evaluation.

^{kk} NBT, Nitro Blue tetrazolium, 2-[2-methoxy-4-[3-methoxy-4-[3-(4-nitrophenyl)-5-phenyltetrazol-2-ium-2-yl]phenyl]phenyl]-3-(4-nitrophenyl)-5-phenyltetrazol-2-ium;dichloride

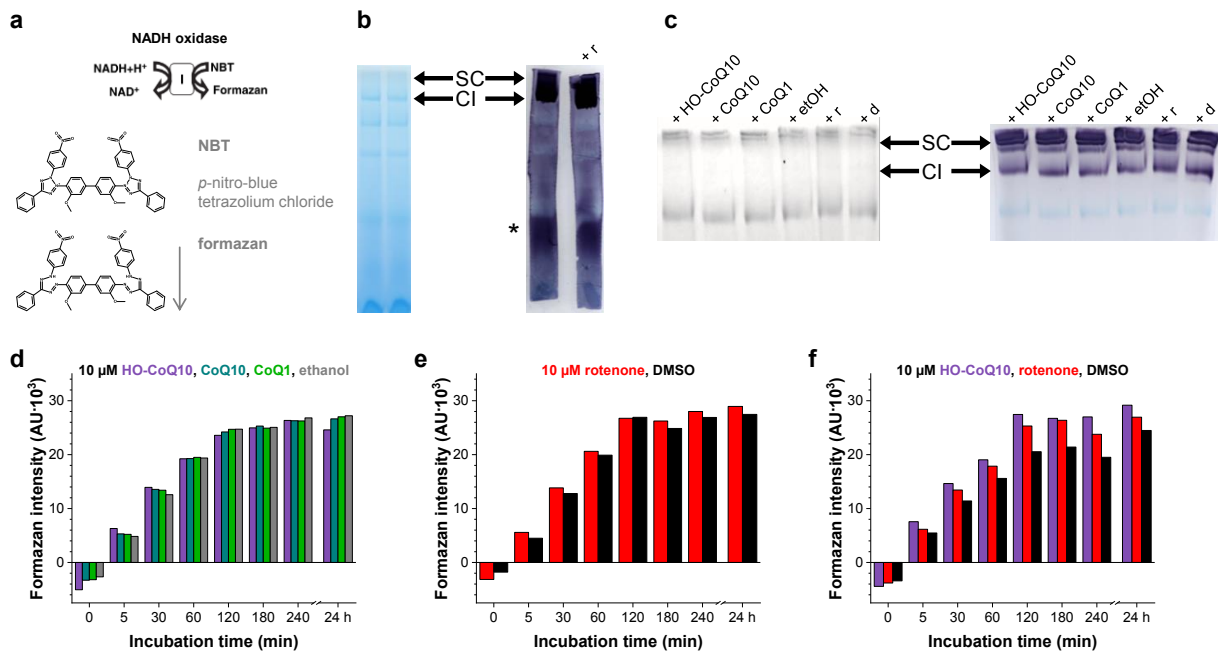


Figure 52 | HO-CoQ10 did not affect Complex I in-gel activity staining. 50 μg bovine heart mitochondria, 140 μM NADH, 1 mg/mL NBT, 10 mM Tris (pH 7.4), incubation at RT; (a) NADH oxidase activity of CI was detected via reduction of NBT to insoluble formazan depositing on the gel, figure adapted from Sabar (2005);²³¹ (b, c) Coomassie Blue staining (left) and NBT staining (right), monomeric Complex I (CI) and supercomplexes (SC) are marked with arrows; CI-unspecific NBT staining marked with *; (d-f) quantification of NBT turnover by monomeric CI; detergents for solubilisation of mitochondria were (b) 2 g/g DDM or (c-f) 10 g/g digitonin; substances (10 μM CoQ or rotenone (r), 1% vehicle, i.e. ethanol or DMSO (d)) were added (c, d, e) during solubilisation or (f) during solubilisation and incubation with NADH and NBT;

HO-CoQ10 did not affect Complex II succinate oxidase activity

Complex II was identified by succinate oxidase activity staining (Figure 53 a) between CIV and the dye front in agreement with its low molecular mass of 130 kDa²³⁵ (Figure 53 b). Since borders of CII bands were not sharp, making quantification difficult, DDM concentration was raised to 5 g/g for experiments with CoQ (c). Succinate oxidase activity was reduced by malonate (b, ± malo) but was not affected by HO-CoQ10, CoQ10 and CoQ1 (c). Since NBT was reduced via PMS by electrons from FADH₂ (a), this assay allowed only evaluation of CII activity influenced at the dicarboxylate-binding site suggesting a role for HO-CoQ10 at the Q-binding site of CII.

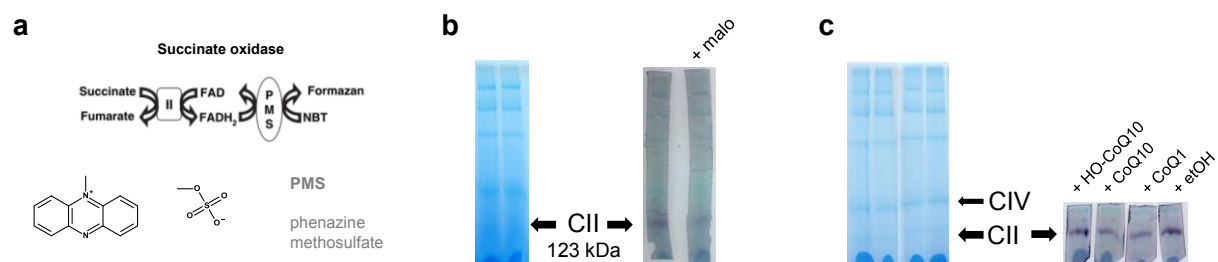


Figure 53 | Complex II in-gel activity was not influenced by HO-CoQ10. 50 μg bovine heart mitochondria, 84 mM succinate, 0.2 mM PMS, 2 mg/mL NBT, 10 mM Tris (pH 7.4); (a) succinate oxidase activity of CII was detected via PMS-mediated NBT conversion to insoluble formazan depositing on the gel, figure adapted from Sabar (2005);²³¹ (b, c) Coomassie Blue staining (left) and NBT staining (right), Complex II (CII) is marked with arrows; detergents for solubilisation of mitochondria were (b) 2 g/g DDM or (c) 5 g/g DDM, substances were added during in-gel activity staining: (b) 5 mM malonate, incubation at RT for 22 h, (c) 10 μM CoQ at 37 °C for 24 h;

3.8 Influence of HO-CoQ10 and CoQ10 on mitochondrial ROS production

Inhibition of the electron transport chain often leads to increased production of ROS. This is true for e.g. the inhibition of CIII by antimycin A or CI by rotenone and a supply of NADH equivalents.⁵⁰ In this thesis, it was found that exogenously supplied HO-CoQ10 and CoQ10 inhibit the mitochondrial ETC, whereas only HO-CoQ10 reduced CI and CII oxidoreductase activities. CoQ10, on the other hand, is well known as the only endogenously de-novo synthesized lipid antioxidant in animals.^{19,35} Moreover, HO-CoQ10 with its lower redox potential might be a more effective antioxidant. Consequently, the role of HO-CoQ10 and CoQ10 on mitochondrial ROS production was investigated.

3.8.1 HO-CoQ10 enhanced hydrogen peroxide production of respiring mitochondria

To learn about the anti- and prooxidant properties of HO-CoQ10, its interaction with mitochondrial H₂O₂ production was analysed with a horseradish peroxidase (HRP)-based assay using Amplex[®] UltraRed (AUR) as the substrate. As illustrated in Figure 54, H₂O₂ will oxidize the heme centre of HRP to the highly electrophile ferryl radical state Compound I. To return to its ground state, HRP subsequently needs to take up 2 electrons, from 2 substrates (i.e. 2 AUR). The two AUR radicals formed in this sequence dismutate into the non-detectable educt and the fluorescent, oxidized form (AURox). In sum, 1 H₂O₂ molecule forms 1 fluorescent resorufin derivative, AURox.

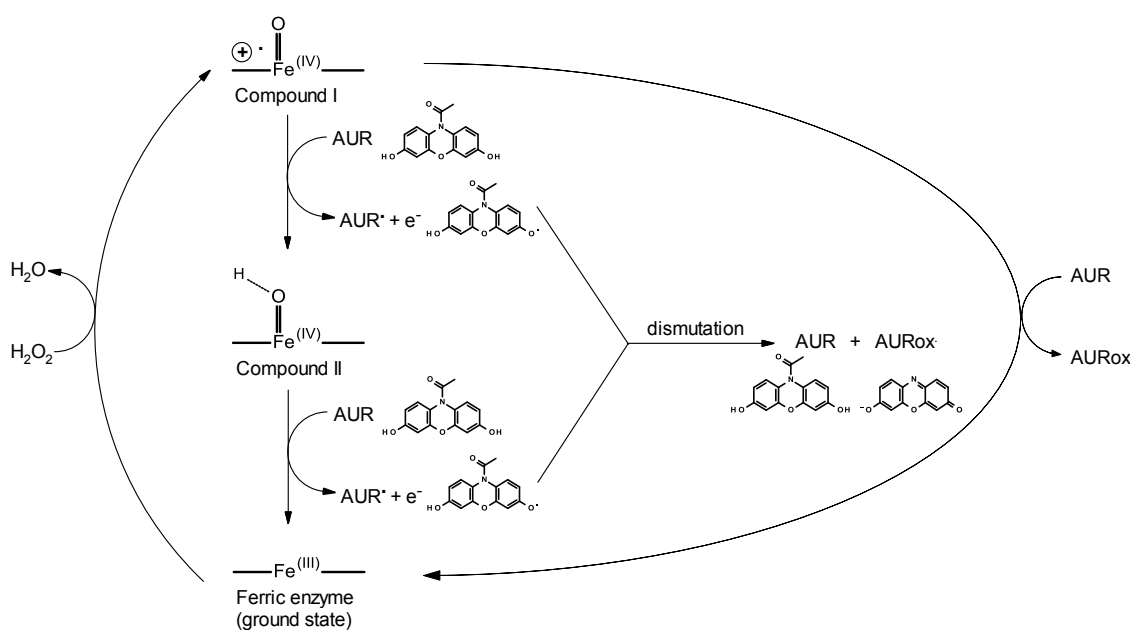


Figure 54 | H₂O₂ detection with the HRP-based fluorescence assay using Amplex[®] UltraRed. Exemplarily, Amplex[®] Red is shown because the chemical structure of its derivative Amplex[®] UltraRed is not published. See text above for description. This scheme is based on Berglund et al. (2002, Fig.1, peroxidase cycle)²³⁶ and Gorris & Walt (2009, Fig.1).²³⁷

To analyse H₂O₂ production by ETC processes, freshly isolated, coupled mouse heart mitochondria were incubated together with AUR, HRP and superoxide dismutase (SOD) to assure immediate dismutation of superoxide to H₂O₂. H₂O₂ production was stimulated by the addition of ETC substrates (and ADP) in respiration buffer together with known inhibitors or Coenzyme Q. It is important to note that H₂O₂ production measured in the supernatant of isolated mitochondria is influenced by the antioxidant potential of the

mitochondrial preparation, H_2O_2 release, as well as its reaction with non-mitochondrial particles in the extramitochondrial solution. Besides, we are detecting accumulating, non-reversible AUrox formation, so the increase in fluorescence signal only shows net H_2O_2 production rates and AUrox accumulation but not H_2O_2 concentrations accumulated in the extramitochondrial solution.

Increasing concentrations of mitochondria were incubated together with HRP and AUR to directly measure H_2O_2 , i.e. AUrox formation rate. **Figure 55** shows an increase of H_2O_2 production proportional to mitochondrial input up to 50 $\mu\text{g}/\text{mL}$ mitochondrial protein when pyruvate and malate were supplied as Complex I substrates (**b** and **c**). Without any ETC substrate, H_2O_2 production was negligible (**a**). Hence, H_2O_2 detected in these experiments is directly associated with NADH production from Krebs cycle and therefore most likely Complex I-associated. CI-linked H_2O_2 production rates were with ~ 20 $\text{pmol}/(\text{min} \cdot \text{mg})$ (**b**) in agreement with measurements from Nickel et al. (2015)⁸⁹ using MHM isolated from the same mouse strain (BL6N). Production rates in presence of saturating ADP concentrations were reduced in **c**, matching the hypothesis that increasing oxygen consumption at constant $[O_2]$ decreases one-electron reduction of oxygen to superoxide.²³⁸ In contrast, Nickel et al. did not report an ADP-linked reduction of H_2O_2 production in heart mitochondria from BL6N mice possessing an intact nicotinamide nucleotide transhydrogenase (*Nnt*) gene due to NNT activity in reverse-mode.⁸⁹ Similarly, measurements shown in **Figure 56 b** and **Figure 57 d** did not show an effect of ADP on H_2O_2 production rate (m + PM + water vs. m + PM + A + water), although in the experiment in **Figure 55 b** and **c** H_2O_2 production was slightly decreased in presence of ADP.

As a positive control antimycin A was added to mitochondria (**d**) inducing H_2O_2 production at the Q_0 site by locking the ubiquinol-derived semiquinone radical. High mitochondrial input led to a fast saturation of the AUrox signal within a short period of time. Therefore, 100 $\mu\text{g}/\text{mL}$ mitochondrial protein was used for following experiments to allow measurements without saturation of AUrox signal.

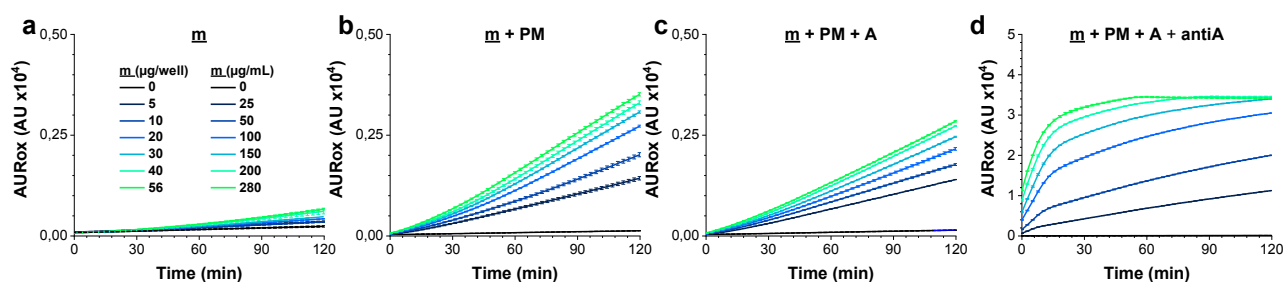


Figure 55 | H_2O_2 detection in coupled mouse heart mitochondria. AUrox formation by the turnover of HRP in presence of produced H_2O_2 was measured at 37 °C using increasing concentrations of mitochondria (m) were used. (**a**) Mitochondria in respiration buffer (RB1), together with (**b**) the CI substrates pyruvate and malate (PM, 5 mM), (**c**) PM and 1 mM ADP (A), (**d**) PM, ADP and the CIII inhibitor antimycin A (antiA, 10 μM)

Sample: freshly isolated, coupled MHM; buffer: RB1, 50 μM AUR, 0.5 U/mL HRP, 50 U/mL SOD; analysis: mean of single traces from triplets of 1 independent mitochondrial preparation;

Complex I-linked H_2O_2 production was examined in **Figure 56** and **Figure 57** (**a**, **d**) by challenging mitochondria with inhibitors of the respiratory chain complexes I-III or CoQs.

Since mitochondrial ROS production is dependent on oxygen concentration,²³⁹ AUrox formation did not increase linearly in presence of PM, ADP and vehicle controls (**Figure 56 a**). Although Amplex assays were

performed in 96-well plates open to atmospheric oxygen, high H_2O_2 production rates and therefore fast oxygen consumption may have led to decreasing oxygen concentrations during the measurements. Grivennikova et al.²³⁹ suggested analysing initial rates of resorufin production. Nevertheless, because AUrox formation showed an initial lag-phase, maximal AUrox production rates were compared for all conditions which were derived from the maximal value of the first derivative of the curves.

Adding HO-CoQ10 in concentrations causing maximal respiratory inhibition, resulted in similar (Figure 57 d) or slightly lower (Figure 56 b and e) H_2O_2 production rates compared to blocking respiration with rotenone (rot = 0.97- and 1.28-fold the value of HO-CoQ10, respectively). CoQ10 slightly reduced PM-linked H_2O_2 production (Figure 56 a and b; see also Figure 57 a and d). Ethanol did not influence H_2O_2 formation (Figure 56 a and b). The CII inhibitor malonate did not affect H_2O_2 formation (d and e) assuring that PM-induced H_2O_2 production is not influenced by CII-linked ROS production. Antimycin A addition resulted in variable but always high production rates (e, antiA = 7-fold the value of HO-CoQ10).

In control measurements without mitochondria, HO-CoQ10 slightly increased AUrox production rate (Figure 56 c, f). This increase might be due to a possible interaction of AUR or AUR radicals with HO-CoQ10. Since HO-CoQ10 was present in its oxidized state and has a more negative reduction potential than the AUR analogue Amplex® Red ($E^0(AR^{\bullet}/AR) = 1.14 V$),²⁴⁰ a redox reaction resulting in oxidation and thereby production of AUR• and fluorescent AUrox is unlikely. Serrano et al. (2009)²⁴¹ observed oxidation of AR in presence of dietary antioxidants like gallic acid through a mechanism involving the oxidative pathway of HRP in absence of H_2O_2 . Antioxidant activity was determining AR oxidation which was decreased but still visible with oxidized species of gallic and ascorbic acid.²⁴¹

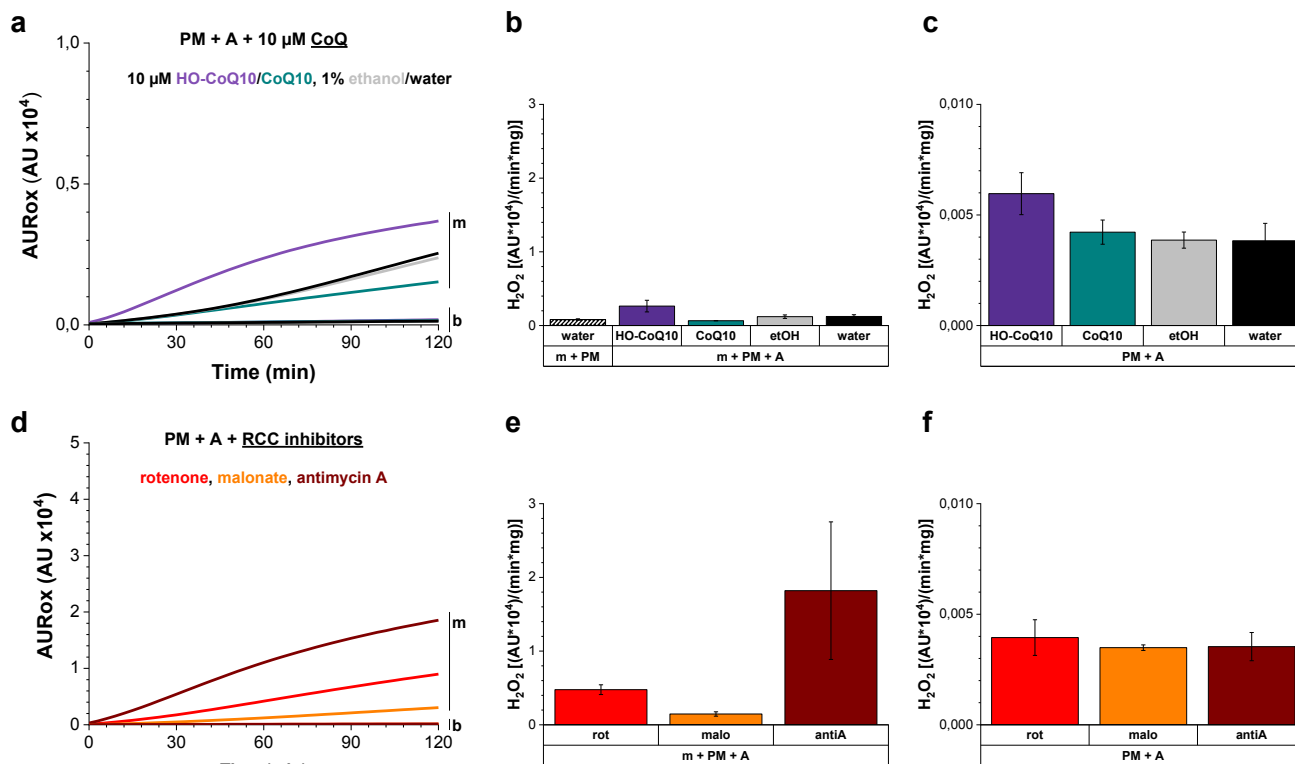


Figure 56 | HO-CoQ10, rotenone and antimycin A increased Complex I-linked H_2O_2 production. 100 $\mu g/mL$ (20 $\mu g/200\text{-}\mu L$ well) mitochondria (m) were incubated with Complex I substrates (PM, 5 mM pyruvate/malate), 1 mM ADP (A), and (a-c) 10 μM CoQs (HO-

CoQ10, CoQ10, 1% ethanol or water as vehicle control) or (d-f) inhibitors of respiratory chain complexes (RCCs) I, II, and III (using 0.5 μ M rotenone (rot), 5 mM malonate (malo), and 10 μ M antimycin A (antiA), respectively). Control measurements were performed with buffer alone (b).

(a, d) AURox accumulation of representative measurements; (b, e) maximal AURox production rates with mitochondria; (c, f) maximal AURox production rates in buffer controls without mitochondria, expanded scale as compared to panels b and e;

Sample: freshly isolated, coupled MHM; buffer: RB1, 50 μ M AUR, 0.5 U/mL HRP, 50 U/mL SOD; analysis: mean \pm SEM from triplets of 3 independent mitochondrial preparations;

In **Figure 57**, mitochondria were supplied with substrates for RCC I, II, and GPDH. AURox formation with CoQ and known inhibitors of the same complex was compared.

Complex II-linked H_2O_2 production was measured using succinate to feed electrons into CII and rotenone to inhibit CI. Indeed, the dicarboxylate-binding site inhibitor malonate decreased H_2O_2 production (**Figure 57 b and e**). This demonstrates that the substrate combination of succinate and rotenone allows examining H_2O_2 formation at Complex II excluding reverse electron transfer (RET) to CI. Unlike CoQ10 that did not affect CII-linked H_2O_2 release, HO-CoQ10 enhanced ROS production to a similar extent as seen for CI, suggesting both CI and CII as ROS production sites in presence of HO-CoQ10. Nevertheless, ROS may be formed at CIII, since that production site has not been blocked by non-ROS inducing inhibitors like stigmatellin. To elucidate if HO-CoQ10 induced ROS production via CII, the effect of low succinate concentrations (0.1 mM) should be tested since inhibitor-induced ROS production at CII was inhibited by high succinate concentration.⁵²

To elucidate if the H_2O_2 production sites are at CI and CII or at the upstream CIII, a protocol to measure CIII-linked activity indirectly was used. Adding glycerol-3-phosphate (G3P) will reduce the endogenous CoQ pool via Glycerol-3-phosphate dehydrogenase (mGPDH) that in turn feeds electrons into CIII. In agreement with studies on rat heart mitochondria by Mráček et al.,¹⁸⁶ H_2O_2 production rate measured in presence of G3P (**Figure 57 c and f, water**) was lower than with PM (a and d, **water**). When ROS production was induced by antimycin A, mGDPH-dependent ROS production was higher (**Figure 57 c and f, antiA**) than via CI blocked with rotenone (a and d, **rot**). Neither ethanol nor CoQ10 affected G3P-linked AURox production (c, f). HO-CoQ10 more than halved basal production rate. This argues for HO-CoQ10 facilitating ROS production directly via CI and CII but not CIII which is in line with HO-CoQ10 inhibiting NADH:CoQ1 and succinate:CoQ1 oxidoreductase but not decyl-ubiquinol:cytochrome *c* oxidase activity (cf. **section 3.7** on p. 97).

As performed by Mráček et al. (2008),¹⁸⁶ a CIII inhibitor not stimulating ROS production can be used to distinguish ROS produced at CIII and GPDH. Even though in their study myxothiazol was used, it induced ROS formation but to a considerably lower extent than antimycin A.^{56,186} Since stigmatellin completely abolishes ROS production at the Q_o site preventing electron transfer to the Rieske protein and consequently oxidation of QH_2 , it is the appropriate tool to evaluate CIII-derived ROS production.²⁴² Combining HO-CoQ10 with stigmatellin or antimycin A will show if electrons are banked up at mGPDH or CIII. In parallel, the influence of HO-CoQ10 on mGPDH activity should be assessed by measuring CoQ reduction photometrically.

Antimycin A induced considerably higher H_2O_2 production in isolated mitochondria (**Figure 56 b, e and Figure 57 f**) with any given substrates than HO-CoQ10. Because of that, it is unlikely that HO-CoQ10 acts through the same mechanism as antimycin A, i.e. locking the CoQ10 semiquinone radical that in turn reacts with O_2 .

Furthermore, mitochondrial $O_2^{\bullet-}/H_2O_2$ production should be verified using another experimental approach, e.g. electrochemical detection without fluorescent sensors, and H_2O_2 production should be analysed simultaneously with oxygen consumption.

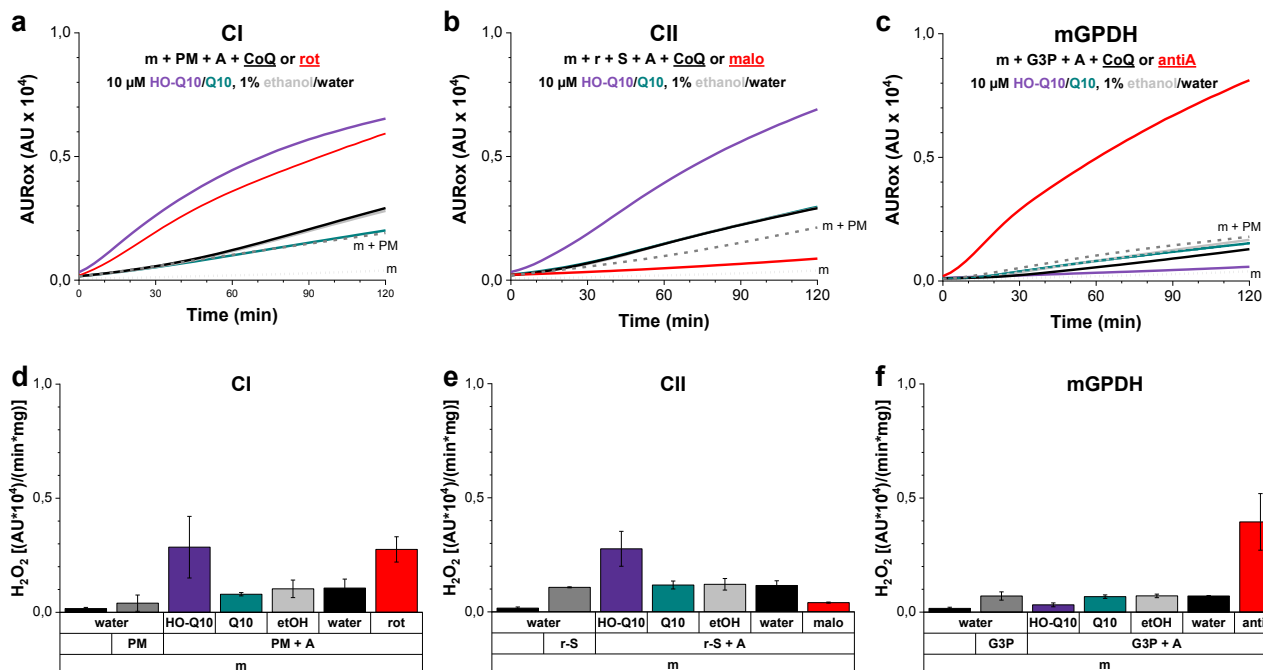


Figure 57 | HO-CoQ10 increased CI- and CII-linked H_2O_2 production and reduced mGPDH-linked H_2O_2 production. 100 μ g/mL (20 μ g/200- μ L well) mitochondria (m) were incubated with substrates for CI/CII/mGPDH (substrates, see below), 1 mM ADP and 10 μ M CoQs (HO-CoQ10, CoQ10, 1% ethanol or water as vehicle control) or complex-specific inhibitors (inhibitors, see below). (a, b, c) AUrox accumulation of representative measurements: solid lines, m + substrate + ADP + CoQ/vehicle/inhibitor; dashed grey line, m + substrate; dotted black line, mitochondria alone; (d-f) maximal H_2O_2 production rate;

Sample: freshly isolated, coupled MHM; buffer: RB1, 50 μ M AUR, 0.5 U/mL HRP, 50 U/mL SOD; substrates: Complex I: PM, 5 mM pyruvate/malate; Complex II: 0.5 μ M rotenone, 10 mM succinate; mGPDH (mitochondrial glycerol-3-phosphate dehydrogenase): G3P, 10 mM glycerol-3-phosphate; inhibitor: Complex I: rot, 0.5 μ M rotenone; Complex II: malo, 5 mM malonate; antiA, 10 μ M antimycin A; mGPDH: inhibition of Complex III with 10 μ M antimycin A (antiA); analysis: mean \pm SEM from triplets of 2 independent mitochondrial preparations;

Since HO-CoQ10 increased CI-linked AUrox formation rate, accumulation of H_2O_2 in the extramitochondrial solution was examined in **Figure 58**. Mitochondria were incubated in a well plate at 37 $^{\circ}$ C. Then, CI substrates PM and saturating ADP were added as indicated. To detect H_2O_2 accumulation in the supernatant, mitochondria were not incubated together with HRP and AUR, but samples were taken at selected times and admixed with assay buffer to measure fluorescence. No H_2O_2 release was detectable when mitochondria were energized with PM and ADP. Only application of 10 μ M antimycin A resulted in a significant increase of extramitochondrial H_2O_2 . Since the locked semiquinone radical is located at the Q_o site of CIII, ROS are directly released into the mitochondrial intermembrane space. Hence, HO-CoQ10 is obviously not participating in ROS formation at the Q_o site of CIII. To localize HO-CoQ10-induced H_2O_2 formation, experiments should be repeated with rotenone. As rotenone induces ROS-production in the mitochondrial matrix, H_2O_2 release into the supernatant is lower (cf. **Figure 56 e**). Due to antioxidant activity of the supernatant from crude mitochondrial extracts,⁵⁰ extramitochondrial H_2O_2 might not accumulate and therefore would only be detectable when

mitochondria are incubated together with the detector. Furthermore, HO-CoQ10-induced ROS production might be undetectable due to interaction of exogenously supplied CoQ with ROS.

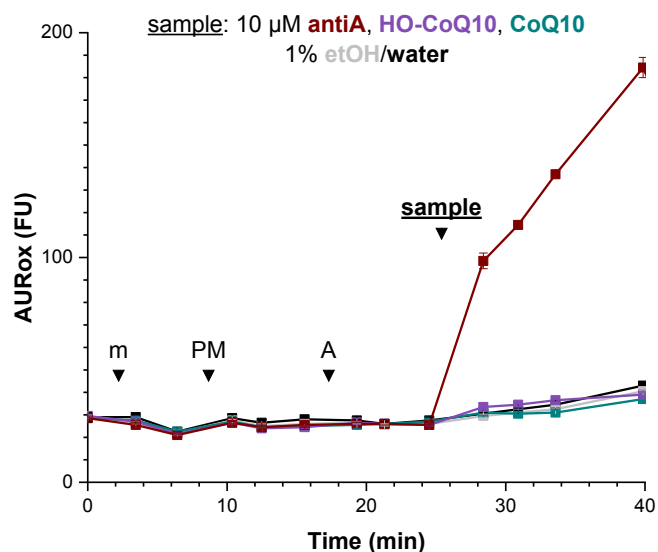


Figure 58 | HO-CoQ10 did not change extramitochondrial H₂O₂ concentration. 200 μg/mL MHM were incubated in RB1 at 37 °C and 5 mM pyruvate/malate (PM), ADP (A), and CoQs (10 μM CoQ10, HO-CoQ10), solvent controls (1% ethanol/water) or 10 μM antimycin A were added at indicated times. Extramitochondrial H₂O₂ was quantified for indicated time points: samples were resuspended, 50-μL aliquots were retrieved and admixed with 50 μL assay buffer;

Sample: freshly isolated, coupled MHM; assay buffer: RB1, 100 μM AUR, 1 U/mL HRP; analysis: mean ± SEM from duplets of 1 independent mitochondrial preparation;

3.8.2 Simultaneous superoxide detection and oximetry in mitochondria using electron spin resonance spectroscopy

Since HO-CoQ10 favoured CI- and CII-linked H₂O₂ production, the precursor superoxide (O₂^{•-}) should be detected. To look at superoxide production dependent on respiration of coupled mitochondria was of special interest. Therefore, a procedure to measure superoxide and oxygen concentration simultaneously using electron paramagnetic resonance (EPR; ESR, electron spin resonance) spectroscopy was established. As unpaired electrons are detected and the radical must be reasonably stable in a chemically complex environment, the spin probe CMH^{II} was utilized to measure superoxide radicals (Figure 59 a). The membrane-permeable hydroxylamine will immediately react with O₂^{•-} forming a stable nitroxyl radical CM[•] (reaction of superoxide and CMH: 1.2 x 10⁴ M⁻¹s⁻¹).²⁴³ The oxygen sensor trityl^{III} was used to follow oxygen consumption (b).

To measure oxygen consumption rates most accurately, it was essential to shorten measuring intervals as much as possible. The lab's standard protocol was adjusted by decreasing the sweep width and time constant to measure every 10 s instead of 60 s. Modulation amplitude had to be changed to measure both trityl and CM radicals simultaneously without over-broadening the narrow trityl signal. As can be seen from measurements at ambient oxygen concentration and in anoxic conditions in Figure 59 e and f, line width and peak-to-peak

^{II} CMH, 1-hydroxy-3-methoxycarbonyl -2,2,5,5-tetramethylpyrrolidine

^{III} Trityl, tetrathiatritylmethyl radical

height (i.e. radical intensity) of trityl absorption (dashed lines) are very sensitive to changes of the modulation amplitude (MA). Different from the nitroxyl radical tempol (solid lines), used as a model for CM radical, peak-to-peak height of trityl signals did not steadily increase with MA. The decrease of radical intensity was correlated to line broadening. As a compromise for both radicals, 0.8 G MA was chosen for experiments. As suggested from recent publications,^{125,126} the peak-to-peak height of the trityl signal, not the commonly-used line width was evaluated for oximetric measurements as difference in O₂-saturated to O₂-depleted solution was far more pronounced (cf. dashed black line and dashed blue line in e and f at 0.8 G MA).

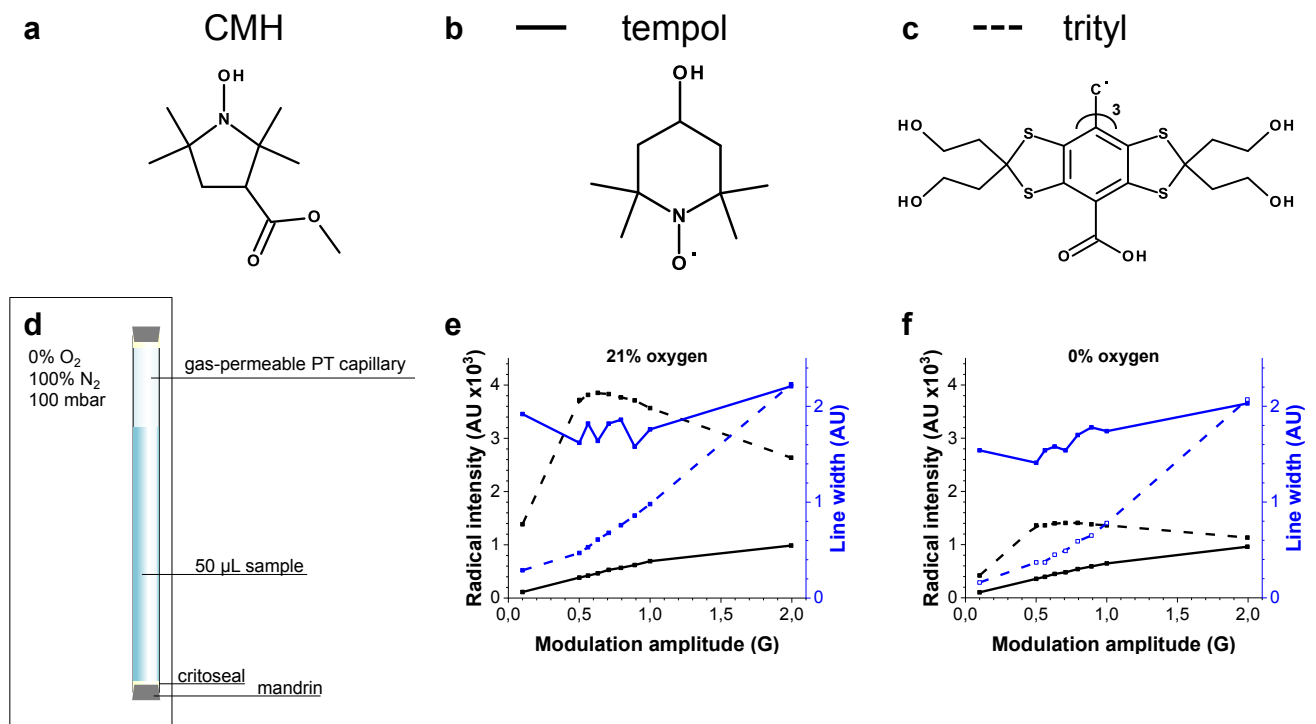


Figure 59 | Measuring superoxide and oxygen simultaneously using an EPR-based assay. (a) Hydroxylamine spin probe for superoxide CMH, (b) stable nitroxyl radical tempol used as a model substance for the nitroxide radical CM[•] formed by reaction of CMH with superoxide, (c) oxygen sensor trityl; measurements to determine ideal detection parameters were performed at (e) ambient oxygen concentration of 21% in a glass capillary or at (f) anoxic conditions in a gas-permeable PT capillary (depicted in panel d) located in 100% nitrogen atmosphere and 100 mbar overpressure to deplete oxygen from the solution; (e, f) comparison of radical intensity (i.e. peak-to-peak height, black) and line width (blue) of 4 µM tempol (solid lines) and 4 µM trityl (dashed lines) in RB1 at changing modulation amplitudes; T : 37 °C

Respiration measurements were performed at 37 °C in glass capillaries that did not allow diffusion of air oxygen into the solution. This permitted detection of oxygen consumption by the sample. Mitochondria were preincubated together with the CI substrates pyruvate and malate, and the oxygen sensor trityl in respiration buffer (RB1) at 37 °C. Just before the recording, a mixture of ADP with inhibitors or CoQ, and CMH were added and the sample was transferred into the glass capillary (Figure 60 a).

Trityl signal and therefore oxygen concentration stayed constant when mitochondria were measured alone (b, dashed line, m). The initial decrease of the trityl signal, observed in all measurements (b, dashed lines), was due to temperature adjustment of the capillary at the beginning of the measurement since signal intensity was higher at RT (c). Supplying PM induced oxygen consumption (b, dashed line, + PM). Addition of ADP increased

oxygen consumption (b, dashed line, + PM + A) and decreased superoxide production (b, solid lines: cf. dark grey, + PM and light grey, + PM + A). as has been reported earlier.^{89,238} In contrast to studies of Nickel et al. (2015),⁸⁹ superoxide production rate was not reduced upon ADP supply. Nevertheless, total CM radical and therefore superoxide concentration was lowered since their formation stopped with O₂ depletion. Surprisingly, CM radical formation (rate) was the highest when mitochondria were measured in absence of any substrate (b, black solid line) without any relevant decrease of the trityl signal.

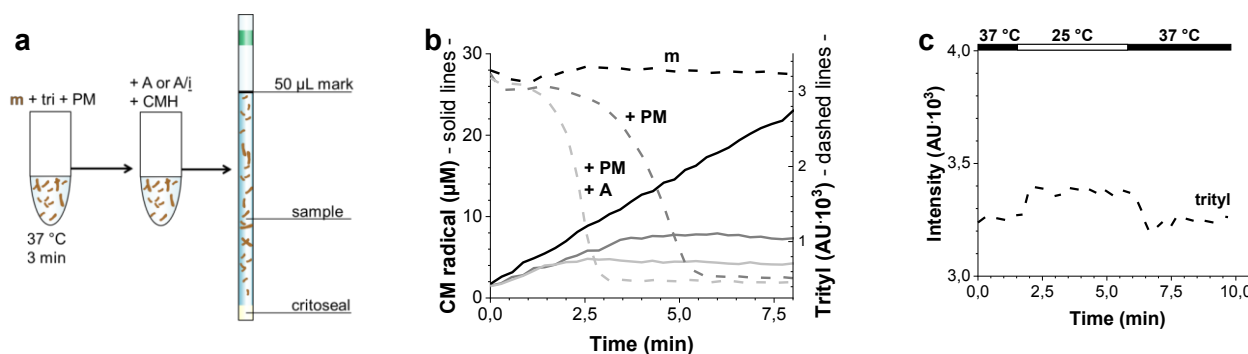


Figure 60 | Mitochondrial superoxide production and oxygen consumption. (a) Sample preparation: 1. preincubation of mitochondria (m) with 4 µM trityl (tri) and 5 mM pyruvate/malate (PM) at 37 °C for 3 min, 2. addition of ADP (A), or a mixture of ADP and inhibitor/CoQ (A/i), and CMH, 3. transfer into and measurement of the sample in 50-µL glass capillary; (b) simultaneous measurement of superoxide production and oxygen consumption of 50 µg (1 mg/mL) freshly isolated MHM (m, black) alone, and supplied with PM (pyruvate/malate, 5 mM, dark grey) or PM + A (ADP, 1 mM, light grey); (c) behaviour of 3.2 µM trityl signal intensity upon temperature changes from 37 °C to 25 °C; (b, c) CM radical concentration (solid lines) and trityl signal intensity (dashed lines) are plotted.

Sample: freshly isolated, coupled mouse heart mitochondria (BL6J); buffer: RB1 + 4 µM trityl, 0.3 mM CMH; T: 37 °C;

Increasing input of mitochondrial protein from 2.5 µg (50 µg/mL) to 50 µg (1 mg/mL) per capillary, resulted in increasing oxygen consumption and concomitant superoxide production rate in presence of PM and ADP (Figure 61). In contrast to oxygen measurements using a Clark-type electrode, decrease of trityl signal is not linear due to the fact that absorption intensity of trityl is not linearly dependent on oxygen concentration (data not shown).

At high mitochondria concentrations, when oxygen was rapidly consumed during the measurement, CM radical concentration decreased after depletion of oxygen (Figure 61 a, 25 µg and b 20-50 µg) though this effect was not always apparent (cf. Figure 60 b, light grey, solid line, 50 µg). Analogously to the H₂O₂ quantification with Amplex® Red (AR), where H₂O₂ oxidizes AR to resorufin, the reaction of superoxide with the spin probe is irreversible and the accumulation of oxidized CMH, not superoxide concentration is detected. Recently, Grivennikova et al. (2018) observed loss of resorufin in absence of oxygen when mitochondrial Complex I was reduced by NADH. Complex I was attributed an NADH:resorufin oxidoreductase activity reducing resorufin (Res) to the colourless dihydroresorufin (ResH₂).²³⁹ The midpoint potential for CM•/CMH (+150 mV vs. SHE)²⁴⁴ is more positive than of Res/ResH₂ (-120 mV at pH 7.5 vs. HE, Twigg (1945)²⁴⁵ as cited in Grivennikova (2018)²³⁹). Therefore, it is plausible that CM radical can be an alternative acceptor for CI as well. Other enzymes like cytosolic DT-diaphorase²⁴⁶ and microsomal NADPH:cytochrome reductase²⁴⁷ have shown resorufin reductase activity. Thus, contaminations in the crude mitochondrial extract together with CI and other unidentified enzymes or redox-active components may be responsible for loss of CM• signal due to reduction to CMH.

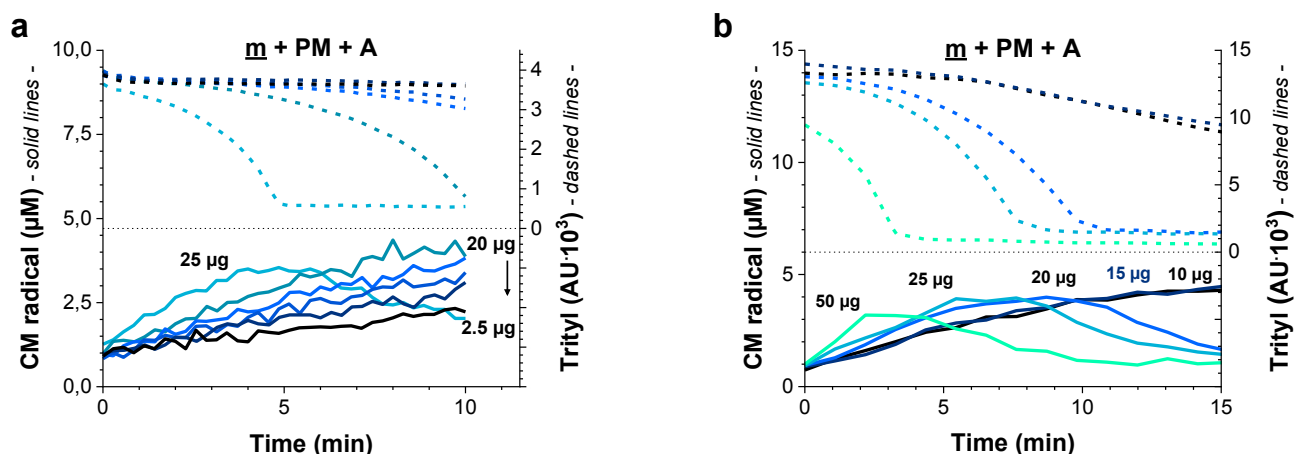


Figure 61 | Oxygen consumption and CM[•] formation in dependence of mitochondrial input. Mouse heart mitochondria (m) were incubated with 5 mM pyruvate/malate (PM) and 1 mM ADP (A); mitochondrial input is indicated in µg/50-µL glass capillary and colour-coded; CM[•] formation (*solid lines*) and trityl signal intensity (*dashed lines*) is plotted; (a) 2.5, 5, 10, 15, 20, 25 µg mitochondrial protein/50 µL (i.e. 50-500 µg/mL); (b) 10, 15, 20, 25, 50 µg mitochondrial protein/50 µL (i.e. 200-1000 µg/mL);

Sample: freshly isolated, coupled mouse heart mitochondria (BL6J); *buffer:* RB1 + 4 µM trityl, 0.3 mM CMH; *T:* 37 °C;

To elucidate the effect of CoQs on superoxide production, the influence of RCC inhibitors on PM-linked respiration and superoxide production was evaluated first (Figure 62 a). Background CMH oxidation was not influenced by substrates, ADP and inhibitors (data not shown). As expected, CII inhibition with 5 mM malonate did not affect respiration nor superoxide production. Even though rotenone reduced oxygen consumption more than antimycin A, CM radical formation rate was lower than with antimycin A. Since antimycin A provokes ROS formation at the outer site of the IMM, produced superoxide might be less prone to elimination by matrix antioxidants like SOD. As can be seen in b, HO-CoQ10 decreased respiration but did not increase CM[•] production rate, when CM[•] formation rate at the end of the respective measurement was subtracted. Raw data of samples containing HO-CoQ10 and CoQ10 (displayed in c) show higher CM[•] formation. This was caused by mitochondria-independent oxidation of CMH as can be seen in buffer control measurements in d. Production of CM radical was dependent on HO-CoQ10 concentration (data not shown). Both HO-CoQ10- and CoQ10-accelerated CM[•] production was not reduced by chelation of iron and copper with DF and DETC (25 µM and 5 µM, respectively; data not shown). When 50 U/mL superoxide dismutase was added, CM[•] formation was not abolished, but both production rates were decreased to the same level (data not shown). This implies that superoxide formation in presence of CoQs is one factor of increased CM[•] production which is more pronounced for HO-CoQ10 than for CoQ10 (Figure 62 d). Additionally, higher CM[•] formation rate in presence of oxygen (d) than under anoxic conditions (b, end of measurement) indicates an oxygen-dependent reaction.

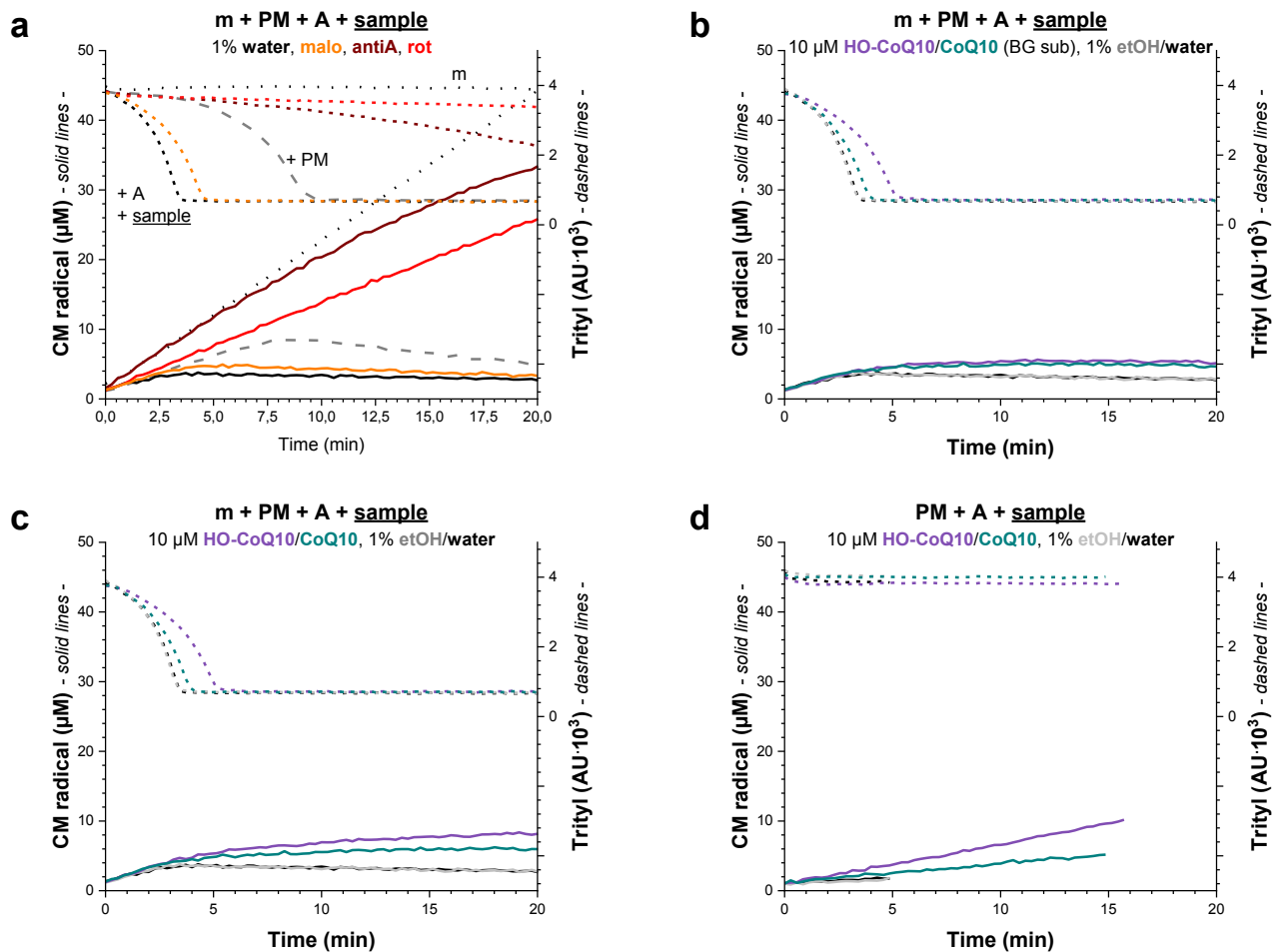


Figure 62 | Inhibition of respiration and production of CM* induced by RCC inhibitors and CoQ. 25 µg/50 µL (0.5 mg/mL) mouse heart mitochondria (m, black dotted lines) were incubated with 5 mM pyruvate/malate (PM, grey dashed lines), and a mixture of 1 mM ADP (A) and inhibitor or CoQ/solvent was added. CM* formation (solid lines) and trityl signal intensity (dashed lines) is plotted. (a) ADP was applied together with RCC inhibitors rotenone (rot, 0.5 µM), malonate (malo, 5 mM) or antimycin A (antiA, 10 µM). (b, c) ADP was applied together with 10 µM CoQ (HO-CoQ10/CoQ10) or vehicle controls (1% ethanol/water final concentration). In panel b, terminal slopes of CM* production in absence of oxygen (fitted within the interval 3 min after oxygen depletion to end of measurement) was subtracted from traces of samples treated with CoQ in panel c; (d) control measurements of applied substances with CoQ and solvents; Sample: freshly isolated, coupled mouse heart mitochondria; buffer: RB1 + 4 µM trityl, 0.3 mM CMH; T: 37 °C;

Unfortunately, oxygen measurements were not consistent as can be seen from measurements of mitochondria treated with vehicle controls (Figure 63) known not to interfere with respiration from oximetric measurement using the Clark-type electrode. Though CM radical formation rate was always comparable, oxygen consumption differed drastically under identical conditions. This might have been caused by inhomogeneous distribution of mitochondria within the capillary resulting in inhomogeneous oxygen consumption in the vial. In comparison to the sample chamber of Clark-type electrodes (see Figure 25 on p. 77) in which samples are constantly stirred, this is not possible in the EPR spectrometer.

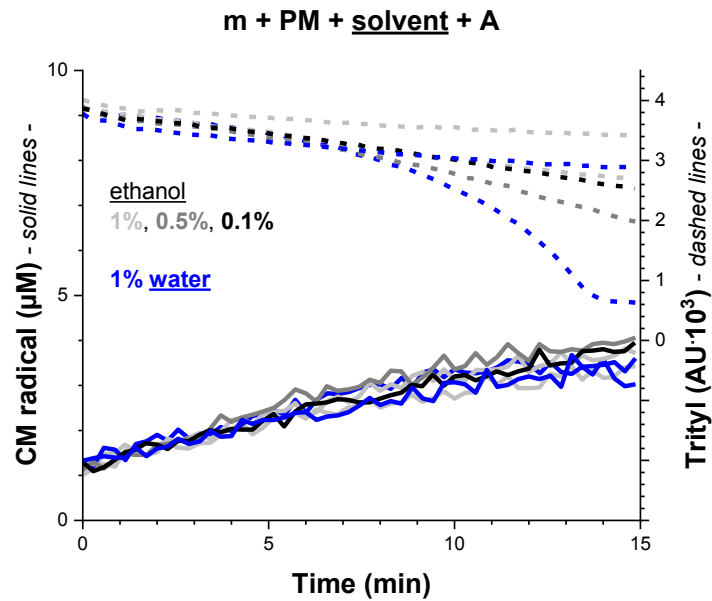


Figure 63 | High variability of oxygen consumption measurements. 10 $\mu\text{g}/50 \mu\text{L}$ (200 $\mu\text{g}/\text{mL}$) mouse heart mitochondria (m) were incubated with 5 mM pyruvate/malate (PM) and a mixture of 1 mM ADP (A) and vehicle control (1% water or 0.1-1% ethanol, final concentrations) was added. CM^{\bullet} formation (solid lines) and trityl signal intensity (dashed lines) is plotted; Sample: freshly isolated, coupled mouse heart mitochondria; buffer: RB1 + 4 μM trityl, 0.3 mM CMH; T: 37 $^{\circ}\text{C}$;

As superoxide production was not enhanced by the addition of HO-CoQ10 in coupled mouse heart mitochondria, the main ROS production site should be on the matrix side of the IMM or in the matrix itself. Similar to rotenone, known to induce superoxide production at the matrix side, initial CM^{\bullet} radical formation was not affected.

Since ROS production is dependent on oxygen concentration²³⁹ and inhibition of oxygen consumption on HO-CoQ10, the influence of oxygen supply of mitochondria might mask direct effects on superoxide production. Therefore, gas-permeable PT capillaries (cf. Figure 59 d) should be used for future measurements to establish stable oxygen conditions.

3.9 Low-temperature electron spin resonance spectroscopy (EPR) of respiratory chain complexes I and II

Since HO-CoQ10 inhibited Complex I and Complex II, and simultaneously stimulated ROS production feeding electrons into these complexes, electron distribution in energized and blocked states of the RCCs was examined.

Within the electron transport chain e^- are channelled via flavine molecules, iron-sulphur clusters, hemes, and copper centres as depicted in **Figure 64**. Iron-sulphur clusters of Complex I consist of $[2\text{Fe-2S}]^{2+}$ and $[4\text{Fe-4S}]^{4+}$ that are diamagnetic in their oxidized state. The ground spin state of these clusters can be described via the interaction of their spin centres as $S = 0^{\text{m}}$ with 2 antiferromagnetically coupled ferric irons (Fe^{III}) and 2 antiferromagnetically coupled ferric iron pairs that are ferromagnetically coupled, respectively. Taking up an e^- , one iron atom will be oxidized to Fe^{II} resulting in a total electron spin of $S = \frac{1}{2}$.^{oo} Consequently, $[2\text{Fe-2S}]$ as well as $[4\text{Fe-4S}]$ clusters, present in respiratory chain complexes I, II, and III, are paramagnetic and thus EPR detectable in their reduced state only. Due to the fact that the S3 cluster from complex II contains an odd number of iron atoms ($[3\text{Fe-4S}]^{+1}$), its total electron spin equals $1/2$. When S3 is reduced, the total spin state has an integer value with $S = 2$ and thus is not EPR detectable.

The spectral line width decreases with increasing spin relaxation time (proportional to $1/(T_1 \text{ or } T_2)$). When relaxation times are very short, spectra are too broad for detection. Since this is the case for Fe-S clusters, measurements need to be performed at low temperatures slowing down relaxation considerably. Relaxation time and therefore optimal sample temperature increases from $[4\text{Fe-4S}]$ via $[3\text{Fe-2S}]$ to $[2\text{Fe-2S}]$.

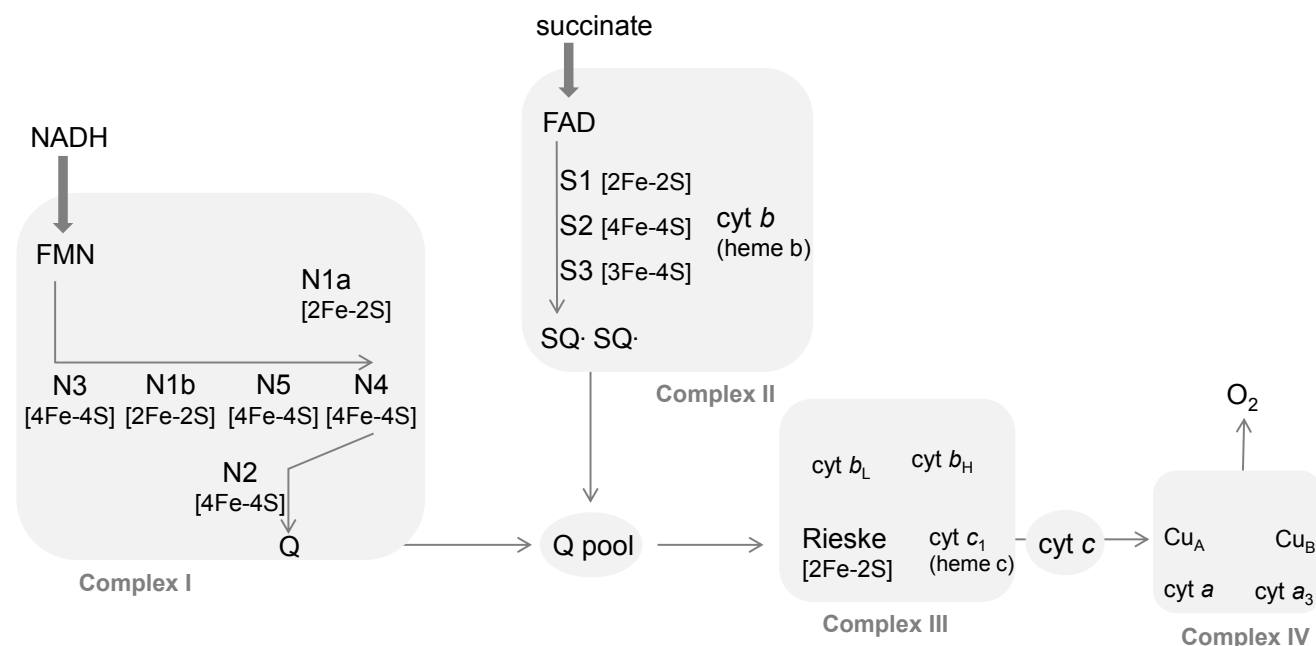


Figure 64 | Electron transport along the electron transport chain. Bold arrow, $2 e^-$ transfer; thin arrow, $1 e^-$ transfer; redox centres are aligned by their redox potentials; for CI only EPR-detectable clusters are listed; cluster N1a is not visible in bovine heart mitochondria; scheme according to Svistunenko (2006) Fig. 4²⁴⁸

^m Fe^{III} has an electron configuration of $\text{Ar } 3d^5$ with 5 single electrons per d orbital. Therefore, $S = 5/2 - 5/2 = 0$ for $[2\text{Fe-2S}]^{2+}$ or $S = 2 \cdot 5/2 - 2 \cdot 5/2$ for $[4\text{Fe-4S}]^{4+}$ clusters.

^{oo} Fe^{II} has an electron configuration of $\text{Ar } 3d^6$ with one fully occupied d orbital and 4 single electrons. Therefore, $S = 5/2 - 4/2 = 1/2$ for $[2\text{Fe-2S}]^{3+}$ or $S = 2 \cdot 5/2 - 5/2 - 4/2 = 1/2$ for $[4\text{Fe-4S}]^{5+}$ clusters.

To analyse and establish the detection of Fe-S clusters in Complex I and II, high input of sample was necessary. Due to that fact and that RCC activities were tested in bovine heart mitochondria, this was the sample of choice. The following table lists Fe-S cluster signals of RCCs I-III and SQ[•] detected within this thesis (**bold**) compared to literature values.

Table 15 | g-factors of measured EPR signals and literature values. Clusters are specified in their EPR-detectable state. g-values determined experimentally in this work (**bold**) are compared to literature values from indicated references. g-tensor components are given as g_{\max} , g_{int} and g_{\min} .

	Redox centres	Fe-S cluster	g_{\max}	g_{int}	g_{\min}	Symmetry g-tensor	Temp (K)	Ref.
Complex I	N1b	[2Fe-2S] ¹⁺	2.02 2.02	1.93 1.94	1.90 1.93-1.92	rhombic	40 40	248-250
	N2	[4Fe-4S] ³⁺	2.04-2.05 2.06-2.05	1.91-1.92 1.93-1.92	1.91-1.92 1.92	axial, (rhombic) ²⁵⁰	16 12	248-250
	N3	[4Fe-4S] ³⁺	2.03-2.04 2.04	1.93 1.93	1.86 1.87-1.86	rhombic	9 9	248-250
	N4	[4Fe-4S] ³⁺	2.1 2.11-2.10	1.93 1.94-1.93	1.88 1.89-1.88	rhombic	7	248-250
	N5	[4Fe-4S] ³⁺	2.07-2.06	1.93	1.90	rhombic	n. d.	248,249
Complex II	S1	[2Fe-2S] ¹⁺	2.02 2.03	1.93 1.94-1.93	1.915 1.92-1.91	rhombic	40 33.2	248,249
	S2	[4Fe-4S] ³⁺	2.02 2.03	1.94-1.93	1.92-1.91	rhombic	9.5	249
	S3	[3Fe-4S] ox	2.017 2.015	2.000 2.00	1.97 1.98	rhombic	9	248
CIII	Rieske	[2Fe-2S] ¹⁺	2.01 ?	1.91	1.78	rhombic		248
	SQ[•]	-	2.005 1.99-2.00	-	-	isotropic		249

3.9.1 Reduction of Fe-S clusters from Complex I and influence of rotenone and CoQ

Complex I was analysed in lysed bovine heart mitochondria by reducing its Fe-S clusters with NADH in phosphate buffer. Varying the sample temperature between 5 and 40 K and comparing to spectra of isolated CI of the strictly aerobic yeast *Yarrowia lipolytica*²⁵¹ and bovine heart,²⁴⁹ signals could be assigned to the iron-sulphur centres shown in Figure 65 a and are compared to literature values in Table 15. Clusters N1 to N4 are named with increasing numbers according to their increasing spin relaxation rates and therefore decreasing optimal detection temperature. Overlays in Figure 65 b-e allow direct comparison of signal patterns of BHM in buffer (**black traces**) to their NADH-energized state (**cyan traces**) and to blocking NADH-derived electrons at their transition to CoQ by rotenone (**red traces**). All identified signals are assigned in Figure 65 f-h.

At 40 K, the g_{\max} component of cluster N1b at $g = 2.02$ was identified comparing untreated BHM to NADH-reduced samples (b, **40 K** in f and g). The axial spectrum of cluster N2 was most prominent at 16 K (c, **16 K** in f

and g). At 9 K, g_{\max} of N3 was barely visible and g_{int} of N1b, N3 and N4 were superposing (d, 9 K in f and g). Nevertheless, g_{\min} of cluster N3 and N4 as well as g_{\max} of N4 could be clearly assigned. Cluster N5 was not detectable.

At 16 K a sharp isotropic signal with $g = 1.99\text{-}2.00$ was observed (c) that might be attributed to a semiquinone radical since it was still visible at 40 K (b). This isotropic signal was more prominent when antimycin A, known for locking the CoQ10 semiquinone radical at the Q_o site of CIII, was present (cf. g : 40 K, grey line (BHM + antiA + NADH) and f, g, h: 40 K). Ohnishi et al. (1998)²⁴⁹ described a SQ^\bullet observed in tightly coupled bovine heart submitochondrial particles (SMPs) activated with NADH at $g = 2.00$, also observed by several other groups.²⁵² Semiquinone radicals are formed during NADH oxidation because Fe-S clusters can transport only one electron at a time. So, CoQ10 will be reduced in two steps. Rotenone binding to the Q-binding site of Complex I should abolish the radical. This behaviour could not be observed within this work as the SQ^\bullet signal intensity was equal in NADH-energized mitochondria in presence and absence of rotenone (b, cf. red and cyan line) and was already present before NADH supply (black line). Comparing CCCP-uncoupled and tightly coupled bovine heart SMPs, Vinogradov et al. (1995)²⁵³ observed a SQ radical ($g = 2.00$) only in the latter. Since in this work, BHM were lysed by several freeze-thaw cycles, it was not surprising to find the absorption pattern of uncoupled SMPs more resembling. Additionally, studies showed splitting of N2 absorption when SQ^\bullet was present²⁵³ which could not be observed, further indicating that the observed organic radical was not located at CI. To analyse the behaviour of the CI-derived SQ radical, measurements should be performed at 40 K^{253,254} with tightly coupled mitochondria. Number of scans and sample concentration needs to be increased to account for absorption intensity loss at higher temperatures. Q_i and Q_o site inhibitors antimycin A and myxothiazol, respectively, can be used to eliminate CIII-derived SQ^\bullet and carboxin to abolish CII-derived SQ^\bullet .²⁵⁵ Isolated CI might be more appropriate to examine CI-derived SQ radicals because no inhibitors of other complexes, possibly interfering with CoQs, are necessary.

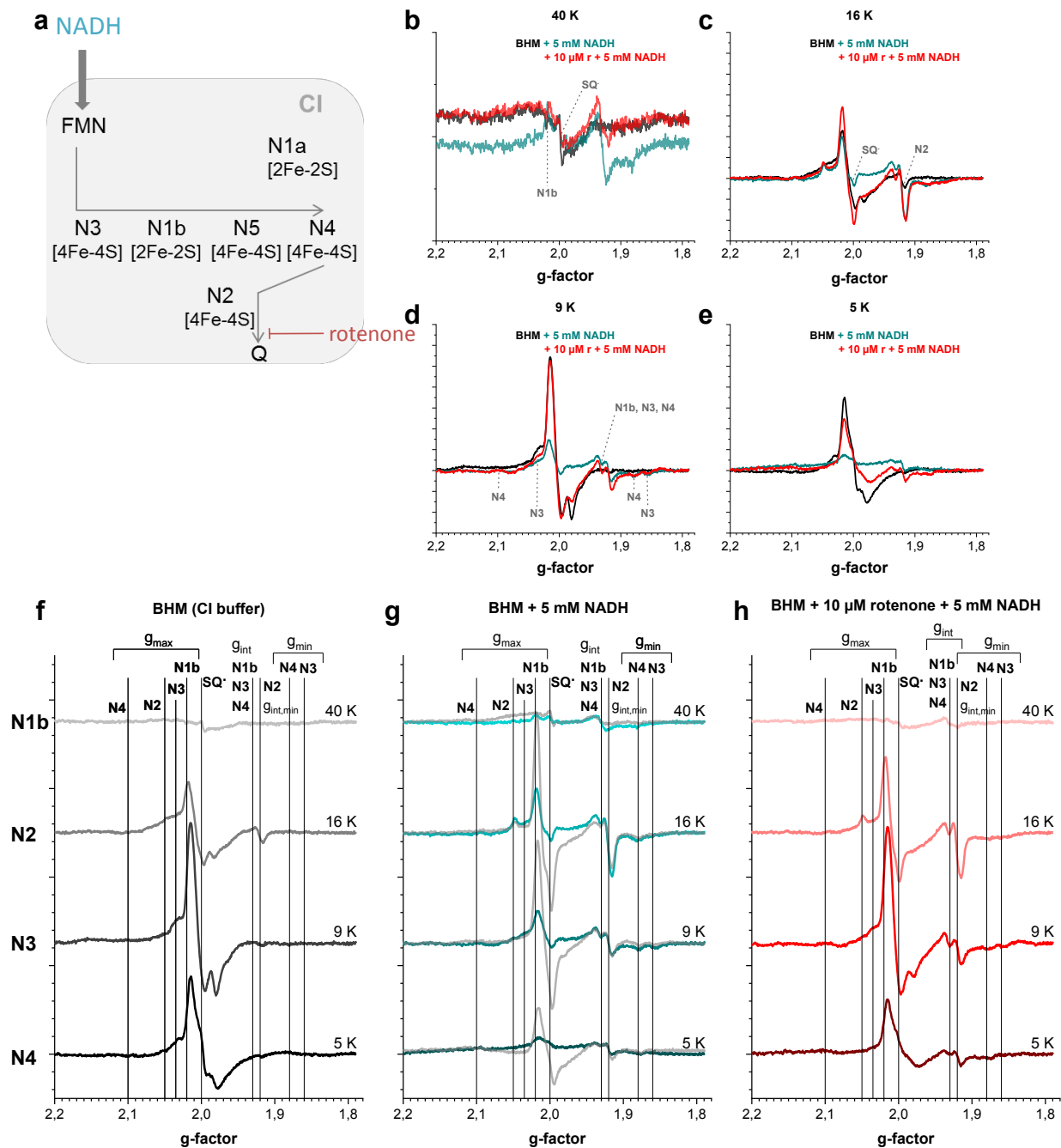


Figure 65 | Temperature-dependence of CI-associated EPR signals. (a) Electron flow from NADH to CoQ in CI and inhibition by rotenone at Q-binding site; overlays of BHM treated with NADH or rotenone and NADH at (b) 40 K, (c) 16 K, (d) 9 K and (e) 5 K; temperature variation of (f) BHM (g) energized with NADH and (h) pretreated with rotenone (same spectra as shown in panels b-e); (f) most prominent Fe-S cluster of CI is mentioned for each temperature on the left to the diagram, (g) grey lines: CI buffer contained 10 μM antimycin A, compare **Figure 66 a**;

Sample: 1.5 mg BHM subjected to 3 freeze-thaw cycles; buffer: 50 mM KP_B (pH 7.4), 0.1% BSA; temperature: 9-40 K as indicated; procedure: Samples were rethawed to add the indicated substances subsequently and refrozen before each measurement. Temperature dependence was performed on one sample without interrupting thawing steps.

As drafted in **Figure 66 a**, in a next step, CI-associated signals were examined while passing-on of electrons from CI via CIII was intervened by preincubation of BHM with the CIII inhibitor antimycin A. Complex I was then reduced by NADH addition. Eventually, electron transfer from the terminal Fe-S cluster N2 to CoQ was blocked using rotenone prior to or after reduction.

Figure 66 e displays subsequent addition of increasing NADH concentrations to BHM. Complex I-related signals of the clusters N3, N1b, N4, and N2 increased with NADH concentration. The g_{\max} component of N3 decreased. The N3 g_{int} component increased but was superposed and not separable from N1b and N4. An absorption signal with its dip at a g-factor of 1.985 dropped drastically (marked with *), but its origin could not be identified yet. Though absorption changes were completed with 1 mM NADH and therefore CI was fully reduced, 5 mM NADH was chosen for all experiments to provide sufficient substrate for multiple thaw-freeze-cycles.

Upon reduction of CI with 5 mM NADH, the influence of rotenone blocking electron transfer from N2 to CoQ on CI signals was observed in Figure 66 f. After elimination of g_{\max} of cluster N3 and the non-identified minimal turning point signal with $g = 1.985$ (marked with *) in presence of NADH, these signals reappeared upon rotenone supply. With increasing rotenone concentration the g_{int} signals of clusters N1b, N4, and N2 decreased slightly, indicating a changed electron occupation of CI Fe-S clusters. 10 μM rotenone was selected for CI inhibition in following experiments since 50 μM changed spectral shape inconsistently, maybe due to secondary solvent effects by increasing the DMSO content to 5%.

In Figure 66 g, the addition sequence was reversed. First, 10 μM rotenone was added thereby fully blocking further transport of electrons according to the observation in (f). Addition of rotenone had little effect on BHM signal pattern only slightly decreasing the signal at $g = 1.985$ (g, red spectrum, marked with *). As observed in absence of CI blockers (e), NADH addition to rotenone-blocked BHM again decreased this signal and N3 though to a lower extent (g). In contrast, the maximum at $g = 2.02$ was increasing.

Figure 66 b compares different states of BHM from f demonstrating that feeding electrons into CI (cyan spectrum) leads to increased electron occupation of clusters N1b, N4, N2 and decreased occupation of the first Fe-S cluster N3 receiving electron directly from FMN (cf. Figure 6 b on p. 17). Then again, blocking electrons at the Q-binding site (red spectrum) increased probability of electron allocation at N3. The signal at $g = 1.985$ (marked with *) was most pronounced when BHM were untreated or NADH-energized and electron conduction was blocked. Therefore, the signal at $g = 1.985$ might be associated to the g_{\min} component of cluster S3 from CII, which is only detectable in its oxidized state and was most intense at 9 K (cf. Table 15 on p. 124 and Figure 65 h on p. 126). When electron transfer from ubiquinol to CIII was inhibited by antimycin A, reverse electron transfer to CII might have occurred.

When first rotenone was added to BHM (Figure 66 c, red spectrum), addition of NADH (cyan spectrum) only slightly reduced peak intensity at $g=2.03$ (N3) but did not abolish the signal as observed in absence of rotenone (b, cyan spectrum) suggesting that electrons cannot be efficiently transported past cluster N3. Figure 66 d compares antimycin A-preincubated mitochondria (black spectrum) with treatment of NADH and rotenone in different orders taken from diagrams b (red spectrum) and c (cyan spectrum). When NADH was added on top of rotenone (cyan spectrum), signal intensities at $g = 2.02$ and $g = 2.00$ were slightly higher than with inversed addition sequence (red spectrum). $g = 2.02$ may be associated to the g_{\max} component of cluster S2 from Complex II as electrons might be transmitted via RET from reduced CoQ to CII and intensity was highest at 9 K (cf. Table 15 on p. 124 and Figure 65 h on p. 126). To avoid superposition of the absorption signals

by antimycin A-induced SQ radicals at the Q_o site of CIII (Figure 65 g, 40 K, grey lines), all following experiments were performed omitting antimycin A from the assay buffer.

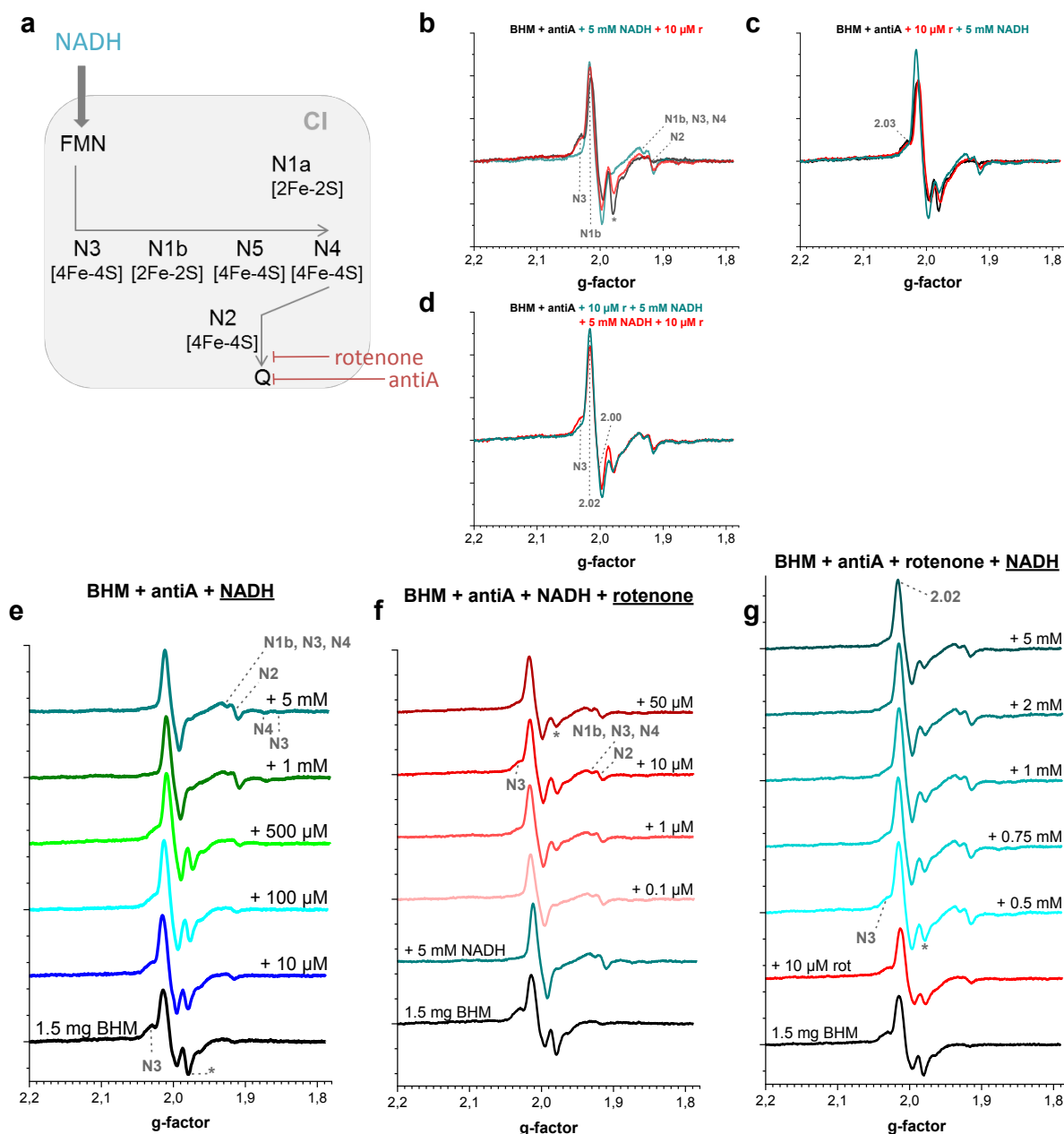


Figure 66 | Reduction of CI with increasing NADH and blocking e^- transfer at CI and CIII. (a) Redox centres of CI; electron transfer was blocked at Q_o site of CIII with 10 μ M antimycin A (antiA) in every measurement and with rotenone (r) at the transition from Fe-S cluster N2 to CoQ when indicated. Overlay of BHM treated with (b) NADH and then rotenone or (c) rotenone and then NADH. (d) Overlay comprises measurements from panels b and c. BHM were energized with (e) increasing concentrations of the CI substrate NADH and then (f) inhibited with increasing concentrations of rotenone (and its solvent DMSO) or with (g) 10 μ M rotenone and increasing [NADH]. In panels e, f, and g concentration of underlined substance was changed and final concentrations are indicated; non-identified changing signal marked with *;

Sample: 1.5 mg BHM subjected to 3 freeze-thaw cycles; buffer: 50 mM KPB (pH 7.4), 0.1% BSA, 10 μ M antiA; temperature: 9 K; procedure: see Figure 65; subsequent measurements from bottom to top per diagram;

Having analysed the signal patterns of NADH-reduced mitochondria blocked at different sites (CI and CIII) and determined the best concentration of rotenone and NADH, CoQs were added to NADH-energized mitochondria

to examine their influence on Fe-S clusters of Complex I (Figure 67 and Figure 68). As can be seen from Figure 67 a, rotenone severely affected the signal pattern of NADH-energized mitochondria as has also been observed for inversed addition sequence described in Figure 65 d (p. 126). In contrast to the CI inhibitor rotenone, HO-CoQ10 (b), which was shown to inhibit Complex I in precedent photometric experiments, did not drastically influence absorption patterns. Upon adding CoQ to NADH-energized mitochondria in addition to N4 and N3, a new signal at $g_{\min} = 1.89$ was detectable in b. Since treatment with CoQ1 (c) and the solvent control (d) also showed this additional dip, it might be attributed to N5 that should be visible better at 5 K.

HO-CoQ10 did not change the electron distribution pattern of NADH-energized mitochondria indicating that the inhibitory mechanism by HO-CoQ10 is different from rotenone. Additionally, electron flow from NADH to CoQ did not seem to be inhibited in the same way or extent as with rotenone.

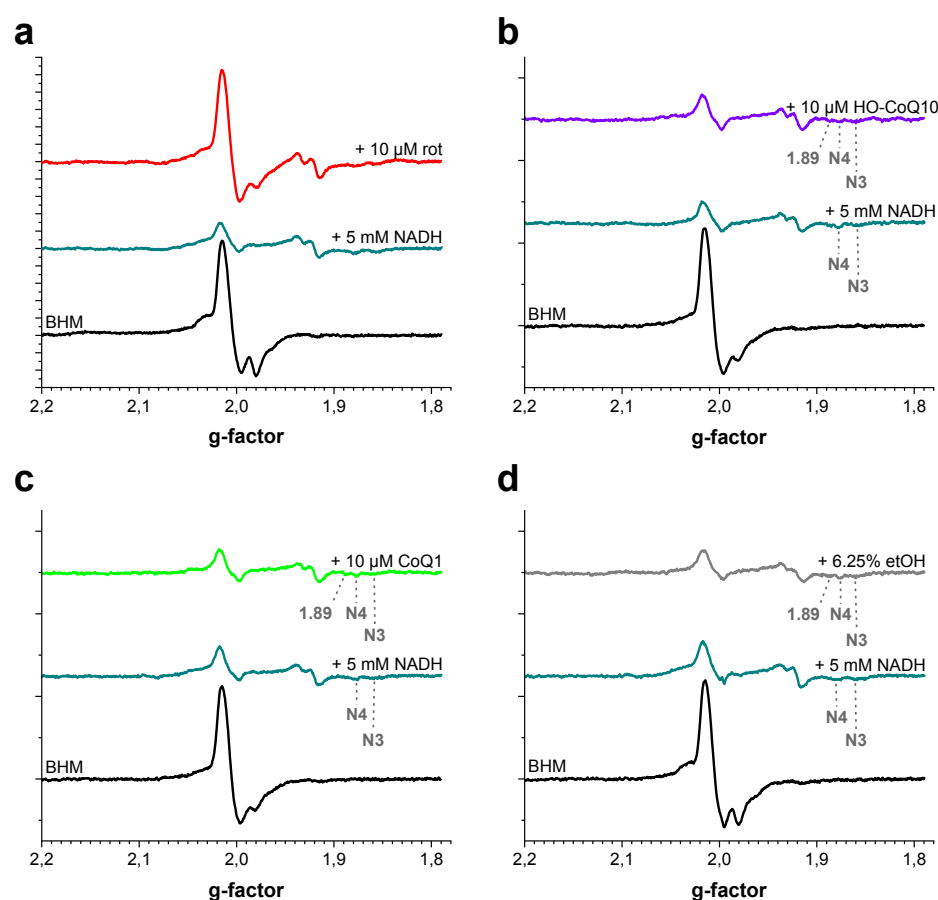


Figure 67 | Influence of HO-CoQ10 on CI-related EPR signals. BHM were energized with 5 mM NADH and treated with (a) 10 μ M rotenone, (b) 10 μ M HO-CoQ10, (c) 10 μ M CoQ1 or (d) 6.25% ethanol as vehicle control for CoQs.

Sample: 1.5 mg BHM subjected to 3 freeze-thaw cycles; buffer: 50 mM KPB (pH 7.4), 0.1% BSA; temperature: 9 K; procedure: see Figure 65; subsequent measurements from bottom to top per diagram;

For the experiments shown in Figure 68 effects of CIII blocker antimycin A on rotenone and HO-CoQ10-treated mitochondria and their order of application were examined. When HO-CoQ10 was added to NADH-activated mitochondria N4 intensity decreased slightly (a) but no additional signal at $g_{\min} = 1.89$ as observed in Figure 67 c was detected. In both experiments especially the small signals in the $g \approx 1.88$ region (g_{\min} of N3, N4 N5), however, have to be considered with precaution since signal-to-noise ratio was quite low making it mandatory to evaluate more scans per sample in future experiments.

When antimycin A was added to NADH-activated mitochondria, absorption patterns were not affected (Figure 68 a, d). Then again, when antimycin A was added on top of HO-CoQ10-treated mitochondria, N4-correlated intensity was abolished and absorption at $g_{\max} = 2.02$ and $g_{\text{int}} = 2.005$, that might be correlated to N1b and SQ• or oxidized cluster S3 of Complex II, increased as visible in b and the overlay in c. These considerable changes imply that HO-CoQ10 affected electron allocation of CI, CII and/or CIII which was only visible when further e⁻ transport was blocked. Of course, solvent controls and non-hydroxy CoQ variants need to be tested extensively.

Signal pattern of NADH-energized BHM was not affected by subsequent addition of antimycin A (Figure 68 d middle trace). Surprisingly, when mitochondria were preincubated with antimycin A and then energized with NADH differences in absorption pattern in the region between $g = 2.02$ and 2.00 were obvious (Figure 65 g compare NADH-energized BHM (cyan) to preincubation with antimycin A (grey)). Signal intensities at $g = 2.02$ and 2.00 corresponding to either N1b and SQ•, respectively, oxidized S3 or their superposition were much higher, when BHM were preincubated with antimycin A (Figure 65 g).

NADH-energized mitochondria that were treated with antimycin A and rotenone subsequently (d) showed identical signal patterns also when addition sequence of inhibitors was reversed (e).

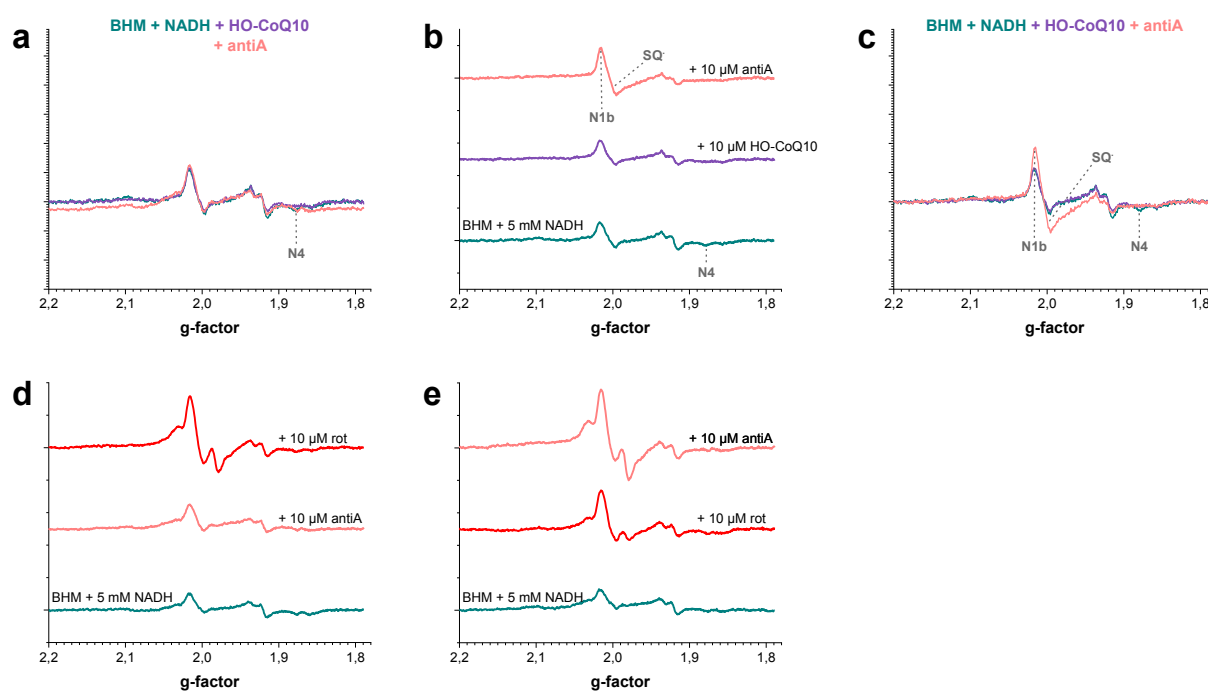


Figure 68 | Preincubation with HO-CoQ10 changed CI-related signal upon antimycin A addition. BHM were reduced with 5 mM NADH and treated with 10 μM sample (HO-CoQ10 or rotenone). 10 μM antimycin A was added to NADH-energized mitochondria or after sample addition. (a) Overlay of NADH-energized BHM treated with HO-CoQ10 or antimycin A (from single spectra of panels b and d), (b) subsequent addition of HO-CoQ10 and antimycin A to NADH-energized mitochondria; (c) overlay of single spectra from panel b; NADH-energized BHM were (d) first treated with antimycin A, then rotenone or (e) first treated with rotenone, then antimycin A; Sample: 1.5 mg BHM subjected to 3 freeze-thaw cycles; buffer: (a, b) 50 mM KPb (pH 7.4); (c, d) 50 mM KPb (pH 7.4), 0.1% BSA; temperature: 9 K; procedure: see Figure 65; subsequent measurements from bottom to top per diagram;

3.9.2 Identification of Fe-S clusters from Complex II and influence of atpenin A5

To measure CII-derived signals, first rotenone was added to block CI and thus the formation of oxaloacetate that would inhibit CII as stated before (Figure 69 a, b). Then, succinate was supplied in increasing concentrations. Cluster S3 was correlated to $g = 2.015$, 2.00 and 1.98 decreasing with addition of succinate since the [3Fe-4S] cluster is only EPR detectable in its oxidized state (b) and the signal can be measured best at 9 K (c and Table 15 on p. 124). g_{\max} and g_{int} of cluster S1 were visible starting from a concentration of 10 mM succinate since it was otherwise overlaid by S3. Cluster S2 should be visible at 9 K²⁴⁹ but was not assigned because it is not succinate-reducible.²⁵⁶

When mitochondria were exposed to succinate without preincubation with rotenone, S3 signals were reduced and a sharp signal at $g = 1.997$ appeared (d, e). To confirm its putative source from an organic radical (SQ \cdot) measurements at higher temperature are necessary. Upon turnover of succinate to oxaloacetate, CII will be inhibited. Since succinate is metabolized to fumarate and malate subsequently, formation of NADH by malate dehydrogenase might lead to partial CI reduction and formation of SQ \cdot at the Q-binding site of CI. Rotenone addition indeed abolished $g = 1.997$ suggesting the source of the putative organic radical (d, SQ \cdot) to the Q-binding site of CI. Further reduction of S3 and S1 in presence of rotenone (d, e) suggests that CI inhibition is important to fully reduce CII.

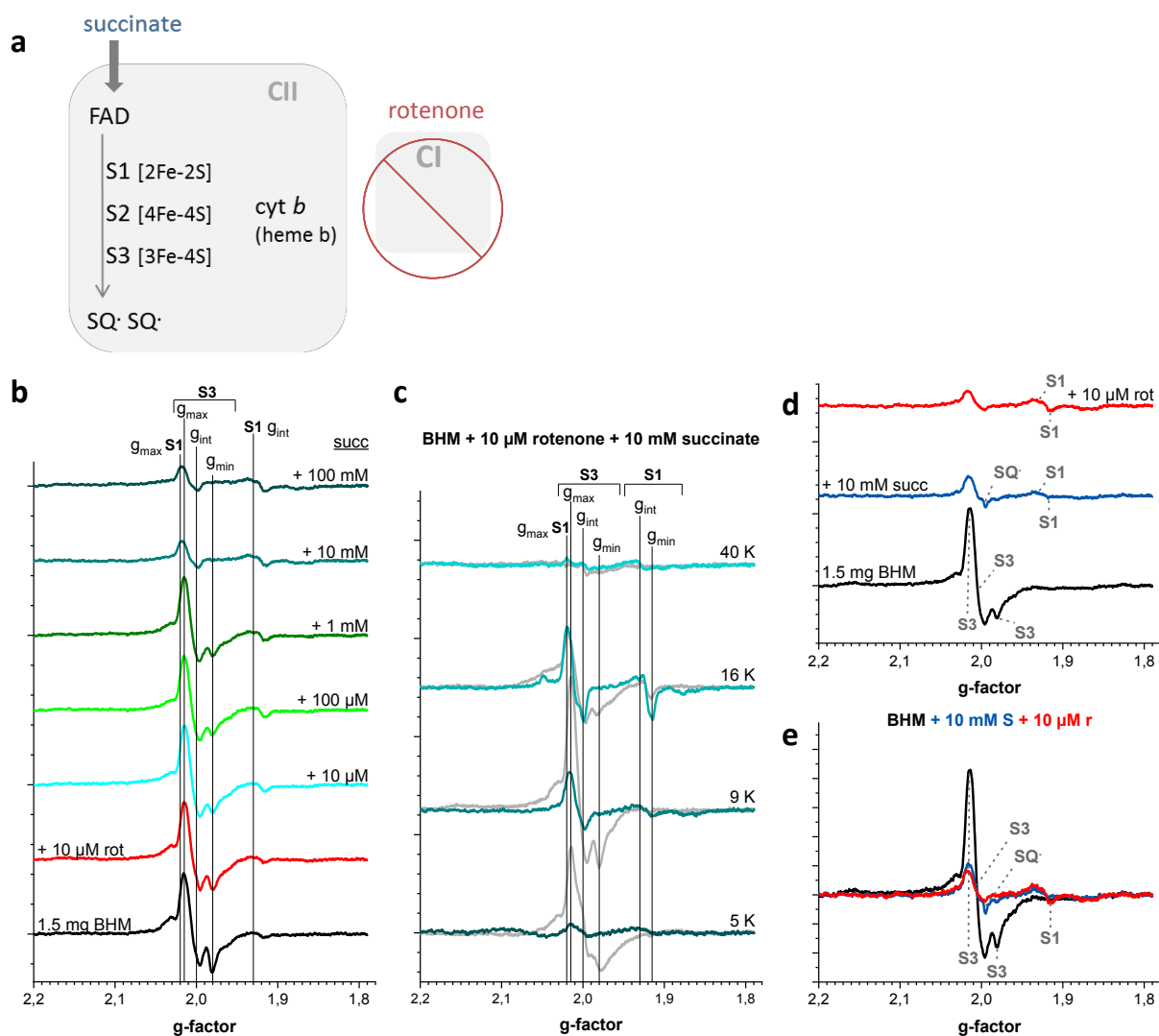


Figure 69 | Identification of CII-related Fe-S clusters in succinate-energized mitochondria. (a) Redox centres of CII, CI was blocked with rotenone; (b) BHM treated with rotenone and increasing concentrations of succinate (final concentration is indicated), (c) temperature-dependence of CII signals comparing BHM (grey lines) to BHM with rotenone and 10 mM succinate (cyan lines), (d) BHM energized with succinate, then treated with rotenone, (e) overlay of single spectra from panel d; Sample: 1.5 mg BHM subjected to 3 freeze-thaw cycles; buffer: 50 mM KPB (pH 7.4); temperature: (a, c, d) 9 K, (b) as indicated; procedure: see **Figure 65**; subsequent measurements from bottom to top per diagram; concentration of underlined substance was changed and final concentrations are indicated;

The impact of Q-binding site blocker atpenin A5 (AA5) on the CII absorption pattern was less prominent than the impact of rotenone on CI signals (cf. **Figure 70 b** and **Figure 67 a**). Adding AA5 decreased the g_{\max} absorption of S3 (**Figure 70 b**), indicating further reduction of cluster S3 of CII because electron transfer to CoQ and CIII was stopped (overlay from **b** in **c**). Preincubating rotenone-treated mitochondria with AA5 before addition of succinate further reduced the S3-associated signal (**d** and orange in **e**) in comparison to atpenin addition following succinate (**e**, brown) as can be seen from the overlay in **e**. Since a decrease of S3 signal is associated to its reduced state, this observation indicates that the final Fe-S cluster S3 has a higher electron occupancy when transfer to CoQ is efficiently blocked with AA5.

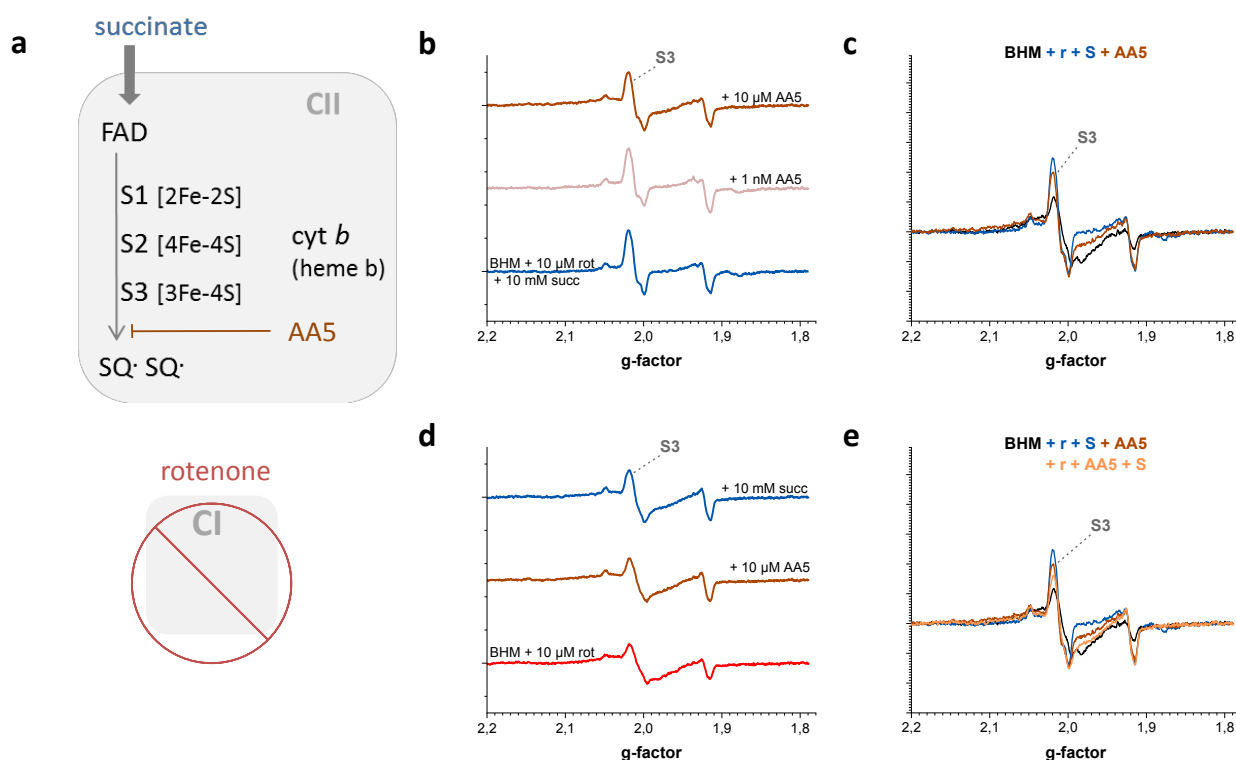


Figure 70 | Atpenin A5 and especially its preincubation reduced Fe-S cluster S3 of CII. (a) Redox centres of CII, mitochondria were preincubated with rotenone to block CI, electron transfer to CoQ was blocked with atpenin A5 (AA5) when indicated; (b) succinate-energized mitochondria were treated with increasing concentrations of AA5, (c) overlay of spectra from panel b, (d) mitochondria were pretreated with AA5 before energizing with succinate, (e) overlay of single spectra from panels b and d: mitochondria (BHM, black) supplied with rotenone and succinate (r + S, blue) and inhibited with 10 μM AA5 (+ AA5, brown) vs. mitochondria preincubated with rotenone and AA5 and then supplied with succinate (r + AA5 + S, orange); Sample: 1.5 mg BHM subjected to 3 freeze-thaw cycles; buffer: 50 mM KPB (pH 7.4), temperature: 16 K; procedure: see **Figure 65**; subsequent measurements from bottom to top per diagram;

Since preincubating mitochondria with antimycin A and atpenin A5 before substrate supply intensified spectral changes, visible for example in **Figure 65 g** (p. 126) and **Figure 70 e**, respectively, the effect of CoQs

should be examined with a similar procedure. Furthermore, effect of HO-CoQ10 on NADH-energized mitochondria was only visible when electron transfer to CIII was blocked (Figure 68 a and c, p. 130). Hence, experiments combining different blockers with HO-CoQ10 should be performed to pinpoint the effect of HO-CoQ10 on electron occupation in the ETC.

4 Discussion

Production of a constitutional isomeric mixture of 2- and 3-HO-CoQ10 with high purity

Various studies have been performed examining a variety of CoQ derivatives.²⁵⁷⁻²⁶⁰ Surprisingly, the direct precursor of CoQ, demethyl-CoQ (carrying one hydroxy group instead of a methoxy group on 2- or 3-position of the quinone moiety, structure see **Figure 2 d, e** on p. 10) had never been in focus of a functional study, even though it was identified at least 42 years ago in the *E. coli* mutant *ubiG*⁻⁸⁷. Recently, our group and a cooperating group of electrochemists started examining hydroxy substitutes of CoQ focussing on physicochemical properties using in-depth characterized reaction mixtures.^{5,7}

HO-CoQ cannot be purchased but needed to be synthesized and purified for this study. The nucleophilic substitution of one methoxy group by hydroxide was definitely proven with 2-D NMR identifying the final, isolated product as an isomeric mixture of 2-HO-CoQ10 (2-[(2E,6E,10E,14E,18E,22E,26E,30E,34E)-3,7,11,15,19,23,27,31,35,39-decamethyltetraconta-2,6,10,14,18,22,26,30,34,38-decaenyl]-6-hydroxy-5-methoxy-3-methyl-1,4-benzoquinone) and 3-HO-CoQ10 (2-[(2E,6E,10E,14E,18E,22E,26E,30E,34E)-3,7,11,15,19,23,27,31,35,39-decamethyltetraconta-2,6,10,14,18,22,26,30,34,38-decaenyl]-5-hydroxy-6-methoxy-3-methyl-1,4-benzoquinone) in a ratio of 2:1. Within this thesis for the first time, HO-CoQ10 was produced in sufficient amounts and high purity of > 92% to perform functional studies. Of course, purity can and should be further increased by performing multiple additional runs of semi-preparative HPLC, reducing the amount of sample input per run, and optimizing separation effect of HO-CoQ10 from CoQ10 and other impurities. Completely eliminating CoQ10 from the reaction mixture alone would already result in a purity of 94%.

Bogeski et al. (2011)⁸ successfully synthesized mono- as well as disubstituted CoQ1 derivatives exchanging one or both methoxy groups of CoQ1. Though monosubstituted CoQ1 was more abundant with both their chemical and biosynthetic approach as shown by LC-MS/MS, dihydroxy-CoQ1 was found in substantial amounts.⁸ Pettersson (1964)¹²⁹ exemplified the directed conversion of fully substituted 2,3-dimethoxy-5,6-dimethyl-1,4-benzoquinone to its mono- or dihydroxy analogue by demethylation at 2- and/or 3-position in aqueous solution modulating the hydroxyl anion concentration and incubation time. Nevertheless, the yield of dihydroxy compounds might be limited by condensation reactions resulting in dimers^{6,261-263} and oxidative ring opening.^{262,264} Indeed, nucleophilic substitution of CoQ0 resulted only in formation of monohydroxy compounds and dimeric structures of dihydroxy dimers,²⁶³ and byproducts of HO-CoQ10 synthesis included CoQ10 derivatives with opened ring structures carrying two carboxylic acid groups.¹¹

The mixture of 2- and 3-HO-CoQ10 in the product might be problematic because it has been shown that the location of methoxy substitutes is important for functionality with the 3-methoxy being more sensitive: Substitution of the methoxy groups with H at 3-position of decyl-UQ resulted in complete loss of succinate:Q oxidoreductase activity, whereas substitution at the 2-position yielded 30% acceptor activity compared to decyl-UQ.²⁶⁰

Eventually, there are two main approaches to target a controlled synthesis of mono- and dihydroxy CoQ10. Apart from incubation time, changing hydroxide availability in the THF phase can be achieved by slightly decreasing the NaOH concentration of the aqueous phase because miscibility of NaOH and THF increases upon

decrease in ionic strength. However, sodium hydroxide concentration needs to be high enough for a two-phase system since the THF phase is necessary to keep the reactant dissolved. A sophisticated approach is biocatalysis which can be specifically engineered.²⁶⁵ For example, the CYP450 monooxygenase CYP1B1 used to produce Hydroxy Q1 by Bogeski et al. (2011) can be mutated to synthesize regiospecific monohydroxy and dihydroxy CoQ10. Finally, separation of constitutional isomers in principle should be possible via HPLC. In our hands isomers could not be purified. However, establishment of elution protocols was not focussed on this task. Nevertheless, it should be possible since separation was successful for 2- and 3-H-substitutes of decyl-ubiquinone.²⁶⁰

CoQ10 supplied to cells and mitochondria

As CoQ10 supplementation is challenging due to its low solubility in aqueous solutions, and solubility of CoQ10 is correlated to uptake by cells and intracellular distribution,¹³⁸ it was crucial to find a reliable dissolution method for biological experiments. Even though organic solvents like dimethyl sulfoxide, chloroform, methanol, and ethanol have been used to study primary cells and cell lines using final concentrations up to 200 μM CoQ10 (Table 10 on p. 64), within this thesis only ethanol was found to be an adequate solvent for dissolving CoQ10 in aqueous media (cf. section 3.2 on p. 63). CoQ10 and HO-CoQ10 could be dissolved in ethanol up to concentrations of 1 and 5 mM, respectively, resulting in a stable stock solution at room temperature. Nevertheless, stock solutions need to be handled and stored cautiously to avoid precipitation of CoQ and evaporation of the solvent.

Using a final concentration of 1% ethanol (170 mM ethanol) in buffer or medium did not adversely affect viability of cancer cell lines (Figure 23: 1% water, black; 1% etOH, grey; p.75) and did not induce apoptosis in Jurkat T cells over a period of 24 h (Figure 24, p. 76), even though other studies observed effects of lower concentrations.^{266,267}

Ethanol was shown to drastically interfere with ADP-stimulated and uncoupled succinate-linked respiration of guinea pig liver mitochondria reducing respiration to 26% and 43%, respectively, with only 0.3% ethanol.²⁶⁸ Other studies using rat liver mitochondria observed ethanol-induced inhibition of oxidative phosphorylation with an IC₅₀ of 4.7%, though up to 2% ethanol did not significantly inhibit ATP production.²⁶⁹ However, in view of experiments performed with isolated, coupled mouse heart mitochondria in this thesis showing no influence on respiration (e.g. Figure 28, p. 81) and ROS production (Figure 57, p. 116), 1% ethanol is compatible for experiments with isolated mitochondria.

Since utilizing ethanolic stock solutions limited the maximal concentration of CoQ10 and HO-CoQ10 in 1% ethanol to 10 and 50 μM , respectively, another dissolution method was introduced. Many studies apply ready-to-use water-soluble CoQ10 formulations^{188,190} that are not available for HO-CoQ10. The patented procedure from Borowy-Borowski et al. (2004)⁹⁶ to enclose CoQ10 in nanomicelles formed with the polyoxyethanyl-conjugate Cholesterol-PEG 600 was adopted for HO-CoQ10. Following this protocol, an aqueous solution of CoQ10 and HO-CoQ10 of a concentration as high as 10 mM was achieved (Figure 18, p. 66). Furthermore, handling of the water-based stock solution is easy and concentrations up to 230 mM CoQ10 are possible according to Borowy-Borowski (2004). Unfortunately, successful preparation of the stock solutions was inconsistent and the procedure needs refining. Additionally, in contrast to HO-CoQ10 dissolved in ethanol,

experiments applying HO-CoQ10-Cholesterol-PEG on isolated mouse heart mitochondria did not show any immediate inhibitory effect on ADP-stimulated respiration even though a 10-fold higher concentration (i.e. 100 μ M HO-CoQ10) could be used (Figure 32 b, p. 86). Borowy-Borowski demonstrated accumulation of CoQ10 in cells (6-fold compared to untreated control) and mitochondria (10-fold compared to untreated control), when cells were incubated with water-soluble CoQ10-PCS for three days.²⁷⁰ Furthermore, reduction of H₂O₂ formation by isolated mitochondria treated with water-soluble CoQ10 prepared according to the same procedure was observed^{190,271} indicating that in principle CoQ10 uptake by mitochondria was not the reason why no effect on mitochondrial respiration was observed in this thesis. Since antioxidant activity of CoQ10 is not limited to CoQ10 localized in the inner mitochondrial membrane, it is not clear if water-soluble CoQ10 integrates into the inner mitochondrial membrane and is released from PCS micelles without prolonged incubation. Hence, localisation to the inner mitochondrial membrane and availability for RCCs seems to be essential for the inhibitory effect of HO-CoQ10.

Other options to increase concentrations in water and/or in samples should be explored, e.g. liposomes using mixtures of phospholipids,²⁷² and electroporation to increase the probability of mitochondrial uptake. Another sophisticated approach to introduce CoQ into the inner mitochondrial membrane is the conjugation with triphenylphosphonium cation (TPP⁺).²⁷³ However, TPP⁺ cannot be attached to CoQ10. Therefore, Kelso et al. (2001) attached TPP⁺ to its analogue decyl-ubiquinone and called it mitoQ.²⁷⁴ Currently, our group (Katerina Stankoska) is working on the introduction of hydroxy groups to mitoQ which will enable us to work with a HO-CoQ analogue definitively located in the IMM.

HO-CoQ10 is a component of bovine heart mitochondria

HO-CoQ was detected in eukaryotes for the first time by LC-MS (section 3.3.3, p. 70). To distinguish existence of 2- and/or 3-HO-CoQ10, NMR analysis of the substance is necessary and can be performed either by isolation of the endogenously detected substance after chromatographic separation or directly via HPLC coupled to NMR detection. The mitochondrial concentration of HO-CoQ10 was estimated to be 100 μ M in phospholipids of crude bovine heart mitochondria. Assuming an average molecular weight for phospholipids of 800 g/mol,²⁷⁵ a content of 0.268 mg PL¹⁵⁹ and 10 nmol CoQ10 per mg mitochondrial protein, a molar ratio of 1:333:11 700 for HO-CoQ10:CoQ10:PL can be calculated. Considering the variability of detected HO-CoQ10 and CoQ10 in the present thesis, no definite concentrations could be determined. Thus, HO-CoQ10 content might have been underestimated.

Even though concentrations were determined in whole mitochondria and not in mitochondrial membranes, concentrations in mitochondrial membranes can be estimated. Calculating molar CoQ concentrations using CoQ contents in rat liver mitochondria (Table 1 on p. 14) and phospholipid contents in whole mitochondria, IMM, and OMM of pig heart mitochondria^{pp,276} or in whole mitochondria and IMM of beef heart mitochondria,^{qq,159} CoQ concentrations were similar in whole mitochondria and the IMM but halved in the

^{pp} PL content in pig heart mitochondria (mg/mg protein): mitochondria, 0.3; IMM, 0.48; OMM, 8.5²⁷⁶

^{qq} PL content in beef heart mitochondria (mg/mg protein): mitochondria, 0.268; IMM, 0.260 or 0.387¹⁵⁹

OMM. Nonetheless, distribution of HO-CoQ10 within mitochondrial membranes might be distinctive and a mechanism to rapidly modulate respiratory activity and ROS signalling.

Since CoQ10 is present in all organs and cellular membranes, HO-CoQ10 is most likely to be found ubiquitously as well. Nevertheless, this thesis was focussed on possible functions of HO-CoQ10 in mitochondria.

HO-CoQ10 and CoQ10 inhibit respiration

One main goal was to test the effect of the two substances, Coenzyme Q10 and HO-CoQ10 on the mitochondrial electron transport chain. The experiments were performed using isolated mouse and beef heart mitochondria and are summarized in **Figure 71**. These results showed clearly that HO-CoQ10 is reducing CI-, CII-, and CIII-linked respiration (**Figure 28**, p. 81) as well as NADH:CoQ1 oxidoreductase and succinate:CoQ1 oxidoreductase activities but not decyl-ubiquinol:cytochrome *c* oxidoreductase activity in photometric assays of the single respiratory chain complexes I, II, and III, respectively (CI, see **Figure 43 a**, p. 100; CII, see **Figure 46**, p. 103; CIII, see **Figure 48**, p. 105). Surprisingly, submicromolar CoQ10 drastically intervened with CI- and CII-linked respiration. However, this effect was only visible at low mitochondrial input reducing oxygen consumption rate to approximately 50% or less (**Figure 38 d**, p. 94 and **Figure 39 d**, p. 95), whereas respiration of quadrupled mitochondrial input was unaffected by 10 μ M CoQ10 (**Figure 28**, p. 81). In line with the observation of CoQ10 reducing respiration, Bergamini et al. (2012) reported decreased uncoupled respiration of whole cells pretreated with 10 μ M CoQ10 for 24 h.¹⁸⁹ This effect was only visible when CoQ10 was applied as an ethanolic solution but not when a water-soluble formulation was used.¹⁸⁹ The authors suggested that incorrect insertion into the IMM was responsible.¹⁸⁹

Being the endogenous electron acceptor of CI and CII, CoQ10 in contrast to HO-CoQ10 did not markedly affect NADH:CoQ1 and succinate:CoQ1 oxidoreductase activities (CI, see **Figure 43 a**, p. 100; CII, see **Figure 46**, p. 103). Furthermore, HO-CoQ10 but not CoQ10 regulated ROS production in coupled mouse heart mitochondria stimulating H₂O₂ formation linked to CI and CII substrates and downregulating H₂O₂ formation linked to G3P (**Figure 57**, p. 116). Therefore, it is conclusive that HO-CoQ10 exhibits two distinct mechanisms to influence ETC activity: 1. HO-CoQ10 directly inhibits RCC activity by interaction with their Q-binding sites, since oxidase activities of CI and CII were unaffected (cf. **section 3.7.6**, p. 109) and inhibition of CIII was only seen when low concentrations of artificial quinols were provided (**Figure 30 c**, p. 83). 2. Another, membrane-associated mechanism is inherent to both HO-CoQ10 and CoQ10 which was observed in mitochondria with intact membranes and did not appear, when the CoQ analogues with short side chains CoQ1 and decyl-UQ were applied (**Figure 32 c**, p. 86). Underlying mechanisms for the latter hypothesis will be discussed in detail in the following chapter and then, explanations for RCC-associated mechanism are proposed.

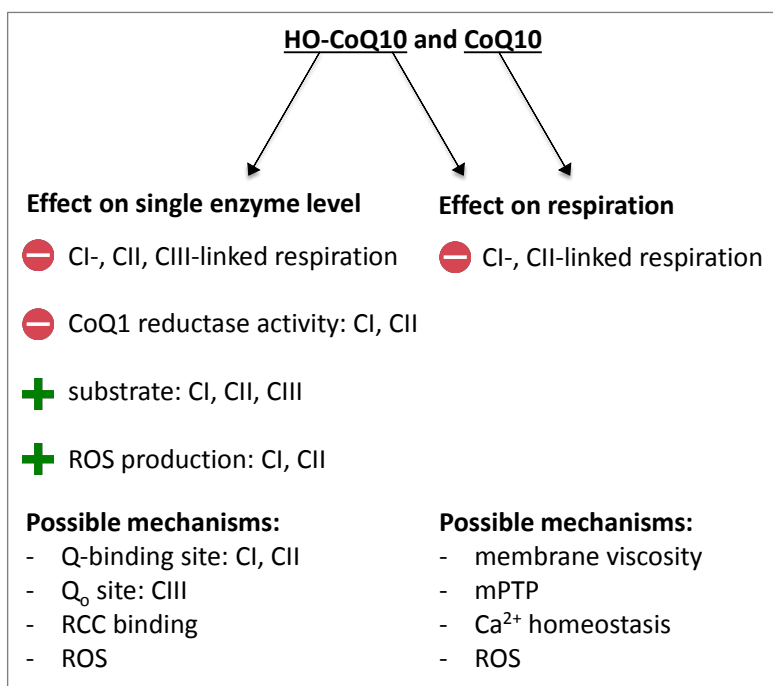


Figure 71| Observed effects of CoQ10 and its hydroxy derivative HO-CoQ10 on the mitochondrial electron transport chain. Respiration and ROS experiments were performed with freshly isolated coupled mitochondria isolated from mouse heart, RCC activities were analysed with uncoupled, lysed mitochondria isolated from bovine heart. ⊖ marks reduction and ⊕ increase by CoQ.

CoQ10 and HO-CoQ10 inhibit respiration by changing biophysical membrane properties

Coenzyme Q10 is known to influence biophysical membrane properties. Similar to cholesterol, but more effectively, CoQ10 increased the order of the hydrophobic region of lipid membranes.²⁷ Since the quinone moiety was essential to this effect, CoQ10 was assumed to intercalate between phospholipids with the head group located near the polar layer of the membrane.³¹ Cholesterol was shown to increase membrane microviscosity and therefore decrease membrane fluidity in biomimetic mitochondrial membranes²⁷⁷ and rat liver mitochondria.²⁷⁸ Simultaneously, cholesterol impaired ATP production.²⁷⁷ Increased membrane viscosity was shown to decrease respiration rates which could be restored by addition of membrane-fluidizing sterols.²⁷⁷ Increasing unsaturated lipid composition, known to enhance membrane fluidity, in *E. coli* membranes and yeast mitochondria, increased respiration rates.²⁷⁹ In contrast, enhancing membrane fluidity by increasing unsaturated lipid composition in *E. coli* membranes and yeast mitochondria increased respiration rates.²⁷⁹ Ubiquinone diffusivity was reported to be enhanced simultaneously with increasing the portion of membrane-fluidizing lipids, thereby tightly regulating respiratory flux.²⁷⁹ As stated by Budin et al. (2018), membrane viscosity might control the efficiency of the respiratory chain by other mechanisms like impairing substrate uptake or changing individual RCC enzyme activity.²⁷⁹ Although cholesterol was shown to decrease membrane fluidity and impair ATP production, it did not affect ADP uptake.²⁸⁰ "It has generally been accepted that increased membrane fluidity reduces the physical barrier to oxygen permeation".²⁸¹ In reverse, increased membrane viscosity should impair passive permeation of oxygen. Since CIV-linked respiration was not reduced by CoQ10 (Figure 28 d, p. 81), decreased oxygen supply in mitochondria cannot be the reason for reduced respiration in our experiments. To assure this statement, additional experiments increasing the CoQ10-to-mitochondria ratio should be performed. Also, replenished oxygen concentration should be

measured upon exhaustion of an ETC substrate or ADP, e.g. using phosphorescent oxygen sensors.²⁸²⁻²⁸⁴ NADH:CoQ1 oxidoreductase and succinate:CoQ1 oxidoreductase activities were not affected by CoQ10 (CI: **Figure 43 a**, p. 100; CII: **Figure 46**, p. 103) further pointing towards a membrane-dependent effect.

Since calcium has been shown to decrease membrane fluidity by binding to low-affinity sites,²⁸⁵ the observed potentiating effect of calcium might be due to an additional increase of viscosity. Since lateral diffusion of CoQ in mitochondrial membranes has been shown to be considerably faster than ETC rates, under standard conditions electron transfer is not diffusion-limited.²⁸⁶ Thus a slight decrease of CoQ diffusivity induced by Ca-binding to phospholipids should not impact respiration in absence of exogenous CoQ10.

Furthermore, HO-CoQ10 and CoQ10 offer additional calcium binding sites in the membrane. Unpublished data by Katerina Stankoska and Nikolina Mitreska^{185,224} revealed that not only HO-CoQ10 like suggested by Bogeski et al. (2011) but also native ubiquinones are capable of calcium-binding. In their reduced state and in absence of H-bonds from water to the quinol oxygen, 2 quinols probably bind 2 Ca²⁺ ions, thereby releasing protons and forming a calcium-quinolate complex (**Figure 72 d, e, f**). CoQ-calcium complexes might consist of agglomerates of multiple CoQ molecules, and thereby might have a stronger effect on membrane properties. Exogenous application of CoQ elevates the ratio of CoQ to other membrane components increasing the probability of multiple CoQ-calcium complexes which is why calcium did not decrease respiration when endogenous amounts of CoQ were present (CI: **Figure 38 a and b**, p. 94; CII: **Figure 39 a**, p. 95).

More hydrophilic CoQ derivatives have been shown to be located in shallower regions of the lipid bilayer, nearer to the polar surface than CoQ10.²⁶ Thus, their influence on the acyl chain order might be negligible which may be the reason why the smaller CoQ analogue CoQ1 did not modulate mitochondrial respiration (**Figure 40**, p. 96). **Figure 72 a-c** illustrates the link between CoQ10 content, calcium binding, and the order of the membrane changing its viscosity, and thereby quinone diffusivity which eventually impacts mitochondrial respiration.

To validate this hypothesis, further work should focus on examining mitochondrial membrane fluidity in dependence of CoQ10 enrichment and calcium presence by, e.g. measuring fluorescence anisotropy with fluorescent probes intercalating between lipids of membranes.^{278,287,288} Possible impairment of electron transfer between enzymes and CoQ can be tested by measuring CI-CIII and CII-CIII (NADH and succinate:cytochrome *c* oxidoreductase) activities without interference of artificial quinone acceptors. Diffusion coefficients of CoQ10 can be assessed by fluorescence after photobleaching (FRAP) experiments with fluorescence-marked CoQ10 (NBD conjugated to carbonyl group of quinone moiety).²⁷⁹ If decreased membrane fluidity can be confirmed, experiments should be repeated with compounds decreasing and increasing membrane fluidity, e.g. cholesterol^{277,278} and A₂C (2-(2-methoxyethoxy)ethyl-8-(cis-2-*n*-octylcyclopropyl)octane,²⁷⁸ respectively.

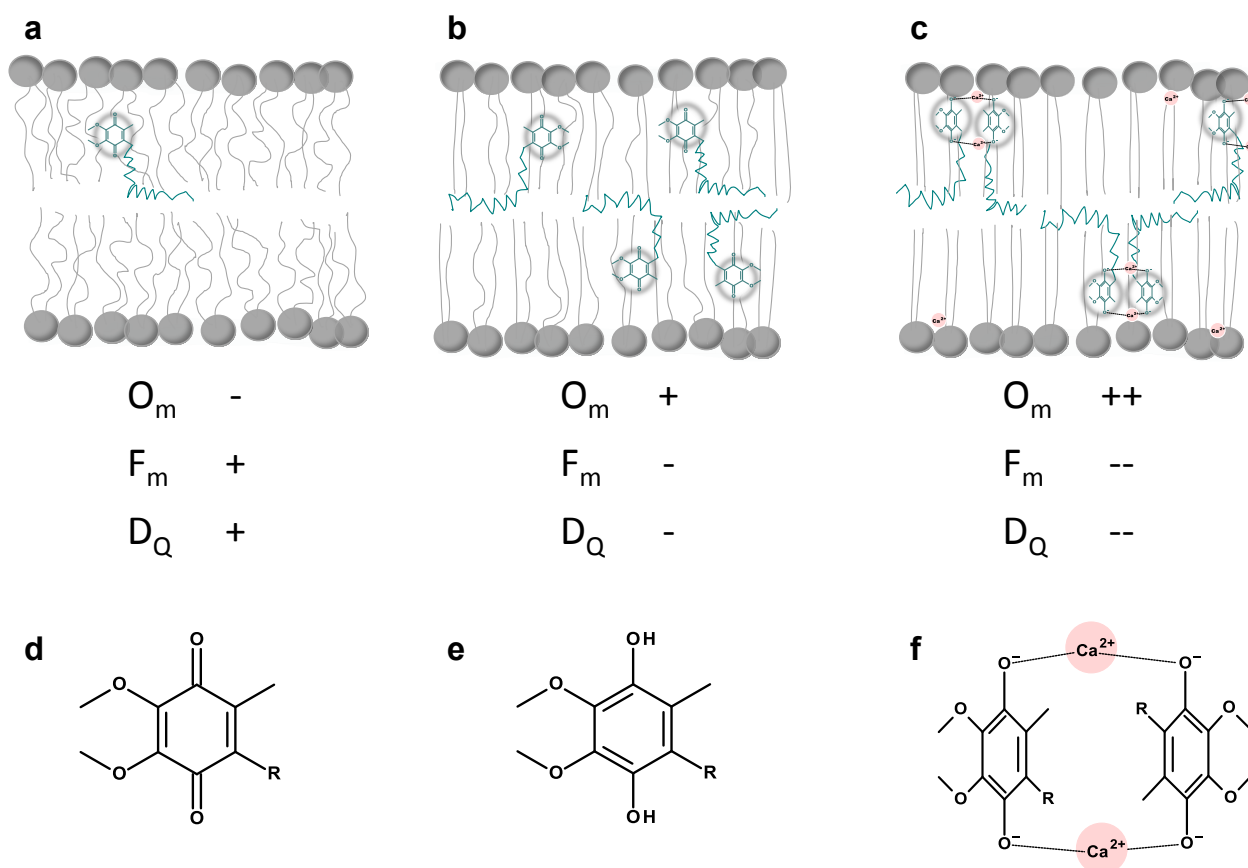


Figure 72 | Proposed model of CoQ10 and Ca²⁺ regulating respiration by changing membrane fluidity. Panels a-c depict the correlation between membrane integration of CoQ and order of the membrane acyl chain region (O_m) influencing membrane fluidity (F_m) and consequently CoQ diffusivity (D_Q). (a) The quinone moiety of CoQ10 is thought to be located near the polar side of the lipid membrane. (b) Increased content of CoQ10 intercalated between phospholipids reduces membrane fluidity by increasing the order of the acyl chains. Enhanced microviscosity, in turn, reduces diffusivity of CoQ. (c) Calcium binding to PL and CoQ further decreases membrane fluidity and Q diffusivity. (d) Oxidized and (e) reduced form of CoQ10, R = isoprene chain consisting of 10 isoprene units; (f) Proposed Ca²⁺-binding of CoQ10 at the deprotonated oxygen atoms at 1- and 4-position, sandwiching 2 Calcium ions between 2 quinols.

HO-CoQ10 is an inhibitor of the Q-binding site of respiratory chain complexes I, II, and III

HO-CoQ10 exhibits an inhibitory effect on single respiratory enzymes CI and CII and at the same time enhances H₂O₂ production linked to these complexes. Usually, ROS production is associated to an electron backup in a respiratory chain complex which increases the probability of electrons to slip and reduce oxygen to produce superoxide anion radicals, that in turn react via spontaneous and enzymatic dismutation to hydrogen peroxide. However, different to rotenone, HO-CoQ10 did not change electron occupation of Complex I detected by low-temperature EPR (Figure 67 a and b, p. 129), but changed absorption spectra of a following antimycin A treatment (Figure 68 a and c, p. 130). Hence, it is plausible that electron passage through Complex I is not hindered by HO-CoQ10. Furthermore, Complex II showed HO-CoQ10 reductase activity when HO-CoQ10 was supplied in high concentrations (Figure 50 c, p. 108). The requirement of high HO-CoQ10 concentrations to detect CII activity might be due to the decreased water solubility of CoQs with long isoprene chains since in comparison to CoQ1 also higher CoQ10 concentrations were necessary (cf. Figure 50 a and b). However, this can also be explained by partial reduction to the semiquinone radical.

Comparing redox properties of CoQ10 and HO-CoQ10 in aqueous solution, the redox potential of the hydroxy derivative was determined to be only 80 mV more negative than the redox potential of CoQ10.^{185,rr} Considering that the last Fe-S cluster transferring electrons to CoQ has a redox potential of -200 mV in Complex I and +60 mV in Complex II and that CII showed HO-CoQ10 reductase activity, it is likely that CI is able to reduce HO-CoQ10 under ideal experimental conditions as discussed before (section 3.7.4 on p. 106).

Since Fe-S clusters transfer one electron at a time, redox potentials of $Q/SQ^{\bullet-}$ and $SQ^{\bullet-}/Q^{2-}$ couples need to be compared. Assumptions are made on basis of electrochemical data although electron transitions and redox potentials might vary since they are highly dependent on the surrounding as well as availability of H-bonds and protons. Nonetheless, comparing quinone derivatives with their monohydroxylated forms,^{ss} it is obvious that even though quinone/quinol pairs of the hydroxy analogues have a more negative redox potential, their midpoint potential of the first electron transfer from Q to $SQ^{\bullet-}$ is more positive. Therefore, the reduction of HO-CoQ10 to its semiquinone radical should be facilitated in comparison to CoQ10. However, the second reduction of $SQ^{\bullet-}$ to Q^{2-} was found to have a remarkably lower redox potential. Therefore, complete reduction of HO-CoQ10 might be hindered. Thus, HO-CoQ10-induced CI- and CII-linked ROS formation might be a result from one-electron transfer to HO-CoQ10 producing HO- SQ^{\bullet} . As the semiquinone radical of HO-CoQ10 has been observed to be remarkably less stable than the CoQ10-derived radical,¹⁸⁵ the HO- SQ^{\bullet} is prone to react with oxygen and thus might be the source of elevated ROS formation.

To substantiate this hypothesis, the source of ROS should be located using non-ROS-inducing inhibitors of the other complexes. Additionally, the HO-CoQ10-derived SQ^{\bullet} should be detectable in absence of oxygen using low-temperature EPR. Inclusion of oxygen in the medium should result in ROS formation and consequently abolish the radical. Furthermore, inhibitors known to eliminate appearing SQ^{\bullet} at the Q-binding site, like rotenone, atpenin A5, and TFFA,⁵⁴ can identify the site of semiquinone formation.

Apart from acting on the Q-binding site, CoQ could also affect RCC activity by binding to other sites of the respiratory chain complexes, thus changing activity directly or via influencing affinity of cardiolipin and phospholipids known to modulate RCC activities.²⁸⁹⁻²⁹¹ Since HO-CoQ10 induced CI- and CII-linked ROS formation, the local increase of ROS might secondarily decrease RCC activity.^{292,293}

HO-CoQ10 neither affected cell viability nor proliferation

Even though HO-CoQ10 enhanced ROS formation and inhibited CI, CII, as well as mitochondrial respiration, HO-CoQ10 did not induce cell death or reduce proliferation of different cell lines under standard cell culture conditions (section 3.4, p. 74). In contrast, ETC inhibitors are known to inhibit proliferation and induce cell death.^{294,295}

Uptake of the substances might be one critical factor, even though it has been shown that incubation with 10 μ M ethanolic CoQ10 for 5 d increased cellular CoQ10 50-fold to 3 000 pmol/mg.¹⁶⁷ However, activities of RCCs of CoQ10-deficient cells were not fully re-established upon CoQ10 supplementation, indicating that

^{rr} $E_{p,mid}$ of CoQ10 and HO-CoQ10: 80 and 0 mV, respectively; vs. SHE, measured with glassy carbon electrodes modified by NH_2 -functionalized carbon nanotubes, KP, pH 7, cyclic and square wave voltammetry¹⁸⁵

^{ss} 1,4-naphtoquinone and 2-hydroxy-1,4-naphtoquinone,²⁹⁸ 2,5-dimethyl-1,4-benzoquinone and 3-hydroxy-2,5-dimethyl-1,4-benzoquinone¹⁸⁵

mitochondrial uptake of exogenous CoQ10 is a limiting factor. In fact, intraperitoneal administration of ³H-labelled CoQ10 showed that only 0.5% of total CoQ10 taken up by rat liver tissue reached mitochondria.²⁹⁶ Assuming an uptake of 0.5% from the observed 3 000 pmol/mg¹⁶⁷ into mitochondria would have resulted in an increase of CoQ10 concentration of 15 pmol/mg mitochondrial protein. Taking this estimate into account suggests that also HO-CoQ10 can be enriched in mitochondria but does not exhibit a deleterious effect on the tested cancer cell lines.

Cancer cells evolved a multitude of coping mechanisms to evade cell death, e.g. switching to aerobic glycolysis.²⁹⁷ Thus, cancer cells might have lost HO-CoQ10 sensitivity during cancer progression. Since this study only considered immortalized cell lines and did not test impact on primary cells which might be considerably different, it can be speculated that HO-CoQ10 acts as a cellular modulator of energy metabolism.

Conclusion

The inhibitory effect of CoQ10 on respiration seems counterintuitive because CoQ10 is an essential component of the mitochondrial electron transport chain, and primary CoQ10 deficiency is successfully treated by oral CoQ10 supplementation. However, CoQ10 has a high turn-over rate, is synthesized in every tissue and can be adaptively regulated implying that CoQ10 levels are kept in steady-state concentrations but may be rapidly changed on demand. HO-CoQ10 inhibits respiratory chain complexes tested in reactions with exogenously applied quinones. Future experiments should address the influence of HO-CoQ10 on more physiological levels. Therefore, it will be essential to follow the accumulation of exogenous HO-CoQ10 in cells and mitochondria to allow estimation of active concentrations. Moreover, modulation of endogenous HO-CoQ10 and CoQ10 levels will permit experiments without exceeding physiological concentrations. Endogenous HO-CoQ10 was detected in highly metabolic active heart tissue in small amounts. Quantification in different tissues, cellular compartments, metabolic activities and pathological conditions may lead to defining physiological roles of HO-CoQ10.

Literature

1. Brunmark, A. & Cadenas, E. *REDOX AND ADDITION CHEMISTRY OF QUINOID COMPOUNDS AND ITS BIOLOGICAL IMPLICATIONS*. *Free Radical Biology & Medicine* **7**, (1989).
2. James, A. M., Smith, R. A. J. & Murphy, M. P. Antioxidant and prooxidant properties of mitochondrial Coenzyme Q. *Arch. Biochem. Biophys.* **423**, 47–56 (2004).
3. Vollhardt, K. P. C. & Schore, N. E. *Organische Chemie*. (WILEY-VCH Verlag, 2009).
4. Berg, J. M. *Stryer Biochemie (deutsche Ausgabe)*. (WILEY-VCH Verlag, 2010).
5. Bogeski, I. *et al.* Calcium binding and transport by coenzyme Q. *J. Am. Chem. Soc.* **133**, 9293–9303 (2011).
6. Gulaboski, R. *et al.* Hydroxylated derivatives of dimethoxy-1,4-benzoquinone as redox switchable earth-alkaline metal ligands and radical scavengers. *Sci. Rep.* **3**, 1–8 (2013).
7. Gulaboski, R. *et al.* New insights into the chemistry of Coenzyme Q-0: A voltammetric and spectroscopic study. *Bioelectrochemistry* **111**, 100–108 (2016).
8. Bogeski, I. *et al.* Calcium binding and transport by coenzyme Q. *J. Am. Chem. Soc.* **133**, 9293–9303 (2011).
9. Benett, I. M. *et al.* Active transport of Ca²⁺ by an artificial photosynthetic membrane. *Nature* **420**, 398–401 (2002).
10. Gawlitzka, A. Redox Eigenschaften von hydroxiliertem 2,6-Dimethoxybenzochinon, Coenzym Q1 und Q10. (Unpublished bachelor thesis, Saarland University, 2012).
11. Slowik, E. J. Hydroxyliertes Coenzym Q10 Synthese, Lokalisation und ROS-Homöostase. (Unpublished master thesis, Saarland University, 2014).
12. Slowik, E. J. Versuchsprotokoll zum Advanced Modul II Signalleitung und Transport: Darstellung von dihydroxyliertem Coenzym Q10. (Unpublished report, Saarland University, 2013).
13. Bernhardt, R. Cytochromes P450 as versatile biocatalysts. *J. Biotechnol.* **124**, 128–145 (2006).
14. Stefely, J. A. & Pagliarini, D. J. Biochemistry of Mitochondrial Coenzyme Q Biosynthesis. *Trends Biochem. Sci.* **42**, 824–843 (2017).
15. Marbois, B. N. & Clarke, C. F. The COQ7 gene encodes a protein in *Saccharomyces cerevisiae* necessary for ubiquinone biosynthesis. *J. Biol. Chem.* **271**, 2995–3004 (1996).
16. Hsu, A. Y., Poon, W. W., Shepherd, J. A., Myles, D. C. & Clarke, C. F. Complementation of *coq3* Mutant Yeast by Mitochondrial Targeting of the *Escherichia coli* UbiG Polypeptide: Evidence That UbiG Catalyzes Both O-Methylation Steps in Ubiquinone Biosynthesis. *Biochemistry* **35**, 9797–9806 (1996).
17. Acosta, M. J. *et al.* Coenzyme Q biosynthesis in health and disease. *Biochim. Biophys. Acta - Bioenerg.* **1857**, 1079–1085 (2016).
18. Turunen, M., Olsson, J. & Dallner, G. Metabolism and function of coenzyme Q. *Biochim. Biophys. Acta - Biomembr.* **1660**, 171–199 (2004).
19. Bentinger, M., Tekle, M. & Dallner, G. Coenzyme Q - Biosynthesis and functions. *Biochem. Biophys. Res. Commun.* **396**, 74–79 (2010).
20. Löw, P., Peterson, E., Edlund, C., Brunk, U. & Appelkvist, E. L. Nonmembrane associated dolichol in rat liver. *Lipids* **27**, 1–9 (1992).
21. Zhang, Y., Turunen, M. & Appelkvist, E.-L. Restricted Uptake of Dietary Coenzyme Q Is in Contrast to the Unrestricted Uptake of α -Tocopherol into Rat Organs and Cells. *J. Nutr.* **126**, 2089–2097 (1996).
22. Guidotti, G. Membrane Proteins. *Annu. Rev. Biochem.* **41**, 731–752 (1972).
23. Lotan, R. & Nicolson, G. L. Plasma membranes of eukaryotes. in *Advanced Cell Biology* (eds. Schwartz, L. M. & Azar, M. M.) 129–154 (1981).
24. Miami University. Table 4-1 Amounts of Lipid, Protein, and Carbohydrate in Different Biological Membranes. *Oxford, OH* (2008). Available at: https://www.cas.miamioh.edu/~meicenrd/anatomy/Ch2_Ultrastructure/TABLE.gif. (Accessed: 18th April 2019)

25. Pearson Education. Inc. Chapters 7 and 8: Membranes, Table 7-1. 19 (2012). Available at: <https://slideplayer.com/slide/7574395/>. (Accessed: 18th April 2019)
26. Afri, M. *et al.* Active oxygen chemistry within the liposomal bilayer Part III: Locating Vitamin E, ubiquinol and ubiquinone and their derivatives in the lipid bilayer. *Chem. Phys. Lipids* **131**, 107–121 (2004).
27. Hernández, V. A., Eriksson, E. K. & Edwards, K. Ubiquinone-10 alters mechanical properties and increases stability of phospholipid membranes. *Biochim. Biophys. Acta - Biomembr.* **1848**, 2233–2243 (2015).
28. Kingsley, P. B. & Feigenson, G. W. ¹H-NMR study of the location and motion of ubiquinones in perdeuterated phosphatidylcholine bilayers. *BBA - Bioenerg.* **635**, 602–618 (1981).
29. Hauß, T., Dante, S., Haines, T. H. & Dencher, N. A. Localization of coenzyme Q10 in the center of a deuterated lipid membrane by neutron diffraction. *Biochim. Biophys. Acta - Bioenerg.* **1710**, 57–62 (2005).
30. Haines, T. H. Do sterols reduce proton and sodium leaks through lipid bilayers? *Prog. Lipid Res.* **40**, 299–324 (2001).
31. Eriksson, E. K., Agmo Hernández, V. & Edwards, K. Effect of ubiquinone-10 on the stability of biomimetic membranes of relevance for the inner mitochondrial membrane. *Biochim. Biophys. Acta - Biomembr.* **1860**, 1205–1215 (2018).
32. Sévin, D. C. & Sauer, U. Ubiquinone accumulation improves osmotic-stress tolerance in *Escherichia coli*. *Nat. Chem. Biol.* **10**, 266–272 (2014).
33. Katsikas, H. & Quinn, P. J. *THE POLYISOPRENOID CHAIN LENGTH INFLUENCES THE INTERACTION OF UBIQUINONES WITH PHOSPHOLIPID BILAYERS.* *Biochimica et Biophysica Acta* **689**, (1982).
34. Quinn, P. J. Lipid–lipid interactions in bilayer membranes: Married couples and casual liaisons. *Prog. Lipid Res.* **51**, 179–198 (2012).
35. Ernster, L. & Forsmark-Andrée, P. Ubiquinol: an endogenous antioxidant in aerobic organisms. *Clin. Investig.* **71**, 60–65 (1993).
36. Crane, F. L. Biochemical Functions of Coenzyme Q 10. *J. Am. Coll. Nutr.* **20**, 591–598 (2001).
37. Nohl, H. & Gille, L. The bifunctional activity of ubiquinone in lysosomal membranes. *Biogerontology* **3**, 125–131 (2002).
38. Nohl, H., Kozlov, A. V., Staniek, K. & Gille, L. The multiple functions of coenzyme q. *Bioorg. Chem.* **29**, 1–13 (2001).
39. Echtay, K. S., Winkler, E. & Klingenberg, M. Coenzyme Q is an obligatory cofactor for uncoupling protein function. *Nature* **408**, 609–613 (2000).
40. Echtay, K. S., Winkler, E., Frischmuth, K. & Klingenberg, M. Uncoupling proteins 2 and 3 are highly active H⁺ transporters and highly nucleotide sensitive when activated by coenzyme Q (ubiquinone). *Proc. Natl. Acad. Sci. U. S. A.* **98**, 1416–1421 (2001).
41. Walter, L. *et al.* Three classes of ubiquinone analogs regulate the mitochondrial permeability transition pore through a common site. *J. Biol. Chem.* **275**, 29521–29527 (2000).
42. Papucci, L. *et al.* Coenzyme Q10 prevents apoptosis by inhibiting mitochondrial depolarization independently of its free radical scavenging property. *J. Biol. Chem.* **278**, 28220–28228 (2003).
43. Sazanov, L. A. A giant molecular proton pump: structure and mechanism of respiratory complex I. *Nat. Rev. Mol. Cell Biol.* **16**, 375–388 (2015).
44. Mitchell, P. Protonmotive redox mechanism of the cytochrome b-c1 complex in the respiratory chain: Protonmotive ubiquinone cycle. *FEBS Lett.* **56**, 1–6 (1975).
45. Van Vranken, J. G., Na, U., Winge, D. R. & Rutter, J. Protein-mediated assembly of succinate dehydrogenase and its cofactors. *Critical Reviews in Biochemistry and Molecular Biology* **50**, 168–180 (2015).
46. Hirst, J. Towards the molecular mechanism of respiratory complex I. *Biochem. J.* **425**, 327–339 (2010).
47. Hägerhäll, C. Succinate: quinone oxidoreductases: Variations on a conserved theme. *Biochim. Biophys. Acta - Bioenerg.* **1320**, 107–141 (1997).

48. Fato, R. *et al.* Differential effects of mitochondrial Complex I inhibitors on production of reactive oxygen species. *Biochim. Biophys. Acta - Bioenerg.* **1787**, 384–392 (2009).
49. Fato, R., Bergamini, C., Leoni, S. & Lenaz, G. Mitochondrial production of reactive oxygen species: role of complex I and quinone analogues. *Biofactors* **32**, 31–39 (2008).
50. Murphy, M. P. How mitochondria produce reactive oxygen species. *Biochem. J.* **417**, 1–13 (2009).
51. Genova, M. L. *et al.* The site of production of superoxide radical in mitochondrial Complex I is not a bound ubiquinone but presumably iron-sulfur cluster N2. *FEBS Lett.* **505**, 364–368 (2001).
52. Siebels, I. & Dröse, S. Q-site inhibitor induced ROS production of mitochondrial complex II is attenuated by TCA cycle dicarboxylates. *Biochim. Biophys. Acta - Bioenerg.* **1827**, 1156–1164 (2013).
53. Quinlan, C. L. *et al.* Mitochondrial complex II can generate reactive oxygen species at high rates in both the forward and reverse reactions. *J. Biol. Chem.* **287**, 27255–64 (2012).
54. Grivennikova, V. G., Kozlovsky, V. S. & Vinogradov, A. D. Respiratory complex II: ROS production and the kinetics of ubiquinone reduction. (2017). doi:10.1016/j.bbabi.2016.10.008
55. Kluckova, K. *et al.* Ubiquinone-binding site mutagenesis reveals the role of mitochondrial complex II in cell death initiation. *Cell Death Dis.* **6**, (2015).
56. Starkov, A. A. & Fiskum, G. Myxothiazol induces H₂O₂ production from mitochondrial respiratory chain. *Biochem. Biophys. Res. Commun.* **281**, 645–650 (2001).
57. Turrens, J. F., Alexandre, A. & Lehninger, A. L. *Ubisemiquinone Is the Electron Donor for Superoxide Formation by Complex III of Heart Mitochondria.* *ARCHIVES OF BIOCHEMISTRY AND BIOPHYSICS* **237**, (1985).
58. Schägger, H. & Pfeiffer, K. Supercomplexes in the respiratory chains of yeast and mammalian mitochondria. *EMBO J.* **19**, 1777–1783 (2000).
59. Acín-Pérez, R., Fernández-Silva, P., Peleato, M. L., Pérez-Martos, A. & Enriquez, J. A. Respiratory Active Mitochondrial Supercomplexes. *Mol. Cell* **32**, 529–539 (2008).
60. Letts, J. A. & Sazanov, L. A. Clarifying the supercomplex: The higher-order organization of the mitochondrial electron transport chain. *Nat. Struct. Mol. Biol.* **24**, 800–808 (2017).
61. Genova, M. L. & Lenaz, G. Functional role of mitochondrial respiratory supercomplexes. *BBA - Bioenerg.* **1837**, 427–443 (2014).
62. Moreno-Lastres, D. *et al.* Cell Metabolism Mitochondrial Complex I Plays an Essential Role in Human Respirasome Assembly. *Cell Metab.* **15**, 324–335 (2012).
63. Kovářová, N. *et al.* High Molecular Weight Forms of Mammalian Respiratory Chain Complex II. *PLoS One* **8**, (2013).
64. Guo, R., Zong, S., Wu, M., Gu, J. & Yang, M. Architecture of Human Mitochondrial Respiratory Megacomplex I2III2IV2. *Cell* **170**, 1247–1257 (2017).
65. Guo, R., Gu, J., Zong, S., Wu, M. & Yang, M. Structure and mechanism of mitochondrial electron transport chain. *Biomed. J.* **41**, 9–20 (2018).
66. Acín-Pérez, R. *et al.* Respiratory Complex III Is Required to Maintain Complex I in Mammalian Mitochondria. *Mol. Cell* **13**, 805–815 (2004).
67. Diaz, F., Fukui, H., Garcia, S. & Moraes, C. T. Cytochrome c Oxidase Is Required for the Assembly/Stability of Respiratory Complex I in Mouse Fibroblasts. *Mol. Cell. Biol.* **26**, 4872–4881 (2006).
68. Maranzana, E., Barbero, G., Falasca, A. I., Lenaz, G. & Genova, M. L. Mitochondrial Respiratory Supercomplex Association Limits Production of Reactive Oxygen Species from Complex I. *Antioxid. Redox Signal.* **19**, 1469–1480 (2013).
69. Lopez-Fabuel, I. *et al.* Complex I assembly into supercomplexes determines differential mitochondrial ROS production in neurons and astrocytes. *PNAS* **113**, 13063–13068 (2016).
70. Greggio, C. *et al.* Enhanced Respiratory Chain Supercomplex Formation in Response to Exercise in Human Skeletal Muscle. *Cell Metab.* **25**, 301–311 (2017).
71. Bianchi, C., Fato, R., Genova, M. L., Castelli, G. P. & Lenaz, G. Structural and functional organization of Complex I in the mitochondrial respiratory chain. *BioFactors* **18**, 3–9 (2003).

72. Bianchi, C., Genova, M. L., Parenti Castelli, G. & Lenaz, G. The mitochondrial respiratory chain is partially organized in a supercomplex assembly: kinetic evidence using flux control analysis. *J. Biol. Chem.* **279**, 36562–9 (2004).
73. Blaza, J. N., Serreli, R., Jones, A. J. Y., Mohammed, K. & Hirst, J. Kinetic evidence against partitioning of the ubiquinone pool and the catalytic relevance of respiratory-chain supercomplexes. *PNAS* **111**, 15735–15740 (2014).
74. Fedor, J. G. & Hirst, J. Mitochondrial Supercomplexes Do Not Enhance Catalysis by Quinone Channeling. *Cell Metab.* **28**, 525–531 (2018).
75. Letts, J. A., Fiedorczuk, K. & Sazanov, L. A. The architecture of respiratory supercomplexes. *Nat. Publ. Gr.* **537**, (2016).
76. Milenkovic, D., Blaza, J. N., Larsson, N.-G. & Hirst, J. The Enigma of the Respiratory Chain Supercomplex. *Cell Metab.* **25**, 765–776 (2017).
77. Denton, R. M. Regulation of mitochondrial dehydrogenases by calcium ions. *BBA - Bioenerg.* **1787**, 1309–1316 (2009).
78. Denton, R. M., McCormack, J. G. & Edgell, N. J. Role of Calcium Ions in the Regulation of Intramitochondrial Metabolism. *Biochem. J.* **190**, 107–117 (1980).
79. Yamada, E. W. & Huzel, N. J. The calcium-binding ATPase inhibitor protein from bovine heart mitochondria. Purification and properties. *J. Biol. Chem.* **263**, 11498–11503 (1988).
80. Das, A. M. & Harris, D. A. Control of mitochondrial ATP synthase in heart cells: inactive to active transitions caused by beating or positive inotropic agents. *Cardiovasc. Res.* **24**, 411–417 (1990).
81. Palmieri, L. *et al.* Citrin and aralar1 are Ca²⁺-stimulated aspartate/glutamate transporters in mitochondria. *EMBO J.* **20**, 5060–5069 (2001).
82. Satrústegui, J., Pardo, B. & del Arco, A. Mitochondrial Transporters as Novel Targets for Intracellular Calcium Signaling. *Physiol. Rev.* **87**, 29–67 (2007).
83. Nosek, M. T., Dransfield, D. T. & Aprille, J. R. Calcium stimulates ATP-Mg/Pi carrier activity in rat liver mitochondria. *J. Biol. Chem.* **265**, 8444–50 (1990).
84. Solien, J., Haynes, V. & Giulivi, C. Differential requirements of calcium for oxoglutarate dehydrogenase and mitochondrial nitric-oxide synthase under hypoxia: Impact on the regulation of mitochondrial oxygen consumption. *Comp. Biochem. Physiol. Part A* **142**, 111–117 (2005).
85. Ghafourifar, P. & Richter, C. Nitric oxide synthase activity in mitochondria. *FEBS Lett.* **418**, 291–296 (1997).
86. Brown, G. C. & Cooper, C. E. Nanomolar concentrations of nitric oxide reversibly inhibit synaptosomal respiration by competing with oxygen at cytochrome oxidase. *FEBS Lett.* **356**, 295–298 (1994).
87. Wallace, B. J. & Young, I. G. AEROBIC RESPIRATION IN MUTANTS OF ESCHERICHIA COLI ACCUMULATING QUINONE ANALOGUES OF UBIQUINONE. *Biochim. Biophys. Acta* **461**, 75–83 (1977).
88. Schindelin, J. *et al.* Fiji: an open-source platform for biological-image analysis. *Nat. Methods* **9**, 676–682 (2012).
89. Nickel, A. G. *et al.* Reversal of mitochondrial transhydrogenase causes oxidative stress in heart failure. *Cell Metab.* **22**, 472–484 (2015).
90. Pallotti, F. & Lenaz, G. Isolation and subfractionation of mitochondria from animal cells and tissue culture lines. in *Methods in Cell Biology* **65**, 1–35 (2001).
91. Bohnert, M. *et al.* Central Role of Mic10 in the Mitochondrial Contact Site and Cristae Organizing System. *Cell Metab.* **21**, 747–755 (2015).
92. Cell.BioMol.Net (2005-2008). Buffer Calculator. Available at: <http://www.biomol.net/en/tools/buffercalculator.htm>. (Accessed: 5th September 2018)
93. Malz, F. Chapter 2 - Quantitative NMR in the Solution State NMR. in *NMR Spectroscopy in Pharmaceutical Analysis* (eds. Holzgrabe, U., Diehl, B. & Wawer, I.) 43–62 (Elsevier Science, 2008). doi:<http://dx.doi.org/10.1016/B978-0-444-53173-5.00002-0>
94. Gottlieb, H. E., Kotlyar, V. & Nudelman, A. NMR chemical shifts of common laboratory solvents as trace impurities. *J. Org. Chem.* **62**, 7512–7515 (1997).

95. Park, J. *et al.* Coenzyme Q10 protects neural stem cells against hypoxia by enhancing survival signals. *Brain Res.* **1478**, 64–73 (2012).
96. Borowy-Borowski, H., Sodja, C., Docherty, J., Walker, P. R. & Sikorska, M. Unique technology for solubilization and delivery of highly lipophilic bioactive molecules. *J. Drug Target.* **12**, 415–424 (2004).
97. Wishart, D. S. *et al.* DrugBank 5.0: a major update to the DrugBank database for 2018. *Nucleic Acids Res.* **46**, D1074–D1082 (2018).
98. Wagmann, L. *et al.* In vitro metabolic fate of nine LSD-based new psychoactive substances and their analytical detectability in different urinary screening procedures. *Anal. Bioanal. Chem.* (2019). doi:10.1007/s00216-018-1558-9
99. Meyer, M. R. *et al.* Qualitative studies on the metabolism and the toxicological detection of the fentanyl-derived designer drugs 3-methylfentanyl and isofentanyl in rats using liquid chromatography-linear ion trap-mass spectrometry (LC-MS n). doi:10.1007/s00216-011-5528-8
100. Richter, L. H. J. *et al.* Development and application of a LC-HRMS/MS method for analyzing antihypertensive drugs in oral fluid for monitoring drug adherence. *Anal. Chim. Acta* **1070**, 69–79 (2019).
101. Dinger, J., Meyer, M. R. & Maurer, H. H. In vitro cytochrome P450 inhibition potential of methylenedioxy-derived designer drugs studied with a two-cocktail approach. *Arch. Toxicol.* **3**, 305–318 (2016).
102. Remane, D., Meyer, M. R., Wissenbach, D. K. & Maurer, H. H. Ion suppression and enhancement effects of co-eluting analytes in multi-analyte approaches: systematic investigation using ultra-high-performance liquid chromatography/mass spectrometry with atmospheric-pressure chemical ionization or electrospray ionization. *Rapid Commun. Mass Spectrom.* **24**, 3103–3108 (2010).
103. Richter, L. H. J., Maurer, H. H. & Meyer, M. R. New psychoactive substances: Studies on the metabolism of XLR-11, AB-PINACA, FUB-PB-22, 4-methoxy- α -PVP, 25-I-NBOMe, and meclonazepam using human liver preparations in comparison to primary human hepatocytes, and human urine. *Toxicol. Lett.* **280**, 142–150 (2017).
104. Caspar, A. T., Brandt, S. D., Stoeber, A. E., Meyer, M. R. & Maurer, H. H. Metabolic fate and detectability of the new psychoactive substances 2-(4-bromo-2,5-dimethoxyphenyl)-N-[(2-methoxyphenyl)methyl]ethanamine (25B-NBOMe) and 2-(4-chloro-2,5-dimethoxyphenyl)-N-[(2-methoxyphenyl)methyl]ethanamine (25C-NBOMe) in human and rat urine by GC-MS, LC-MSn, and LC-HR-MS/MS approaches. *J. Pharm. Biomed. Anal.* **134**, 158–169 (2017).
105. Richter, L. H. J., Beck, A., Flockerzi, V., Maurer, H. H. & Meyer, M. R. Cytotoxicity of new psychoactive substances and other drugs of abuse studied in human HepG2 cells using an adopted high content screening assay. *Toxicol. Lett.* **301**, 79–89 (2019).
106. Caspar, A. T., Kollas, A. B., Maurer, H. H. & Meyer, M. R. Development of a quantitative approach in blood plasma for low-dosed hallucinogens and opioids using LC-high resolution mass spectrometry. *Talanta* **176**, 635–645 (2018).
107. Richter, L. H. J., Kaminski, Y. R., Noor, F., Meyer, M. R. & Maurer, H. H. Metabolic fate of desomorphine elucidated using rat urine, pooled human liver preparations, and human hepatocyte cultures as well as its detectability using standard urine screening approaches. *Anal. Bioanal. Chem.* **408**, 6283–6294 (2016).
108. Helfer, A. G., Michely, J. A., Weber, A. A., Meyer, M. R. & Maurer, H. H. Orbitrap technology for comprehensive metabolite-based liquid chromatographic-high resolution-tandem mass spectrometric urine drug screening - Exemplified for cardiovascular drugs. *Anal. Chim. Acta* **891**, 221–233 (2015).
109. Richter, L. H. J., Flockerzi, V., Maurer, H. H. & Meyer, M. R. Pooled human liver preparations, HepaRG, or HepG2 cell lines for metabolism studies of new psychoactive substances? A study using MDMA, MDD, butylone, MDPPP, MDPV, MDPB, 5-MAPB, and 5-API as examples. *J. Pharm. Biomed. Anal.* **143**, 32–42 (2017).
110. Backes, C. S. *et al.* Natural killer cells induce distinct modes of cancer cell death: Discrimination, quantification and modulation of apoptosis, necrosis and mixed forms. *J. Biol. Chem.* **293**, 16348–16363

- (2018).
111. Backes, C. Untersuchung zytotoxischer Mechanismen in humanen natürlichen Killerzellen. (Doctoral dissertation, Saarland University, 2016).
 112. Bio-Rad Laboratories. DC Protein Assay Instruction Manual: 5.1 Standard Assay Protocol. 1–17
 113. Mela, L. & Seitz, S. Isolation of Mitochondria with Emphasis on Heart Mitochondria from Small Amounts of Tissue. *Methods Enzymol.* **55**, 39–46 (1979).
 114. Nickel, A. G. *et al.* Reversal of mitochondrial transhydrogenase causes oxidative stress in heart failure. *Cell Metab.* **22**, 472–484 (2015).
 115. Tao, Z., Goodisman, J. & Soudi, A.-K. Oxygen Measurement via Phosphorescence: Reaction of Sodium Dithionite with Dissolved Oxygen. *J Phys Chem A.* **112**, 1511–1518 (2008).
 116. Gnaiger, E. *O2k Quality Control 1: Polarographic oxygen sensors and accuracy of calibration. Mitochondrial Physiology Network* **06.03(16)**, (Oroboros Instruments Corp, 2016).
 117. Gnaiger, E. *Service of the Polarographic Oxygen Sensor OroboPOS. Mitochondrial Physiology Network* **19.18(B04)**, (Oroboros Instruments Corp, 2011).
 118. Fasching, M. & Gnaiger, E. *O2k Quality Control 2: Instrumental oxygen background correction and accuracy of oxygen flux. Mitochondrial Physiology Network* **14.06(06)**, (Oroboros Instruments Corp, 2016).
 119. Fasching M & Fontana-Ayoub. Oroboros O2k-Protocols Chemicals: Mitochondrial respiration medium-MiR06, Version 06. *Mitochondrial Physiol. Netw.* **14.13**, 1–4 (2016).
 120. Thermo Fisher Scientific. *Catalog numbers C3008MP, F6774: Calcium Calibration Buffer Kits.* (Author, 2014).
 121. Chris Patton. WinMAXC32. (2002).
 122. Frazier, A. E. & Thorburn, D. R. Biochemical Analyses of the Electron Transport Chain Complexes by Spectrophotometry. in *Mitochondrial Disorders. Methods in Molecular Biology (Methods and Protocols)*, vol 837 (ed. Wong, P. D. L.) 49–62 (Humana Press, 2012). doi:10.1007/978-1-61779-504-6_4
 123. Horvath, S. Complex IV in-gel activity staining. in (ed. van der Laan, M.) 15–17 (2015).
 124. Jung, C., Higgins, C. M. & Xu, Z. Measuring the quantity and activity of mitochondrial electron transport chain complexes in tissues of central nervous system using blue native polyacrylamide gel electrophoresis. *Anal. Biochem.* **286**, 214–223 (2000).
 125. Vogt, T. *et al.* Overcoming Intrinsic Multidrug Resistance in Melanoma by Blocking the Mitochondrial Respiratory Chain of Slow-Cycling JARID1Bhigh Cells. *Cancer Cell* **23**, 811–825 (2013).
 126. Thierbach, S. *et al.* Substrate-Assisted O₂ Activation in a Cofactor-Independent Dioxygenase. *Chem. Biol.* **21**, 217–225 (2014).
 127. Ahmed, M. & Khan, Z. H. Electronic absorption spectra of benzoquinone and its hydroxy substituents and effect of solvents on their spectra. *Spectrochim. Acta - Part A Mol. Biomol. Spectrosc.* **56**, 965–981 (2000).
 128. Flaig, W. & Salfeld, J. C. Nachweis der Bildung von Hydroxy-p-benzochinon als Zwischenprodukt bei der Autoxydation von Hydrochinon in schwach alkalischer Lösung. *Naturwissenschaften* 5–16 (1960).
 129. Pettersson, G. Synthesis of 2,3-Dihydroxy-5,6-dimethyl-1,4-benzoquinone and its Monomethyl Ether. *Acta Chem. Scand.* **18**, 2309–2312 (1964).
 130. Kim, E.-A., Kim, J.-Y., Chung, H.-J. & Lim, S.-T. Preparation of aqueous dispersions of coenzyme Q10 nanoparticles with amylo maize starch and its dextrin. *LWT - Food Sci. Technol.* **47**, 493–499 (2012).
 131. Nepal, P. R., Han, H.-K. & Choi, H.-K. Enhancement of solubility and dissolution of Coenzyme Q10 using solid dispersion formulation. *Int. J. Pharm.* **383**, 147–153 (2010).
 132. Beg, S., Javed, S. & JKohli, K. Bioavailability Enhancement of Coenzyme Q10: An Extensive Review of Patents. *Recent Pat. Drug Deliv. Formul.* **4**, 245–257 (2010).
 133. Tsai, K. L. *et al.* A novel mechanism of coenzyme Q10 protects against human endothelial cells from oxidative stress-induced injury by modulating NO-related pathways. *J. Nutr. Biochem.* **23**, 458–468 (2012).

134. Noh, Y. H. *et al.* Inhibition of oxidative stress by coenzyme Q10 increases mitochondrial mass and improves bioenergetic function in optic nerve head astrocytes. *Cell Death Dis.* **4**, e820 (2013).
135. Xu, J. *et al.* Hsp70 expression induced by Co-Enzyme Q10 protected chicken myocardial cells from damage and apoptosis under in vitro heat stress. *Poult. Sci.* **96**, 1426–1437 (2017).
136. Bahar, M. *et al.* Exogenous coenzyme Q10 modulates MMP-2 activity in MCF-7 cell line as a breast cancer cellular model. *Nutr. J.* **9**, 62 (2010).
137. Duberley, K. E. *et al.* Effect of Coenzyme Q10 supplementation on mitochondrial electron transport chain activity and mitochondrial oxidative stress in Coenzyme Q10 deficient human neuronal cells. *Int. J. Biochem. Cell Biol.* **50**, 60–63 (2014).
138. Bergamini, C., Moruzzi, N., Sblendido, A., Lenaz, G. & Fato, R. A water soluble CoQ 10 formulation improves intracellular distribution and promotes mitochondrial respiration in cultured cells. *PLoS One* **7**, e33712 (2012).
139. Eghbal, M. A., Abdoli, N. & Azarmi, Y. Efficiency of hepatocyte pretreatment with coenzyme Q10 against statin toxicity. *Arh. Hig. Rada Toksikol.* **65**, 101–108 (2014).
140. Åberg, F., Appelkvist, E. L., Dallner, G. & Ernster, L. Distribution and redox state of ubiquinones in rat and human tissues. *Arch. Biochem. Biophys.* **295**, 230–234 (1992).
141. Turkowicz, M. J. & Karpińska, J. Analytical problems with the determination of coenzyme Q10 in biological samples. *BioFactors* **39**, 176–185 (2013).
142. Li, L., Pabbisetty, D., Carvalho, P., Avery, M. A. & Avery, B. A. Analysis of CoQ10 in rat serum by ultra-performance liquid chromatography mass spectrometry after oral administration. *J. Pharm. Biomed. Anal.* **46**, 137–142 (2008).
143. Kubo, H. *et al.* Food content of ubiquinol-10 and ubiquinone-10 in the Japanese diet. *J. Food Compos. Anal.* **21**, 199–210 (2008).
144. Gonzáles-Mañas, J. M., Vito, M. D., Gurtubay, J.-I. G. & Goñi, F. M. The interaction of Triton X-100 with purple membranes. Detergent binding, spectral changes and membrane solubilization. *Eur. J. Biochem.* **188**, 673–678 (1990).
145. Ferreiro-Barros, C. C., Sugawara, E. K. & Sanches, L. R. *Determination of a method for extraction of coenzyme Q10 in human plasma: optimization of the use of surfactants and other variables.* **10**, (2012).
146. Mosca, F., Fattorini, D., Bompadre, S. & Littarru, G. P. Assay of coenzyme Q10 in plasma by a single dilution step. *Anal. Biochem.* **305**, 49–54 (2002).
147. Tang, P. H. *et al.* Measurement of reduced and oxidized coenzyme Q9 and coenzyme Q10 levels in mouse tissues by HPLC with coulometric detection. *Clin. Chim. Acta* **341**, 173–184 (2004).
148. Tang, Z. *et al.* Rapid assessment of the coenzyme Q10 redox state using ultrahigh performance liquid chromatography tandem mass spectrometry. *Analyst* **139**, 5600–5604 (2014).
149. Bongard, R. D. *et al.* Coenzyme Q1 as a probe for mitochondrial complex I activity in the intact perfused hyperoxia-exposed wild-type and *Nqo1*-null mouse lung. *Am. J. Physiol. Cell. Mol. Physiol.* **302**, L949–L958 (2012).
150. Duberley, K. E. C. *et al.* Coenzyme Q10 quantification in muscle, fibroblasts and cerebrospinal fluid by liquid chromatography/tandem mass spectrometry using a novel deuterated internal standard. *Rapid Commun. Mass Spectrom.* **27**, 924–930 (2013).
151. Duncan, A. J. *et al.* Determination of coenzyme Q10 status in blood mononuclear cells, skeletal muscle, and plasma by HPLC with di-propoxy-coenzyme Q10 as an internal standard. *Clin. Chem.* **51**, 2380–2 (2005).
152. Edlund, P. O. Determination of coenzyme Q10, α -tocopherol and cholesterol in biological samples by coupled-column liquid chromatography with coulometric and ultraviolet detection. *J. Chromatogr. B Biomed. Sci. Appl.* **425**, 87–97 (1988).
153. Lass, A., Agarwal, S. & Sohal, R. S. Mitochondrial ubiquinone homologues, superoxide radical generation, and longevity in different mammalian species. *J. Biol. Chem.* **272**, 19199–19204 (1997).
154. Sohal, R. S. *et al.* Effect of coenzyme Q10 intake on endogenous coenzyme Q content, mitochondrial electron transport chain, antioxidative defenses, and life span of mice. *Free Radic. Biol. Med.* **40**, 480–

- 487 (2006).
155. Lass, A., Forster, M. J. & Sohal, R. S. Effects of coenzyme Q10 and α -tocopherol administration on their tissue levels in the mouse: Elevation of mitochondrial α -tocopherol by coenzyme Q10. *Free Radic. Biol. Med.* **26**, 1375–1382 (1999).
 156. Kamzalov, S., Sumien, N., Forster, M. J. & Sohal, R. S. Coenzyme Q Intake Elevates the Mitochondrial and Tissue Levels of Coenzyme Q and α -Tocopherol in Young Mice. *J. Nutr.* **133**, 3175–3180 (2003).
 157. Kucharská, J., Braunová, Z., Uličná, O., Zlatoš, L. & Gvozdjaková, A. Deficit of Coenzyme Q in heart and liver mitochondria of rats with streptozotocin-induced diabetes. *Physiol. Res.* **49**, 411–418 (2000).
 158. Kwong, L. K. *et al.* Effects of coenzyme Q10 administration on its tissue concentrations, mitochondrial oxidant generation, and oxidative stress in the rat. *Free Radic. Biol. Med.* **33**, 627–638 (2002).
 159. Krebs, J. J. R., Hauser, H. & Carafoli, E. Asymmetric distribution of phospholipids in the inner membrane of beef heart mitochondria. *J. Biol. Chem.* **254**, 5308–5316 (1979).
 160. Estornell, E. *et al.* Saturation kinetics of coenzyme Q in NADH and succinate oxidation in beef heart mitochondria. *FEBS Lett.* **311**, 107–109 (1992).
 161. Lakowicz, J. R. & Hogen, D. Chlorinated hydrocarbon-cell membrane interactions studied by the fluorescence quenching of carbazole-labeled phospholipids: Probe synthesis and characterization of the quenching methodology. *Chem. Phys. Lipids* **26**, 1–40 (1980).
 162. Chitra, M., Sukumar, E., Suja, V. & Shyamala Devi, C. S. Antitumor, Anti-Inflammatory and Analgesic Property of Embelin, a Plant Product. *Chemother.* **19940**, 109–113 (1994).
 163. Coutelle, O. *et al.* Embelin inhibits endothelial mitochondrial respiration and impairs neoangiogenesis during tumor growth and wound healing. *EMBO Mol. Med.* **6**, 624–639 (2014).
 164. Shcherbo, D. *et al.* Practical and reliable FRET/FLIM pair of fluorescent proteins. *BMC Biotechnol.* **9**, 1–6 (2009).
 165. Porter, A. G., Ng, P. & Jänicke, R. U. Death substrates come alive. *BioEssays* **19**, 501–507 (1997).
 166. Nicholson, D. W. & Thornberry, N. A. Caspases: killer proteases. *Trends Biochem. Sci.* **22**, 299–306 (1997).
 167. Duberley, K. E. *et al.* Effect of Coenzyme Q10 supplementation on mitochondrial electron transport chain activity and mitochondrial oxidative stress in Coenzyme Q10 deficient human neuronal cells. *Int. J. Biochem. Cell Biol.* **50**, 60–63 (2014).
 168. Messer, J. I., Jackman, M. R. & Willis, W. T. Pyruvate and citric acid cycle carbon requirements in isolated skeletal muscle mitochondria. *Am. J. Physiol. Physiol.* **286**, C565–C572 (2004).
 169. Gnaiger, E. Chapter 3. Mitochondrial pathways to Complex I: respiratory substrate control with pyruvate, malate and glutamate. in *Mitochondrial Pathways and Respiratory Control* 32–28 (Steiger Druck GmbH, 2014).
 170. Ackrell, B. A. C., Kearney, E. B. & Mayr, M. Role of oxalacetate in the regulation of mammalian succinate dehydrogenase. *J. Biol. Chem.* **249**, 2021–2027 (1974).
 171. Kearney, E. B., Ackrell, B. A. C. & Mayr, M. Tightly bound oxalacetate and the activation of succinate dehydrogenase. *Biochem. Biophys. Res. Commun.* **49**, 1115–1121 (1972).
 172. Bock, R. M. & Alberty, R. A. Studies of the Enzyme Fumarase. I. Kinetics and Equilibrium. *J. Am. Chem. Soc.* **75**, 1921–1925 (1953).
 173. Chien, T.-F. & Burkhard, R. K. Stoichiometry and Calculated Enthalpy Change for Mitochondrial Oxidation of Succinate by Ferricyanide. *J. Biol. Chem.* **250**, 553–556 (1975).
 174. Palmieri, F., Quagliariello, E. & Klingenberg, M. Kinetics and Specificity of the Oxoglutarate Carrier in Rat-Liver Mitochondria. *Eur. J. Biochem.* **29**, 408–416 (1972).
 175. Storey, B. T. Inhibitors of energy-coupling site 1 of the mitochondrial respiratory chain. *Pharmacol. Ther.* **10**, 399–406 (1980).
 176. Tocilescu, M. A., Fendel, U., Zwicker, K., Kerscher, S. & Brandt, U. Exploring the ubiquinone binding cavity of respiratory complex I. *J. Biol. Chem.* **282**, 29514–29520 (2007).
 177. Dervartanian, D. V. & Veeger, C. Studies on succinate dehydrogenase. I. Spectral properties of the purified enzyme and formation of enzyme-competitive inhibitor complexes. *BBA - Enzymol. Subj.* **92**,

- 233–247 (1964).
178. Lemasters, J. J. The ATP-to-Oxygen Stoichiometries of Oxidative Phosphorylation by Rat Liver Mitochondria. *J. Biol. Chem.* **259**, 13123–13130 (1984).
179. Capel, F. *et al.* Due to reverse electron transfer, mitochondrial H₂O₂ release increases with age in human vastus lateralis muscle although oxidative capacity is preserved. *Mech. Ageing Dev.* **126**, 505–511 (2005).
180. Cino, M. & Del Maestro, R. F. Generation of hydrogen peroxide by brain mitochondria: The effect of reoxygenation following postdecapitative ischemia. *Arch. Biochem. Biophys.* **269**, 623–638 (1989).
181. Chouchani, E. T. *et al.* Ischaemic accumulation of succinate controls reperfusion injury through mitochondrial ROS. *Nature* **515**, 431–435 (2014).
182. Barrientos, A., Fontanesi, F. & Díaz, F. Evaluation of the mitochondrial respiratory chain and oxidative phosphorylation system using polarography and spectrophotometric enzyme assays. *Curr. Protoc. Hum. Genet.* **Chapter 19**, 1–13 (2009).
183. Käppeli, O. & Fiechter, A. A convenient method for the determination of oxygen solubility in different solution. *Biotechnol. Bioeng.* **23**, 1897–1901 (1981).
184. Shchukarev, S. A. & Tolmacheva, T. A. Solubility of oxygen in ethanol-water mixtures. *Zhurnal Strukt. Khimii* **9**, 16–21 (1968).
185. Stankoska, K. Personal communication. (Department of Biophysics, Saarland University, 2018).
186. Mráček, T., Pecinová, A., Vrbacký, M., Drahotka, Z. & Houštěk, J. High efficiency of ROS production by glycerophosphate dehydrogenase in mammalian mitochondria. *Arch. Biochem. Biophys.* **481**, 30–36 (2009).
187. HOUŠTĚK, J., CANNON, B. & LINDBERG, O. Glycerol-3-Phosphate Shuttle and Its Function in Intermediary Metabolism of Hamster Brown-Adipose Tissue. *Eur. J. Biochem.* **54**, 11–18 (1975).
188. Takahashi, K. & Takahashi, M. Exogenous administration of coenzyme Q10 restores mitochondrial oxygen consumption in the aged mouse brain. *Mech. Ageing Dev.* **134**, 580–586 (2013).
189. Bergamini, C., Moruzzi, N., Sblendido, A., Lenaz, G. & Fato, R. A water soluble CoQ 10 formulation improves intracellular distribution and promotes mitochondrial respiration in cultured cells. *PLoS One* **7**, e33712 (2012).
190. Naderi, J. *et al.* Water-soluble formulation of Coenzyme Q10 inhibits Bax-induced destabilization of mitochondria in mammalian cells. *Apoptosis* **11**, 1359–1369 (2006).
191. Casey, J. R., Grinstein, S. & Orlowski, J. Sensors and regulators of intracellular pH. *Nat. Rev. Mol. Cell Biol.* **11**, 50–61 (2010).
192. Powell, K. J. *et al.* Chemical speciation of environmentally significant heavy metals with inorganic ligands. Part 1: The Hg₂⁺, Cl⁻, OH⁻, CO₃²⁻, SO₄²⁻, and PO₄³⁻ aqueous systems (IUPAC Technical Report). *Pure Appl. Chem.* **77**, 739–800 (2005).
193. Monomagnesium phosphate. Available at: http://www.fao.org/fileadmin/user_upload/jecfa_additives/docs/monograph5/additive-507-m5.pdf. (Accessed: 5th October 2018)
194. Racz, G. J. & Soper, R. J. Solubility of dimagnesium phosphate trihydrate and trimagnesium phosphate. *Can. J. Soil Sci* **48**, 265–269 (1968).
195. Taylor, A. W., Frazier, A. W., Gurney, E. L. & Smith, J. P. Solubility products of di- and trimagnesium phosphates and the dissociation of magnesium phosphate solutions. *Trans. Faraday Soc.* **59**, 1585–1589 (1963).
196. Calcium biphosphate, CID=24454. *Database, National Center for Biotechnology Information. PubChem* Available at: <https://pubchem.ncbi.nlm.nih.gov/compound/Calcium-biphosphate>. (Accessed: 11th June 2019)
197. Lyerla, J. R. High-resolution nuclear magnetic resonance spectroscopy. *Methods Exp. Phys.* **16**, 241–369 (1980).
198. Thermo Fisher Scientific. Fura and Indo Ratiometric Calcium Indicators: Product Information (MP 01200). 1–6 (2011).

199. Grynkiewicz, G., Poenie, M. & Tsien, R. Y. A new generation of Ca²⁺-indicators with greatly improved fluorescence properties. *Journal of Biological Chemistry* **260**, 3440–3450 (1985).
200. Raju, B., Murphy, E., Levy, L. A., Hall, R. D. & London, R. E. A fluorescent indicator for measuring cytosolic free magnesium. *Am. J. Physiol.* **256**, C540-8 (1989).
201. Hyrc, K. L., Bownik, J. M. & Goldberg, M. P. Ionic selectivity of low-affinity ratiometric calcium indicators: mag-Fura-2, Fura-2FF and BTC. *Cell Calcium* **27**, 75–86 (2000).
202. Molecular Probes Inc. Fluorescent Magnesium Indicators: Product Information (MP 01290). 1–4 (2005).
203. Atar, D., Backx, P. H., Appel, M. M., Gao, W. D. & Marban, E. Excitation-transcription coupling mediated by zinc influx through voltage-dependent calcium channels. *J. Biol. Chem.* **270**, 2473–2477 (1995).
204. Tsien, R. Y. & Pozzan, T. Measurement of Cytosolic Free Ca²⁺ with Quin2. *Methods Enzym.* **172**, 230–244 (1989).
205. Paredes, R. M., Etzler, J. C., Watts, L. T., Zheng, W. & Lechleiter, J. D. Chemical calcium indicators. *Methods* **46**, 143–151 (2008).
206. Bertero, E. & Maack, C. Calcium signaling and reactive oxygen species in Mitochondria. *Circ. Res.* **122**, 1460–1478 (2018).
207. Territo, P. R., French, S. A., Dunleavy, M. C., Evans, F. J. & Balaban, R. S. Calcium activation of heart mitochondrial oxidative phosphorylation. Rapid kinetics of mVO₂, NADH, and light scattering. *J. Biol. Chem.* **276**, 2586–2599 (2001).
208. Gellerich, F. N. *et al.* The regulation of OXPHOS by extramitochondrial calcium. *Biochimica et Biophysica Acta - Bioenergetics* **1797**, 1018–1027 (2010).
209. Esposti, M. D. *et al.* Incorporation of ubiquinone homologs into lipid vesicles and mitochondrial membranes. *Arch. Biochem. Biophys.* **210**, 21–32 (1981).
210. Gottschalk, K. E., Hiskey, R. G., Pedersen, L. G. & Koehler, K. A. A theoretical study of malonate and formate calcium binding by ab initio techniques. *J. Mol. Struct. THEOCHEM* **87**, 155–159 (1982).
211. Head-Gordon, M., Deerfield, D. W., Hiskey, R. G., Fox, D. J. & Pedersen, L. G. Interaction of calcium and magnesium ions with malonate and the role of the waters of hydration: a quantum mechanical study. *J. Am. Chem. Soc.* **113**, 1892–1899 (2005).
212. Miyadera, H. *et al.* Atpenins, potent and specific inhibitors of mitochondrial complex II (succinate-ubiquinone oxidoreductase). *Proc. Natl. Acad. Sci.* **100**, 473–477 (2003).
213. Kuznetsov, A. V & Gnaiger, E. Laboratory Protocol Complex I (NADH:Ubiquinone Oxidoreductase; EC 1.6.5.3) Mitochondrial Membrane Enzyme. *Mitochondrial Physiology Network* **8**, 1–9 (2010).
214. Spinazzi, M., Casarin, A., Pertegato, V., Salviati, L. & Angelini, C. Assessment of mitochondrial respiratory chain enzymatic activities on tissues and cultured cells. *Nat. Protoc.* **7**, 1235–1246 (2012).
215. Kirby, D. M., Thorburn, D. R., Turnbull, D. M. & Taylor, R. W. Biochemical Assays of Respiratory Chain Complex Activity. *Methods Cell Biol.* **80**, 93–119 (2007).
216. Fischer, B. E., Häring, U. K., Tribolet, R. & Sigel, H. Metal ion/buffer interactions. Stability of binary and ternary complexes containing 2-amino-2(hydroxymethyl)-1,3-propanediol (Tris) and adenosine 5'-triphosphate (ATP). *Eur. J. Biochem.* **94**, 523–30 (1979).
217. Ferreira, C. M. H., Pinto, I. S. S., Soares, E. V. & Soares, H. M. V. M. (Un)suitability of the use of pH buffers in biological, biochemical and environmental studies and their interaction with metal ions-a review. *RSC Advances* **5**, 30989–31003 (2015).
218. Good, N. E. & Izawa, S. [3] Hydrogen ion buffers. in *Methods in Enzymology* **24**, 53–68 (Academic Press, 2004).
219. Covington, A. K. & Danish, E. Y. Measurement of magnesium stability constants of biologically relevant ligands by Simultaneous use of pH and ion-selective electrodes. *J. Solution Chem.* **38**, 1449–1462 (2009).
220. Janssen, A. J. M. *et al.* Spectrophotometric assay for complex I of the respiratory chain in tissue samples and cultured fibroblasts. *Clin. Chem.* **53**, 729–734 (2007).
221. Porcelli, A. M. *et al.* pH difference across the outer mitochondrial membrane measured with a green

- fluorescent protein mutant. *Biochem. Biophys. Res. Commun.* **326**, 799–804 (2005).
222. Llopis, J., McCaffery, J. M., Miyawaki, A., Farquhar, M. A. & Tsien, R. Y. Measurement of cytosolic, mitochondrial, and Golgi pH in single living cells with green fluorescent protein. *Cell Biol.* **95**, 6803–6808 (1990).
223. Molyneux, S. L. & Lever, M. Fluorescence is less sensitive than ultraviolet or electrochemical detection for measurement of coenzyme Q10 in plasma. *Clin. Chim. Acta* **358**, 198–200 (2005).
224. Mitreska, N. personal communication. (Department of Biophysics, Saarland University, 2018).
225. James, A. M., Cochemé, H. M., Smith, R. A. J. & Murphy, M. P. Interactions of mitochondria-targeted and untargeted ubiquinones with the mitochondrial respiratory chain and reactive oxygen species: Implications for the use of exogenous ubiquinones as therapies and experimental tools. *J. Biol. Chem.* **280**, 21295–21312 (2005).
226. Wittig, I., Karas, M. & Schägger, H. High Resolution Clear Native Electrophoresis for In-gel Functional Assays and Fluorescence Studies of Membrane Protein Complexes. *Mol. Cell. Proteomics* **6**, 1215–1225 (2007).
227. Vinothkumar, K. R., Zhu, J. & Hirst, J. Architecture of mammalian respiratory complex I. *Nature* **515**, 80–84 (2014).
228. Guerrero-Castillo, S. *et al.* The Assembly Pathway of Mitochondrial Respiratory Chain Complex I. *Cell Metab.* **25**, 128–139 (2017).
229. Yan, L.-J. & Forster, M. J. Resolving mitochondrial protein complexes using nongradient blue native polyacrylamide gel electrophoresis. *Anal. Biochem.* **389**, 143–149 (2009).
230. Schägger, H. Respiratory chain supercomplexes. *IUBMB Life* **52**, 119–128 (2001).
231. Sabar, M., Balk, J. & Leaver, C. J. Histochemical staining and quantification of plant mitochondrial respiratory chain complexes using blue-native polyacrylamide gel electrophoresis. *Plant J.* **44**, 893–901 (2005).
232. Abcam. ab109720 – Complex I Enzyme Activity Dipstick Assay Kit. 1–19 (2017).
233. Willis, J. H. *et al.* Isolated deficiencies of OXPHOS complexes I and IV are identified accurately and quickly by simple enzyme activity immunocapture assays. *Biochim. Biophys. Acta - Bioenerg.* **1787**, 533–538 (2009).
234. Hock Ngu, L. *et al.* A catalytic defect in mitochondrial respiratory chain complex I due to a mutation in NDUFS2 in a patient with Leigh syndrome. *BBA - Mol. Basis Dis.* **1822**, 168–175 (2012).
235. Schägger, H., Cramer, W. A. & von Jagow, G. Analysis of molecular masses and oligomeric states of protein complexes by blue native electrophoresis and isolation of membrane protein complexes by two-dimensional native electrophoresis. *Anal. Biochem.* **217**, 220–230 (1994).
236. Berglund, G. I. *et al.* The catalytic pathway of horseradish peroxidase at high resolution. *Nature* **417**, 463–468 (2002).
237. Gorris, H. H. & Walt, D. R. Mechanistic Aspects of Horseradish Peroxidase Elucidated through Single-Molecule Studies. *J. Am. Chem. Soc.* **131**, 6277–6282 (2009).
238. Balaban, R. S., Nemoto, S. & Finkel, T. Mitochondria, oxidants, and aging. *Cell* **120**, 483–495 (2005).
239. Grivennikova, V. G., Kareyeva, A. V. & Vinogradov, A. D. Oxygen-dependence of mitochondrial ROS production as detected by Amplex Red assay. *Redox Biol.* **17**, 192–199 (2018).
240. Debski, D. *et al.* Mechanism of oxidative conversion of Amplex® Red to resorufin: Pulse radiolysis and enzymatic studies. *Free Radic. Biol. Med.* **95**, 323–332 (2016).
241. Serrano, J. *et al.* Dietary antioxidants interfere with Amplex Red-coupled-fluorescence assays. *Biochem. Biophys. Res. Commun.* **388**, 443–449 (2009).
242. Starkov, A. A. & Fiskum, G. Regulation of brain mitochondrial H₂O₂ production by membrane potential and NAD(P)H redox state. *J. Neurochem.* **86**, 1101–1107 (2003).
243. Dikalov, S. I., Li, W., Mehranpour, P., Wang, S. S. & Zafari, A. M. Production of extracellular superoxide by human lymphoblast cell lines: Comparison of electron spin resonance techniques and cytochrome C reduction assay. *Biochem. Pharmacol.* **73**, 972–980 (2007).
244. Bui, N. N. Voltammetric and Electron Spin Resonance Studies of Cyclic Hydroxylamine CMH and Its

- Application to Monitor Transient Radicals in Dioxygenase Enzymes. (Doctoral dissertation, Saarland University, 2016).
245. TWIGG, R. S. Oxidation-Reduction Aspects of Resazurin. *Nature* **155**, 401–402 (1945).
246. Nims, R. W., Prough, R. A. & Lubet, R. A. Cytosol-mediated reduction of resorufin: A method for measuring quinone oxidoreductase. *Arch. Biochem. Biophys.* **229**, 459–465 (1984).
247. Dutton, D. R., Reed, G. A. & Parkinson, A. Redox cycling of resorufin catalyzed by rat liver microsomal NADPH-cytochrome P450 reductase. *Arch. Biochem. Biophys.* **268**, 605–616 (1989).
248. Svistunenko, D. A., Davies, N., Brealey, D., Singer, M. & Cooper, C. E. Mitochondrial dysfunction in patients with severe sepsis: An EPR interrogation of individual respiratory chain components. *Biochim. Biophys. Acta - Bioenerg.* **1757**, 262–272 (2006).
249. Ohnishi, T. Iron-sulfur clusters/semiquinones in Complex I. *Biochim. Biophys. Acta - Bioenerg.* **1364**, 186–206 (1998).
250. Wright, J. J., Salvadori, E., Bridges, H. R., Hirst, J. & Roessler, M. M. Small-volume potentiometric titrations: EPR investigations of Fe-S cluster N2 in mitochondrial complex I. *J. Inorg. Biochem.* **162**, 201–206 (2016).
251. Angerer, H. *et al.* A scaffold of accessory subunits links the peripheral arm and the distal proton-pumping module of mitochondrial complex I. *Biochem. J.* **437**, 279–88 (2011).
252. Hirst, J. & Roessler, M. M. Energy conversion, redox catalysis and generation of reactive oxygen species by respiratory complex I. *Biochim. Biophys. Acta - Bioenerg.* **1857**, 872–883 (2016).
253. Vinogradov, A. D. *et al.* Energy-dependent Complex I-associated ubisemiquinones in submitochondrial particles. *FEBS Lett.* **370**, 83–87 (1995).
254. Burbaev, Ds., Moroz, I., Kotlyar, A., Sled, V. & Vinogradov, A. *Ubisemiquinone in the NADH-ubiquinone reductase region of the mitochondrial respiratory chain.* **254**, (1989).
255. Magnitsky, S. *et al.* EPR characterization of ubisemiquinones and iron-sulfur cluster N2, central components of the energy coupling in the NADH-ubiquinone oxidoreductase (complex I) in situ. *J. Bioenerg. Biomembr.* **34**, 193–208 (2002).
256. Ohnishi, T., Lim, J., Winter, D. B. & King, T. E. Thermodynamic and EPR characteristics of a HiPIP type iron sulfur center in the succinate dehydrogenase of the respiratory chain. *J. Biol. Chem.* **251**, 2105–2109 (1976).
257. Duveau, D. Y. *et al.* Synthesis and characterization of mitoQ and idebenone analogues as mediators of oxygen consumption in mitochondria. *Bioorganic Med. Chem.* **18**, 6429–6441 (2010).
258. Lenaz, G. Quinone specificity of Complex I. *Biochimica et Biophysica Acta - Bioenergetics* **1364**, 207–221 (1998).
259. Fash, D. M. *et al.* Effects of alkyl side chain modification of coenzyme Q10 on mitochondrial respiratory chain function and cytoprotection. *Bioorganic Med. Chem.* **21**, 2346–2354 (2013).
260. Gu, L. Q., Yu, L. & Yu, C. A. Effect of substituents of the benzoquinone ring on electron-transfer activities of ubiquinone derivatives. *BBA - Bioenerg.* **1015**, 482–492 (1990).
261. Erdtman, H., Granath, M., Linholt, S. C. & Sörensen, N. A. Studies on Humic Acids. V. The Reaction of p-Benzoquinone with Alkali. *Acta Chem. Scand.* **8**, 811–816 (2008).
262. Flaig, W., Ploetz, T. & Biergans, H. Zur Kenntnis der Huminsäuren, XIV. Mitteilung Bildung und Reaktionen einiger Hydroxy-chinone. *Justus Liebigs Ann. Chem.* **597**, 196–213 (1955).
263. Gulaboski, R. *et al.* New insights into the chemistry of Coenzyme Q-0: A voltammetric and spectroscopic study. *Bioelectrochemistry* **111**, 100–108 (2016).
264. Schulze, H. & Flaig, W. Zur Kenntnis der Huminsäuren, IV. Mitteilung. Über die Ringsprengung mehrwertiger Phenole mit Sauerstoff in alkalischem Medium. *Justus Liebigs Ann. Chem.* **575**, 231–241 (1952).
265. Dong, J. *et al.* Biokatalytische Oxidationsreaktionen - aus der Sicht eines Chemikers. *Angew. Chemie* **130**, 9380–9404 (2018).
266. Kapasi, A. A. *et al.* Ethanol promotes T cell apoptosis through the mitochondrial pathway. *Immunology* **108**, 313–320 (2003).

267. Rehman, S. *et al.* Ethanol and vitamin D receptor in T cell apoptosis. *J. Neuroimmune Pharmacol.* **8**, 251–261 (2013).
268. Lovett, G. S. & Sweetman, A. J. The analysis of drug action on mitochondrial oxidative phosphorylation. The choice of organic solvent for water-insoluble drugs. *Methods Find. Exp. Clin. Pharmacol.* **5**, 695–9 (1983).
269. Syed, M., Skonberg, C. & Hansen, S. H. Effect of some organic solvents on oxidative phosphorylation in rat liver mitochondria: Choice of organic solvents. *Toxicol. Vitro.* **27**, 2135–2141 (2013).
270. Borowy-Borowski, H., Sikorska-Walker, M. & Walker, P. R. Corrected publication: Water-soluble compositions of bioactive lipophilic compounds. 1–5 (2009).
271. Ma, D. *et al.* Inhibition of stress induced premature senescence in presenilin-1 mutated cells with water soluble Coenzyme Q10. *Mitochondrion* **17**, 106–115 (2014).
272. Xia, S., Xu, S. & Zhang, X. Optimization in the preparation of coenzyme Q10 nanoliposomes. *J. Agric. Food Chem.* **54**, 6358–6366 (2006).
273. Murphy, M. P. Targeting lipophilic cations to mitochondria. *Biochim. Biophys. Acta - Bioenerg.* **1777**, 1028–1031 (2008).
274. Kelso, G. F. *et al.* Selective targeting of a redox-active ubiquinone to mitochondria within cells: Antioxidant and antiapoptotic properties. *J. Biol. Chem.* **276**, 4588–4596 (2001).
275. Hallermayer, G. & Neupert, W. Lipid Composition of Mitochondrial Outer and Inner Membranes of *Neurospora crassa*. *Hoppe. Seylers. Z. Physiol. Chem.* **355**, (1974).
276. Jane Comte, B. M. and D. C. G. Lipid composition and protein profiles of outer and inner membranes from pig heart mitochondria. Comparison with microsomes. *Biochim. Biophys. Acta* **419**, 271–284 (1976).
277. Torres, M. J. *et al.* 17 β -Estradiol Directly Lowers Mitochondrial Membrane Microviscosity and Improves Bioenergetic Function in Skeletal Muscle. *Cell Metab.* **27**, 167–179 (2018).
278. Colell, A. *et al.* Cholesterol Impairs the Adenine Nucleotide Translocator-mediated Mitochondrial Permeability Transition through Altered Membrane Fluidity*. (2003). doi:10.1074/jbc.M210943200
279. Budin, I. *et al.* Viscous control of cellular respiration by membrane lipid composition. *Science (80-)*. **362**, 1186–1189 (2018).
280. Yu, W. *et al.* Altered cholesterol metabolism in Niemann-Pick type C1 mouse brains affects mitochondrial function. *J. Biol. Chem.* **280**, 11731–11739 (2005).
281. Dumas, D., Latger, V., Viriot, M. L., Blondel, W. & Stoltz, J. F. Membrane fluidity and oxygen diffusion in cholesterol-enriched endothelial cells. *Clin. Hemorheol. Microcirc.* **21**, 255–261 (1999).
282. Dmitriev, R. I., Zhdanov, A. V., Ponomarev, G. V., Yashunski, D. V. & Papkovsky, D. B. Intracellular oxygen-sensitive phosphorescent probes based on cell-penetrating peptides. *Anal. Biochem.* **398**, 24–33 (2010).
283. Dmitriev, R. I. & Papkovsky, D. B. Optical probes and techniques for O₂ measurement in live cells and tissue. *Cell. Mol. Life Sci.* **69**, 2025–2039 (2012).
284. Fercher, A., Borisov, S. M., Zhdanov, A. V., Klimant, I. & Papkovsky, D. B. Intracellular O₂ sensing probe based on cell-penetrating phosphorescent nanoparticles. *ACS Nano* **5**, 5499–5508 (2011).
285. Sauerheber, R. D., Lewis, U. J., Esgate, J. A. & Gordon, L. M. Effect of calcium, insulin and growth hormone on membrane fluidity. A spin label study of rat adipocyte and human erythrocyte ghosts. *BBA - Biomembr.* **597**, 292–304 (1980).
286. Gupte, S. *et al.* Relationship between lateral diffusion, collision frequency, and electron transfer of mitochondrial inner membrane oxidation-reduction components. *Proc. Natl. Acad. Sci.* **81**, 2606–2610 (2006).
287. Ziegelh offer, A. *et al.* Involvement of Membrane Fluidity in Endogenous Protective Processes Running on Subcellular Membrane Systems of the Rat Heart. *Physiol. Res* **61**, 11–21 (2012).
288. Waczulikova, I. *et al.* Mitochondrial membrane fluidity, potential, and calcium transients in the myocardium from acute diabetic rats. *J. Physiol. Pharmacol* **85**, 372–381 (2007).
289. Shaikh, S. R., Sullivan, E. M., Alleman, R. J., Brown, D. A. & Zeczycki, T. N. Increasing mitochondrial

- membrane phospholipid content lowers the enzymatic activity of electron transport complexes. *Biochemistry* **53**, 5589–5591 (2014).
290. Sharpley, M. S., Shannon, R. J., Draghi, F. & Hirst, J. Interactions between Phospholipids and NADH:Ubiquinone Oxidoreductase (Complex I) from Bovine Mitochondria. doi:10.1021/bi051809x
291. Schwall, C. T., Greenwood, V. L. & Alder, N. N. The stability and activity of respiratory Complex II is cardiolipin-dependent. *Biochim. Biophys. Acta - Bioenerg.* **1817**, 1588–1596 (2012).
292. Petrosillo, G., Casanova, G., Matera, M., Ruggiero, F. M. & Paradies, G. Interaction of peroxidized cardiolipin with rat-heart mitochondrial membranes: Induction of permeability transition and cytochrome c release. *FEBS Lett.* **580**, 6311–6316 (2006).
293. Paradies, G. *et al.* Decrease in Mitochondrial Complex I Activity in Ischemic/Reperfused Rat Heart: Involvement of Reactive Oxygen Species and Cardiolipin. *Circ. Res.* **94**, 53–59 (2004).
294. Chen, Y., McMillan-Ward, E., Kong, J., Israels, S. J. & Gibson, S. B. Mitochondrial electron-transport-chain inhibitors of complexes I and II induce autophagic cell death mediated by reactive oxygen species. *J. Cell Sci.* **120**, 4155–4166 (2007).
295. Li, N. *et al.* Mitochondrial complex I inhibitor rotenone induces apoptosis through enhancing mitochondrial reactive oxygen species production. *J. Biol. Chem.* **278**, 8516–8525 (2003).
296. Bentinger, M., Dallner, G., Chojnacki, T. & Swiezewska, E. Distribution and breakdown of labeled coenzyme Q10 in rat. *Free Radic. Biol. Med.* **34**, 563–575 (2003).
297. Hanahan, D. & Weinberg, R. A. Hallmarks of cancer: the next generation. *Cell* **144**, 646–74 (2011).
298. Frontana, C. & González, I. The role of intramolecular hydrogen bonding in the electrochemical behavior of hydroxy-quinones and in semiquinone stability. *J. Braz. Chem. Soc.* **16**, 299–307 (2005).

Acknowledgements

Mein erster Dank richtet sich an meinen Chemielehrer Herrn Hauck. Seine ansteckende Begeisterung für die und hervorragende Lehre der Naturwissenschaften hat mich mit der Faszination, die Welt verstehen und ergründen zu wollen, dazu motiviert ein naturwissenschaftliches Studium aufzunehmen und war meine Eintrittskarte in die Grundlagenforschung. Meine Kunstlehrerin Frau Webersberger-Maier hat mir gelehrt immer wieder über den Tellerrand hinauszublicken, Kreativität roh ihren Lauf zu lassen und in neue Richtungen zu denken und mir damit wichtige Qualitäten für die Wissenschaft mitgegeben.

Ein großer Dank geht an Prof. Dr. Markus Hoth, der mich so herzlich in seine Arbeitsgruppe aufgenommen hat und mich immer wieder mit seinem Enthusiasmus für die Wissenschaft, der Freiheit bei der Wahl von und in meinen Projekten sowie dem entgegengebrachten Vertrauen motiviert hat. Bei Dr. Reinhard Kappl, Prof. Dr. Markus Hoth und Prof. Dr. Ivan Bogeski möchte ich mich für den Einstieg in die spannende Forschungswelt der Redoxbiologie bedanken und die Möglichkeit in ein Projekt einzusteigen, das mir erlaubte viele, verschiedene Methoden unterschiedlicher Disziplinen zu erlernen und immer wieder meinen wissenschaftlichen Horizont zu erweitern. Einen besonderen Dank an Reinhard u. a. für die Unterstützung, Wertschätzung und motivierenden Worte. Dem Redox-Club danke ich für viele, spannende Diskussionen und lehrreiche Seminare. Dr. Monika Bozem möchte ich für ihre Ideen, Diskussions- und fortwährende Hilfsbereitschaft danken.

Für die hervorragende technische Unterstützung bedanke ich mich bei dem gesamten technischen Personal, insbesondere Josef Marx, Susanne Renno, Sandra Janku, Cora Hoxha, Andrea Armbrüster, Gertrud Schwär und Kathrin Förderer. Ich bedanke mich bei Gerhard Bracic für seine Unterstützung und die Zurverfügungstellung und Optimierung seiner Programme, Rüdiger Stumpf für seine große Hilfsbereitschaft bei technischen Fragestellungen aller Art. Zudem möchte ich der gesamten Arbeitsgruppe danken, die immer wieder mit Rat und Tat beiseite stand, insbesondere Carsten Kummerow, Dalia Alansary und Eva Schwarz.

Für die schöne Zeit und die vielen Diskussionen möchte ich meinen Bürokollegen besonders danken: Dr. Nguyen Bui, Katerina Stankoska, Nikolina Mitreska, Phillip Knapp, Hannah Heintz und Sofia Schnell.

Ein großer Dank geht an Dr. Josef Zapp für die ausführlichen Vor- und Nachbesprechungen aller NMR-Messungen. Prof. Dr. Markus R. Meyer danke ich für seine große Hilfs- und Diskussionsbereitschaft bei allen massenspektrometrischen Experimenten. Prof. Dr. Christoph Maack danke ich für die Zusammenarbeit, den Zugang zum Oxygraphen und insbesondere Dr. Alexander G. Nickel, Nina Schnellbach und Michelle Gulentz für die Einführung in und Unterstützung bei Experimenten mit Mausmaterial. Prof. Dr. Martin van der Laan danke ich für den freien Zugang zu seinem Labor und Geräten, Florian Wollweber für die Zurverfügungstellung von Probenmaterial und Dr. Karina von der Malsburg für die Unterstützung bei Western Blot und BN-PAGE.

Ein inniger Dank an meinen Mann, Dr. Sven Kappel, der im Laufe unseres Studiums unzählige Protokolle und Abschlussarbeiten Korrektur gelesen hat und nie müde wurde, wenn ich jedes einzelne Experiment Revue passieren lassen oder die Durchführung bis ins letzte Detail durchsprechen wollte. Danke für die unzähligen Male, die Du mich im Dunkeln vom Institut abgeholt hast und deine immerwährende, grenzenlose Unterstützung, damit ich mich voll und ganz auf meine Abschlussarbeiten konzentrieren konnte.

Publications

Bozem, M., Knapp, P., Mirčeski, V., Slowik, E. J., Bogeski, I., Kappl, R., Heinemann, C. and Hoth, M. Electrochemical Quantification of Extracellular Local H₂O₂ Kinetics Originating from Single Cells. *Antioxidants & Redox Signaling*. **29** (6): 501-517 (2018).

Slowik, E. J., Bui, N. N., Bogeski, I., Thierbach, S., Bozem, M., Hoth, M., Kappl, R. Detection of H₂O₂ and superoxide using a horseradish peroxidase assay: an electron spin resonance approach. *ACTA PHYSIOLOGICA*. **214**: 173-174 (2015).

Slowik, E. J., Zapp, J., Meyer, M. R., Holzmann, C., Bogeski, I., Hoth, M., Kappl, R. HO-CoQ10 synthesis in a two-phase system. (in preparation)

Slowik, E. J., Hoth, M., Bogeski, I., Kappl, R. Regulation of mitochondrial respiration and ROS homeostasis by exogenous CoQ10 and HO-CoQ10. (in preparation)

Slowik, E. J., Stankoska, K., Bui, N. N., Zapp, J., Meyer, M. R., Hoth, M., Kappl, R., Bogeski, I. The widely used channel blocker 2-APB is ROS sensitive. (in preparation)

Stankoska, K., Slowik, E. J., Mitreska, N., Zapp, J., Meyer, M. R., Hoth, M., Kappl, R. Redox properties and Calicium-binding of Coenzyme Q10, mitoQ and their hydroxy analogues. (in preparation)